Univerza v Ljubljani
Fakulteta za matematiko in fiziko

Andreja Šarlah

Vpliv ograjujoče površine na fluktuacije nematske ureditve v tekočem kristalu

disertacija

Ljubljana, 2001

University of Ljubljana
Faculty of Mathematics and Physics

Andreja Šarlah

Effect of the confining substrates on nematic order-fluctuations in liquid crystals

Thesis

Ljubljana, 2001

Na raziskovalni poti me je od vseh začetkov usmerjal in vodil prof. dr. Slobodan Žumer. Za njegove nasvete in ravno pravo mero priganjanja ter usmerjanja, s kom naj se še pogovorim in kateri poster bi si bilo dobro še ogledati, se mu najlepše zahvaljujem.

Vesela sem, da sem bila od vsega začetka deležna majhnih raziskovalnih skrivnosti, ki jih je z nami delil Primož. Postale so že kar legendarne in jih z veseljem prenašamo na mlajše rodove. Primož, hvala tudi za pripombe, ki si jih imel ob prebiranju ne čisto zadnjih verzij mojih člankov.

Za prijetno delovno vzdušje ste skrbeli Anamarija, Gregor in Daniel, del časa pa tudi Jure, Primož, Fahimeh in Matej. Daniel in Grega, hvala za vse naše pogovore, zaradi katerih je bil marsikateri ne nujno raziskovalni problem videti precej manjši, ali pa ga sploh ni bilo več.

Nenazadnje hvala vam, mami, oči in Katarina, ker me vedno podpirate in ste ponosni name. Hvala tudi tebi Grega, ker skrbiš za prijetno vzdušje, kadar nisem v službi, in še posebej zato, ker se te, kot praviš, ne da odgnati.

Povzetek

Delo je posvečeno študiju vpliva ograjujoče površine na fluktuacije nematskega ureditvenega parametra – posredno preko spremembe povprečne ravnovesne ureditve in neposredno preko spremembe robnih pogojev za fluktuacije. Posebej se posvečam sistemom, v katerih so v bližini faznih in strukturnih prehodov pomembne tudi nedirektorske prostostne stopnje ureditvenega parametra. Za kolektivne fluktuacije ureditvenega parametra v heterofaznem sistemu — nematik v stiku z razurejujočo površino — je značilen mehek fluktuacijski način fluktuacij skalarnega ureditvenega parametra, ki predstavlja fluktuacije debeline staljene omočitvene plasti. Nematsko hibridno celico označujejo tri različne urejene strukture. Prehod med njimi je lahko tako nezvezen kot tudi zvezen. Posebej študiram dvoosno strukturo, v kateri je direktorsko polje nedeformirano na račun staljenega reda in povečane stopnje urejenosti v notranjosti celice. Strukturni prehod iz dvoosne v upognjeno direktorsko strukturo vodi mehek direktoski fluktuacijski način. Močno upočasnjene so tudi fluktuacije stopnje urejenosti. Spremembe urejenosti, ki so posledica ograditve, povzročajo strukturni in psevdo Casimirjev privlak ali odboj med stenami. Spremenjena simetrija ureditve pa spremeni van der Waalsovo silo, ki jo tekoči kristal posreduje med stenama.

Ključne besede: nematski tekoči kristali, ograditev, fluktuacije, fazni prehod, strukturni prehod, močenje, van der Waalsova sila, strukturna sila, stabilnost

PACS: 61.30.-v, 61.30.Cz, 61.30.Hn, 64.70.Md, 68.15.+e, 68.60.Dv, 78.67.-n

Abstract

The thesis deals with effects of the confining substrates onto the nematic order parameter fluctuations, both, through changing the equilibrium average order and through changing the boundary conditions. A special attention is paid to systems in which in the vicinity of phase and structural transitions certain degrees of freedom differ significantly from the ones in the bulk. In the analysis of collective excitations in a nematic liquid crystal in contact with disordering substrates, a soft fluctuation mode is discovered. It represents fluctuations of the thickness of the molten wetting layers. In hybrid nematic film, there are three possible ordered structures and the structural transition between them can be either discontinuous or it can become continuous. In biaxial structure, the director field is undistorted at the expense of the decreased order and increased biaxiality of the order in the middle of the film. At the transition to structure with bent director field, the spectrum of collective excitations is characterized by soft director fluctuations and in addition, fluctuations of the degree of order and of the parameter of biaxiality become softer as well. Surface-induced change of the order gives rise to the structural and pseudo-Casimir interaction between the confining walls and the changed symmetry of the order changes the van der Waals interaction.

Keywords: nematic liquid crystals, confinement, fluctuations, phase transition, structural transition, wetting, van der Waals force, structural force, stability

PACS: 61.30.-v, 61.30.Cz, 61.30.Hn, 64.70.Md, 68.15.+e, 68.60.Dv, 78.67.-n

Contents

Razširjeni povzetek

Uvod

Snovi v naravi obstajajo v treh osnovnih agregatnih stanjih: plinastem, tekočem in trdnem. Pri mnogo snoveh meje med različnimi agregatnimi stanji niso ostre, ampak obstajajo te tudi v vmesnih stanjih. Tekočekristalna faza označuje stanje, v katerem snov teče kot tekočina, vendar ima optične lastnosti podobne kot trdne snovi, saj je delno urejena. Tekočekristalne faze so značilne za snovi, ki jih tvorijo organske molekule močno anizotropnih oblik: paličaste organske verige z dobro definirano dolgo osjo in diskaste molekule, katerih sestavni del je mreža benzenskih obročev. Ureditev molekul v tekočekristalni fazi je lahko odvisna predvsem od temperature — *termotropni tekoči kristali* — ali predvsem od koncentracije tekočekristalne snovi v topilu — *liotropni tekoči kristali*. V doktorskem delu obravnavam prve.

Najpreprostejša tekočekristalna faza je nematska. V njej so molekule v povprečju urejene okrog določene smeri v prostoru, ki ji pravimo *direktor*, težišča molekul pa so enakomerno porazdeljena po prostoru. Za nematske tekoče kristale je značilna cilindrična simetrija, tako da sta smeri direktorja $\hat{n}$ in $-\hat{n}$ enakovredni. Optična os snovi v enoosni nematski fazi sovpada s smerjo direktorja. Pod vplivom zunanjih dejavnikov ali polj se v nematski ureditvi lahko pojavi nova značilna smer, ki jo opiše sekundarni direktor, simetrija pripadajoče ureditve pa je dvoosna. Pri ohlajanju nematskega tekočega kristala lahko ta ali preide v trdno kristalno strukturo ali pa v eno naslednjih, bolj urejenih tekočekristalnih faz [4,5].

Tekoče kristale so prvič opazili, oziroma o njihovem obstoju poročali, že davnega leta 1888 [2]. Botanik Friedrich Reinitzer je pod mikroskopom opazoval taljenje rastlinskega holesterola. Kristal se je stalil v motno tekočino in Reinitzer je pravilno ugotovil, da njena motnost ni posledica nečistosti vzorca, ampak posebnih fizikalnih lastnosti stanja snovi. Moten videz tekočih kristalov je namreč posledica močenga sipanja svetlobe, ki se od sipanja na izotropnih tekočinah razlikuje za kar do 6 velikostnih redov [4,5].

Zanimanje za tekoče kristale se je povečalo v drugi polovici prejšnega stoletja, ko so spoznali, da so tekoči kristali snovi, ki bi se jih dalo s pridom uporabiti v

industriji prikazalnikov. Raziskave so bile najprej vezane na velike vzorce tekočih kristalov, v katerih so površinski efekti zanemarljivi. V njih je red odvisen le od temperature in zunanjih električnih in magnetnih polj. Poleg ravnovesne ureditve snovi v tekočekristalni fazi je vedno več zanimanja deležna tudi dinamika spreminjana ureditve [9–16]. Pri tem se zanimamo za kolektivna gibanja — termične fluktuacije ureditve —, ki imajo vpliv na povprečen makroskopski red. Kolektivne termične fluktuacije so predvsem pomembne, ker so takrat največje, v bližini faznih prehodov. Kasneje so zaradi tehnoloških potreb pa tudi zaradi zanimanja za osnovne fizikalne pojave postali precej bolj zanimivi ograjeni tekoči kristali [8]. V njih so zaradi velikega razmerja površine glede na prostornino sistema vplivi površine na urejenost tekočega kristala nezanemarljivi. Na efektivno interakcijo tekočekristalne snovi z ograjujočo površino vpliva tako interakcija molekul obeh materialov, ki se razlikuje od interakcije med molekulami tekočega kristala, kot tudi manjkajoče število sosedov.

V doktorskem delu predstavljam rezultate svojih raziskav vpliva ograjujoče površine na fluktuacije nematskega ureditvenega parametra. Površina vpliva na fluktuacije neposredno z robnimi pogoji in posredno preko spremenjene povprečne ravnovesne ureditve, ki predstavlja potencial za fluktuacijske načine. Ločim dva primera: (i) sisteme, v katerih je vpliv površine vezan na njeno neposredno bližino [15,24,23], in (ii) sisteme, v katerih površina spremeni ureditev v celotnem tekočekristalnem sistemu [21,23]. V obeh primerih me najbolj zanima pojav mehkih fluktuacijskih načinov, ki jih v neograjenih tekočekristalnih sistemih ne zasledimo. Njihov obstoj pomeni, da je fazni oziroma strukturni prehod zvezen, medtem ko je fazni prehod v neograjenih sistemih nezvezen. Nadalje me zanimajo najznačilnejše opazljivke v ograjenih sistemih, sile, ki jih spremenjena ureditev povzroča med ograjujočimi stenami. Omejim se na strukturne sile, ki so posledica spremenjene povprečne ravnovesne ureditve, psevdo Casimirjeve sile, ki izvirajo v spremenjenem spektru termičnih fluktuacij, in van der Waalsove sile, ki so sicer posledica fluktuacij elektromagnetnega polja, a prav tako zavisijo od nehomogenosti in anizotropije tekočega kristala med stenami [31]. Sile med ograjujočimi stenami lahko merimo z različnimi spektroskopskimi metodami, naprimer z mikroskopom na atomsko silo [67], pri katerem prevzame vlogo ene od sten kar tipalo mikroskopa, ali preko njihovega vpliva na stabilnost tekočekristalnih nanosov, ki imajo eno prosto površino [104,158]. V delu obravnavam slednji primer.

V doktorskem delu najprej pojasnim nekaj osnovnih pojmov, ki jih potrebujem za opis ureditve v tekočem kristalu in za opis termičnih fluktuacij. Sledi definicija in opis določitve sil med ograjujočimi površinami ter komentar vpliva interakcij

v tekočekristalnem nanosu na njegovo stabilnost. Nato se podrobneje posvetim van der Waalsovi sili, kjer sledijo novi rezultati za silo med anizotropnimi sredstvi [31]. Konkretni izračuni vpliva ograjujoče površine na fluktuacije nematskega ureditvenega parametra so vezani na heterofazni sistem nematika v stiku s površino, ki tali red [15,24,23], in na hibridni nematski sistem, v katerem je zaradi nasprotujočih si vplivov ograjujočih površin nematski red močno deformiran [21,23]. V obeh primerih izračunam strukturno silo [29], medtem ko so rezultati za psevdo Casimirjevo silo le navedeni. V heterofaznem sistemu se zaradi nehomogenosti reda v sistemu pojavi dodatna "stena" — fazna meja med izotropno in nematsko fazo. Povprečno ureditev v heterofaznem sistemu renormaliziram glede na van der Waalsovo silo, ki deluje med fazno mejo in mejo med tekočim kristalom in trdno ograjujočo površino. V hibridnem sistemu določim sile v plasti tekočega kristala in študiram njegovo stabilnost napram spinodalnemu razomočenju [30]. Delo zaključim s pregledom opravljenega in izpostavitvijo odprtih vprašanj.

Fenomenološka teorija

Fenomenološka teorija opiše tekoče kristale v bližini faznega prehoda, ko se sistemu nezvezno spremenijo nekateri termodinamski potenciali in zvezno ali nezvezno njegova makroskopska urejenost [38]. Večja urejenost sistema je povezana z zmanjšanjem njegove simetrije. Za opis posameznega sistema je pomembna določitev parametra, ki opiše spremembo ureditve — *ureditveni parameter*. Ta ustreza fizikalni opazljivki, ki se ji vrednost ob faznem prehodu spremeni z nič na vrednost različno od nič. Izhajajoč z mikroskopske porazdelitve molekul predstavlja ureditveni parameter prvi nekonstantni neničelni moment v porazdelitveni funkciji, na makroskopskem nivoju pa se odraža z vplivom na fizikalne količine istega ranga (skalar, vektor, tenzor,...). Pri enoosnem nematskem tekočem kristalu je $f(\theta) = \sum_{n=0}^{\infty} f_n P_n(\cos\theta)$, kjer je θ kot med dolgo osjo molekule in smerjo direktorja. Zaradi cilindrične simetrije ureditve so vsi lihi momenti porazdelitve enaki nič, prvi nekonstantni neničelni moment pa ustreza brezslednemu tenzorju 2. reda

$$\mathsf{Q} = \frac{1}{2} S \left(3\hat{n} \otimes \hat{n} - \mathsf{I}\right), \tag{1}$$

kjer je $S = \langle (3\cos^2\theta - 1)/2 \rangle$ skalarni ureditveni parameter, ki meri stopnjo urejenosti glede na os direktorja [4]. Kadar so vse molekule poravnane vzporedno direktorju, je $S = 1$, ob popolnem neredu — enakomerni porazdelitvi molekul po kotu θ — pa je $S = 0$. Najnižja vrednost skalarnega ureditvenega parametra $S = -1/2$ ustreza molekulam enakomerno porazdeljenim v ravnini pravokotni na direktor. V splošnem je nematski red lahko zaradi zunanjih vplivov deformi-

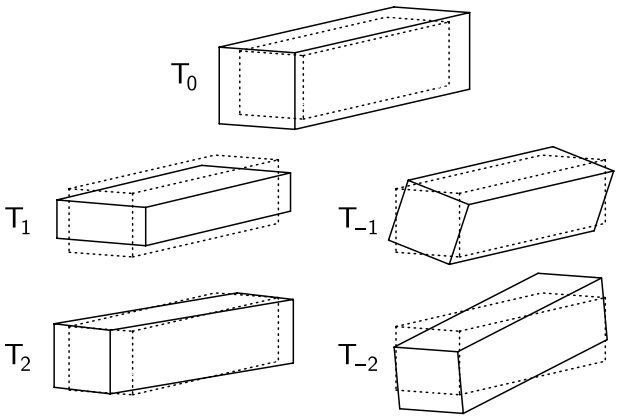

Slika 1 Shematska predstavitev odstopanj od enoosnega reda, ki ustrezajo posameznim amplitudam q_m.

ran. V najsplošnejšem primeru ga opiše 5 neodvisnih parametrov: dva kota, ki določata smer direktorja, skalarni ureditveni parameter glede na direktor, kot sekundarnga direktorja in stopnja dvoosnosti $P = (3/2)\langle \sin^2\theta \cos 2\phi \rangle$, kjer je ϕ kot glede na sekundarni direktor v ravnini pravokotni na direktor, $\mathsf{Q} = \frac{1}{2}S\left(3\hat{n}\otimes\hat{n} - \mathsf{I}\right) + \frac{1}{2}P\left(\hat{e}_1\otimes\hat{e}_1 - \hat{e}_2\otimes\hat{e}_2\right)$. Včasih je smiselnejša parametrizacija ureditvenega parametra glede na bazne tenzorje brezslednega tenzorja 2. reda $\mathsf{Q} = \sum_{i=-2}^{2} q_m \mathsf{T}_m$, kjer so [32,33]

$$\begin{aligned} \mathsf{T}_0 &= \frac{3\hat{n}\otimes\hat{n} - \mathsf{I}}{\sqrt{6}}, \\ \mathsf{T}_1 = \frac{\hat{e}_1\otimes\hat{e}_1 - \hat{e}_2\otimes\hat{e}_2}{\sqrt{2}} &\quad , \quad \mathsf{T}_{-1} = \frac{\hat{e}_1\otimes\hat{e}_2 + \hat{e}_2\otimes\hat{e}_1}{\sqrt{2}}, \\ \mathsf{T}_2 = \frac{\hat{e}_1\otimes\hat{n} + \hat{n}\otimes\hat{e}_1}{\sqrt{2}} &\quad , \quad \mathsf{T}_{-2} = \frac{\hat{e}_2\otimes\hat{n} + \hat{n}\otimes\hat{e}_2}{\sqrt{2}}. \end{aligned} \tag{2}$$

Amplitude v razvoju, q_m, predstavljajo skalarni ureditveni parameter (q_0), stopnjo dvoosnosti ureditve (q_1) in smer sekundarnega direktorja v ravnini, ki jo določata enotska vektorja $\hat{e}_1$ in $\hat{e}_2$, (q_{-1}), ter odstopanja direktorja od smeri $\hat{n}$ v ravnini z vektorjem $\hat{e}_1$ (q_2) ali z vektorjem $\hat{e}_2$ (q_{-2}). Pomen posameznih amplitud je shematsko predstavljen na sliki 1.

Urejenost in s tem simetrija nematske tekočekristalne faze se odraža na simetriji tenzorskih opazljivk. V primeru enosne ureditve se tenzor magnetne susceptibilnosti zapiše kot

$$\underline{\chi} = \frac{2}{3}\chi_a \mathsf{Q} + \chi_i \mathsf{I}, \tag{3}$$

kjer je $\chi_a = \chi_\parallel - \chi_\perp$ anizotopija suscepibilnosti in sta $\chi_\parallel$ ter $\chi_\perp$ susceptibilnosti popolnoma urejenega sistema v smeri direktorja in pravokotno nanj. $\chi_i = (\chi_\parallel + 2\chi_\perp)/3$ je povprečna magnetna susceptibilnost oziroma njen izotropni del.

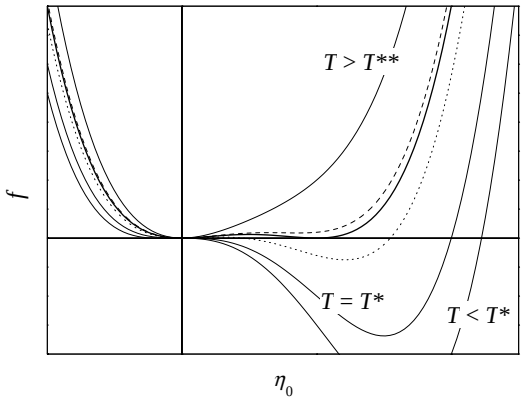

Slika 2 Prosta energija sistema z nezveznim faznim prehodom kot funkcija ureditvenega parametra za različne temperature. Krepko je narisana prosta energija pri temperaturi prehoda, črtkana in pikčasta črta pa ustrezata temperaturam $T_{NI} < T < T^{**}$ oziroma $T^* < T < T_{NI}$.

Do spremembe urejenosti pride pri faznih prehodih. Fenomenološki opis faznih prehodov temelji na definiciji ureditvenega parametra in razvoju proste energije sistema po simetrijsko dovoljenih invariantah ureditvenega parametra [34,38]. Razvoj velja v okolici zveznih faznih prehodov in se ga da uporabiti tudi pri opisu nezveznih prehodov, predvsem šibko nezveznih. Invariante tenzorskega nematskega ureditvenega parametra so potence operatorja sled na tenzorju. V bližini faznega prehoda se gostota proste energije torej zapiše kot

$$f_{hom} = f_{izo} + \frac{1}{2}\tilde{A}\,\mathrm{tr}\,\mathsf{Q}^2 - \frac{1}{3}B\,\mathrm{tr}\,\mathsf{Q}^3 + \frac{1}{4}C(\,\mathrm{tr}\,\mathsf{Q}^2)^2, \tag{4}$$

kjer so $\tilde{A}$, B in C parametri, ki jih določimo fenomenološko. Člen v prvi potenci je identično enak nič, saj je nematski ureditveni parameter brezsleden, kar zagotavlja, da je rešitev $\mathsf{Q} = 0$ ekstrem proste energije. Člen tretjega reda nakazuje, da bo fazni prehod nezvezen, ta potenca pa je simetrijsko dovoljena, ker rešitvi Q in $-\mathsf{Q}$ ustrezata različnim fizikalnim stanjem [enačba (3)]. Kadar člen tretjega reda simetrijsko ni dovoljen, je fazni prehod zvezen. Člen četrtega reda poskrbi za obstoj globalnega minimuma proste energije, višji členi v razvoju pa so zanemarljivi, razen kadar je $C < 0$. Fenomenološki parametri $\tilde{A}$, B in C so v splošnem temperaturno odvisni. Parameter $\tilde{A}$ mora pri T^* menjati predznak, če naj pod to temperaturo izotropna faza ne bo več možna rešitev. $\tilde{A}$ je torej funkcija lihih potenc $(T - T^*)$, ponavadi pa zadošča, da upoštevamo le najnižji člen, $\tilde{A} = A(T - T^*)$. V bližini prehoda lahko privzamemo, da sta parametra B in C konstantna. Za tipične tekoče kristale je $A \sim 10^5$ J/m^{3}K in $B \sim C \sim 10^6$ J/m^3 [4]. Prosta energija sistema z nezveznim faznim prehodom je upodobljena na sliki 2.

V obsežnem tekočem kristalu je povrprečna smer ureditve konstantna in se s

temperaturo spreminja le stopnja urejenosti okrog direktorja. Izotropna faza je stabilna nad temperaturo prehoda $T_{NI} = T^* + B^2/27AC$ in metastabilna v temperaturnem intervalu $T_{NI} > T > T^*$. Ob prehodu sta v ravnovesju izotropna faza in nematska faza s stopnjo urejenosti $S_c = 2B/3\sqrt{6}C \sim 0{,}2 - 0{,}4$. Nematska faza je stabilna pod temperaturo prehoda, ko se stopnja urejenosti spreminja kot $S/S_c = 0{,}75(1 + \sqrt{1 - 8\theta/9})$, kjer je $\theta = (T - T^*)/(T_{NI} - T^*)$, in metastabilna za $T_{NI} < T < T^{**} = T^* + B^2/24AC$ (glej sliko 2). Ob prehodu iz izotropne v nematsko fazo se sprosti latentna toplota $q_l = B^4/729C^3[T_{NI}/(T_{NI} - T^*)] \sim 10^6$ J/m^3 [147]; za primerjavo, latentna toplota ob zmrzovanju vode je $q_l \sim 3 \cdot 10^8$ J/m^3.

Pod vplivom zunanjih polj, največkrat gre za vpliv ograjujočih sten, je povprečna smer nematske ureditve lahko različna v različnih delih sistema. Deformacija ureditvenega parametra zviša prosto energijo. Njen prispevek zapišemo s simetrijsko dovoljenimi gradientnimi členi. V bližini faznega prehoda je deformacija ureditvenega parametra vezana predvsem na krajevno spreminjanje stopnje urejenosti, zato takrat ne pridejo do izraza vsi vidiki elastičnosti sistema in zadošča opis z eno elastično konstanto,

$$f_{el} = \frac{1}{2} L \, \nabla \mathsf{Q} \vdots \nabla \mathsf{Q}, \tag{5}$$

kjer je $L =\sim 10^{-11}$ N do 10^{-10} N [4]. Globoko v nematski fazi, ko je stopnja urejenosti približno konstantna po celotnem vzorcu, so deformacije ureditvenega parametra vezane na elastične deformacije direktorskega polja. Te ponavadi opišemo v okviru Frankove elastične teorije [42], ki razdeli prispevke k prosti energiji na prispevek pahljačne, zvojne in upogibne deformacije.

Spontane deformacije ureditvenega parametra ni, saj ta viša prosto energijo sistema. Seveda pa je ureditveni parameter lahko deformiran zaradi vpliva ograjujočih sten. Na mikroskopskem nivoju so interakcije med nevtralnimi molekulami van der Waalsove interakcije kratkega dosega ($1/r^6$). V fenomenološki teoriji jih zato ponavadi nadomestimo s kontaktnimi interakcijami. V okviru direktorskega opisa nematika opiše sklopitev s površino Rapini–Papoularjev izraz [49], ki sta ga za popolnejši tenzorski opis prilagodila Nobili in Durand [17],

$$f_S = \frac{1}{2} G \, \mathrm{tr} \, (\mathsf{Q} - \mathsf{Q}_{S_i})^2 \delta(z - z_S), \tag{6}$$

kjer je G moč sklopitve s površino, Q_S je tenzorski ureditveni parameter, ki ga vsiljuje ograjujoča površina, ta pa se nahaja pri $z = z_S$. Izraz predstavlja prvi člen v razvoju proste energije zaradi interakcije s površino. Višji členi ponavadi niso potrebni, razen pri opisu temperaturne odvisnosti ekstrapolacijske dolžine. Ta nam pove, ali je energijsko ugodnejša deformacija direktorskega polja, pri čemer je le-to v soglasju z redom, ki ga vsiljuje površina, ali pa je ugodneje kršiti robne pogoje in se pri tem izogniti zvišanju proste energije zaradi deformacije, $\lambda \sim L/G$. Moč vpliva

površine meri razmerje ekstrapolacijske dolžine in tipične dolžinske enote v sistemu: sklopitev s površino je močna, kadar je $\lambda/d \to 0$, in je šibka, če je $\lambda/d \gg 1$.

V nadaljevanju bomo računali z brezdimenzijskimi količinami: ureditveni parameter bomo zapisali glede na stopnjo urejenosti ob prehodu v obsežnem sistemu, $\hat{\mathsf{Q}} = \mathsf{Q}/S_c$, dolžine bomo merili v tipičnih enotah sistema d ($\hat{x}_i = x_i/d$ in $\hat{\nabla} = d\nabla$) ali s korelacijsko dolžino $\xi_{NI} = \zeta d = \sqrt{27CL/B^2} \sim 10$ nm, temperaturo s $\theta = (T - T^*)/(T_{NI} - T^*)$ in prosto energijo v enotah $\tilde{f} = L\xi_{NI}^{-2}(2B^2/27C^2)$. Znak $\widehat{\cdots}$ bomo v nadaljevanju spustili. Brezdimenzijska gostota proste energije je potem

$$f = f_{izo} + \frac{1}{2}\theta \,\mathrm{tr}\,\mathsf{Q}^2 - \sqrt{6}\,\mathrm{tr}\,\mathsf{Q}^3 + \frac{1}{2}(\,\mathrm{tr}\,\mathsf{Q}^2)^2 + \frac{1}{2}\zeta^2 \nabla\mathsf{Q}\vdots\nabla\mathsf{Q}. \tag{7}$$

Površinski prispevek h gostoti proste energije je

$$f_S = \frac{1}{2} g \,\mathrm{tr}\,(\mathsf{Q} - \mathsf{Q}_S)^2 \delta(z - z_S), \tag{8}$$

kjer je $g = (\xi_{NI}^2/Ld)G$ ali $g = (3\xi_{NI}^2/2d)\lambda^{-1}$, če uporabimo zapis z ekstrapolacijsko dolžino.

Korelacijske dolžine fluktuacij

Fenomenološka teorija faznih prehodov se zanima le za povprčno vrednost ureditvenega parametra in pri tem zanemarja krajevna in časovna odstopanja od povprečja. Ta so predvsem pomembna v okolici zveznih faznih prehodov. Tudi v obsežnem sistemu je ureditveni parameter odvisen od kraja, $\eta(\vec{r}) = \eta_0 + \Delta(\vec{r})$, a je $\langle\eta(\vec{r})\rangle = \eta_0$ in torej $\langle\Delta(\vec{r})\rangle = 0$. Tu η označuje vsako od petih prostostnih stopenj nematske ureditve. Vsaj na majhnih področjih so molekule vedno urejene. Pomembno pa je, kako velika so ta področja. Povezanost oziroma korelacijo v urejenosti nam opiše korelacijska funkcija $\Gamma(\vec{r}) = \langle\eta(\vec{r})\eta(0)\rangle - \langle\eta(\vec{r})\rangle\langle\eta(0)\rangle = \langle\Delta(\vec{r})\Delta(0)\rangle$. Razvijemo korelacijsko funkcijo v Fourierovo vrsto po ravnih valovih, ki so v sistemih z zvezno translacijsko simetrijo naravna izbira lastnih funkcij, in dobimo $\Gamma(\vec{r}) = \sum_{\vec{q}} \tilde{\Gamma}(\vec{q})\,\mathrm{e}^{-i\vec{q}\cdot\vec{r}}$, kjer je $\tilde{\Gamma}(\vec{q}) = \langle|\tilde{\Delta}(\vec{q})|^2\rangle$. Amplitude lastnih funkcij $\tilde{\Delta}(\vec{q})$ določimo iz proste energije,

$$\mathcal{F} = \int \mathrm{d}^3 r\; f = \mathcal{F}_0 + \frac{\mathcal{V}}{2}\sum_{\vec{q}} \left(\frac{\partial^2 f}{\partial\eta^2} + Lq^2\right)|\tilde{\Delta}(\vec{q})|^2 + \mathcal{O}(|\tilde{\Delta}(\vec{q})|^3), \tag{9}$$

s pomočjo ekviparticijskega teorema, $\tilde{\Gamma}(\vec{q}) = k_B T/\mathcal{V}(L\xi^{-2} + Lq^2)$, kjer je $\xi = \sqrt{L/(\partial^2 f/\partial\eta^2)}$ korelacijska dolžina danega fluktuacijskega načina. V direktnem prostoru dobimo namreč $\Gamma(\vec{r}) = \frac{k_B T}{4\pi L r}\,\mathrm{e}^{-r/\xi}$. Kadar je korelacijska dolžina končna, pojema korelacija urejenosti z eksponentom razdalje in fluktuacije niso pomembne. V primeru neskončne korelacijske dolžine je korelacija dolgega dosega in pojema obratno sorazmerno z razdaljo.

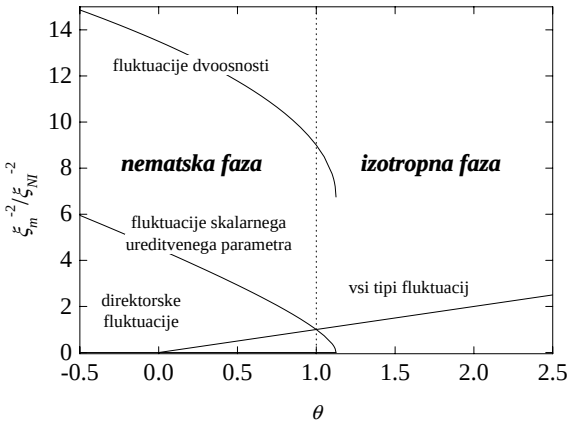

Slika 3 Temperaturna odvisnost korelacijskih dolžin petih prostostnih stopenj nematskega reda v (meta)stabilni izotropni in enoosni nematski fazi.

Izpišimo zdaj korelacijske dolžine posameznih prostostnih stopenj enoosne nematske ureditve, ki jo opiše ureditveni parameter $\mathsf{Q} = a_0\mathsf{T}_0$,

$$\begin{aligned} \xi_0^{-2}/\xi_{NI}^{-2} &= \theta - 6a_0 + 6a_0^2, \\ \xi_{\pm1}^{-2}/\xi_{NI}^{-2} &= \theta + 6a_0 + 2a_0^2, \\ \xi_{\pm2}^{-2}/\xi_{NI}^{-2} &= \theta + 3a_0 + 2a_0^2. \end{aligned} \tag{10}$$

V izotropni fazi so ravnovesne vrednosti vseh parametrom q_m enake 0, tako da so korelacijske dolžine vseh fluktuacijskih načinov enake, $\xi_I^{-2}/\xi_{NI}^{-2} = \theta$. V nematski fazi se korelacijske dolžine posameznih fluktuacijskih načinov s temperaturo spreminjajo kot kaže slika 3. Ob prehodu iz izotropne v nematsko fazo ali ob prehodu v nasprotni smeri ostajajo korelacijske dolžine vseh fluktuacijskih načinov končne, kar je še ena značilnost nezveznih faznih prehodov. Zato pa korelacijska dolžina ξ_I divergira na meji stabilnosti izotropne faze ($\theta = 0$ oziroma pri T^*), korelacijska dolžina stopnje urejenosti nematske faze $\xi_{N,0}$ pa divergira pri najvišji temperaturi pregrete nematske faze ($\theta = 9/8$ oziroma pri T^{**}). V bližini faznega prehoda je $\xi_{N,0}^{-2}/\xi_{NI}^{-2} \approx 6 - 5\theta$ in $\xi_{N,\pm1}^{-2}/\xi_{NI}^{-2} \approx 18 - 9\theta$, korelacijska dolžina direktorskih fluktuacij pa je neskončna na celotnem območju nematske faze.

Dinamika ureditvenega parametra

Termodinamsko ravnovesje sistema je določeno z minimumom njegove proste energije, $\mathcal{F} = \int \mathrm{d}\mathcal{V} f$. V okviru fenomenološke teorije štejemo v prosto energijo le prispevke povprečnega makroskopskega reda, ki se krajevno spreminja kvečjemu na razdaljah večjih od nekaj tipičnih dolžin molekul. Z minimizacijo dobimo Euler–Lagrangeve enačbe

$$\frac{\delta f}{\delta \mathsf{Q}} = 0, \tag{11}$$

kjer je funkcionalni odvod $\delta/\delta\mathsf{Q} = \partial/\partial\mathsf{Q} - \nabla\cdot(\partial/\partial\nabla\mathsf{Q})$ in k f prispevajo volumski členi v prosti energiji. Površinski členi določajo robne pogoje.

Zdaj pa si predstavljajmo sistem, ki ga malo izmaknemo iz ravnovesja. Takrat je $\delta f/\delta\mathsf{Q}$ različen od 0 in predstavlja generalizirano silo, ki vleče sistem nazaj v ravnovesje. Približevanje ravnovesju je proces, pri katerem se zgublja energija. Opišemo ga z viskozno silo, ki je po analogiji z viskozno silo v mehaniki sorazmerna s hitrostjo, tokrat s hitrostjo spreminjanja ureditvenega parametra [7,54,52],

$$\frac{\delta f}{\delta \mathsf{Q}} = -\gamma^{-1}\frac{\partial \mathsf{Q}}{\partial t}, \tag{12}$$

kjer je γ^{-1} posplošeni viskozni koeficient. V primeru nematskega tekočega kristala, ko je ureditveni parameter tenzor drugega reda, je posplošeni viskozni koeficient tenzor 3. reda. V obravnavi ga nadomestim z izotropnim tenzorjem in s tem s skalarnim koeficientom. V brezdimenzijski obliki določa generalizirana viskoznost tipični čas za reorientacije direktorja, $\tau_a = 27C\gamma^{-1}/B^2 \sim 10^{-8}$ s [32,4]. Enačba (12) je znana kot Landau–Halatnikova enačba ali Ginzburg–Landauov časovno odvisni model, ki sta ga leta 1954 prva predlagala Landau in Halatnikov [7]. Do istega rezultata pridemo s striktno obravnavo disipativnega anizotropnega sistema z zanemaritvijo makroskopskih masnih tokov [52,53].

Časovno spreminjanje fluktuacijskih načinov opiše v tem najpreprostejšem relaksacijskem opisu eksponentno pojemanje, $b_i \propto \mathrm{e}^{-\mu_i t}$, kjer je $\mathsf{Q}(\vec{r},t) = \mathsf{A}(\vec{r}) + \mathsf{B}(\vec{r},t)$, $\|\mathsf{B}\| \ll \|\mathsf{A}\|$, in je μ_i relaksacijska hitrost danega fluktuacijskega načina. V primeru homogenega nematika je $\mu_i \propto (\xi_i^{-2} + q^2)$. Korelacijska dolžina fluktuacij ne predstavlja torej le velikosti otočkov določenega reda, ampak je tudi v zvezi s hitrostjo relaksacije vzbujenega stanja. Relaksacija je tem počasnejša in posledično vzbujeno stanje tem bolj trdoživo, čimvečja je njegova korelacijska dolžina. Ločimo dva posebna primera glede na obnašanje disperzijske relacije za dolgovalovne deformacije $\vec{q} \to 0$ (v končnem sistemu si mislimo limito zvezne funkcije, ki bi v ustreznih diskretnih vrednostih ustrezala naši funkciji). Relaksacijska hitrost **mehkega fluktuacijskega načina** pade od prehodu v limiti $\vec{q} \to 0$ na 0, medtem ko je stran od prehoda različna od nič. Za **Goldstoneov fluktuacijski način** pa je značilno, da je njegova relaksacijska hitrost enaka 0 na celotnem območju urejene faze. Omenimo še, da je Goldstoneov fluktuacijski način posledica zlomljene rotacijske simetrije izotropne faze [36,37]. Goldstoneove fluktuacije v nematskem tekočem kristalu so direktorske fluktuacije. Te so odgovorne za močno sipanje svetlobe na nematikih, o čemer smo govorili v uvodu. Mehkih fluktuacijskih načinov v neograjenih nematikih ni, saj spremljajo zvezne fazne prehode, lahko pa se pojavi zaradi vpliva površin.

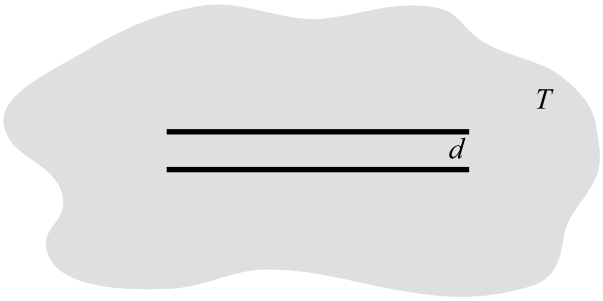

Slika 4 Shema ograjenega tekočekristalnega sistema za študij sil: pri spremembi razmika med ograjujočima stenama se prostornina in površina tekočega kristala ne spremenita.

Strukturna in psevdo Casimirjeva sila

Zaključimo predstavitev fenomenološke teorije opisa faznega prehoda pri tekočih kristalih s predstavitvijo sil, ki delujejo na tanko plast nematika, kadar je ta v stiku s stenami. Zaradi prisotnosti sten se spremeni tako povprečna ravnovesna ureditev v tekočem kristalu, kot tudi spekter fluktuacij. Spremenjeni ureditvi ustreza drugačna prosta energija, kot enaki prostornini neograjenega tekočega kristala (glej sliko 4). V splošnem je prirastek proste energije odvisen od razdalje med stenama, zaradi česar se steni ali privlačita ali odbijata. Termodinamska definicija sile je

$$\vec{F} = -\left(\frac{\partial \mathcal{F}}{\partial \vec{r}}\right)_{\mathcal{V},\mathcal{A}}. \tag{13}$$

Strukturna sila imenujemo del sile, ki izhaja iz spremenjenega povprečnega ravnovesnega reda, $F = -\partial\Delta\mathcal{F}_{MF}/\partial d = -\partial\mathcal{F}_{MF}/\partial d + f_{neo}\mathcal{A}$, kjer je $\mathcal{F}_{MF}$ prosta energija sistema v okviru fenomenološke teorije povprečnega polja, enaki prostornini neograjenega tekočega kristala pa znotraj iste teorije ustreza prosta energija $f_{neo}\mathcal{A}$.

Psevdo Casimirjeva sila izhaja iz spremenjene proste energije fluktuacij. To določa fazni integral po vseh možnih konfiguracijah fluktuirajočih polj [54,38],

$$\mathcal{F}_{CAS} = -k_B T \ln\left(\int \mathcal{D}b\, \mathrm{e}^{-\mathcal{H}[b]/k_B T}\right), \tag{14}$$

kjer je k_B Boltzmannova konstanta in T temperatura. $\mathcal{H}[b] = L/2\{\int[\xi^{-2}b^2 + (\nabla b)^2]\mathrm{d}\mathcal{V} + \sum_i \lambda_i^{-1}\int b^2 \mathrm{d}\mathcal{A}\}$ je Hamiltonian za fluktuacije v harmonskem približku. Izračun proste energije fluktuacij je ponavadi precej zapleten, predvsem pa moti njena divergenca, ki za odpravo katere je razvitih več metod [155]. Za občutek povejmo nekaj o splošnih lastnosti psevdo Casimirjeve sile, ki temeljijo na robnih pogojih za fluktuacije. V primeru močne sklopitve s stenami, $\lambda_{1,2} \ll d$, ali šibke sklopitve, $\lambda_{1,2} \gg d$, je psevdo Casimirjeva interakcija med stenami privlačna. Nasprotno

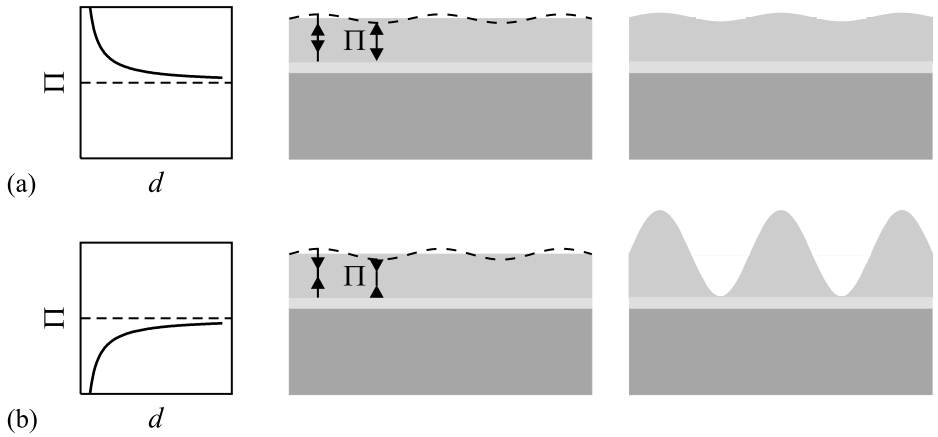

Slika 5 Shematski prikaz (a) oslabitve kapilarnih valov v primeru odbojne sile na plast tekočega kristala in (b) ojačitve kapilarnih valov.

je interakcija v primeru mešanih robnih pogojev, torej šibke sklopitve z eno steno in močne z drugo, odbojna [27,63,64].

Študiju strukturnih in psevdo Casimirjevih sil se v delu posvečam zaradi študija stabilnosti tankih tekočekristalnih plasti. Plast tekočega kristala je v stiku s trdno steno, eno površino pa ima prosto, v stiku z zrakom. Zaradi termičnih fluktuacij prosta površina ni ravna, ampak so na njej vzbujeni kapilarni valovi, ki povzročijo, da se debelina filma s krajem spreminja. Na plast zaradi njene strukture, termičnih fluktuacij ureditvenih in elektromagnetnih polj, deluje skupna sila, odvisna od debeline filma, $\Pi(d)$. (Tudi, kadar bomo govorili o sili, bomo v resnici mislili silo na enoto površine, torej na dodatni tlak v plasti.) Ko se debelina filma veča, se mora velikost sil, ki delujejo nanj, zmanjševati. Slednje ne velja le pri debelinah, ko se spreminja značaj sile iz odbojne v privlačno ali obratno. Za zdaj imejmo v mislih le monotono padajoče odbojne sile in monotono rastoče privlačne sile, splošni izrazi pa bodo veljali tudi za prevojna območja. Če torej deluje na plast odbojna sila, bo odboj v stanjšanih delih večji kot odboj v odebeljenih delih in bo sila povzročila zmanjšanje razlik v debelini. Nasprotno bo večji privlak v tanjših delih in manjši privlak v debelejših povzročil še dodatno povečanje razlik v debelini, dokler se ne bo na stanjšanem delu prosta površina dotaknila trdne podlage in se bo film razgradil v kapljice tekočega kristala in suha področja. Opisanemu mehanizmu razomočenja trdne podlage preko ojačitve kapilarnih valov pravimo *spinodalno razomočenje*; shematsko je predstavljen na sliki 5. Razmišljanje lahko posploĭmo v pravilo: film je stabilen napram spinodalnemu razomočenju, če je v okolici povprečne debeline filma sila padajoča funkcija debeline ($\Pi'(d) < 0$), medtem ko je v nasprotnem primeru ($\Pi'(d) > 0$) film nestabilen. Povedano zapišemo formalno z relaksacijskim časom za

kapilarne valove [73,74],

$$\frac{1}{\tau_q} = \frac{d_0^3}{3\eta}\left[\gamma q^4 - q^2\Pi'(d_0)\right], \tag{15}$$

ki je pozitiven — in s tem zagotavlja eksponentno pojemanje vzbujenih stanj — za poljuben val, če je $\Pi' < 0$, oziroma postane negativen za določene vrednosti valovnega vektorja $\vec{q}$ za $\Pi' > 0$; takrat se dani val ojači.

Van der Waalsova sila

Van der Waalsova sila med dvema nevtralnima molekulama združuje disperzijsko interakcijo med fluktuirajočimi dipoli, ki nastanejo zaradi trenutne prerazporeditve elektronov v molekulah, in orientacijsko interakcijo med fluktuirajočimi stalnimi dipoli. Pripadajoča energija pada z razdaljo kot $1/r^6$, pri velikih oddaljenostih med molekulama pa se disperzijski prispevek zmanjša (za velike razdalje se približuje odvisnosti $1/r^7$ [91,68]). Zmanjšanje disperzijske interakcijske energije je posledica končne hitrosti svetlobe — ko postane čas, ki ga elektromagnetno polje vzbujenega dipola potrebuje, da doseže drugo molekulo primerljiv tipičnemu življenskemu času danega vzbujenega stanja, se zgublja fazna povezava med interagirajočima molekulama. Pojav imenujemo *retardacija*.

Kadar interagirajo med seboj molekule, ki tvorijo makroskopska telesa, radi prevedemo mikroskopske interakcije na makroskopske. Najenostavnejši način je, da kar seštejemo dvodelčne interakcije med vsemi pari molekul, kot da bi bili izolirani. Za ravninsko geometrijo pada energija pripadajoče interakcije v približku brez upoštevanja retardacije kot $1/d^2$ (v limiti močne retardacije $1/d^3$). V trdnih snoveh je gostota molekul precej večja, da bi upravičila približek "idealnega plina". Molekule vplivajo druga na drugo, kar bi morali upoštevati z večdelčnimi interakcijami. Na mezoskopskih in makroskopskih razdaljah lahko pozabimo na "zrnatost" snovi in jo obravnavamo kot kontinuum. V tem približku lahko o van der Waalsovi interakciji med makroskopskimi telesi govorimo v smislu spremembe proste energije sistema, ker smo telesi iz neskončne oddaljenosti približali na končno razdaljo. S tem smo spremenili spekter in pripadajočo prosto energijo elektromagnetnega valovanja v dielektrični snovi. Spremenjeni fluktuacijski načini v splošnem zavisijo od razdalje med telesoma, kar vodi do privlaka ali odboja med njima.

Z opisom van der Waalsove sile med makroskopskimi telesi se je na nivoju opisa idealnega plina prvi ukvarjal Hamaker [92]. Kasneje je Lifshitz opis za trdna telesa popravil s kontinuumskim opisom [93], na nivoju kvantne teorije polja pa so se z njim ukvarjali Dzyaloshinskii in sodelavci [94,95]. Vsi opisi so vezani na izotropna makroskoska telesa. Kihara in Honda sta v 60-ih letih predstavila van der Waalsovo silo med optično enoosnimi telesi, vendar rezultata nista komentirala. Tako se še

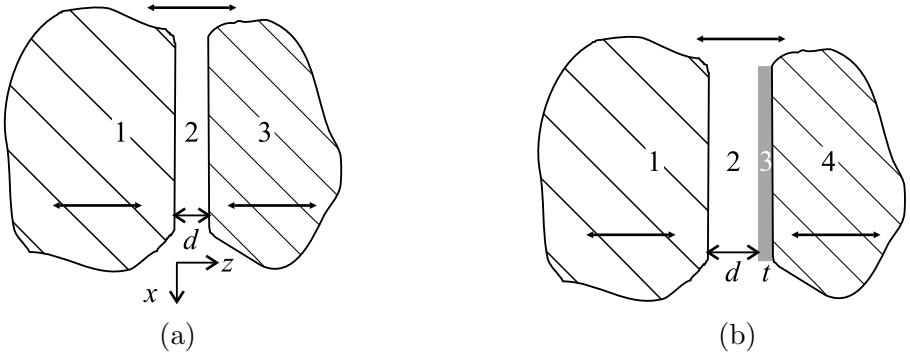

Slika 6 Shema sistema, v katerem študiram van der Waalsovo silo: (a) dve polneskončni makroskopski telesi, ki ju ločuje plast tretje snovi z debelino d; (b) pogosto je na trdni podlagi še dodatna plast oksida, vode,... z debelino t. Puščice označujejo smer optičnih osi.

vedno tudi za opis van der Waalsove sile med močno anizotropnimi sredstvi uporabljajo izrazi za izotropna sredstva. Eden od razlogov za to, je poleg neznanosti izraza za enoosna sredstva tudi to, da za silo med izotropnimi sredstvi obstajajo poenostavljeni izrazi za izračun sile [89] za anizotropna sredstva pa ne.

Ker je v tekočih kristalih dielektrična in optična anizotropija precej velika, sem se lotila študija van der Waalsove sile med optično anizotropnimi sredstvi. Omejila sem se na edino geometrijo in simetrijo sistema, ki nas privede do končnega analitičnega rezultata za van der Waalsovo silo: dve polneskončni makroskopski telesi, med katerima je ravninska plast tretje snovi. Telesa so v splošnem optično enoosna, optične osi pa so v vseh snoveh pravokotne na mejne površine, tako da je tudi simetrija celotnega sistema enoosna. Shema študiranega sistema je predstavljena na sliki 6. Čeprav se morda zdi, da smo za študiran sistem postavili preveč omejitev, da bi lahko govorili o kakšnih splošnejših vplivih dielektrične anizotropije na van der Waalsovo silo, pa ne smemo pozabiti, da je to edini sistem, glede katerega lahko kaj povemo, poleg tega pa opiše tudi precej tekočekristalnih sistemov, ki jih opisujem v tem delu, pa tudi sistemov, ki so sicer predmet raziskav [77–85].

Van der Waalsova interakcija je posledica spremenjenih elektromagnetnih fluktuacijskih načinov. Te določajo Maxwellove enačbe. V enoosnem sistemu, ki ga študiram, lahko elektromagnetne fluktuacijske načine razdelimo na transverzalne magnetne (TM) in transverzalne električne (TE). Načini v polneskončnih sredstvih eksponentno pojemajo z vdorno globino

$$\bar{\rho}_{TM}(\omega) = \left[\frac{\epsilon_\perp}{\epsilon_\parallel}\left(\kappa^2 - \frac{\omega^2}{c^2}\epsilon_\parallel\right)\right]^{1/2},$$
$$\rho_{TE}(\omega) = \left(\kappa^2 - \frac{\omega^2}{c^2}\epsilon_\perp\right)^{1/2}, \qquad (16)$$

kjer je κ valovni vektor v ravnini meje med sredstvoma. Z upoštevanjem robnih pogojev na meji sredstev, dobimo sekularno enačbo, katere rešitve so frekvence elektromagnetnih fluktuacijskih načinov. Te določajo prosto energijo sistema,

$$\Delta\mathcal{F} = k_B T \sum_{\vec{\kappa}} \left[\sum_i \ln\left(2\sinh\tfrac{\hbar\omega_i}{2k_BT}\right) - \sum_{i'} \ln\left(2\sinh\tfrac{\hbar\omega_{i'}}{2k_BT}\right)\right], \tag{17}$$

kjer teče vsota i po frekvencah v sistemu s končno razdaljo med polneskončnima makroskopskima telesoma d, vsota i' pa po frekvencah sistema $d \to \infty$, ko je celoten prostor napolnjen samo z vmesno snovjo. Sekularne enačbe nam ni treba eksplicitno rešiti, ker lahko vsote v enačbi (17) prevedemo z integracijo po kompleksni ravnini [102,100] na

$$\Delta\mathcal{F} = \frac{k_B T \mathcal{A}}{2\pi} \int_0^\infty \mathrm{d}\kappa\kappa \sum_{n=-\infty}^{\infty} \ln\frac{D(i\xi_n)}{D_0(i\xi_n)}, \tag{18}$$

kjer je $\mathcal{A}$ površina mejnih ploskev, $D(\omega) = 0$ sekularna enačba za sestavljen sistem in $D_0(\omega) = 0$ sekularna enačba za homogen sistem vmesne snovi; $\xi_n = 2\pi k_B T n/\hbar$. Silo, ki izhaja iz povečanja proste energije zaradi prisotnosti sten, zračunamo po enačbi (13).

V triplastnem sistemu [glej sliko 6 (a)] je

$$D^R_{TM}(\omega) = 1 + \bar{\Delta}^R_{12}(\omega)\bar{\Delta}^R_{23}(\omega)\mathrm{e}^{-2\bar{\rho}_2(\omega)d} = 0, \tag{19}$$

kjer je

$$\bar{\Delta}^R_{ij}(\omega) = \frac{\epsilon_{i\perp}(\omega)\bar{\rho}_j(\omega) - \epsilon_{j\perp}(\omega)\bar{\rho}_i(\omega)}{\epsilon_{i\perp}(\omega)\bar{\rho}_j(\omega) + \epsilon_{j\perp}(\omega)\bar{\rho}_i(\omega)}, \tag{20}$$

in

$$D^R_{TE}(\omega) = 1 + \Delta^R_{12}(\omega)\Delta^R_{23}(\omega)\mathrm{e}^{-2\rho_2(\omega)d} = 0, \tag{21}$$

kjer je

$$\Delta^R_{ij}(\omega) = \frac{\rho_i(\omega) - \rho_j(\omega)}{\rho_i(\omega) + \rho_j(\omega)}. \tag{22}$$

Za izračun van der Waalsove sile moramo poznati še funkcijsko odvisnost dielektrične konstante od frekvence. Dielektrična konstanta je povezana s polarizabilnostjo molekul α kot $\epsilon = 1 + n\alpha/\epsilon_0$, kjer je n gostota molekul. K polarizabilnosti molekule prispeva več mehanizmov: reorientacija permanentnih dipolov, reorientacija ionov in deformacija elektronskega oblaka. Permenentni dipoli sledijo zunanjemu polju le pri zelo nizkih frekvencah, meja za reorientacijo ionov je v infrardečem območju, pri frekvencah v območju vidne svetlobe pa zunanjemu polju sledi le še elektronski oblak, ki se deformira zaradi skokov elektronov v vzbujena stanja. Pri izračunu van der Waalsove sile je pomembna vrednost statične dielektrične konstante, $\epsilon(0)$, in pa

konstante pri $\omega = in\xi_1$. Ker je $\xi_1 = 2{,}5\cdot 10^{14}\ \mathrm{s}^{-1}$ v območju, kjer je polarizabilnost le še posledica elektronskih prehodov, vzamemo za $\epsilon(i\xi_n) = 1 + \frac{n^2-1}{1+\xi_n^2/\omega_e^2}$. Privzeli smo, da je v snovi en tipičen elektronski prehod, ki je v vseh snoveh (približno) enak; $\omega_e \sim 2\pi\cdot 3\cdot 10^{15}\mathrm{s}^{-1}$ [89]. Zdaj lahko izračunamo van der Waalsovo silo

$$\begin{aligned}\Pi(d,T) &= \frac{k_BT}{16\pi d^3}\frac{\epsilon_{2_\parallel}(0)}{\epsilon_{2_\perp}(0)}\int_0^\infty \mathrm{d}x\ x^2\frac{\bar\Delta_{12}\bar\Delta_{23}\,\mathrm{e}^{-x}}{1+\Delta_{12}\Delta_{23}\,\mathrm{e}^{-x}} \\ &+\frac{k_BT}{\pi d^3}\sum_{n=1}^{\infty}{}'\tilde d^3\int_1^\infty \mathrm{d}p\ p^2\left(\frac{\Delta_{12}^R\Delta_{23}^R\,\mathrm{e}^{-2p\tilde d}}{1+\Delta_{12}^R\Delta_{23}^R\,\mathrm{e}^{-2p\tilde d}}+\frac{\epsilon_{2_\parallel}}{\epsilon_{2_\perp}}\frac{\bar\Delta_{12}^R\bar\Delta_{23}^R\,\mathrm{e}^{-2p\tilde d}}{1+\bar\Delta_{12}^R\bar\Delta_{23}^R\,\mathrm{e}^{-2p\tilde d}}\right),\end{aligned} \tag{23}$$

kjer smo upoštevali, da je ϵ soda funkcija argumenta. Prvi člen v izrazu predstavlja statičen odziv sistema, oziroma prispevek stalnih dipolov, medtem ko je drugi člen posledica dinamičnega odziva. Funkcije $\bar\Delta_{ij} = \bar\Delta_{ij}(0)$, $\Delta_{ij}^R = \Delta_{ij}^R(i\xi_n)$ in $\bar\Delta_{ij}^R = \bar\Delta_{ij}^R(i\xi_n)$ so določene v enačbah (20) in (22); $\tilde d = d\sqrt{\epsilon_{2_\perp}}\xi_n/c$. V enačbi (23) smo integracijo po valovnem vektorju κ nadomestili z integracijo po brezdimenzijskem parametru $p = \rho_2(\kappa)c/(\xi_n\sqrt{\epsilon_{2_\perp}})$, tako da so

$$\begin{aligned}\bar\Delta_{ij} &= \frac{\bar\epsilon_i-\bar\epsilon_j}{\bar\epsilon_i+\bar\epsilon_j} \quad , \quad \bar\epsilon_i = \sqrt{\epsilon_{i_\parallel}\epsilon_{i_\perp}}, \\ \Delta_{ij}^R &= \frac{s_i-s_j}{s_i+s_j} \quad , \quad s_i = \sqrt{p^2-1+\epsilon_{i_\perp}/\epsilon_{2_\perp}}, \\ \bar\Delta_{ij}^R &= \frac{\bar\epsilon_i\bar s_j-\bar\epsilon_j\bar s_i}{\bar\epsilon_i\bar s_j+\bar\epsilon_j\bar s_i} \quad , \quad \bar s_i = \sqrt{p^2-1+\epsilon_{i_\parallel}/\epsilon_{2_\parallel}},\end{aligned} \tag{24}$$

in $\epsilon_i = \epsilon_i(i\xi_n)$, če ni navedeno drugače. Enoosnost zunanjih polneskončnih makroskopskih teles renormalizira dielektrično konstanto, $\epsilon_i \to \sqrt{\epsilon_{i_\parallel}\epsilon_{i_\perp}}$. Po drugi strani enoosnost snovi, ki je vrinjena med makroskopski telesi ne renormalizira le dielektrične konstante, ampak tudi samo moč interakcije.

Izračun van der Waalsove sile iz izraza v enačbi (24) je precej zamuden, odvisnost sile od parametrov snovi pa precej nejasna. Izraz se poenostavi v neretardiranem približku, $c \to \infty$. Približek velja dobro za majhen razmik med makroskopskima telesoma ($d \lesssim \lambda_e = 2\pi c/\omega_e \sim 100$ nm). Pri večjih razdaljah ne dobimo pričakovanega zmanjšanja dosega sile. Velikokrat nas natančna odvisnost od razmika med telesoma niti ne zanima, saj je v sistemu ena od sil dominantna, druge pa predstavljajo le popravek. Dominantna je lahko van der Waalsova sila ali pa morebitne elektrostatične sile ali druge. V tem primeru je pomemben predvsem značaj sile (odbojna ali privlačna) in njena velikost. Vse te podatke nam v zadostni natančnosti nudi tudi približek brez retardacije. V približku brez retardacije je $\Pi = -A/6\pi d^3$, kjer je

$$A = -\frac{3k_BT}{4}\sum_{n=0}^{\infty}{}'\frac{\epsilon_{2_\parallel}(i\xi_n)}{\epsilon_{2_\perp}(i\xi_n)}\int_0^\infty \mathrm{d}x\ x^2\frac{\bar\Delta_{12}(i\xi_n)\bar\Delta_{23}(i\xi_n)\mathrm{e}^{-x}}{1+\bar\Delta_{12}(i\xi_n)\bar\Delta_{23}(i\xi_n)\mathrm{e}^{-x}}, \tag{25}$$

Hamakerjeva konstanta. Črtica nad vsoto označuje, da moramo člen z $n = 0$ množiti z 1/2; funkcijo $\bar{\Delta}_{ij} = \bar{\Delta}_{ij}(i\xi_n)$ smo definirali v enačbi (24). Integral v enačbi (25) je analitično izračunljiv, vsoto po n pa izvedemo z nekaj nadaljnimi približki: upoštevamo, da je $|\bar{\Delta}_{ij}| \ll 1$, zato zanemarimo člene višjega reda kot $\bar{\Delta}_{12}\bar{\Delta}_{23}$. Pri sobni temperaturi je $\xi_1/\omega_e = (k_BT/\hbar c)\lambda_e \sim 1/80 \ll 1$, zato lahko vsoto po n nadomestimo z integralom po ξ. Upoštevamo še, da je $\bar{\Delta}_{ij}(i\xi) \approx \frac{\bar{n}_i^2-\bar{n}_j^2}{\bar{n}_i^2+\bar{n}_j^2+2\xi^2/\omega_e^2}$, kjer smo zanemarili člene tipa $[(\Delta n_i/n_{i_\parallel})^2 \pm (\Delta n_j/n_{j_\parallel})^2](\xi/\omega_e)^2$ in višjih redov v $(\Delta n_i/n_{i_\parallel})$ in (ξ/ω_e). Tu je $\Delta n_i = n_{i_\parallel} - n_{i_\perp}$ in ima v primeru tekočih kristalov vrednost do $10\% \cdot n_{i_\parallel}$. Tako dobimo končni izraz za Hamakerjevo konstanto za enoosna sredstva

$$\begin{aligned} A \;=\; A^{\nu=0} + A^{\nu>0} &= \frac{3}{4}k_BT\frac{\epsilon_{2_\parallel}}{\epsilon_{2_\perp}}\frac{\bar{\epsilon}_1-\bar{\epsilon}_2}{\bar{\epsilon}_1+\bar{\epsilon}_2}\frac{\bar{\epsilon}_3-\bar{\epsilon}_2}{\bar{\epsilon}_3+\bar{\epsilon}_2} \\ &+ \frac{3\hbar\omega_e}{8\sqrt{2}}(\bar{n}_1^2-\bar{n}_2^2)(\bar{n}_3^2-\bar{n}_2^2)\left[\frac{\sqrt{2}(n_{2_\parallel}^2-n_{2_\perp}^2)}{n_{2_\perp}(2n_{2_\perp}^2-\bar{n}_1^2-\bar{n}_2^2)(2n_{2_\perp}^2-\bar{n}_3^2-\bar{n}_2^2)}\right. \\ &\left. - \frac{2n_{2_\parallel}^2-\bar{n}_1^2-\bar{n}_2^2}{\sqrt{\bar{n}_1^2+\bar{n}_2^2}(2n_{2_\perp}^2-\bar{n}_1^2-\bar{n}_2^2)(\bar{n}_1^2-\bar{n}_3^2)} + \frac{2n_{2_\parallel}^2-\bar{n}_3^2-\bar{n}_2^2}{\sqrt{\bar{n}_3^2+\bar{n}_2^2}(2n_{2_\perp}^2-\bar{n}_3^2-\bar{n}_2^2)(\bar{n}_1^2-\bar{n}_3^2)}\right], \end{aligned} \tag{26}$$

kjer je $\bar{a}_i = \sqrt{a_{i_\parallel}a_{i_\perp}}$ in je a ali statična dielektrična konstanta ϵ ali lomni količnik v področju vidne svetlobe n. Prvi člen v enačbi (26), $A^{\nu=0}$, ponovno predstavlja statični odziv sistema, drugi člen, $A^{\nu>0}$, pa ustreza dinamičnemu odzivu.

Kot že pri splošnem izrazu, je tudi zdaj jasno razvidno, da anizotropija okolnih sredstev le renormalizira dielektrično konstanto in lomni količnik, medtem ko je vloga vmesnega sredstva večja. V primeru, da bi bila vsa tri sredstva izotropna, se izraz v enačbi (26) poenostavi v znan izraz [89]

$$\begin{aligned} A \;=\; &\frac{3}{4}k_BT\frac{\epsilon_{2_\parallel}}{\epsilon_{2_\perp}}\frac{(\bar{\epsilon}_1-\bar{\epsilon}_2)^2}{(\bar{\epsilon}_1+\bar{\epsilon}_2)^2} + \frac{3\hbar\omega_e}{8\sqrt{2}}(\bar{n}_1^2-\bar{n}_2^2)^2 \\ &\times\left[\frac{\sqrt{2}(n_{2_\parallel}^2-n_{2_\perp}^2)}{n_{2_\perp}(2n_{2_\perp}^2-\bar{n}_1^2-\bar{n}_2^2)^2} + \frac{(\bar{n}_1^2+\bar{n}_2^2)^2+4\bar{n}_2^4-2(\bar{n}_1^2+\bar{n}_2^2)(3n_{2_\parallel}^2-n_{2_\perp}^2)}{2(\bar{n}_1^2+\bar{n}_2^2)^{3/2}(2n_{2_\perp}^2-\bar{n}_1^2-\bar{n}_2^2)^2}\right]. \end{aligned} \tag{27}$$

Značaj van der Waalsove interakcije je odvisen od medsebojne relacije med statičnimi dielektričnimi konstantami in lomnimi količniki interagirajočih snovi. Znak statične Hamakerjeve konstante je določen z relacijami med statičnimi dielektričnimi konstantami: za $\bar{\epsilon}_2 < \bar{\epsilon}_1, \bar{\epsilon}_3$ ali $\bar{\epsilon}_2 > \bar{\epsilon}_1, \bar{\epsilon}_3$ je konstanta pozitivna zato je statični del van der Waalsove interakcije privlačen, za $\bar{\epsilon}_1 < \bar{\epsilon}_2 < \bar{\epsilon}_3$ ali $\bar{\epsilon}_1 > \bar{\epsilon}_2 > \bar{\epsilon}_3$ je konstanta negativna in ustrezni del van der Waalsove interakcije odbojen. Podobni pogoji veljajo za dinamičen del Hamakerjeve konstante. Izkaže se, da je del izraza (26) v oglatih oklepajih pozitivno definiten in je torej znak konstante določen z znakom produkta $(\bar{n}_1^2-\bar{n}_2^2)(\bar{n}_3^2-\bar{n}_2^2)$. Za $\bar{n}_2 < \bar{n}_1, \bar{n}_3$ ali $\bar{n}_2 > \bar{n}_1, \bar{n}_3$ je dinamični

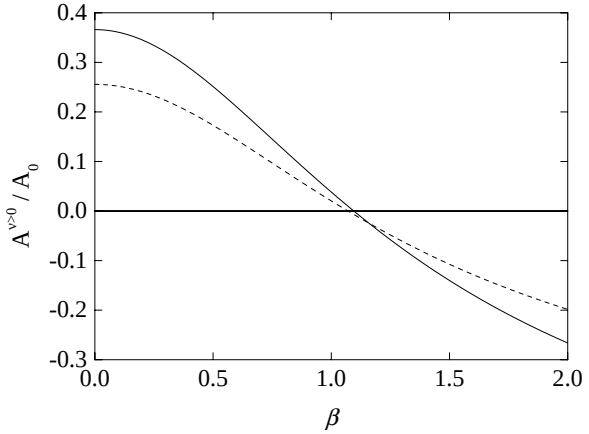

Slika 7 Dinamični del Hamakerjeve konstante za enoosna sredstva kot funkcija parametra $\beta = n_1/n_{2_\perp}$. Polna črta označuje konstanto izračunano po enačbi (26) za enoosna sredstva, črtkana črta pa označuje konstanto v približku izotropnih sredstev, kjer je $(n_i^{iso})^2 = (n_{i_\parallel}^2 + 2n_{i_\perp}^2)/3$. Hamakerjeva konstanta je merjena v enotah $A_0 = 3\hbar\omega_e n_{2_\perp}/8\sqrt{2}$, $n_{2_\parallel}/n_{2_\perp} = 1{,}2$ in $n_3/n_{2_\perp} = 0{,}67$.

del Hamakerjeve konstante pozitiven in interakcija privlačna, za $\bar{n}_1 < \bar{n}_2 < \bar{n}_3$ ali $\bar{n}_1 > \bar{n}_2 > \bar{n}_3$ pa je konstanta negativna in interakcija odbojna. Enaki pogoji veljajo za značaj izotopne Hamakerjeve konstante [enačba (27)], če renormalizirane parametre nadomestimo z izotropnimi. Kot je bilo omenjeno že na začetku, do sedaj ni bil znan enostaven izraz za van der Waalsovo silo med enoosnimi sredstvi. Zato je bila ta sila določena iz izrazov za izotropna sredstva, kjer so bili vstopni parametri za Hamakerjevo konstanto izotropni deli ustreznih tenzorjev, $\epsilon^{iso} = (\epsilon_\parallel + 2\epsilon_\perp)/3$ oziroma $(n^{iso})^2 = (n_\parallel^2 + 2n_\perp^2)/3$. Kot je razvidno iz pogojev, ki smo jih ravnokar zapisali in kot se vidi na sliki 7, se lahko tako določena van der Waalsova sila od prave precej razlikuje po velikosti, v ozkem intervalu anizotorije pa celo po značaju interakcije.

V nadaljevanju se bomo posvetili neposrednim vplivom ograjujočih sten na nematski red in fluktuacije nematskega ureditvenega parametra. Najprej se bomo posvetili lokalnim vplivom površin na nematski tekočekristalni red. Lokalizirane variacije reda so značilne za spreminjanje stopnje nematskega reda, medtem ko se deformacije, povezane s frustracijami direktorskega polja, ponavadi raztezajo po celotnem tekočekristalnem vzorcu.

Heterofazni nematski sistem

Kadar je nematski tekoči kristal v stiku s površino, ki vsiljuje močan nematski red, se tik ob površini tudi pri temperaturah nad prehodom v urejeno nematsko fazo

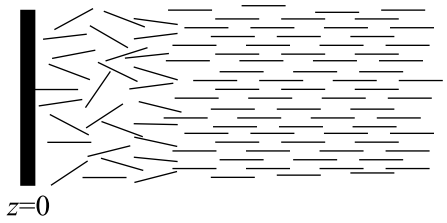

Slika 8 Shema ureditve molekul v nematskem tekočem kristalu v stiku z razurejujočo steno.

pojavi mezoskopska urejena plast. Pojav imenujemo (orientacijsko) *močenje*, opisani sistem pa *paranematski sistem*. Podoben pojav opazimo pod temperaturo prehoda, ko se ob površini, ki vsiljuje močan nered, med steno in nematsko fazo pojavi dobro definirana plast izotropne faze (glej sliko 8). Tu opisujem predvsem slednji primer, ki ga imenujem *površinsko staljeni nematski sistem*. Orientacijsko močenje je lahko delno ali popolno. Pri delnem močenju je površinska plast le delno (raz)urejena, njena debelina pa je končna tudi tik ob prehodu v fazo, ki jo vsiljuje tudi površina. Fazni prehod je nezvezen. Pri popolnem močenju opazimo pred faznim prehodom površinski prehod, kjer se delno (raz)urejena površinska plast skokovito (raz)uredi, nato pa njena debelina ob približevanju prehodu močno narašča in v polneskončnem sistemu ob faznem prehodu divergira. Fazni prehod je v primeru popolnega močenja zvezen.

Močenje v polneskončnem sistemu, predvsem paranematskem, so od prvega zapisa leta 1976 študirali v mnogih skupinah [18,50,108–111,59,60,14]. Tu predstavljam predvsem študij dinamike v nematski plasti s staljenim redom ob površinah. Obravnava je vezana na Landau–de Gennesovo teorijo in opis tekočega kristala s tenzorskim nematskim ureditvenim parametrom. Smektičnega urejanja tik ob površini ne upoštevam, saj je to, posebej v izotropni fazi, zelo majhno. Homeotropno smer nematskega direktorja določa šibko zunanje magnetno polje, ki pa je dovolj močno, da premaga morebitno drugačno preferenčno smer direktorja na meji obeh faz [120–125]. Njegovega vpliva na stopnjo urejenosti v obravnavi ni potrebno upoštevati. Prav tako ne upoštevamo šibke sklopitve med variacijo stopnje urejenosti in deformacijami direktorskega polja [119]. Ravnovesni povprečni ureditveni parameter torej zapišemo kot $\mathsf{Q} = a_0\mathsf{T}_0$, kjer je $\hat{n} = \hat{e}_z$ in je os z v smeri normale na plast, ureditveni parameter, ki ga vsiljuje površina pa je $\mathsf{Q}_S = a_S\mathsf{T}_0$, kjer je $a_S < 1$.

Na sliki 9 so predstavljeni profili stopnje nematske urejenosti pri različnih temperaturah in močeh vpliva površine. V primeru nematika v stiku z razurejujočimi stenami pride do popolnega omočenja stene z izotropno fazo le, če stena vsiljuje popoln nered ($a_S = 0$) in je sklopitev dovolj močna ($G \gtrsim 0{,}0023$ J/m^2). V obratnem paranematskem sistemu lahko dobimo popolno omočenje za vse vrednosti vsiljevanega ne-

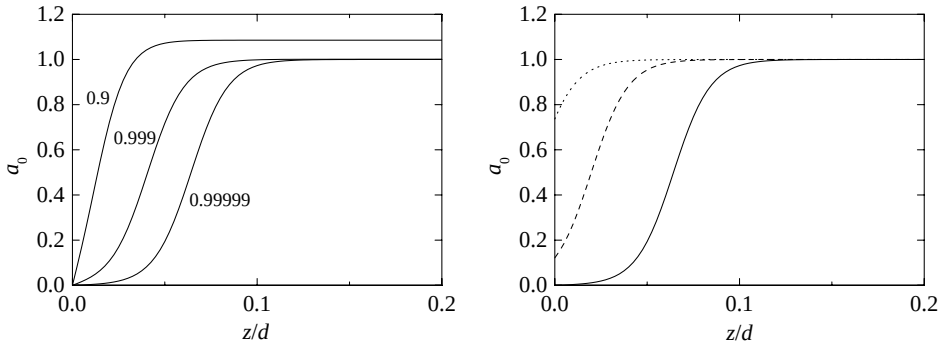

Slika 9 Stopnja nematske urejenosti v nematiku s staljenima površinskima plastema v bližini prehoda v izotropno fazo. (a) Temperaturna odvisnost: $a_S = 0$, $G \to \infty$, profili pa so označeni z vrednostjo ustrezne brezdimenzijske temperature. (b) Odvisnost od moči sklopitve s površino: $\theta = 1-10^{-5}$, $a_S = 0$ ter $G \to \infty$ (polna črta), 0,001 J/m^2 (črtkana črta) in 0,0003 J/m^2 (pikčasta črta).

matskega reda, ki je večji od reda ob prehodu v neograjenem sistemu ($a_S > 1$), mejna vrednost sklopitve G, ki dovoljuje popolno omočenje pa je odvisna od a_S; na primer $G(a_S = 1{,}1) = 0{,}0006$ J/m^2. Eden od znakov, da je omočenje popolno, je rast omočitvene plasti, ko se približujemo prehodu v izotropno fazo. Na sliki 10 (a) lahko jasno razločimo med divergentnim naraščanjem debeline omočitvene plasti v primeru popolnega omočenja in obnašanjem, značilnim za delno omočenje, ko doseže površinska plast končno obliko že pred prehodom. V končnem vzorcu nematskega tekočega kristala debelina omočitvene plasti seveda ne more divergirati, ker se obe omočitveni plasti prej združita, vendar kaže temperaturna odvisnost $d_W(T - T_{NI})$ tipično logaritemsko odvisnost. Zaradi končne prečne dimenzije je fazni prehod tudi v primeru popolnega omočenja stene z izotropno fazo rahlo nezvezen. Poleg tega nastopi prehod pri nižji temperaturi (višji v primeru paranematskega sistema), vendar je razlika komaj zaznavna — v celici debeline 792 nm je $\theta_{NI} = 0{,}99274$, v debelejših celicah pa še manj.

Predvsem v neposredni bližini faznega prehoda sestavljata heterofazni sistem površinska plast z redom, kot ga vsiljuje površina, in notranji del sistema, v katerem se vpliv površine ne pozna in je tekoči kristal urejen tako, kot bi bil pri dani temperaturi v neograjenem sistemu. Obe področji loči dobro definirana fazna meja, tem bolj, čim bližje smo faznemu prehodu. Obe fazi imata sicer enake izotropne dielektrične lastnosti, vendar pa se razlikujeta v simetriji. Pri obravnavi van der Waalsove sile v anizotropnih sredstvih smo ugotovili, da sta taki snovi z vidika van der Waalsove interakcije različni. Zato fazna meja med njima predstavlja novo steno v sistemu, v omočitveni plasti pa k tlaku prispeva tudi van der Waalsov tlak. Ker je omočitvena

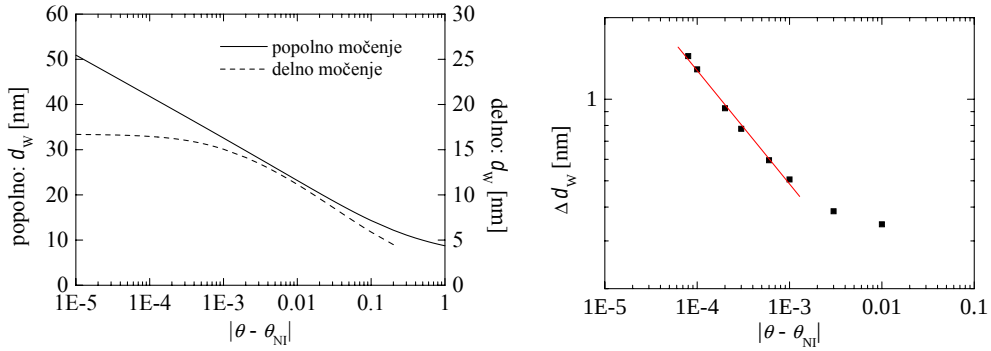

(a) (b)

Slika 10 (a) Temperaturna odvisnost debeline staljene površinske plasti v primeru popolnega in delnega močenja. Parametri računa: $a_S = 0$, $d = 792$ nm ter $G \to \infty$ v primeru popolnega močenja in $G = 0{,}001$ J/m^2 v primeru delnega močenja. (b) Renormalizacija debeline omočitvene plasti zaradi van der Waalsove sile na fazno mejo. Logaritemsko divergenco s kritičnim eksponentom 0 zamenja potenčna divergenca $\Delta d_W \propto (T - T_{NI})^{-\nu}$ s kritičnim eksponentom $\nu = 0{,}5$.

plast precej tanjša od celotne debeline celice, sem obravnavala tridelni sistem trdne stene, omočitvene plasti in nezmotenega tekočega kristala. Blizu prehoda, kjer je fazna meja dobro definirana, nadomestimo profil skalarnega ureditvenega parametra s stopničasto funkcijo in izračunamo prispevek k prosti energiji zaradi van der Waalsove interakcije. Ta je v primeru nematika s staljenimi površinami privlačna in prispeva k stanjšanju omočitvene plasti, v primeru paranematske celice pa odbojna in poveča ravnovesno debelino plasti. Temperaturna odvisnost van der Waalsovega popravka k debelini omočitvene plasti je narisana na sliki 10 (b). V področju dobro definirane fazne meje ima popravek potenčno odvisnost od razlike temperatur $T - T_{NI}$, kritični eksponent določen iz prilagoditve pa da vrednost blizu 0,5.

Fluktuacije ureditvenega parametra

Obravnavamo sistem z enakimi robnimi pogoji na obeh ograjujočih stenah, zato je ravnovesni povprečni profil simetričen glede na sredino celice in ima enako simetrijo tudi potencial za fluktuacije. Kot je znano, so lastne funkcije sodega operatorja bodisi sode ali lihe glede na dano simetrijsko ravnino [130], kar velja tudi za harmonski operator za fluktuacije ureditvenega parametra. Zato rešujem enčbe le na eni polovici celice, pri čemer za fluktuacijske načine velja, da ima na sredini ničlo bodisi fluktuacijski profil (lihi načini) ali njegov odvod (sodi načini).

Vpliv površin lahko študiramo ob primerjavi dimenzijsko in geometrijsko enakega sistema, v katerem pa ograjujoče stene vsiljujejo prav tak red, kot bi ga imel neograjeni tekoči kristal. V takem sistemu je stopnja urejenosti v celici konstantna. Fluk-

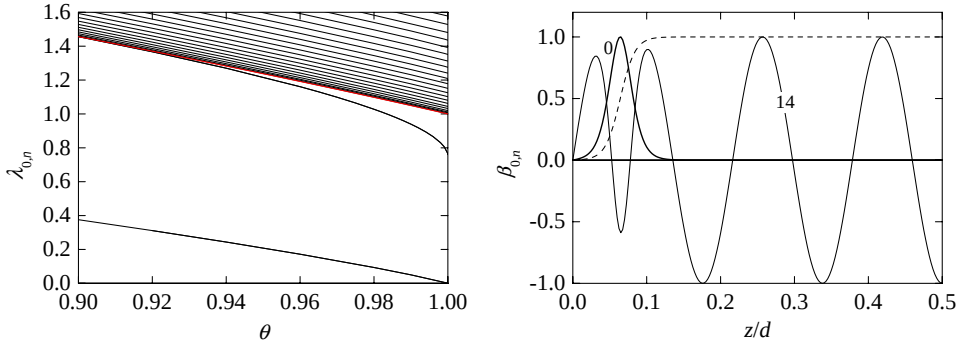

(a) (b)

Slika 11 (a) Spekter fluktuacij stopnje urejenosti, za katerega je značilen mehki osnovni fluktuacijski način, in (b) upodobitev profila dveh fluktuacijskih načinov — številka, ki označuje posamezni način, pove število vozlov med obema stenama — skupaj z ravnovesnim povprečnim profilom za $\theta = 1-10^{-5}$. ($G \to \infty$ in $a_S = 0$)

tuacijski načini v konstantnem (škatlastem) potencialu so sinusi, $\sin q_z z$, kjer je $q_z = \zeta(n+1)\pi$, pripadajoče relaksacijske hitrosti pa so

$$\widetilde{\lambda}_i = \xi_{N,i}^{-2}/\xi_{NI}^{-2} + \zeta^2 \left[(n+1)\,\pi\right]^2, \tag{28}$$

kjer so $\xi_{N,i}$ korelacijske dolžine definirane v enačbi (10) z $a_0 = 0{,}75(1+\sqrt{1-8\theta/9})$. V bližini faznega prehoda je $\xi_{N,0}^{-2}/\xi_{NI}^{-2} \approx 6-5\theta$ in $\xi_{N,\pm1}^{-2}/\xi_{NI}^{-2} \approx 18-9\theta$, medtem ko je $\xi_{N,\pm2}^{-2}/\xi_{NI}^{-2} = 0$ na celotnem temperaturnem intervalu nematske ureditve.

Spekter fluktuacij v nematskem sistemu s razurejujočimi površinami se od homogenega sistema najbolj razlikuje po obstoju mehkega fluktuacijskega načina, s tipično temperaturno odvisnostjo $\lambda_{0,0} = \pm C|\theta - \theta_{NI}|$ ($C_{nem} = 3{,}0$ in $C_{para} = 5{,}6$). Ta ustreza fluktuacijam debeline omočitvene plasti. Pri osnovnem načinu fluktuirata debelini obeh plasti z nasprotno fazo in povrzročata krčenje oziroma širjenje osrednjega nematskega dela. Prvi lihi način je po energiji enak osnovnemu (prvemu sodemu) kadar je debelina celice dovolj velika, da omočitveni plasti ne "čutita" povezave. Način predstavlja fluktuacije položaja osrednjega dela. Od homogenega spektra se ločita še prva naslednja lihi in sodi način, ki spreminjata obliko fazne meje. Višji načini skorajda ne čutijo razurejujočega vpliva sten. Spekter fluktuacij stopnje urejenosti in profili nekaj fluktuacijskih načinov stopnje urejenosti so predstavljeni na sliki 11.

Mehki fluktuacijski način je še en znak za zveznost faznega prehoda, ki spremlja sisteme s popolnim omočenjem. Kadar je močenje le delno, je $\lambda_{0,0} > 0$ in narašča z oddaljenostjo od režima popolnega omočenja. Na sliki 12 je predstavljena odvisnost relaksacijske hitrosti mehkega načina od moči površinske sklopitve za $a_S = 0$ v primeru nematika v stiku z razurejujočima stenama in $a_S = 1{,}1$ v primeru parane-

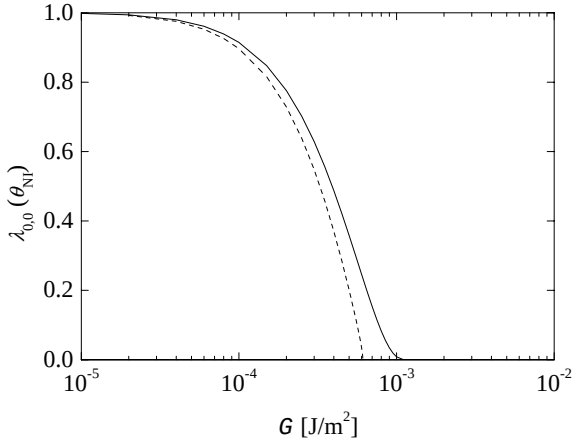

Slika 12 Relaksacijska hitrost osnovnega načina fluktuacij stopnje urejenosti v sistemu nematika v stiku z razurejujočima stenama (polna črta) in v paranematskem sistemu (črtkana črta). V območju delnega močenja, $G < G_c$, je $\lambda_{0,0} > 0$. Kritična vrednost G je za nematik s staljenimi površinami 0,0023 J/m^2 ($a_S = 0$) in v paranematskem sistemu $G_c = 0{,}0006$ J/m^2 ($a_S = 1{,}1$). V paranematskem sistemu sta oba režima ločena z omočitvenim prehodom, medtem ko je v primeru nematika v stiku z razurejujočimi površinami prehod nekoliko zabrisan.

matika. Režima popolnega in delnega omočenja loči kritična vrednost sklopitve, sistem pa iz enega režima preide v drugega z omočitvenim prehodom. Ta je v primeru nematika v stiku z razurejujočimi stenami nekoliko zabrisan, ker je popolno omočenje vezano na sam rob faznega diagrama (G, a_S), na $a_S = 0$.

V nematiku v stiku z razurejujočimi stenami ni drugih fluktuacijskih načinov, katerih relaksacijska hitrost bi ob prehodu padla na 0, medtem ko je v paranematiku tak še najnižji direktorski način, ki je lokaliziran znotraj nematske omočitvene plasti. Zmanjšanje njegove relaksacijske hitrosti na 0 je posledica dejstva, da so direktorske fluktuacije v nematski fazi, ki postane ob prehodu stabilna, Goldstoneove. V heterofaznem nematiku se zaradi povečanja debeline omočitvene plasti ob prehodu močno poveča relaksacijska hitrost Goldstoneovih direktorskih fluktuacij. Te so strogo vezane na osrednji nematski del, kjer je njihova korelacijska dolžina neskončna, tako da je povečanje relaksacijske hitrosti posledica efektivnega zmanjšanja debeline "sistema". V nasprotju z direktorskimi fluktuacijami so fluktuacije dvoosnosti energijsko zelo neugodne v nematski fazi. Tako je za nekaj najnižjih načinov ugodneje, da so vezani na tanko izotropno omočitveno plast in se šele višji načini raztezajo tudi po osrednjem delu. Število fluktuacijskih načinov, katerih relaksacijska hitrost se približuje nižji vrednosti v izotropni fazi, je odvisna od debeline omočitvene plasti in s tem od temperature. Spektra fluktuacij dvoosnosti in direktorskih fluktuacij sta narisana na sliki 13.

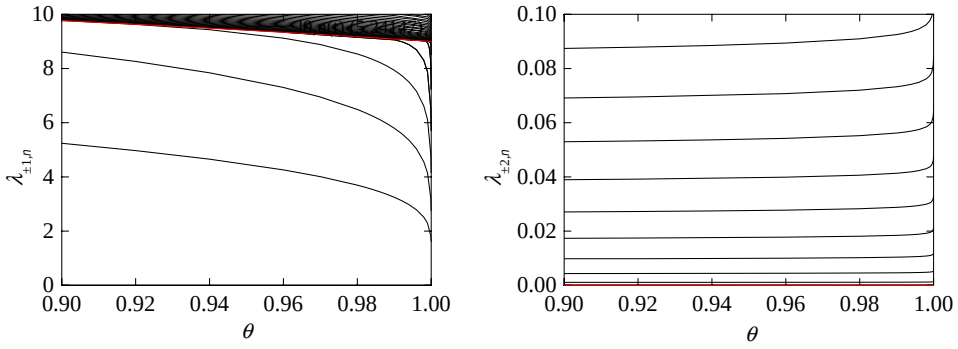

(a) (b)

Slika 13 Spektra fluktuacij (a) dvoosnosti in (b) direktorja v sistemu nematika v stiku z razurejujočima stenama. ($\theta = 1 - 10^{-5}$, $a_S = 0$ in $G \to \infty$)

Ograjujoče stene, ki jih izotropna oziroma nematska faza v tekočekristalnem sistemu popolnoma omoči, močno spremenijo tako povrpečni red kot tudi fluktuacije v bližini prehoda. Zaradi nenasprotujočih si robnih pogojev se steni privlačita. Ravnovesna ureditev je zaznamovana z lokalizirano spremembo ureditvenega parametra, ki je vezana na fazno mejo. Strukturni privlak je zato kratkega dosega. K fluktuacijski psevdo Casimirjevi sili prispeva fluktuacijska interakcija med steno in fazno mejo ter interakcija med obema faznima mejama. Najpomembnejši je vpliv Goldstoneovih direktorskih fluktuacij v nematskem delu sistema, ki vodi do sile dolgega dosega. V paranematskem sistemu je dolgi red interakcije prikrit z eksponentnim padanjem debeline nematskega dela tekočega kristala, tako da je psevdo Casimirjeva sila enakega dosega kot strukturna sila. Nasprotno je psevdo Casmirjeva sila v nematskem sistemu s staljenimi površinami dolgega dosega.

Hibridna nematska celica

V hibridni nematski celici je nematski tekoči kristal ograjen s stenama, ki vsiljujeta enoosni nematski red v različnih smereh. Ponavadi sta vsiljevani smeri pravokotni druga na drugo, tako da je na eni površini vsiljevani red v smeri pravokotno na steno (na primer v smeri osi z) na drugi pa v določeni smeri v ravnini stene (recimo, v smeri osi x). Ker steni vsiljujeta nematski red v različnih smereh, je ureditev med njima vedno deformirana v primerjavi s spontano nematsko ureditvijo v neograjenem sistemu. Podobni nasprotujoči si pogoji pa niso nujno le posledica vsiljevanega reda na ograjujočih površinah, ampak pride do njih tudi v bližini defektov in zaradi geometije sistema. Tako v cilindrični geometriji, kjer ograjujoče stene cilindra vsiljujejo red v radialni smeri, takemu redu nasprotuje simetrija cilindra, ki daje prednost ureditvi vzdolž dolge osi cilindra.

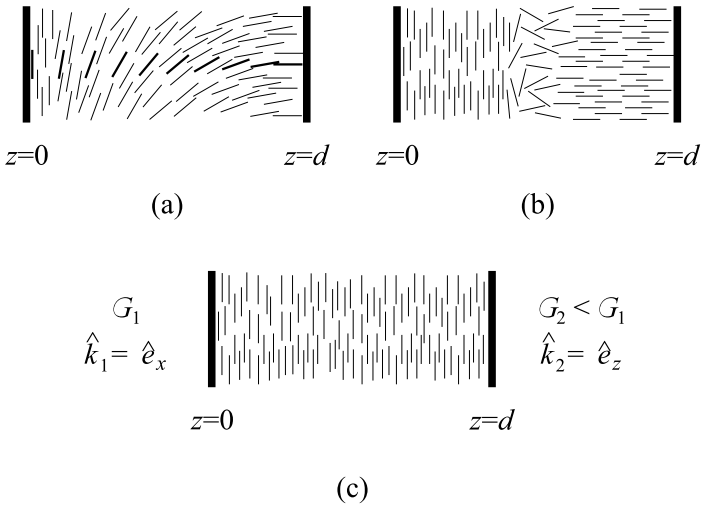

Slika 14 Shema urejenih struktur v hibridni celici: (a) upognjena struktura, (b) dvoosna struktura in (c) homogena struktura.

Študij povprečne ravnovesne ureditve v hibridni celici je ponavadi vezan na temperature globoko v nematski fazi, kjer se zanimamo predvsem za deformacije direktorskega polja in ne toliko za variacije stopnje urejenosti ter morebitne dvoosnosti ureditve. Opis z direktorskim poljem predvidi dve strukturi, katerih stabilnost je odvisna od debeline hibridne celice in relativne moči površinske sklopitve [19]. Za $d < d_c \equiv |\lambda_1 - \lambda_2|$ je stabilna struktura z nedeformiranim direktorskim poljem — *homogena struktura*, saj je energijsko ugodneje, da na površini s šibkejšim sidranjem ni izpolnjen robni pogoj, kot da bi bilo deformirano direktorsko polje. Nasprotno je za $d > d_c$ elastična deformacija direktorskega polja ugodnejša od močnega kršenja robnih pogojev na eni od sten — *upognjena struktura*. Direktorsko polje v celici je upognjeno, smer direktorja na obeh stenah pa se v splošnem razlikuje od vsiljevane smeri. Shema ureditve molekul v obeh opisanih strukturah je predstavljena na sliki 14.

Blizu prehoda v izotropno fazo in, kadar je sidranje na površinah zelo močno ekstrapolacijski dolžini pa približno enaki, so poleg direktorja pomembne tudi ostale prostostne stopnje ureditvenega parametra. Nekaj raziskav ravnovesnih struktur v hibridni celici, kadar so pomembne tudi nedirektorske prostostne stopnje je že bilo narejenih [20,139], z variacijo različnih parametrov, ki vplivajo na stabilnost različnih struktur in fazne prehode med njimi, pa smo védenje o hibridni celici poglobili s študijo tudi mi [21]. Ker je za vse opisane strukture značilno, da leži direktorsko polje v ravnini vsiljevanih smeri x in z, opišemo ureditveni parameter s konstantno trojico enotskih vektorjev $\hat{n} = \hat{e}_y$, $\hat{e}_1 = \hat{e}_z$ in $\hat{e}_2 = \hat{e}_x$, na katerih razpnemo bazne tenzorje T_i [enačba (2)]. Tako z upoštevanjem vseh prostostnih stopenj nematskega reda pri višjih temperaturah popravimo predstavo o že znanih struktu-

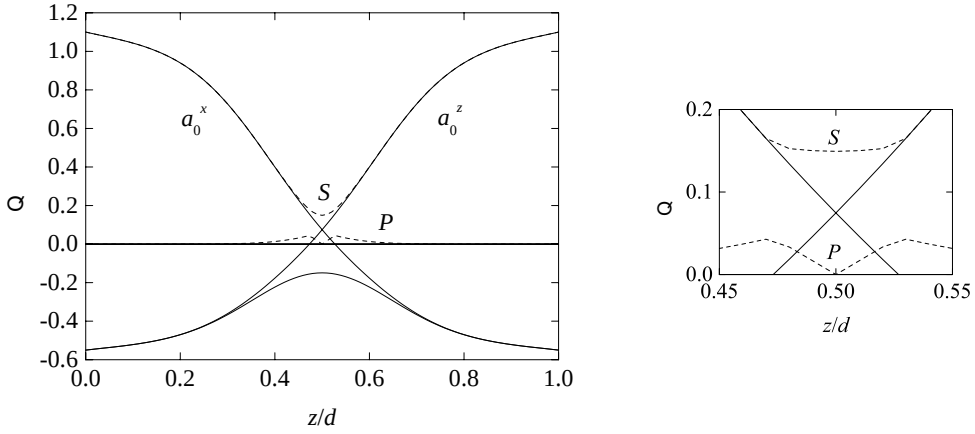

(a) (b)

Slika 15 (a) Ravnovesni profil neničelnih prostostnih stopenj nematskega ureditvenega parametra: stopnja urejenosti glede na osi x [$a_0^x = -(a_0 + \sqrt{3}a_1)/2$] ali z [$a_0^z = (-a_0 + \sqrt{3}a_1)/2$] — krepki polni črti — ali glede na os y (a_0) — tanka polna črta. Črtkani črti označujeta absolutno vrednost stopnje urejenosti [$S = (\sqrt{6}/2)|\mathsf{Q}_{ii}|$, kjer je predznak Q_{ii} nasproten predznaku drugih dveh lastnih vrednosti Q] in dvoosnosti ($P = |\mathsf{Q}_{jj} - \mathsf{Q}_{kk}|/\sqrt{2}$, kjer $j, k \neq i$). (b) Povečan del na območju izmenjave direktorja. ($\theta = 0{,}9$, $\zeta^2 = 0{,}01258$, $a_S = 1{,}1$ in $g_1 = g_2 \to \infty$)

rah, najdemo pa še dodatno strukturo, ki jo imenujemo *dvoosna struktura*. Shemo ureditve molekul v dvoosni strukturi kaže slika 14. V dvoosni strukturi se direktor ob stenah ujema z vsiljevano smerjo. Red ob stenah je enoosen, z oddaljevanjem od sten se zmanjšuje, povečuje pa se dvoosnost. Do preklopa direktorja iz ene smeri v drugo pride na sredini celice, kjer je red močno staljen. V osrednjem, slabih 10 nm debelem, delu hibridne celice so molekule urejene vedno bolj enakomerno v ravnini obeh direktorjev, torej kot bi bil direktor pravokoten na značilno ravnino, stopnja urejenosti pa negativna. Odvisnost ureditvenih parametrov od oddaljenosti od ene od sten kaže slika 15.

Z zmanjševanjem moči sidranja na eni od sten preide dvoosna struktura v homogeno strukturo s homogenim direktorskim poljem, medtem ko stopnja urejenosti pada v smeri proti steni, kjer se direktor in vsiljevana smer direktorja ne ujemata. V isti smeri narašča dvoosnost ureditve. Preobrazba ene strukture v drugo ni povezana s strukturnim ali faznim prehodom, ampak je stvar dogovora o poimenovanju faz. Pojav dvoosne sturkture je vezan na dovolj veliko frustracijo, kvantitativno jo ocenimo z močjo sidranja $G \gtrsim 10^{-4}$ J/m^2. Po drugi strani pa ob nespremenjenih enakih (velikih) močeh sidranja na obeh ograjujočih stenah z nižanjem temperature ali z večanjem debeline hibridne celice pridemo do strukturnega prehoda iz dvoosne strukture v upognjeno strukturo. Prehod je v splošnem šibko nezvezen, kar je razvidno iz slike 16 (a). Ob prehodu, kjer se vrednosti prostih energij ujemata,

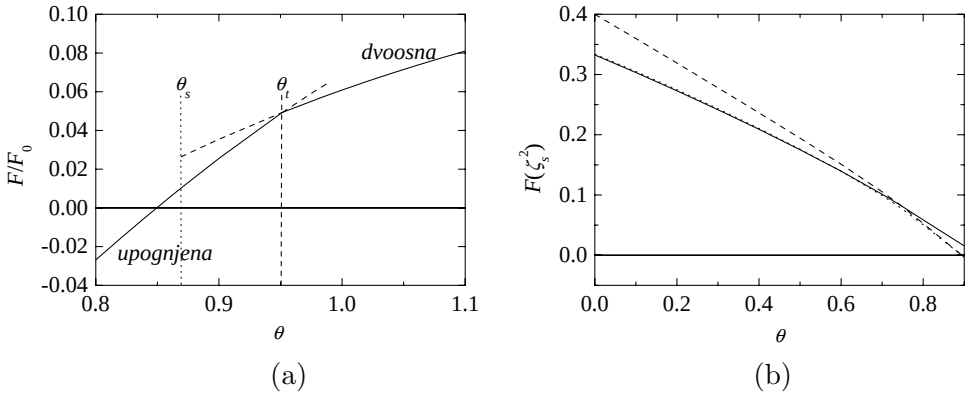

Slika 16 (a) Temperaturna odvisnost proste energije dvoosne in upognjene strukture. Do strukturnega prehoda pride pri $\theta_t = 0{,}951$, dvoosna struktura pa je metastabilna v temperaturnem intervalu $\theta_t > \theta > \theta_s = 0{,}869$. ($\zeta^2 = 0{,}02$, $a_S = 1{,}1$ in $g_1 = g_2 \to \infty$) (b) Temperaturna odvisnost proste energije dvoosne in upognjene strukture pri debelini, ki ustreza meji stabilnosti dvoosne strukture $\zeta_s = \zeta_s(\theta)$. Pod trikritično točko $\theta_{\mathrm{TP}} = 0{,}746$ in $\zeta^2_{\mathrm{TP}} = 0{,}054$ je strukturni prehod zvezen, nad njo pa postane postopoma vedno bolj nezvezen.

sta naklona obeh funkcij različna, črtkano nadaljevanje funkcij pa ustreza prostim energijam metastabilnega stanja dvoosne oziroma upognjene strukture. Pri debelini 56 nm je dvoosna struktura metastabilna v temperatunem intervalu 0,09 K, do strukturnega prehoda pa pride 0,04 K pod temperaturo faznega prehoda v neograjenem sistemu. Latentna toplota povezana s strukturnim prehodom je velikostnega reda $10^4\mathrm{J/m}^3$, kar je za dva velikostna reda manj kot pri faznem prehodu v neograjenem sistemu. Nezvezni strukturni prehod preide pod trikritično točko v zvezni prehod [glej sliko 16 (b)]. Zgornja meja za trikritično točko je v limiti neskončno močnega sidranja $d_{TP} = 34$ nm in $T_{NI} - T_{TP} = 0{,}28$ K.

Obstoj dvoosne strukture smo preverili s primerjavo rezultatov, ki jih da računalniška simulacija z metodo Monte Carlo [148,149]. Mikroskopske interakcije med molekulami "tekočega kristala" smo modelirali s preizkušenim Lebwohl-Lasherjevim potencialom [150], ki dobro opiše nematski sistem. Samo simulacijo na kubični mreži so izvedli v skupini dr. Pasinija in prof. Zannonija v Bologni, obdelavo podatkov in primerjavo z rezultati fenomenološkega opisa pa smo izvedli v naši skupini. Na rezultatih simulacije so bila izračunana različna makroskopska povprečja, ki ustrezajo ureditvenim parametrom, ki jih določamo s fenomenološko teorijo. Poseben poudarek smo posvetili določitvi parametra a_{-1}, ki meri upogib direktorskega polja v celici. Z njim smo razločili med dvoosno in upognjeno strukturo, ki imata v bližini strukturnega prehoda kvalitativno podobno obnašanje ostalih ureditvenih parametrov.

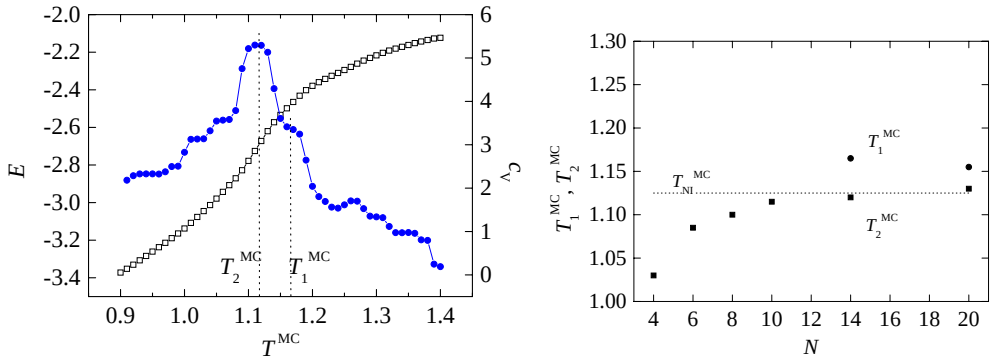

(a) (b)

Slika 17 (a) Energija (kvadratki) in specifična toplota (polni krogci) v 14 plastni hibridni celici. Vrh pri $T_2^{MC} \approx 1{,}115$ ustreza strukturnemu prehodu med dvoosno in upgnjeno strukturo, manjši vrh pri $T_1^{MC} \approx 1{,}165$ pa ustreza ureditvi tekočega kristala v sredini celice. (b) Temperaturi T_1^{MC} in T_2^{MC} kot funkciji števila plasti v celici. Črtkana črta označuje temperraturo prehoda v neograjenem sistemu.

Po pričakovanjih so rezultati Monte Carlo simulacije pokazali obstoj tako dvoosne kot upognjene strukture. Homogene strukture v sistemu ni, ker sta bili moči sidranja na obeh ograjujočih stenah enaki. Simulacija je bila izvedena na različno velikih sistemih ($30 \times 30 \times N'$, kjer je $N' = N + 2 = 6, 8, 10, 12, 16, 22$ in predstavlja N "plasti" molekul ali skupkov molekul tekočega kristala in po 1 krajno "plast" na vsaki strani celice, ki ustreza molekulam ograjujoče stene) in pri različnih vrednostih Monte Carlo temperature ($T^{MC} = k_B T/\epsilon$, kjer je ϵ energija interakcije med sosednjima molekulama), predvsem v okolici prehodov. Na sliki 17 (a) je predstavljena tipična odvisnost energije in specifične toplote hibridne celice v odvisnosti od temperature. Dobro razviden visok vrh specifične toplote ustreza strukturnemu prehodu iz dvoosne strukture v upognjeno. Temperaturo prehoda smo označili s T_2^{MC}. V celici z $N = 14$ plastmi je $T_2^{MC} \approx 1.12$. Temperatua strukturnega prehoda je nižja od temperature faznega prehoda v neograjenem sistemu, ki ustreza $T_{NI}^{MC} = 1.1232$ [152]. Nekoliko skrit v glavni vrh in precej manjši je vrh, ki ustreza ureditvenemu prehodu v sredini celice. Pri visokih temperaturah so urejene le molekule blizu sten, ko pa se omočitveni plasti stakneta, dobimo znano dvoosno strukturo. Temperaturo ureditvenega prehoda smo označili z T_1^{MC}, v 14 plastni celici je njena vrednost $T_1^{MC} \approx 1.18$. Zaradi urejujoče narave sten nastopi ureditev v celici pri temperaturi višji od prehoda v neograjenem sistemu, o čemer smo govorili v poglavju o heterofaznih sistemih. S povečevanjem debeline celice se T_1^{MC} približuje vrednosti T_{NI}^{MC}, prav tako se proti tej vrednosti približuje temperatura strukturnega prehoda T_2^{MC}.

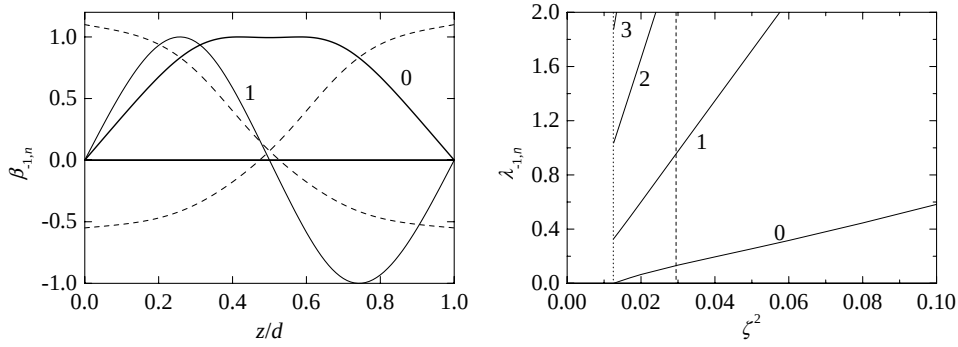

(a) (b)

Slika 18 (a) Relaksacijska hitrost nekaj osnovnih direktorskih fluktuacijskih načinov v odvisnosti od debeline filma. Ker direktorske fluktuacije vodijo strukturni prehod, pade njihova relaksacijska hitrost na 0 ob prehodu v upognjeno strukturo, če je prehod zvezen, oziroma pri debelini, nad katero dvoosna struktura ni več niti metastabilna, v primeru nezveznega prehoda. Pikčasta in črtkana črta ustrezata mejni debelini za stabilnost oziroma debelini prehoda. ($\theta = 0{,}9$, $a_S = 1{,}1$ in $g_1 = g_2 \to \infty$)

Fluktuacije ureditvenega parametra

Pri študiju fluktuacij se zanimamo za fluktuacije v dvoosni strukturi v bližini prehoda v upognjeno strukturo. Ločimo štiri neodvisne fluktuacijske načine.

Direktorske fluktuacije, povezane s fluktuacijami v smeri baznega tenzorja T_{-1}, predstavljajo deformacije direktorskega polja v ravnini (x, z). Njihov osnovni način povzroča prav tako deformacijo direktorskega polja, kot je značilna za upognjeno strukturo. Zato direktorske fluktuacije vodijo strukturni prehod. Njihova relaksacijska hitrost pade ob debelini (temperaturi) prehoda na 0, če je prehod zvezen. V primeru nezveznega prehoda je relaksacijska hitrost direktorskih fluktuacij ob prehodu končna, a pade na 0 pri debelini (temperaturi), ki predstavlja mejo stabilnosti dvoosne strukture. Te lastnosti direktorskih fluktuacij so znak, da prav te fluktuacije predstavljajo mehanizem prehoda. Odvisnost relaksacijske hitrosti direktorskih fluktuacij v primeru nezveznega strukturnega prehoda kaže slika 18 (a).

Fluktuacije dvoosnosti (fluktuacije amplitud β_i v smeri tenzorjev $\mathsf{T}_{\pm 2}$) merijo porazdelitev molekul v ravnini pravokotni na ravnino obeh značilnih smeri v hibridni celici, torej ureditev v ravnini (y, z) in v ravnini (x, y). Prve predstavljajo fluktuacije dvoosnosti v delu celice, kjer je direktor v smeri osi x, medtem ko predstavljajo v delu filma z direktorjem v smeri osi z direktorske fluktuacije. Za drugi tip fluktuacij velja ravno nasprotno. Ker so v urejeni nematski fazi fluktuacije dvoosnosti precej trše od direktorskih fluktuacij, je nekaj najnižjih fluktuacijskih načinov $\beta_{\pm 2}$ lokaliziranih le v $\hat{n} = \hat{e}_z$ oziroma $\hat{n} = \hat{e}_x$ delu filma, kjer predstavljajo direktorske fluktuacije. Višji

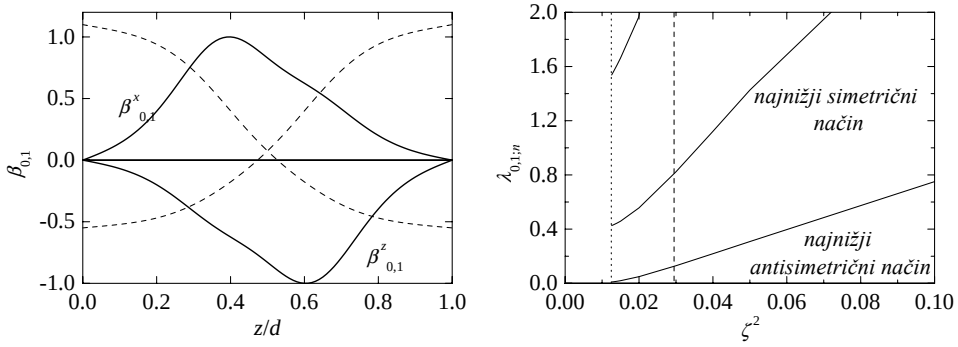

(a) (b)

Slika 19 (a) Profila osnovnega načina fluktuacij stopnje urejenosti. Polni črti predstavljata sklopnjena fluktuacijska načina stopnje urejenosti glede na direktor v smeri osi x oziroma z, črtkani črti pa ustrezata pripadajočima ravnovesnima profiloma. (b) Relaksacijska hitrost nekaj najnižjih fluktuacijskih načinov. Pikčasta in črtkana vertikala ustrezata debelini filma ob meji stabilnosti dvoosne strukture in ob strukturnem prehodu. ($\theta = 0{,}9$, $\zeta^2 = 0{,}01258$, $a_S = 1{,}1$ in $g_1 = g_2 \to \infty$)

načini deformirajo red v celotnem filmu. Fluktuacijski načini ± 2 so degenerirani, njihovi profili pa so zrcalno simetrični glede na sredino filma. Degeneracija se zgubi v filmih, kjer moči sidranja na obeh stenah nista enaki.

Fluktuacije stopnje urejenosti predstavljajo sklopljene fluktuacije obeh neničelnih ravnovesnih ureditvenih parametrov. Upodobimo jih lahko kot fluktuacije stopnje urejenosti glede na oba direktorja v filmu. Načini so sodi ali lihi glede na sredino celice, kar je posledica sodosti poteniciala za fluktuacije [130]. Najnižji fluktuacijski način je najnižji lihi oziroma antisimetrični način. Ta ustreza fluktuacijam debeline omočitvene plasti ob steni in smo ga spoznali že v poglavju o heterofaznem sistemu. Maksimum načina ustreza mestom z največjim naklonom v spreminjanju stopnje urejenosti, kot je razvidno tudi s slike 19 (a). Oba načina sklopljena skupaj predstavljata fluktuacije položaja osrednjega dela, kjer pride do zamenjave lastnih osi ureditvenega tenzorja. Višji načini spreminjajo obliko profilov in s tem izmenjalnega področja. Relaksacijska hitrost osnovnega načina fluktuacij stopnje urejenosti se ob prehodu oziroma ob meji stabilnosti močno zmanjša, vendar ostane končna, saj strukturni prehod ni povezan z mehanizmom urejanja, ki ga te fluktuacije predstavljajo [glej sliko 19 (b)]. Relaksacijska hitrost doseže ob prehodu nižjo vrednost, če gre za prehod v debelejših filmih (prehod dosežemo z nižanjem temperature) oziroma pri temperaturah blizu temperature faznega prehoda v neograjenih sistemih (prehod dosežemo z večevanjem debeline), ko dvoosna struktura izgine, namesto nje pa je pred upognjeno strukturo izotropna faza in je urejen le majhen del molekul tik ob steni.

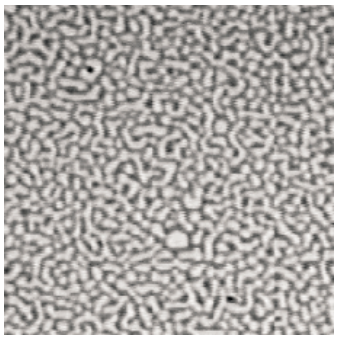

Slika 20 Fotografija tankega nematskega filma po razpadu zaradi spinodalnega razomočenja. Fotografijo so posneli F. Vandenbrouck in sodelavci objavljena pa je v reviji Phys. Rev. Lett. **82**, 2693 (1999).

Stabilnost tankih hibridnih nematskih filmov

Zaradi vpliva površin se povprečni red in fluktuacije v bližini prehoda močno spremenijo, zaradi česar deluje med stenama dodatni tlak. Če je tekočekristalni film ograjen le z ene strani, ostale površine pa so proste, je v odvisnosti od dodatnega tlaka film lahko stabilen ali pa zaradi ojačenja kapilarnih valov razpade v kapljice nematika in vmesna suha področja [104,158]. Primer nematskega filma po spinodalnem razomočenju kaže slika 20.

K tlaku v hibridnem nematskem filmu prispevajo strukturni tlak, psevdo Casimirjev tlak in van der Waalsov tlak [28,30]. Vsi so odvisni od nematske strukture v filmu. Na sliki 21 lahko vidimo odvisnost strukturnega tlaka od ravnovesne strukture in debeline filma. V okviru direktorskega opisa v homogeni strukturi ni strukturnega tlaka, strukturni tlak v upognjeni strukturi pa je močno odbojen in pada z razdaljo kot $1/d^2$. Upoštevanje ostalih prostnostnih stopenj nematske ureditve privede do neničelnega tlaka tudi v homogeni strukturi. Ta je kratkega dosega in zelo šibek, saj je posledica močno lokalizirane in majhne deformacije stopje urejenosti. Popravki k strukturnemu tlaku v upognjeni strukturi so zanemarljivo majhni, saj so nekaj velikostnih redov manjši od glavnega prispevka zaradi elastičnih deformacij direktorskega polja. Tudi strukturni tlak v dvoosni strukturi je odbojen, kar je posledica nasprotujočih si robnih pogojev, ki povzročajo deformacije, tem večje čim manjša je debelina filma [29]. Pri majhnih debelinah je deformacija ureditvenega parametra vezana na celoten film, zato je tam tlak približno enak tlaku v upognjeni strukturi. Z večanjem debeline je deformacija vedno bolj vezana na osrednji izmenjalni del filma, tako da velikost tlaka pade močneje kot v upognjeni strukturi. Primerjani sili ne ustrezata upognjeni in dvoosni strukturi pri istih parametrih, ampak gledamo upognjeno strukturo globoko v nematski fazi, kjer zadošča opis z direktorskim poljem, dvoosno strukturo pa v temperaturnem območju, kjer je ta stabilna, torej v bližini temperature T_{NI}.

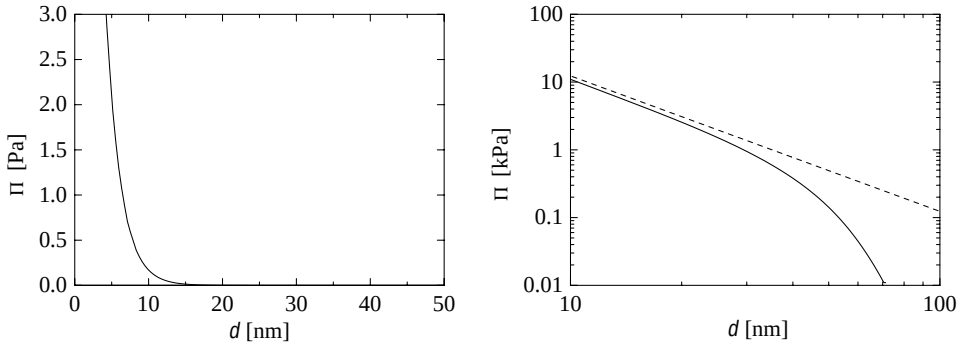

(a) (b)

Slika 21 Strukturna sila na enoto površine v hibridni celici (a) s homogeno strukturo ter (b) z upognjeno (črtkana črta) in dvoosno (polna črta) strukturo. Strukturna sila v hibridni celici z upognjeno ali dvoosno strukturo je nekaj velikostnih redov večja, saj je posledica močnih elastičnih deformacij. Pri debelinah nad nekaj 10 nm pada velikost sile v dvoosni strukturi hitreje kot v upognjeni strukturi, saj postaja deformacija vedno bolj lokalizirana. ($G_1, G_2 \to \infty$, upognjena struktura globoko v nematski fazi in dvoosna struktura blizu temperature T_{NI}.)

V podrobnosti izračuna in lastnosti psevdo Casimirjeve sile se tu ne bomo spuščali. V splošnem je njen izračun v hibridni celici zaradi nehomogenosti ureditvenega parametra zelo otežen. Rezultate, ki jih bomo uporabili pri študiju stabilnosti in interpretaciji eksperimentalnih rezultatov [158], bomo povzeli po študiji Ziherla in sodelavcev [65]. Izračun velja za najpreprostejšo, homogeno, strukturo in to dovolj globoko v nematski fazi, da lahko zanemarimo deformacije stopnje urejenosti. Poleg tega je študirana hibridna celica taka, v kateri stena, ki vsiljuje red v ravnini stene, na makroskopskem skali ne preferira nobene smeri. Na mikroskopskem in mezoskopskem nivoju to seveda nikoli ni res in je rotacijska simetrija zlomljena, ravnovesne strukture pa take, kot smo jih opisali v tem poglavlju. Do pomembne razlike pride pri opisu fluktuacij in fluktuacijske sile, saj opisana stena ne poruši zvezne rotacijske simetrije okrog normale na ograjujoči steni. Psevdo Casimirjeva sila v takem sistemu je potem odvisna od dveh parametrov, razmerja ekstrapolacijskih dolžin $\Lambda = \lambda_H/\lambda_P$ ter razmerja med debelino celice in kritično debelino za prehod v upognjeno strukturo, d/d_c. Odvisnost psevdo Casimirjevega tlaka od debeline filma je upodobljena na sliki 22.

Poleg opisanih strukturnega in psevdo Casimirjevega tlaka prispeva k skupnemu tlaku še van der Waalsov tlak [31]. V eksperimentalnem sistemu, ki ga želimo obravnavati, je bila na trdni steni še dodatna tanka oksidna plast, tako da sistem sestavljajo štiri plasti. Njihove dielektrične in optične lastnosti so zbrane v tabeli 1. Ker imata silicij in njegov oksid različen vpliv na van der Waalsovo interakcijo v

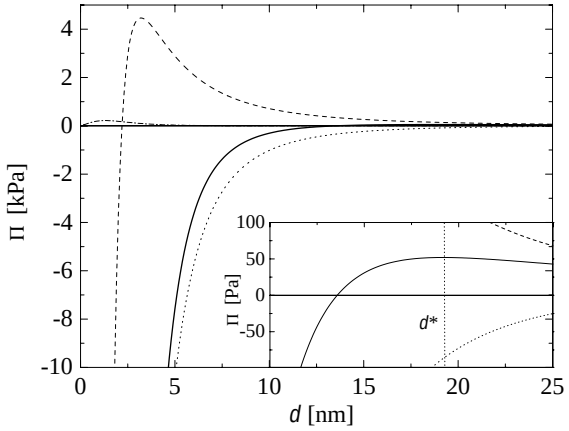

Slika 22 Dodatni tlak v hibridnem nematskem filmu v stiku s trdno steno in s prosto površino globoko v nematski fazi (polna črta). Črtkana črta ustreza van der Waalsovemu tlaku, pikčasta in črtkano pikčasta črta pa psevdo Casimirjevi in strukturni sili. Povečan je del v bližini prehoda tlaka iz naraščajočega z debelino filma v padajočega.

povezavi z danim tekočim kristalom in zrakom, je van der Waalsova sila v sestavljenem sistemu nemonotona. V grobem lahko rečemo, da je privlak pri majhnih debelinah filma posledica interakcije z dodatno oksidno plastjo, medtem ko je pri $d > t$, kjer je t debelina oksidne plasti, njen vpliv zanemarljiv in je odbojni tlak posledica interakcije s silicijem. Pri debelinah $d \sim t$ sta pomembna oba vpliva. Odvisnost van der Waalsovega tlaka od debeline nematskega filma je predstavljen na sliki 22.

Skupni tlak v hibridnem nematskem filmu ima nemonotono odvisnost od debeline. Za debeline manjše od marginalne debeline d^* tlak narašča z debelino, za $d > d^*$ pa pada. V prvem primeru je film nestabilen napram spinodalnemu razomočenju, v drugem je stabilen. Pri sobni temperaturi dobimo za vrednosti parametrov $\lambda_H = 33$ nm in $\lambda_P = 133$ nm ($\Lambda = 0{,}25$ in $d_c = 100$ nm) za marginalno debelino 18 nm,

Tabela 1 Dielektrične in optične lastnosti snovi, ki sestavljajo štiriplastni sistem, pri sobni temperaturi. ϵ je statična dielektrična konstanta in n lomni količnik v območju vidne svetlobe. Vsi parametri so podani pri sobni temperaturi.

material	ϵ		n	
silicij	12		3,5	
silicijev oksid	14		1,5	
5CB	$\epsilon_\parallel$	$\epsilon_\perp$	$n_\parallel$	$n_\perp$
	18,5	7	1,71	1,53

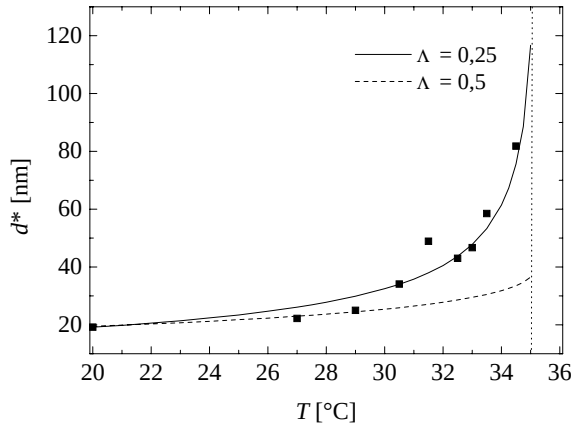

Slika 23 Temperaturna odvisnost marginalne debeline filma za različne vrednosti razmerja ekstrapolacijskih dolžin Λ. Kvadratki označujejo eksperimentalne rezultate, ki so jih izmerili Valignat s sodelavci [154].

kar ustreza rezultatom eksperimenta. Parametra λ_H in λ_P sta primerljiva že znanim vrednostim [159,43,28]. S približevanjem prehodu v izotropno fazo izmerjene vrednosti marginalne debeline močno narastejo. Naraščanja ne opraviči temperaturno spreminjanje dielektirčnih in optičnih lastnosti tekočega kristala, ki so povezane s stopnjo urejenosti. Zaradi spreminjanja le-teh se van der Waalsova in strukturna sila le malo spreminjajo. Tudi eksplicitna temperaturna odvisnost tako van der Waalsove kot tudi psevdo Casimirjeve sile ne da opaženega, skoraj divergentnega obnašanja. Tako obnašanje pojasni temperaturno spreminjanje ekstrapolacijskih dolžin. V okviru direktorskega opisa in z razvojem površinske proste energije do členov drugega reda so ekstrapolacijske dolžine konstantne. Vendar pa rezultati meritev kažejo, da postanejo ob približevanju prehodu pomembni tudi členi višjega reda, tako da se ekstrapolacijske dolžine s temperatuo spreminjajo nekako kot $\lambda \propto S^{-2}(T)$ [17,46–48,16]. Pri interpretaciji spinodalnega razomočenja smo privzeli najpreprostejši model: ekstrapolacijski dolžini se spreminjata na enak način, tako da ostaja njuno razmerje stalno ,ob približevanju temperaturi prehoda pa se povečuje kritična debelina d_c. Ekstrapolacijski dolžni se ujemata z izmerjenimi vrednostmi globoko v nematski fazi, kjer je opis z direktorskim poljem dobro definiran. Na sliki 23 vidimo primerjavo temperaturne odvisnosti izmerjenih vrednosti za marginalno debelino z rezultati našega modela za različne vrednosti parametra Λ. Vrednosti λ_H in λ_P sta izbrani tako, da se ujemata izračunana in izmerjena vrednost marginalne debeline globoko v nematski fazi. Najboljše ujemanje dobimo pri prej omenjenih parametrih. Spinodalno razomočenje je eden od mehanizmov za opazovanje strukturnih in psevdo Casimirjevih sil v tanki plasti tekočega kristala.

Zaključki

V doktorskem delu sem predstavila različne vidike vpliva ograjujočih sten na ravnovesno ureditev in fluktuacije ureditvenega parametra v bližini faznih in strukturnih prehodov. Pokazala sem, pri katerih pogojih privede (raz)urejevalna moč sten do zmanjšnja nezveznosti prehoda oziroma ga celo odpravi in postane prehod zvezen. V vseh študiranih sistemih sem poiskala mehanizme, ki vodijo prehod, poleg teh pa so me zanimali tudi lokalizirani fluktuacijski načini, ki so povezani z obstojem faznih ali strukturnih mej. Fazni prehod v heterofaznem prehodu vodijo fluktuacije stopnje urejenosti, ki so odgovorne za rast omočitvenih plasti, ko se približujemo prehodu. Na omočitveno plast so vezani nižji direktorski načini v paranematskem sistemu in nižji fluktuacijski načini dvoosnosti v nematskem sistemu v stiku z razurejujočimi stenami. Strukturni prehod v hibridni celici vodijo direktorske fluktuacije, saj pri prehodu ne gre za urejanje nematika, ampak spreminjanje ureditve. Strukturni prehod je lahko zvezen ali nezvezen, vmes pa je trikritična točka, katere zgornjo mejo sem določila. Fluktuacije stopnje urejenosti v hibridni celici predstavljajo povezano spreminjanje dveh parametrov, ki opišejo povprečno ravnovesno ureditev. Te prispevajo k urejevanju nematika v celici. Nižji fluktuacijski načini dvoosnosti so zanimivi, ker so lokalizirani v le eni omočitveni plasti, tisti, kjer te fluktuacije predstaljajo direktorske fluktuacije.

Strukture v hibridni celici in prehode med njimi sem študirala tudi ob primerjavi rezultatov, ki jih da Monte Carlo simulacija nematskega tekočega kristala v hibridni celici. Pokazala sem kvalitativno ujemanje rezultatov, za kvantitativno primerjavo pa moramo vzpostaviti še nekaj povezav med temperaturami v okviru Monte Carlo simulacije in fenomenološkega opisa ter med močmi sidranja in vsiljevano stopnjo ureditve.

Ograjujoče stene vplivajo posredno preko vpliva na ureditev tekočega kristala tudi na van der Waalsov tlak v plasti ograjenega tekočega kristala. Ker do zdaj ni bilo znano, kakšen vpliv ima anizotropija snovi na van der Waalsovo interakcijo, sem jo za primer enoosne simetrije sistema določila v tem delu. Pokazala sem, da se v enoosni snovi dielekrične in optične lastnosti renormalizirajo tako, da so pomembni parametri za opis sistema $\sqrt{\epsilon_\parallel \epsilon_\perp}$ in $n_\parallel n_\perp$ ne pa izotropne vrednosti $(\epsilon_\parallel + 2\epsilon_\perp)/3$ in $(n_\parallel^2 + 2n_\perp^2)/3$. Dobljeni rezultat za van der Waalsovo silo, ki razlikuje med neurejenim in urejenim tekočim kristalom, sem uporabila za renormalizacijo debeline omočitvene plasti v heterofaznem sistemu. Van der Waalsova interakcija spremeni kritični eksponent rasti z 0 na 1/2. V nadaljevanju sem popravljen izraz za van der Waalsov tlak uporabila tudi pri določitvi pogojev za stabilnost tankega nematskega filma s hibridnimi robnimi pogoji. Določila sem temperaturno odvisnost mejne debeline, ki se dobro ujema z izmerjenimi vrednostmi.

V raziskavi vpliva ograjujočih sten na fluktuacije nematskega ureditvenega parametra sem pojasnili in raziskala nekaj različnih vidikov, še vedno ostaja nekaj vprašanj, ki sem jih v tej obravnavi izpustila. Tako bi si morali v prihodnosti pogledati še, kakšen je vpliv delnega urejanja molekul ob steni v plasti. Smektično urejanje visoko nad morebitno smektično A fazo, v manjši meri pa se pojavlja tudi v tekočih kristalih brez spontane smektične faze, je posledica zlomljene translacijske simetrije, ki jo povzroči prisotnost stene. Diskretna rast smektičnih plasti bi morala imeti zanimiv vpliv na nematske red in njegove fluktuacije.

S popravljenim izrazom za van der Waalsovo interakcijo v primeru anizotropnih sredstev sem popravila debelino ravnovesne omočitvene plasti. Ker van der Waalsova interakcija spremeni kritični eksponent rasti plasti in s tem položaja fazne meje, na katero je vezan mehki fluktuacijski način, bi bilo treba pogledati, kakšen vpliv ima to na spekter fluktuacij stopnje urejenosti.

Že od vsega začetka smo predpostavili, da se energija v sistemu zgublja le v notranjosti tekočekristalnega sistema. Gibanje molekul ob stenah je sicer res upočasnjeno in je disipacija energije zato tam manjša, vendar pa je različna od nič. Raziskati bi morali vpliv površinske viskoznosti na fluktuacije celotnega ureditvenega parametra.

Pojavi, ki sem jih opisala v tem delu, niso vezani le na opisano planarno geometrijo in seveda ne le na nematske tekoče kristale. Da bi lahko povedali kaj več, kot le načelno pričakovanje podobnih pojavov v kapilarah in drugih geometrijah, bi morali študije razširiti na splošnejše sisteme.

1

Introduction

The matter can exist in three basic states: gas, liquid, and solid state. For a number of materials the limits between these states are not sharp and the material can be found in various intermediate states called *mesophases*. The liquid-crystalline phases denote a cascade of states between liquid and solid state of the matter. In these states, the matter is characterized by some of the liquid-like properties, such as the ability to flow, and solid-like properties, such as partial order, which results in anisotropy of dielectric, magnetic, and optical properties. The materials, which exhibit one or more liquid-crystalline phases, are characterized by highly anisotropic molecular shape: the molecules are either rodlike or disklike. In fact, the molecular shape is irregular, but due to fast molecular rotations it appears rodlike or disklike. The order in liquid crystals is controlled either mainly by temperature —*thermotropic liquid crystals* — or mainly by concentration of liquid-crystalline material in a solution —*lyotropic liquid crystals*. This thesis deals with thermotropic liquid crystals.

The simplest liquid-crystalline phase is a nematic phase. The term nematic was invented by Friedel [1] who studied many properties of the liquid-crystalline phases in the first part of the twentieth century. The name originates in Greek word $\nu\eta\mu\alpha$, which means thread. When observed between crossed polarizers, the defects in nematics produce a threadlike structure. In the nematic phase, the molecules tend to orient in a particular direction in the space, however, their centers of mass are randomly distributed (see Fig. 1.1). The average orientation of long axes of rodlike molecules or discs' normals is denoted as a nematic *director* — $\hat{n}$. In nematic liquid crystals, the states with directors $\hat{n}$ and $-\hat{n}$ are indistinguishable. Therefore, the nematic phase occurs only with achiral materials or with racemic mixtures of chiral molecules. The molecules are not perfectly ordered in the direction of the director, but their order increases with the decreasing temperature. The distribution of molecules around the director is uniform and corresponds to uniaxial symmetry

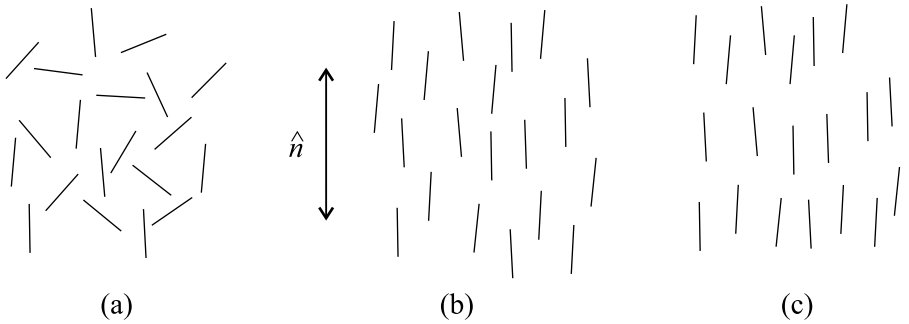

Figure 1.1 Schematic representation of a molecular order in (a) isotropic, (b) nematic, and (c) smectic phase. $\hat{n}$ denotes the average orientation of molecular long axes in nematic in smectic phase.

— the symmetry of a perfect cylinder. The optical axis of a material coincides with the nematic director. Due to external constraints another characteristic direction can occur — a secondary or biaxial director — and the corresponding order is biaxial. On cooling the liquid-crystalline material even further the transition to either crystalline state or to another, more ordered liquid-crystalline phase occurs. In smectic liquid crystals (from Greek $\sigma\mu\epsilon\gamma\mu\alpha$ for soap), the molecules start to arrange in layers. Here layering denotes that the distribution of centers of mass of the molecules becomes periodic along the director.

Liquid crystals were first recognized as an intermediate state between the liquid and the solid state in 1888 by the botanist Friedrich Reinitzer [2] and in 1889 by Otto Lehman [3]. They studied cholesterol in plants through the microscope as it underwent the melting and they observed that at melting the crystal became "cloudy", but fluid. As the cholesterol was heated even more, it transformed into a transparent liquid. Similar experiments were performed even before that, but before Reinitzer and Lehman nobody thought that the intermediate cloudy liquid was different state of a matter and that its nontransparent appearance was not due to the impurities of the material.

The cloudy or opaque appearance of liquid crystals is due to the thermal collective fluctuations of the macroscopic order. The scattering of visible light by nematics is higher by a factor of the order of 10^6 than the scattering by the isotropic liquid in which the scattering is due to density fluctuations [4,5]. The first detailed experimental studies in the field of light scattering from ordered samples are due to Chatelain [6]. In the 40's of the twentieth century he showed from systematic observations of the Rayleigh scattering that the scattering intensity exhibits a pronounced angular variation. An early model put forward to explain this phenomenon assumed the medium to consist of swarms of aligned molecules or of small crystallites, with dimensions comparable to the optical wavelength. Later it became progressively

clear that the high scattering power was an intrinsic property of nematic phases, i.e., the thermal fluctuations of the alignment.

In bulk the order of the molecules of the nematic liquid crystal depends only on temperature and external electric or magnetic fields. Qualitatively, the system can be described by the phenomenological Landau-de Gennes theory [4], which replaces the microscopic interactions between the molecules by an effective interaction and macroscopic order parameter. Using phenomenological mean-field theory the main features of the liquid crystalline systems near the phase transitions can be described. However, the mean-field description neglects the temporal and spatial fluctuations which are especially important in the vicinity of transitions. The first correction to the mean-field equilibrium description is the study of collective order parameter fluctuations [7].

More frequent and physically interesting are confined liquid crystals which fill the pores in porous media, holes in polymer matrix or the space between the two confining substrates in the slab geometry of the LC displays [8]. In the confined liquid crystals, the equilibrium order as well as dynamic properties attracted a lot of attention of experimentalists and theorists. Studies devoted to the determination of the equilibrium order in different confining geometries with various constraining properties [8] have lately been followed by investigations of the pretransitional dynamics. The understanding of collective order fluctuations gives a better insight into equilibrium ordering in the vicinity of phase and structural transitions as well as in the mechanism of the transition itself [9–16]. In confined liquid-crystalline systems, the order of the molecules does not depend only on the interaction between the constituting molecules but also (mainly) on (i) the lack of the neighboring molecules (interactions) near the surface and (ii) interaction between the molecules of the liquid crystal and the confining substrate which differs from the interactions in the bulk liquid crystal. The confinement of the liquid crystal is in the phenomenological theory usually modeled by a first order symmetrically allowed term [17]. The interaction with the confining substrate can result in higher or lower order than expected in bulk [18,14,15], in the spatial dependence and deformation of the order [19–21], and in partial positional —not only orientational— order [22]. Furthermore, the confinement affects also the pretransitional dynamics, both through changing the equilibrium order and through changing the boundary conditions for the fluctuations themselves [8,14,15,21].

The aim of my thesis is to study the effect of different kinds of substrate–liquid crystal interaction onto the macroscopic order of the liquid crystal in the vicinity of phase and structural transitions. The studied order will be both, the equilibrium order within the phenomenological mean-field theory and the collective pretransitional

excitations. Here, the studied excitations are not only the orientational fluctuations, but fluctuations of all five degrees of freedom of the nematic order. In the studied systems, their contribution to the light scattering is nonnegligible in the vicinity of phase transitions [15,23]. The study is focused into the search and determination of geometries and anchoring conditions for the discontinuous transition characteristic for the isotropic–nematic transition to become continuous. With respect to the extent of the deformation caused by the confinement two categories of systems will be treated: (i) systems with the deformation localized to the vicinity of the confining walls and (ii) systems in which the frustration caused by competing boundary conditions is reflected in deformation spread all over the system.

Among the systems with local deformation of the order the systems characterized with the coexistence of the high-temperature isotropic and low-temperature nematic phase are studied. In such systems one of the phases corresponds to the order in bulk at a given temperature, whereas the other phase is induced by the confinement. The two phases are separated by a broad interface where the order progressively changes from one to the other regime. The nematic order in a semi-infinite system in contact with a single wall has been described 20 years ago [18]. Few years ago the substrate induced nematic order in a thin isotropic film (paranematic phase) has been determined together with the corresponding order parameter fluctuations in the vicinity of the transition to the ordered nematic phase [14]. In this thesis, I will focus on the study of order in a heterophase system with substrates which induce disorder. Beside that, the previous study of the paranematic phase is supplemented by considering different kinds of interaction between the liquid crystal and confining substrates. The work related to the disordering substrates is centered on discussion about the collective fluctuations on approaching the phase transition to the disordered isotropic phase and on determination of conditions where the transition becomes continuous [15,24].

In the study of nonlocal deformation of the nematic order caused by the confinement, the hybrid nematic geometry is taken into account. In hybrid nematic cells the liquid crystal is confined by substrates inducing nematic order in different directions, usually close to being perpendicular. Such cells are mainly used for studying anchoring properties of confining substrates but also as switches. As long as the used hybrid cells are thick enough (∼micrometer) and the liquid crystal is deep in the nematic phase the usual director description even though neglecting the variation of the degree of the nematic order is good enough [19]. Nowadays thinner and thinner films are used in which spatial dependence of the degree of nematic order and the biaxiality of the order can be crucial. The pioneering work in describing the hybrid nematic cell with non-director degrees of freedom of the

nematic order has been done a decade ago by Palffy *et. al* [20]. In the thesis, the hybrid nematic geometry is studied in detail. In cells with the cell thickness up to few 100 nanometers different possibilities of the nematic order are discussed. My original contribution to the study of hybrid nematic cells is associated to the determination of pretransitional collective excitations of all five degrees of freedom of the nematic order parameter [21,23]. The study reveals the mechanism for the structural transition between different ordered configurations. Although the work is done for the simple planar geometry it serves as a model system for studying the line defects in cylindrical cavities. In planar hybrid geometry the frustration is caused by mutually perpendicular induced easy axes whereas in cylindrical geometry the frustration is caused by homeotropic anchoring at the wall and topological favoring of the axial alignment [21,25]. The phenomenological description of the nematic liquid crystal is compared to the results obtained by methods which take into account the microscopic interactions among the liquid crystal molecules [26].

The effect of the confinement is reflected in the variations of fields of macroscopic physical observables with respect to the corresponding fields when there are no walls. The perturbed fields are the order parameter fields in ordered liquids, both corresponding to the equilibrium average value and to collective excitations, and in general, the electromagnetic fields. Their variations give rise to the change of the energy of the system which depends of the separation between walls and as a consequence, forces act among them [27–29]. Due to different properties of the confining walls the forces can be either attractive or repulsive, and the samples of the liquid crystal can be either stable (they wet the substrate) or unstable (they disintegrate into small drops). Thus, the determined ordered structures and pretransitional dynamics are used to study stability of liquid-crystalline systems in corresponding geometry and with appropriate properties of the confining walls [30].

A special interest is paid to the van der Waals force even though it is not described in terms of fluctuating order parameter fields, however, it is strongly affected by the confinement. Since there was no appropriate description of this force for the case of anisotropic media I perform a detailed study of van der Waals force, especially, for the case of uniaxial materials which are most common among nematic liquid-crystalline systems [31].

The outline of the thesis is as follows. First, in Chapter 2 the basic theoretical background used to study the nematic liquid crystals is introduced. In Section 2.1 the nematic order parameter is derived from the microscopic description and its influence on the macroscopic physical observables is emphasized. Section 2.2 deals with basics of the phase transitions. The general introduction of basic terminology

which includes the Landau free energy and correlation length of the order parameter is followed by the description of the phenomenological theory of nematic liquid crystals in the vicinity of the isotropic–nematic phase transition. Then, the correlation lengths of all degrees of freedom of the nematic order are determined and discussed in terms of the type of the phase transition. In Section 2.3 the equations describing dissipative dynamics of the system are derived within the continuum description. After arguing the approximations that are made when performing calculations the equations describing pretransitional collective dynamics in nematic liquid crystals are deduced. Section 2.4 deals with forces that arise as a consequence of the influence of the confinement onto the nematic order and with the stability of thin liquid films which is strongly related to forces acting on it. Structural force is due to the changed equilibrium order and pseudo-Casimir force is caused by the change in spectrum and shape of fluctuations of the order parameter. The van der Waals force, which is also affected by the presence of walls, is discussed in more detail. Since I derive original results for the van der Waals force among uniaxial media the discussion of this force is separated from the discussion of other forces and it is gathered in Chapter 3. Chapter 4 deals with heterophase system characterized by "order-melting" substrates. All through the Chapter, the comparison is made to the inverse heterophase system — the paranematic system. In Section 4.1 the equilibrium order is discussed and in Section 4.2 the pretransitional dynamics is determined. Structural and pseudo-Casimir forces acting on a heterophase system are overviewed in Section 4.3. Nematic and isotropic phase give rise to different dielectric and optical properties of the medium. Therefore, the two phase interface represents an additional wall in the system and van der Waals interaction acts among solid–liquid-crystalline interface and the phase boundary. Its effect on the equilibrium order in the heterophase system is argued in Section 4.4. In Chapter 5 non-local deformations caused by the confinement are discussed. First, different possible equilibrium configurations and the structural transitions between them are introduced in Section 5.1. In Section 5.1.1 they are compared to the ones obtained by Monte Carlo simulations of a hybrid nematic cell. The pretransitional dynamics associated with the structural transition is discussed in Section 5.2. In order to study the stability of thin nematic films subject to hybrid confinement the relevant forces are described in Section 5.3, whereas the study of stability is provided in Section 5.4. The thesis ends with conclusions and discussion of open problems in Chapter 6.

2

Phenomenological description

As explained in the Introduction, my thesis deals with nematic liquid crystals and with how they are affected by the presence of walls. Therefore, in this Chapter we will introduce parameters that describe the nematic liquid crystal and present the theoretical frame within which the liquid-crystalline systems will be described.

2.1 Nematic order parameter

In the isotropic phase the medium possesses full symmetry. On the contrary, in the nematic phase the symmetry is lowered because the molecules exhibit collective orientational order. Lower symmetry corresponds to higher order. This order is reflected in the macroscopic physical quantities characteristic for the system. To express the order of the system quantitatively, we need to define the parameter describing the order — the *order parameter*. The latter has to vanish in the isotropic phase and has to become nonzero in the ordered nematic phase. We will derive the order parameter of the nematic liquid crystal from the microscopic approach.

The nematic liquid crystal consists of rodlike molecules characterized by unit vectors along the long axis of the molecule, $\hat{a}$. The molecule is assumed to have complete cylindrical symmetry about $\hat{a}$ which is realized by fast molecular rotations about this axis. In practice, we can distinguish between the "tail" and the "head" of a molecule, however, there are as much heads pointing in the direction of the director as there are tails pointing in the same direction. The orientation of a single molecule is determined by two angles with respect to the laboratory frame (x, y, z), the polar angle θ and the azimuthal angle ϕ; the z axis coincides with the direction of the director. The state of the alignment of molecules is described by a distribution function $f(\theta, \phi)$ which gives the probability of finding molecules in a solid angle $\mathrm{d}\Omega$, $f(\theta, \phi)\mathrm{d}\Omega/\Omega$. In bulk nematic liquid crystals, the uniaxial symmetry does not allow any ϕ dependence of the distribution function, and so the latter can be expanded in

a series

$$f(\theta) = \sum_{n=0}^{\infty} f_n P_n(\cos\theta), \tag{2.1}$$

where $P_n(x)$ are Legendre polynomials and $f_n = (2n+1)\Omega^{-1}\int \mathrm{d}\Omega f(\theta) P_n(\cos\theta)$. From this and because f is normalized, $\Omega^{-1}\int \mathrm{d}\Omega f(\theta) \equiv 1$, $f_0 = 1$, which does not depend on the ordering of molecules and is, thus, inappropriate as an order parameter. Due to the cylindrical symmetry yielding the equivalence of $\hat{n}$ and $-\hat{n}$, $f_n \equiv 0$ for odd parameters n. From the same argument f_n's are nonzero for even parameters n. The first nonzero parameter is

$$\begin{aligned} f_2 &= \frac{5}{\Omega}\int \mathrm{d}\Omega f(\theta) P_2(\cos\theta) = 5\langle P_2(\cos\theta)\rangle \\ &= 5\left\langle \frac{1}{2}\left(3\cos^2\theta - 1\right)\right\rangle \equiv 5S, \end{aligned} \tag{2.2}$$

where S is a *scalar order parameter* which describes the degree of order of molecules about the average orientation. The value of S is in the interval $[-\frac{1}{2}, 1]$: In the case of a perfect nematic order all molecules point in the direction of the director, $\theta = 0$, and $S = 1$. When the distribution of molecules is uniform over all directions $\langle\cos^2\theta\rangle = \frac{1}{3}$ and $S = 0$. The minimum value of S corresponds to a situation when all molecules lie in the plane perpendicular to the director and there is no preferred direction in this plane. Now, up to the first nontrivial term, the distribution function reads

$$\begin{aligned} f(\theta) &= 1 + 5SP_2(\cos\theta) = 1 + 5S\frac{1}{2}\left(3\cos^2\theta - 1\right) \\ &= 1 + 5S\frac{1}{2}\left(3(\hat{n}\cdot\hat{a})^2 - 1\right) = 1 + 5S\frac{1}{2}\left[3(n_i a_i)(n_j a_j) - 1\right] \\ &= 1 + 5S\frac{1}{2}\left[3(n_i n_j)(a_i a_j) - \delta_{i,j} a_i a_j\right] = 1 + 5S\frac{1}{2}\left(3n_i n_j - \delta_{i,j}\right) a_i a_j \\ &= 1 + 5S\frac{1}{2}\left[3(\hat{n}\otimes\hat{n})_{ij} - (\mathsf{I})_{ij}\right] a_i a_j = 1 + 5(\mathsf{Q})_{ij}\, a_i a_j \end{aligned} \tag{2.3}$$

and

$$\mathsf{Q} = \frac{1}{2}S\left(3\hat{n}\otimes\hat{n} - \mathsf{I}\right) \tag{2.4}$$

is the *tensorial order parameter* of the nematic liquid crystal which represents the quadrupolar moment of the distribution, i.e., deviations from the perfect sphere. Here, I is the second rank unit tensor.

If there are external fields acting on the nematic liquid crystal the cylindrical symmetry of the order can be lost. In that case, the tensorial order parameter is somewhat more complicated. With the procedure similar to the one in Eq. (2.3) one ends up with

$$\mathsf{Q} = \frac{1}{2}S\left(3\hat{n}\otimes\hat{n} - \mathsf{I}\right) + \frac{1}{2}P\left(\hat{e}_1\otimes\hat{e}_1 - \hat{e}_2\otimes\hat{e}_2\right) \tag{2.5}$$

where $P = (3/2)\langle \sin^2\theta \cos 2\phi \rangle$ denotes parameter of biaxiality of order, $\hat{e}_1$ represents a secondary director, and $\hat{n}$, $\hat{e}_1$, and $\hat{e}_2$ form the orthonormal triad.

The full tensorial order parameter has five independent degrees of freedom. This can be easily recognized if one considers, that the order parameter is a second rank symmetrical traceless tensor: The second rank tensor has 9 degrees of freedom. Because it is symmetric, $(\mathsf{Q})_{ij} = (\mathsf{Q})_{ji}$, there are 3 degrees of freedom less, and, finally, the constraint $\mathrm{tr}\,\mathsf{Q} = 0$ reduces the number of independent degrees of freedom for one which leads to only 5 independent degrees of freedom. In the parametrization considered in Eqs. (2.4) and (2.5) these degrees of freedom are two angles determining the orientation of the director, the scalar order parameter, the angle specifying the orientation of the secondary director, and the parameter of biaxiality. In most of the thesis the order parameter will be parameterized with respect to the 5 base tensors of the symmetrical traceless tensor [32,33]

$$\begin{aligned} \mathsf{T}_0 &= \frac{3\hat{n}\otimes\hat{n} - \mathsf{I}}{\sqrt{6}}, \\ \mathsf{T}_1 = \frac{\hat{e}_1\otimes\hat{e}_1 - \hat{e}_2\otimes\hat{e}_2}{\sqrt{2}} &\quad , \quad \mathsf{T}_{-1} = \frac{\hat{e}_1\otimes\hat{e}_2 + \hat{e}_2\otimes\hat{e}_1}{\sqrt{2}}, \\ \mathsf{T}_2 = \frac{\hat{e}_1\otimes\hat{n} + \hat{n}\otimes\hat{e}_1}{\sqrt{2}} &\quad , \quad \mathsf{T}_{-2} = \frac{\hat{e}_2\otimes\hat{n} + \hat{n}\otimes\hat{e}_2}{\sqrt{2}}. \end{aligned} \tag{2.6}$$

All the above tensors are traceless and they are orthogonal with respect to the metric $\mathsf{T}_n : \mathsf{T}_m = \mathrm{tr}\,(\mathsf{T}_n\mathsf{T}_m) = \delta_{n,m}$. (With this the magnitude of a tensor can be defined as $\|\mathsf{A}\| = \sqrt{\mathrm{tr}\,\mathsf{A}^2}$.) In this parametrization the order parameter reads

$$\mathsf{Q} = \sum_{m=-2}^{2} q_m \mathsf{T}_m, \tag{2.7}$$

where $q_m = \mathrm{tr}\,(\mathsf{Q}\mathsf{T}_m)$. The multiplicative constants are set so that the amplitude q_0 represents the scalar order parameter, parameters $q_{\pm1}$ are nonzero if the order is biaxial, and parameters $q_{\pm2}$ represent deviations in the orientation of the director with respect to the assumed director $\hat{n}$. If we interpret the nematic order in the eigenframe it can be schematically visualized by a block with the length of sides equal to $\lambda_i + \lambda_>$, where λ_i's are the eigenvalues of the tensor Q and $\lambda_>$ is the largest of them. In the case of uniaxial order the ratio between the sides is $1 : 1 : 4$. Schematic representation of the nematic order is plotted in Fig. 2.1 together with representation of amplitudes along different base tensors T_i.

The order that is represented by a tensorial order parameter is reflected in its influence on the macroscopic tensorial physical quantities, such as magnetic susceptibility. In the eigenframe, the magnetic susceptibility can be written as

$$\underline{\chi} = \begin{pmatrix} \chi_1 & 0 & 0 \\ 0 & \chi_2 & 0 \\ 0 & 0 & \chi_3 \end{pmatrix}, \tag{2.8}$$

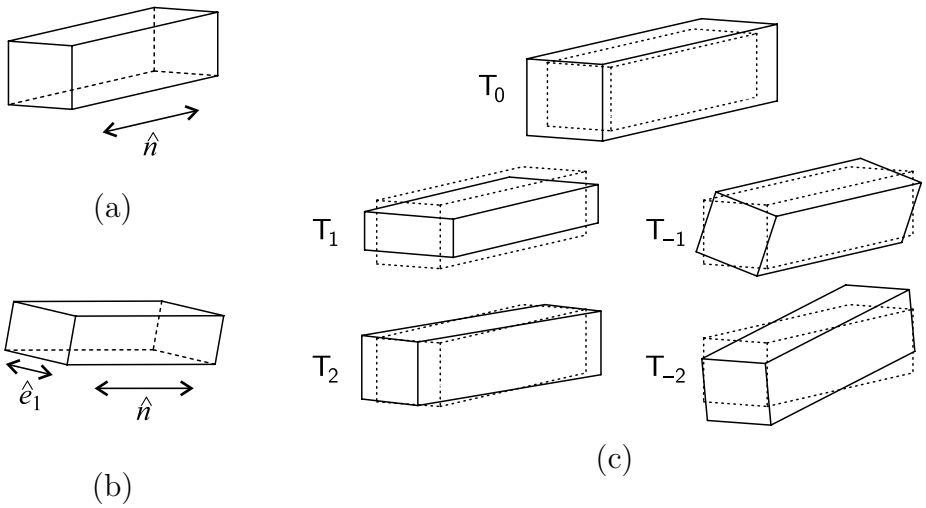

Figure 2.1 Schematic representation of (a) uniaxial and (b) biaxial nematic order. In (c) deviations of amplitudes from the uniaxial nematic order are visualized along base tensors. Variations of the degree of order correspond to a breathing mode (T_0); variations of the degree of biaxiality simultaneously decrease one of the short sides and increase the other by the same amount (T_1), whereas the deviations of the biaxial and nematic director are identified by rotations of the block about the long (T_{-1}) and the two short axes ($\mathsf{T}_{\pm 2}$), respectively.

where $\chi_3 > \chi_1, \chi_2$ are susceptibilities in the direction of the director and in two perpendicular directions $\hat{e}_1$ and $\hat{e}_2$, respectively. By use of the derived order parameter [Eq. (2.5)] and the scalar product $\mathsf{A} : \mathsf{B} = \mathrm{tr}\,(\mathsf{AB})$ it can be rewritten as

$$\underline{\chi} = \frac{2}{3}\chi_a \left[\frac{1}{2} S \left(3\hat{n} \otimes \hat{n} - \mathsf{I}\right)\right] + \chi_b \left[\frac{1}{2} P \left(\hat{e}_1 \otimes \hat{e}_1 - \hat{e}_2 \otimes \hat{e}_2\right)\right] + \chi_i \mathsf{I}. \tag{2.9}$$

Here, $\chi_a = \tilde{\chi}_3 - (\tilde{\chi}_1 + \tilde{\chi}_2)/2$ is the biggest anisotropy of the magnetic susceptibility and $\tilde{\chi}_\alpha = \chi_\alpha / S$ are susceptibilities of the perfectly ordered nematic, $\chi_b = \tilde{\chi}_1 - \tilde{\chi}_2$ is nonzero in biaxially ordered nematic ($\tilde{\chi}_\alpha = \chi_\alpha / P$), and $\chi_i = (\chi_1 + \chi_2 + \chi_3)/3$ is the average magnetic susceptibility, i.e., its isotropic part.

2.2 Phenomenological Landau–de Gennes theory

Before we proceed with the Landau–de Gennes theory of phase transitions in liquid crystals let us first recall the general properties of phase transitions and the basic assumptions within the Landau description of phase transitions.

2.2.1 Landau theory of phase transitions

The term phase transition denotes a change in the medium which is accompanied by discontinuity of some of the thermodynamic potentials and by a change of a certain physical quantity, e.g., density of a medium, macroscopic magnetization or polarization of the material, magnetic, electric and optical properties of the medium, etc. If entropy of the system is a continuous function of thermodynamic variables at the transition then the transition is of *second order* or *continuous* whereas it is of the *first order* or *discontinuous* if the entropy is discontinuous. In the first order transitions, heat is absorbed by the system in going from the low temperature to the high temperature phase. The absorbed heat or the *latent heat* of the transition is $\mathcal{Q}_L = T_c \Delta\mathcal{S}$, where $\Delta\mathcal{S}$ is the difference of the entropies of the two coexisting phases at the transition and T_c is the phase transtition temperature. The two phases of the medium can either possess the same symmetry or the symmetry is changed at the transition. The Landau theory pertains to the latter category of transitions. In the following, the Landau theory will be reviewed [34]. Although it was first established for continuous phase transitions it is used also for describing the discontinuous transitions, however, in this case special care should be taken because the order parameter exhibits a jump at the transition and is, thus, not necessarily small.

In Landau theory, the information about the change of physical quantities as well as of the change of the symmetry of the system is gathered in the order parameter

η_0 which is a macroscopic quantity, $\eta_0 = \mathcal{V}^{-1} \int \mathrm{d}^d r \eta(\vec{r})$, and neglects spatial and temporal fluctuations. The basic concept of the Landau description of phase transitions is the introduction of Landau free energy. The Landau free energy takes into account the symmetry of the system through the power series expansion in terms of the order parameter in the vicinity of the transition. This originates in the Legendre transformation of the grand potential $\Omega(T, h_i)$ of the system with which the external fields h_i related to physical quantities that change with order parameter(s) η_i are replaced by the order parameter(s), $\mathcal{F}(T, \eta_i) = \Omega(T, h_i) + \int \mathrm{d}^d r h_i \eta_i$. From this, the equation of state of the system reads

$$\frac{\partial f}{\partial \eta_i} = h_i, \tag{2.10}$$

where $\mathcal{F} = \int \mathrm{d}^d r f$. When there are no external fields, the equilibrium state is the one that minimizes f. If a solution to Eq. (2.10) with $h_i = 0$ exists for a nonzero η_0 there can be spontaneous order provided that the free energy of the state with nonzero η_0 is lower than the free energy of the state with $\eta_0 = 0$.

The Landau theory assumes that the order parameter is small in the vicinity of the transition so that only the lowest terms required by symmetry and preventing the free energy from diverging are kept in the expansion,

$$f = f_0 + \frac{1}{2} A \eta_0^2 - \frac{1}{3} B \eta_0^3 + \frac{1}{4} C \eta_0^4 + \mathcal{O}(\eta_0^5), \tag{2.11}$$

where f_0 is the free energy density of the disordered phase. Coefficients A, B, and C are determined phenomenologically and are temperature dependent. Coefficient $C > 0$ in order for f to have a local minimum for $\eta_0 < \infty$ whereas the parameter A must change the sign at the temperature below which the solution $\eta_0 = 0$ is not possible anymore so that the solution $\eta_0 > 0$ becomes stable. In the expansion $A = a(T - T^*) + \ldots$ only the first term is taken into account. The transition is discontinuous. Usually, parameters B and C can be regarded as being constants. If at some temperature $B = 0$ the temperature is referred to as a *critical temperature*. In systems with the center of inversion the odd-power terms are not allowed by the symmetry and the phase transition is continuous. If in addition the parameter C is negative in some temperature interval next even-power term has to be added to the expansion and the transition becomes discontinuous. The temperature at which the line of continuous transitions changes to a line of discontinuous transitions between the two phases is denoted as a *tricritical point*.

In the equilibrium, the free energy of the system has its minimum,

$$\begin{aligned} \frac{\partial f}{\partial \eta_0} &= 0 \\ \frac{\partial^2 f}{\partial \eta_0^2} &> 0. \end{aligned} \tag{2.12}$$

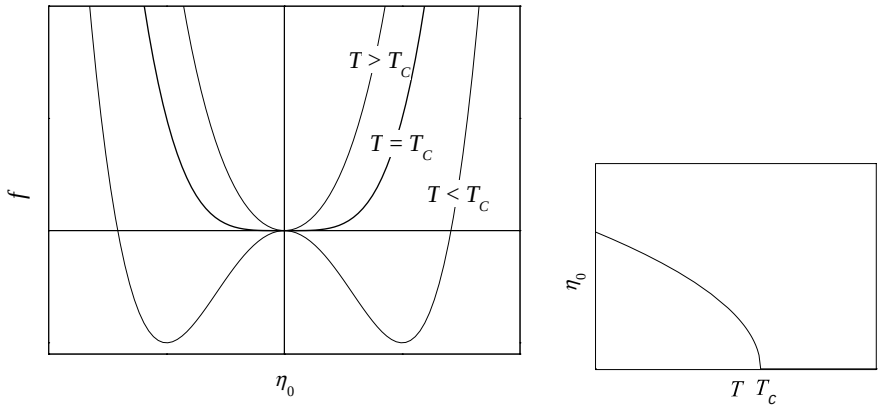

(a) (b)

Figure 2.2 (a) Free energy of a system with a continuous phase transition as a function of the order parameter for various temperatures. (b) Temperature dependence of the order parameter.

If the transition is **continuous** the order parameter $\eta_0^{dis} = 0$ in the disordered phase changes continuously to

$$\eta_0^{ord} = \pm\sqrt{\frac{a}{C}(T - T_c)} \tag{2.13}$$

in the ordered phase which occurs below $T_c = T^*$. Free energy of a system with center of inversion and a continuous phase transition is plotted in Fig. 2.2. In Eq. (2.13) we recognize the well-known critical exponent for the order parameter within the mean-field theories, $\beta = 1/2$. At the phase transition, the first term in Eq. (2.11) vanishes and the free energy of a system is a function of the fourth power of η_0. This means that the free energy of the system is undistinguishable from the equilibrium value even if the order parameter deviates significantly from its equilibrium value. Thus, the continuous phase transition is characterized by increased fluctuations of the order parameter.

At the **discontinuous phase transition** the temperature of the transition is shifted from T^* which is by definition the temperature below which the disordered phase can not exist. Therefore, in the interval $T^* < T < T_c$ the disordered phase with $\eta_0^{dis} = 0$ is metastable whereas it is stable above T_c. Here,

$$T_c = T^* + \frac{2B^2}{9aC}. \tag{2.14}$$

The ordered phase with

$$\begin{aligned} \eta_0^{ord} &= \frac{B}{2C}\left(1 + \sqrt{1 - \frac{4aC}{B^2}(T - T^*)}\right) \\ &= \frac{3}{4}\eta_c\left(1 + \sqrt{1 - 8\theta/9}\right) \end{aligned} \tag{2.15}$$

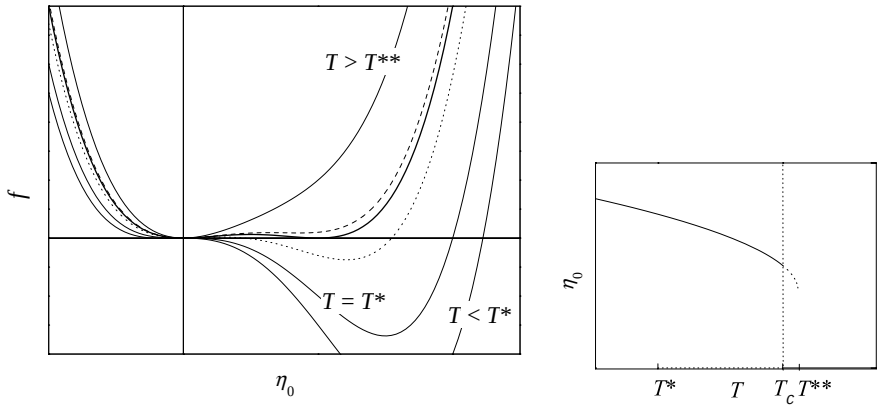

(a) (b)

Figure 2.3 (a) Free energy of a system with a discontinuous phase transition as a function of the order parameter for various temperatures. Dashed and dotted lines correspond to $T_c < T < T^{**}$ and $T^* < T < T_c$, respectively. (b) Temperature dependence of the order parameter in stable (solid line) and metastable state of the appropriate phase (dotted lines).

is stable below T_c and it is metastable in the temperature interval $T_c < T < T^{**} = T^* + B^2/4aC$. Here, $\eta_c = \eta_0^{ord}(T_c)$ and $\theta = (T - T^*)/(T_c - T^*)$. Temperature dependence of the order parameter in (meta)stable (dis)ordered phases is plotted in Fig. 2.3(b) and the free energy of the system as a function of η_0 is plotted in Fig. 2.3(a). The latent heat associated with the transition is

$$\mathcal{Q}_l = T_c \Delta\mathcal{S} = \frac{T_c a \mathcal{V}}{2} \eta_c^2. \tag{2.16}$$

At the phase transition, the free energy has a parabolic shape and the pretransitional fluctuations are much smaller than the pretransitional fluctuations at the continuous transition.

Fluctuations of the order parameter within the mean-field theory

Although in bulk the order is a macroscopic quantity and, on the average, depends only on the external parameters such as temperature, pressure, and external fields, due to finite temperature it is characterized by spatial and temporal deviations from the average value, caused by *thermal fluctuations*. What is important when considering fluctuations is their correlation length which determines how big are the islands characterized by different order. When the correlation length of the fluctuations is small compared to the typical dimensions of the system the fluctuations do not mask the average behavior of the system. On the other hand, highly correlated fluctuations change the order on large scales and perturb the macroscopic appearance of the system. Since we are interested in spatial deviations of the order

parameter with respect to the mean-field value η_0 defined either in Eq. (2.13) or in Eq. (2.15)

$$\eta(\vec{r}) = \eta_0 + \Delta(\vec{r}), \tag{2.17}$$

where $\langle\eta(\vec{r})\rangle = \eta_0$ and $\Delta(\vec{r})$ are spatially-dependent fluctuations, $\langle\Delta(\vec{r})\rangle = 0$. To describe spatial variations of the order parameter a gradient term has to be added in the free energy density which reads in the first nontrivial order $L(\nabla\eta)^2/2$. Here, $L\mathcal{V}^{-2/3}$ is the measure for free energy density associated with deformation of the order parameter and $\mathcal{V}$ is the volume of the system. The correlation function of fluctuations reads

$$\Gamma(\vec{r}) = \langle\eta(\vec{r})\eta(0)\rangle - \langle\eta(0)\rangle^2, \tag{2.18}$$

where we have used the equality $\langle\eta(\vec{r})\rangle = \langle\eta(0)\rangle$ which is due to transitional invariance of the system. Taking into account Eq. (2.17) the correlation function reduces to

$$\Gamma(\vec{r}) = \langle\Delta(\vec{r})\Delta(0)\rangle. \tag{2.19}$$

Because of the continuous translational invariance of the system the functions of $\vec{r}$ can be expanded in a Fourier series, $f(\vec{r}) = \sum_{\vec{q}} \tilde{f}(\vec{q})\, \mathrm{e}^{-i\vec{q}\cdot\vec{r}}$, so that $\tilde{\Gamma}(\vec{q}) = \langle|\tilde{\Delta}(\vec{q})|^2\rangle$. The amplitudes $\tilde{\Delta}(\vec{q})$ are derived from the free energy of the system which can be by applying the Fourier series expansion rewritten in a form

$$\begin{aligned} \mathcal{F} &= \int \mathrm{d}^3 r\; f \qquad (2.20)\\ &= \mathcal{V}(f_0 + \frac{1}{2}A\eta_0^2 - \frac{1}{3}B\eta_0^3 + \frac{1}{4}C\eta_0^4) + \frac{\mathcal{V}}{2}\sum_{\vec{q}}(A - 2B\eta_0 + 3C\eta_0^2 + Lq^2)|\tilde{\Delta}(\vec{q})|^2. \end{aligned}$$

Since the fluctuations are assumed to be small the free energy is written out only up to the quadratic terms in fluctuations. From the equipartition theorem we know that each degree of freedom which enters into the energy with a quadratic term holds the internal energy $k_BT/2$. Taking into account this and the Eq. (2.20) the Fourier transform of a correlation function reads $\tilde{\Gamma}(\vec{q}) = k_BT/\mathcal{V}(A - 2B\eta_0 + 3C\eta_0^2 + Lq^2)$ which gives in the direct space

$$\Gamma(\vec{r}) = \frac{k_BT}{4\pi Lr}\, \mathrm{e}^{-r/\xi}. \tag{2.21}$$

Here, $\xi = \sqrt{L/(A - 2B\eta_0 + 3C\eta_0^2)}$ is the correlation length of fluctuations. For finite ξ, correlations are weak and decrease exponentially whereas for infinite correlation length the correlations are long-range and decrease inversely with distance.

From the result for η_0 in Eq. (2.13) the correlation lengths in the vicinity of a **continuous transition** ($B = 0$) have the following temperature dependence,

$$\xi = \sqrt{\frac{L}{a(T - T_c)}} \quad ; \quad T > T_c,$$

$$\xi = \sqrt{\frac{L}{2a(T_c - T)}} \quad ; \quad T < T_c. \tag{2.22}$$

On approaching the phase transition the correlation length in both, high temperature disordered phase and low temperature ordered phase, diverges. The critical exponent is in both cases $\nu = 1/2$ which is again the common feature of mean-field theories. Due to fluctuations the islands of ordered (disordered) phase occur in the disordered (ordered) phase. Typical dimension of these islands is the correlation length. Far from the transition the correlation length is small and the islands of (dis)ordered phase do not change the macroscopic behavior of the system. Correlations are smaller in the ordered phase. Getting closer to the transition the dimension of islands grows and, finally, at the transition domains of different order extend over the whole system.

In systems with a **discontinuous phase transition** the correlation lengths in the two phases read

$$\begin{aligned} \xi &= \sqrt{\frac{L}{a(T - T^*)}} \quad ; \quad T > T_c, \\ \xi &= \sqrt{\frac{L}{2a(T^* - T) + B^2(1 + \sqrt{1 + 4aC(T^* - T)/B^2})/2C}} \quad ; \quad T < T_c. \end{aligned} \tag{2.23}$$

Neither of them diverges at the phase transition, however, they diverge at the temperature where the given phase ceases to exist even as a metastable phase. Nondivergent behavior of the correlation length of fluctuations at the transition is a characteristics of a discontinuous phase transition and leads to occurrence of metastable phases and a jump of the order parameter at the transition. At the transition, both of the phases are energetically equally favored, thus, the correlation lengths of fluctuations in both phases are equal there.

Goldstone mode and soft mode

As it was derived in Eq. (2.20) the free energy associated with a certain fluctuation mode is

$$\mathcal{F}_{\vec{q}} = \frac{\mathcal{V}L}{2}(\xi^{-2} + q^2). \tag{2.24}$$

In the following Sections this free energy will be related to the relaxation rate $\mu_{\vec{q}}$ for the decrease of the excited mode, $\mu_{\vec{q}} \propto (\xi^{-2} + q^2)$ and consequently, $\mathcal{F}_{\vec{q}} \propto \mu_{\vec{q}}$. There are two specific types of fluctuation modes in which we will be interested in the study of thermal fluctuations in confined nematic liquid-crystalline systems: Goldstone modes and soft modes.

When the correlation length of fluctuations diverges the relaxation rate of a long wavelength mode ($\vec{q} \to 0$) drops down to 0 — the free energy associated with a deformation caused by the mode is very small. *Soft modes* are modes whose relaxation rate drops to zero at the transition whereas it is nonzero elsewhere. From the consideration of correlation lengths we can deduce that the $\vec{q} = 0$ fluctuation mode of the order parameter characteristic for a given continuous transition belongs to the category of soft modes. On the other hand, the relaxation rate of a *Goldstone mode* drops to zero at the transition and stays critical within the entire range of a given ordered phase. At the phase transition from the disordered to the ordered phase the symmetry of the system is typically lowered. This spontaneous breaking of the symmetry is accompanied by a multiple degeneration of the ground state. The system is brought from one ground state to the other by symmetry operations of the high-symmetry phase. If the broken symmetry is continuous a fluctuation mode occurs whose deformation of the system represents a continuous change from one ground state to another and so on. In the thermodynamic limit with $\vec{q} \to 0$ this excitation does not increase the free energy of the system. The mode is called a Goldstone mode and the condition for its existence is stated in a Goldstone theorem [35–37].

Ginzburg criterion

The measure of the importance of fluctuations of the order parameter is the difference between the order parameter and its mean-field value averaged over the correlation volume $\mathcal{V}_\xi \sim \xi^3$,

$$\delta\eta_{\mathrm{cor}} = \mathcal{V}_\xi^{-1} \int_{\mathcal{V}_\xi} \mathrm{d}^d r \;\; (\eta(\vec{r}) - \eta_0)\,, \tag{2.25}$$

where d is the dimensionality of the system. Fluctuations are negligible if in the ordered phase $\langle(\delta\eta_{\mathrm{cor}})^2\rangle = V_\xi^{-1} \int_{V_\xi} \mathrm{d}^d r \;\Gamma(\vec{r}) \ll \eta_0^2$ [38]. Taking into account previously derived correlation function [Eq. (2.21)] and the mean-field value of the order parameter written out in Eq. (2.13), the criterion for the negligibility of fluctuations reads

$$\left(\frac{T_c - T}{T_c}\right)^{(4-d)/2} \gg \frac{I_d}{\Delta c_{\mathrm{v}} \xi_0^d} \frac{k_B T^2}{2T_c^2}. \tag{2.26}$$

Here, $\Delta c_{\mathrm{v}} = a^2 T_c / 2C$ denotes the difference between heat capacity per unit volume in ordered and disordered phase, and $\xi_0 = \sqrt{L/2aT_c}$ is the bare correlation length. Parameter $I_d = \int \mathrm{d}^d x \; x^{-(d-2)} Y(x)$ depends solely on the dimensionality of the system, whereas the integral $Y(x) = \int_0^\infty \mathrm{d}z \; z^{d-1} \int (\mathrm{d}\Omega_d/(2\pi)^d)\, \mathrm{e}^{iz\cos\theta}/(z^2 + x^2)$ comes from the correlation function, $\Gamma(\vec{r}) = (k_B T / L r^{d-2}) Y(r/\xi)$. The criterion was first derived by Ginzburg [39] which yields the name *Ginzburg criterion*. Although the

criterion was derived by considering fluctuations in the ordered phase it also applies in the disordered phase [38].

For $d > 4$ the left hand side of Eq. (2.26) diverges as T approaches T_c and the Ginzburg criterion is always satisfied near the critical point. On the contrary, for $d < 4$, $|T_c - T|^{4-d}$ tends to zero as $T \to T_c$ and the Eq. (2.26) is never satisfied near the critical point. Thus, the mean-field theory provides an adequate description of continuous transitions for $d > 4$ and it breaks down for $d < 4$. The dimension $d_c = 4$ below which the mean-field theory fails to describe the continuous transition adequately is called the *critical dimension*. For $d < d_c$, the mean-field theory is valid far from the phase transition and up to the Ginzburg temperature T_G,

$$\frac{|T_c - T_G|}{T_c} \sim \left(\frac{k_B I_d}{2\Delta c_\mathrm{v} \xi_0^d} \right)^{2/(4-d)} . \tag{2.27}$$

In systems with $d < d_c$, however, with $\xi_0 \to \infty$ the mean-field theory is valid even close to the transition; $\xi_0 \to \infty$ in systems with long-range forces.

2.2.2 Phase transition in a nematic liquid crystal

Isotropic–nematic phase transitions are typically only weakly discontinuous which is reflected in the narrow interval of metastable phases. Typically, the isotropic phase can be undercooled for ~ 1 K and the nematic phase can be overheated for ~ 0.1 K. Therefore, the isotropic–nematic transition can be described within the Landau theory of phase transitions. Here, we will use the extended theory which permits local variations of order parameter, however, the variations are on the lengthscales much larger than the length of a molecule (typically 1 nm) which preserve continuum description of the system. To do this, the free energy is expanded in a power series of scalar invariants of the order parameter and the gradient terms are considered only up to the quadratic term. The order parameter for the isotropic–nematic transition was derived in Section 2.1. Here, we will use the parametrization in terms of five base tensors in Eqs. (2.6) and (2.7), so that in the uniaxial nematic $\mathrm{tr}\,\mathsf{Q}^2 = S^2$.

The free energy of the system must be invariant to all symmetry operations that preserve the system in the high symmetry phase. The isotropic phase has full symmetry. Scalar invariants of a tensor are its trace and determinant. Both invariants are preserved with rotations, however, the determinant changes sign with reflections. Thus, the free energy is expanded in a power series of traces of powers of the order parameter. As defined in Section 2.1, $\mathrm{tr}\,\mathsf{Q} \equiv 0$, so the first nontrivial term is $\mathrm{tr}\,\mathsf{Q}^2$. The absence of the first order term is in accordance with the existence of the stable high temperature phase with $\mathsf{Q} = 0$. There are no other second order terms than $\mathrm{tr}\,\mathsf{Q}^2$ and there is also only one third order invariant, $\mathrm{tr}\,\mathsf{Q}^3$. It is included in the

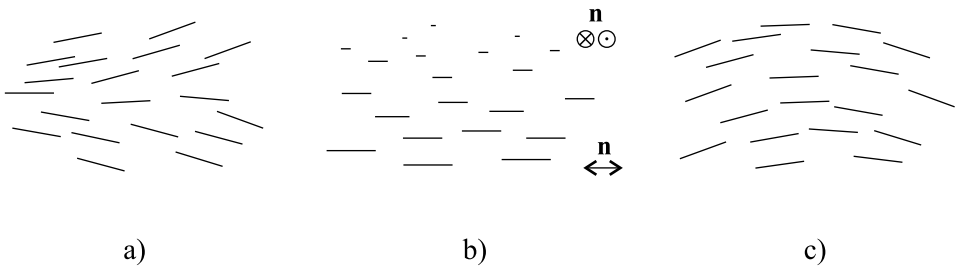

Figure 2.4 Schematic representation of three basic elastic deformations of the director field in an uniaxial nematic liquid crystal: (a) splay with $(\nabla \cdot \hat{n})^2 \neq 0$, (b) twist with $[\hat{n} \cdot (\nabla \times \hat{n})]^2 \neq 0$, and (c) bend with nonzero $[\hat{n} \times (\nabla \times \hat{n})]^2$.

expansion because $\pm\mathsf{Q}$ have different physical meaning; from Eq. (2.9) we can see that for materials with positive magnetic anisotropy, which are studied in this thesis, $\mathsf{Q} > 0$ corresponds to nematic phase in which molecules tend to orient along the director whereas $\mathsf{Q} < 0$ is associated with a nematic phase in which molecules orient in the plane perpendicular to the director. There are two fourth order invariants, $\mathrm{tr}\,\mathsf{Q}^4$ and $(\mathrm{tr}\,\mathsf{Q}^2)^2$, however, for symmetric tensors $\mathrm{tr}\,\mathsf{Q}^4 = (\mathrm{tr}\,\mathsf{Q}^2)^2/2$ and we will use only $(\mathrm{tr}\,\mathsf{Q}^2)^2$ in the expansion. Higher order invariants are not considered here so that the homogeneous part of the free energy density reads

$$f_{hom} = f_{iso} + \frac{1}{2}A(T - T^*)\,\mathrm{tr}\,\mathsf{Q}^2 - \frac{1}{3}B\,\mathrm{tr}\,\mathsf{Q}^3 + \frac{1}{4}C(\mathrm{tr}\,\mathsf{Q}^2)^2, \tag{2.28}$$

where A, B, and C are temperature independent, and T^* is the supercooling temperature. The magnitude of A is typically 10^{-5} J/m^{3}K whereas $B \sim C \sim 10^{-6}$ J/m^3. Since spatial variations of order parameter are allowed gradient terms have to be added to the free energy. There are many symmetry allowed invariants related to gradients of the tensorial order parameter. Up to second order derivatives: $L^{(1)}\mathsf{Q}_{ij,ij}$; $L_1^{(2)}\mathsf{Q}_{ij,k}\mathsf{Q}_{ij,k}$, $L_2^{(2)}\mathsf{Q}_{ij,i}\mathsf{Q}_{kj,k}$, $L_3^{(2)}\mathsf{Q}_{ij,k}\mathsf{Q}_{kj,i}$, $L_4^{(2)}\mathsf{Q}_{ij,ik}\mathsf{Q}_{jk}$, $L_5^{(2)}\mathsf{Q}_{ij,kk}\mathsf{Q}_{ij}$; $L_1^{(3)}\mathsf{Q}_{ij}\mathsf{Q}_{ij,k}\mathsf{Q}_{kl,l}$, $L_2^{(3)}\mathsf{Q}_{ij}\mathsf{Q}_{ik,j}\mathsf{Q}_{kl,l}$, $L_3^{(3)}\mathsf{Q}_{ij}\mathsf{Q}_{ik,k}\mathsf{Q}_{jl,l}$, $L_4^{(3)}\mathsf{Q}_{ij}\mathsf{Q}_{ik,l}\mathsf{Q}_{jk,l}$, $L_5^{(3)}\mathsf{Q}_{ij}\mathsf{Q}_{ik,l}\mathsf{Q}_{jl,k}$, $L_6^{(3)}\mathsf{Q}_{ij}\mathsf{Q}_{ik,l}\mathsf{Q}_{kl,j}$, etc., where $\mathsf{Q}_{ij,k} = \partial\mathsf{Q}_{ij}/\partial x_k$ [40,41]. In the vicinity of the phase transition, one is not interested in elastic deformations of nematic director but rather in spatial variations of the degree of nematic order. Therefore, the pretransitional nematic system is described adequately within the usual one-elastic-constant approximation,

$$f_{el} = \frac{1}{2}L\,\nabla\mathsf{Q} \vdots \nabla\mathsf{Q}. \tag{2.29}$$

Here, $L = L_1^{(2)}$ is typically in order of 10^{-11} N to 10^{-10} N.

Deep in the nematic phase, variations of the scalar order parameter do not play significant role and the main contribution to the elasticity of the system is due to elastic deformations of the director field which contribute to the free energy density

$$f_{el}^{Frank} = \frac{1}{2}\left\{K_{11}(\nabla \cdot \hat{n})^2 + K_{22}[\hat{n} \cdot (\nabla \times \hat{n})]^2 + K_{33}[\hat{n} \times (\nabla \times \hat{n})]^2\right\} \tag{2.30}$$

$$+K_{13}\nabla\cdot[\hat{n}(\nabla\cdot\hat{n})]-K_{24}\nabla\cdot[\hat{n}(\nabla\cdot\hat{n})+\hat{n}\times(\nabla\times\hat{n})].$$

The terms apply to invariants with respect to rotations of the system as a whole, space inversion, and the transformation $\hat{n}\rightarrow-\hat{n}$. Here, the first three terms correspond to three basic deformations of the director field, splay, twist, and bend deformations, respectively. These deformations are schematically represented in Fig. 2.4. The description of the nematic liquid crystal within the frame of elastic deformations of the director whereas the other degrees of freedom of the nematic order are considered to be constant is known as the Frank elastic description [42]. The stiffness of the nematic with respect to a given deformation is determined by parameters K_{ij}; typical magnitude being 10 pN [4]. The other two terms in Eq. (2.30) correspond to splay-twist and saddle-splay deformations, respectively. From their form it can be seen that unlike the three bulklike terms they represent a kind of surface terms, therefore, they are often neglected in studies. In the last decade the interest in these terms was renewed in the studies of spontaneously deformed nematic liquid crystals characterized by stripe-domain structure [43,44]. However, there are still arguments in favor or against these terms. The main reason for that is that unlike the first three terms which are obviously positive definite for the K_{13} and K_{24} terms the existence of the lower limit is not that evident. In fact, it can be shown that the saddle-splay term has the lower limit [45] whereas the K_{13} term does not.

The one-elastic-constant approximation used in Eq. (2.29) corresponds to the case $K_{ii}=K$, $K_{13}=0$, and $K_{24}=K$ in the Frank elastic theory and does not allow any spontaneous deformation of the director field. In the uniaxial nematic liquid crystal parameters L and K relate through $K=9LS^2/2$.

Within the mean-field theory there are no spontaneous elastic deformations since any deformation increases the free energy. As discussed before, if we take into account thermal fluctuations of the director even in bulk the director field is not uniform but bent due to Goldstone director mode. However, when the nematic liquid crystal is subject to interactions with the confining walls the equilibrium order can be also perturbed. In this thesis we are interested in highly constrained nematic liquid crystals where the interaction with the walls and their effect can not be neglected. On the microscopic level, the molecules of the walls and of the liquid crystal attract each other via van der Waals interaction. This interaction is rather short-range since it decreases with distance as $1/r^6$. Therefore, it is assumed that only the molecules that are in a contact with the wall interact with it — contact interaction. On the macroscopic level, this interaction reduces to the quadruple–quadruple interaction and can be, as the interaction between molecules of the liquid crystals, expanded in a power series over scalar invariants. Usually, only the first

order term is taken into account although some experimental evidence suggest that higher orders could be important as well [17,46–48,16]. (Temperature dependence of extrapolation length of the substrate–liquid crystal interaction can not be modelled by taking into account only the quadratic term. This is discussed in more detail in Section 5.4 on page 140.) The contribution from this interaction to the free energy density of a nematic liquid crystal is modeled by an improved expression of the Rapini–Papoular expression [49], first suggested by Nobili and Durand [17],

$$f_S = \frac{1}{2} G \operatorname{tr} (\mathsf{Q} - \mathsf{Q}_{S_i})^2 \delta(z - z_S), \tag{2.31}$$

where G is the strength of the interaction, Q_S is the preferred value of the tensor order parameter at the substrate, and the wall is located at $z = z_S$. In the case of uniaxial nematic order the anchoring strength G can be related to anchoring strength W for the bare director description as $W = 3GS^2$, where S is the scalar order parameter. Often, the anchoring strength is measured in terms of the extrapolation length which denotes the length on which the director field would relax to the one preferred by the substrate. It is the measure for the relevance of the competing elastic distortions vs. violating substrate induced order, $\lambda = K/W$ or, similarly, $\lambda = 3L/2G$. The criterion whether the anchoring is strong or weak is the ratio between the extrapolation length and typical dimension of the system; $\lambda/d \to 0$ corresponds to strong anchoring whereas $\lambda/d \gg 1$ is associated with weak anchoring.

It is useful to rewrite the quantities into a dimensionless form. Thus in the following, all coordinates will be measured in terms of the film thickness d and the correlation length $\xi_{NI} = \zeta d = \sqrt{27CL/B^2} \approx 10$ nm. The order parameter will be rescaled in units of the scalar order parameter of the nematic phase at the phase transition temperature, $S_c = 2B/3\sqrt{6}C$ which is typically between 0.2 and 0.6, and the temperature will be controlled by $\theta = (T - T^*)/(T_{NI} - T^*)$, where $T_{NI} = T^* + B^2/27AC$ is the bulk nematic–isotropic phase transition temperature; the reduced temperatures $\theta = 1$, 0, and 9/8 correspond to the bulk phase transition temperature, and to the supercooling and superheating limits, respectively. Thus, the dimensionless free energy density reads

$$f = f_{iso} + \frac{1}{2}\theta \operatorname{tr} \mathsf{Q}^2 - \sqrt{6} \operatorname{tr} \mathsf{Q}^3 + \frac{1}{2}(\operatorname{tr} \mathsf{Q}^2)^2 + \frac{1}{2}\zeta^2 \nabla\mathsf{Q} \vdots \nabla\mathsf{Q}, \tag{2.32}$$

where f is measured in units of $\tilde{f} = L\xi_{NI}^{-2} S_c^2$ and ∇ corresponds to derivatives with respect to dimensionless coordinates $x_i \leftarrow x_i/d$. The substrate induced contribution to the free energy density is rescaled in

$$f_S = \frac{1}{2} g \operatorname{tr} (\mathsf{Q} - \mathsf{Q}_S)^2 \delta(z - z_S), \tag{2.33}$$

where $g = (\xi_{NI}^2/Ld)G$ or $g = (3\xi_{NI}^2/2d)\lambda^{-1}$ in terms of the extrapolation length. Unless stated otherwise, the calculations will be performed for a nematic liquid crystal 5CB with $A = 0.13\times10^6$ J/m^{3}K, $B = 3.89\times10^6$ J/m^3, $C = 3.92\times10^6$ J/m^3, $L = 9\times10^{-12}$ N, and $T^* = 307.1$ K [50,51]. Here, $S_c \approx 0.27$, $T_{NI} - T^* \approx 1.1$ K, and the latent heat $q_l = B^4/729C^3[T_{NI}/(T_{NI}-T^*)] \approx 1.5\cdot10^6$ J/m^3 which is rather small comparing to the latent heat of the typical first order transition — for melting of ice $q_l = 3.36\cdot10^8$ J/m^3.

2.2.3 Correlation lengths of the nematic order parameter

Again, we will discuss the validity of the mean-field description of the isotropic–nematic phase transition in terms of correlations of fluctuations of the nematic order parameter. In the bulk, the average equilibrium order is uniaxial with the order parameter $\mathsf{Q}_{MF} = \mathsf{A} = a_0\mathsf{T}_0$ and $a_0 = S$. Due to thermal fluctuations, the local order can deviate from the average mean-field value, $\mathsf{Q}(\vec{r}) = \mathsf{A} + \mathsf{B}(\vec{r})$, where $\langle\mathsf{B}(\vec{r})\rangle = 0$ and $\|\mathsf{B}\| \ll \|\mathsf{A}\|$. If B is expanded in terms of the base tensors Eq. (2.6), $\mathsf{B} = \sum_{m=-2}^{2} b_m\mathsf{T}_m$, the free energy density depends only on amplitudes q_m, q being either a or b. By the Fourier expansion and up to the quadratic terms in deviations from the mean-field order, the free energy is decomposed in a mean-field part and a sum of contributions from independent fluctuation modes, $\mathcal{F} = \mathcal{F}_{iso} + \mathcal{V}\tilde{f}(\theta a_0^2/2 - a_0^3 + a_0^4/2) + \sum_m \mathcal{H}_m$, where $\mathcal{H}_m$ is a Hamiltonian associated with a given type of fluctuations,

$$\mathcal{H}_m = \frac{\mathcal{V}\tilde{f}}{2}\xi_{NI}^2 \sum_{\vec{q}} \left(\xi_m^{-2} + q^2\right) |b_{\vec{q}}|^2. \tag{2.34}$$

Here, $\vec{q}$ is the wavevector of a specific fluctuation mode and ξ_m is the correlation length associated with fluctuations of the scalar order parameter ($m = 0$), fluctuations of biaxiality ($m = \pm1$), and director fluctuations ($m = \pm2$), as they were represented in Fig. 2.1(c);

$$\begin{aligned} \xi_0^{-2}/\xi_{NI}^{-2} &= \theta - 6a_0 + 6a_0^2, \\ \xi_{\pm1}^{-2}/\xi_{NI}^{-2} &= \theta + 6a_0 + 2a_0^2, \\ \xi_{\pm2}^{-2}/\xi_{NI}^{-2} &= \theta + 3a_0 + 2a_0^2. \end{aligned} \tag{2.35}$$

Due to the uniaxial symmetry of the nematic phase the two types of fluctuations of biaxiality are degenerated and so are the two types of director fluctuations.

In the isotropic phase, there is no order and all directions are equivalent, therefore, all types of fluctuations must have the same correlation length. Indeed, if we put $a_0 = 0$ in Eqs. (2.35) we find out that the correlation lengths of all degrees of

freedom in the isotropic phase are

$$\xi_I^{-2}/\xi_{NI}^{-2} = \theta. \tag{2.36}$$

As expected, the correlation length does not diverge at the transition where $\theta = 1$, however, it diverges at the supercooling limit of the isotropic phase. On the other hand, in the nematic phase $a_0 = 3/4\,(1 + \sqrt{1 - 8\theta/9})$ and

$$\begin{aligned} \xi_{N,0}^{-2}/\xi_{NI}^{-2} &= \frac{9}{4}\sqrt{1-8\theta/9}\left(1+\sqrt{1-8\theta/9}\right), \\ \xi_{N,\pm1}^{-2}/\xi_{NI}^{-2} &= \frac{27}{4}\left(1+\sqrt{1-8\theta/9}\right), \\ \xi_{N,\pm2}^{-2}/\xi_{NI}^{-2} &= 0. \end{aligned} \tag{2.37}$$

The correlation length of director fluctuations is infinite in the whole range of the stable nematic phase. Director is the order parameter responsible for breaking the full continuous rotational symmetry of the isotropic phase, thus, the director excitation with the infinite wavelength ($\vec{q} \to 0$) is the Goldstone mode. Fluctuations of other degrees of freedom of the nematic order are much more energy consuming. The correlation length of fluctuations of the scalar order parameter diverges at the superheating temperature $\theta^{**} = 9/8$. In the vicinity of the transition to the isotropic phase

$$\begin{aligned} \xi_{N,0}^{-2}/\xi_{NI}^{-2} &\approx 6 - 5\theta, \\ \xi_{N,\pm1}^{-2}/\xi_{NI}^{-2} &\approx 18 - 9\theta. \end{aligned} \tag{2.38}$$

Now we can set the meaning to the correlation length ξ_{NI} — it is the correlation length of fluctuations of the scalar order parameter at the bulk isotropic–nematic phase transition. The hardest type of fluctuations in the uniaxial nematic phase are fluctuations of biaxiality since they oppose to the established symmetry of the phase. Temperature dependence of correlation lengths of different types of fluctuations are depicted in Fig. 2.5.

2.3 Dynamics of the ordered fluid

At a phase transition or on applying external fields the order of the system changes. To describe the changes on the macroscopic level we have to restrict ourselves to phenomena which happen on timescales much larger than the characteristic times for microscopic phenomena — the time between two distinct collisions. The dynamics on the macroscopic level is related to acquiring the equilibrium; the process associated with that is dissipative. In this Section the equations describing the dissipative dynamics will be derived [52,53].

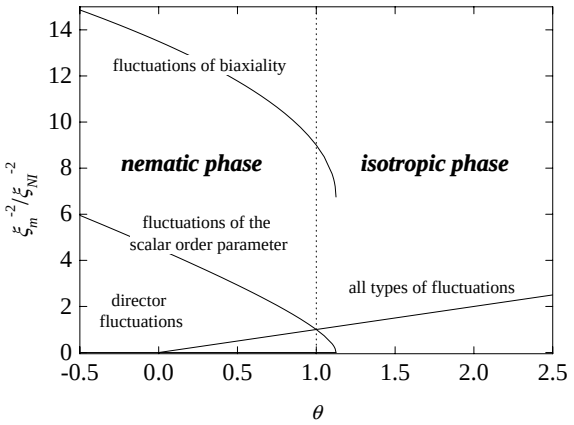

Figure 2.5 Temperature dependence of correlation lengths in the isotropic and nematic phase. Continuations of the lines across the dotted vertical correspond to the correlation lengths in the corresponding metastable phase.

First, we will introduce the basic terminology and physical quantities on the example of a homogeneous body moving in an isotropic liquid. The state and motion of such system is described by a set of macroscopic observables x_i, where $i = 1, .., s$ and s is the total number of degrees of freedom of the system. In general, these are the 3 spatial coordinates, 3 components of the macroscopic velocity of the system, Euler's angles, etc., and components of the order parameter. The entropy of a system is a function of the thermodynamic state of the system, thus, it depends on the just mentioned macroscopic observables, $\mathcal{S} = \mathcal{S}(x_i)$. Let us define thermodynamically conjugate quantities to observables x_i,

$$X_i = -\frac{\partial \mathcal{S}}{\partial x_i}. \tag{2.39}$$

With these, the production of the entropy can be written as

$$\dot{\mathcal{S}} = \frac{\mathrm{d}\mathcal{S}}{\mathrm{d}t} = -\sum_{i=1}^{s} X_i \dot{x}_i. \tag{2.40}$$

In the equilibrium, the entropy reaches its maximum, $\mathrm{d}\mathcal{S} = \sum \partial \mathcal{S}/\partial x_i \ \mathrm{d}x_i = 0$, which is realized if $X_i = 0$ for each i. Simultaneously, the production of entropy is equal to 0. The production of entropy accompanies irreversible processes, i.e., the approach of the equilibrium. Thus, the system which approaches the thermal equilibrium acts like an origin of the entropy. So far as the state of the system is not too far from the equilibrium the linear relations between "flows" x_i's and "forces" X_i's can be assumed [54],

$$\dot{x}_i = -\sum_{j=1}^{s} \gamma_{ij} X_j, \tag{2.41}$$

with *kinetic coefficients* γ_{ij}. (The relaxation of slightly non-equilibrium system is described by $\dot{x}_i = -\sum_j \lambda_{ij} x_j$. From the definition of X_i in Eq. (2.39) and, again, not to far from the equilibrium, the thermodynamic conjugate X_i's can be expanded in $X_i = \sum_j \beta_{ij} x_i$, where $\beta_{ij} = -\partial^2 S/\partial x_i \partial x_j$ and, thus, $\beta_{ij} = \beta_{ji}$. Then, by expressing x_i from the latter expansion and by using this in the expression for $\dot{x}_i$ the Eq. (2.41) follows directly [52].) In 1931 Onsager showed that from the reversibility of dynamical laws governing the microscopic processes behind observable macroscopic phenomena

$$\gamma_{ij} = \gamma_{ji}, \tag{2.42}$$

which is known as the Onsager's reciprocity principle [55,54].

The state of a rigid body under a dissipative motion in a viscous medium is described by generalized coordinates Q_i and impulses P_i, where $i = 1, .., s$. If $\mathcal{H} = \mathcal{H}(Q_i, P_i)$ is the energy of a system then the non-dissipative motion is determined by

$$\dot{P}_i = -\frac{\partial \mathcal{H}}{\partial Q_i}, \tag{2.43}$$

where $P_i = \partial \mathcal{H}/\partial \dot{Q}_i$. When the processes become dissipative the dissipative terms introduced in Eq. (2.41) have to be added to equations of motion [Eq. (2.43)],

$$\dot{P}_i = -\frac{\partial \mathcal{H}}{\partial Q_i} - \sum_{j=1}^{s} \gamma_{ij} X_{P_j}. \tag{2.44}$$

The deviation of the entropy of a closed system, which is not in its equilibrium, from its maximum value equals $\Delta \mathcal{S} = -A_{\min}/T$, where $A_{\min}$ is the minimum work required to bring the system (body in a system) in the given non-equilibrium state and T is the temperature of the system [52]. In the case discussed here $A_{\min} = \Delta \mathcal{H}$, thus, $X_{P_i} = -\partial \mathcal{S}/\partial P_i = 1/T(\partial \mathcal{H}/\partial P_i) = \dot{Q}_i/T$ and $\left(\dot{P}_i\right)_{\text{dis}} = -\sum_{j=1}^{s} \gamma_{ij} \dot{Q}_j$, where $\gamma_{ij} \leftarrow \gamma_{ij}/T$. Since the matrix $\underline{\gamma}$ is fully symmetric the latter eqution can be reduced to $(\dot{P}_i)_{\text{dis}} = -\partial \mathcal{D}/\partial \dot{Q}_i$, where

$$\mathcal{D} = \frac{1}{2} \sum_{i,j=1}^{s} \gamma_{ij} \dot{Q}_i \dot{Q}_j \tag{2.45}$$

is a bilinear form of velocities, which is called the *dissipation function*. Now, the equations of motion can be rewritten in

$$\dot{P}_i = -\frac{\partial \mathcal{H}}{\partial Q_i} - \frac{\partial \mathcal{D}}{\partial \dot{Q}_i}. \tag{2.46}$$

Temporal evolution of the system is determined by a reactive part and a dissipative part describing the part of the energy of the system which converts into heat. The

rate of the decrease of the energy of the system is thus, $\dot{\mathcal{H}} = \sum_i [\dot{Q}_i(\partial\mathcal{H}/\partial Q_i) + \dot{P}_i(\partial\mathcal{H}/\partial P_i)] = \sum_i \dot{Q}_i[(\partial\mathcal{H}/\partial Q_i) + \dot{P}_i] = -\sum_i \dot{Q}_i(\partial\mathcal{D}/\partial\dot{Q}_i) = -2\mathcal{D}$.

The above derived equations of a dissipative motion can be generalized for macroscopic motion of continuum media such as liquids and liquid crystals. Here, we have to take into account the spatial dependence of macroscopic velocity as well as of macroscopic observables. In that case, the entropy of the system is a function of macroscopic observables and their gradients, $\mathcal{S} = \int \mathrm{d}^3 r\ s(x_i, \nabla x_i)$. The production of entropy is then

$$\begin{aligned} \dot{\mathcal{S}} &= \int \mathrm{d}^3 r\ \dot{s} = \int \mathrm{d}^3 r\ \sum_i \left(\frac{\partial s}{\partial x_i}\dot{x}_i + \frac{\partial s}{\partial \nabla x_i}\nabla \dot{x}_i \right) \\ &= \int \mathrm{d}^3 r \sum_i \left(\frac{\partial s}{\partial x_i} - \nabla \frac{\partial s}{\partial \nabla x_i} \right) \dot{x}_i + \int \mathrm{d}^3 r \sum_i \nabla \cdot \left(\frac{\partial s}{\partial \nabla x_i}\dot{x}_i \right), \end{aligned} \tag{2.47}$$

where the first term can be rewritten in terms of products of flows $\dot{x}_i$ and forces X_i,

$$X_i = -\frac{\partial s}{\partial x_i} + \nabla \frac{\partial s}{\partial \nabla x_i}, \tag{2.48}$$

which determine the dissipative nature of the motion. The second term in production of entropy, $\int \mathrm{d}^3 r \sum_i \nabla \cdot [\dot{x}_i(\partial s/\partial \nabla x_i)] = \sum_i \oint_S \mathrm{d}\vec{S} \cdot [\dot{x}_i(\partial s/\partial \nabla x_i)]$, corresponds to dissipation of energy on the surfaces. This can be neglected in bulk systems, however, we will neglect it even in the case of systems with high surface-to-volume ratio.

The deviation of the entropy density from its maximum value is again related to the minimum work required to bring the system in a given non-equilibrium state, $\delta s = -a_{\min}/T$. Due to inhomogeneity of the system we do not now the exact amount of this work, however, we know that it depends on variations of macroscopic observables and their gradients which cause internal friction in the system. The change of the macroscopic velocity for a constant value or the rotation of a system as a whole do not cause any relative internal motion, thus, they do not contribute to the dissipation. Therefore, the minimum work and consequently, the dissipation function do not depend on velocity but rather on its gradient. The work related to changes of the order of the system is phenomenologically determined to be equal to $f(\eta, \nabla\eta)$ as it was written out in Eqs. (2.11) and (2.32). In addition to these contributions there is also a contribution which couples the velocity field and the order of a system.

The equations of motion of a continuum system are written in the same way as for the rigid body [Eqs. (2.44) and (2.46)], however, the energy $\mathcal{H}$ has to be replaced by the energy density $h = \mathcal{H}/\mathcal{V}$. The dissipative part of equation is described by a dissipation function which is constructed to be a bilinear form of invariants of macroscopic observables and their gradients allowed by symmetry. Coefficients

before the terms are determined phenomenologically. The state of the system and its dynamic behavior is further determined by the dynamics of the order parameter(s),

$$\dot{\eta} = -\frac{\partial \mathcal{D}}{\partial \eta}. \tag{2.49}$$

The evolution of the order is purely dissipative. In general, it is coupled to gradients of the velocity field which makes the description even harder.

The energy density of an isotropic fluid reads

$$h = \frac{1}{2}\rho \vec{v}^2 + p, \tag{2.50}$$

where ρ is the density of the fluid, $\vec{v}$ is the spatially dependent macroscopic flow, and p is the pressure in a given point. The state of the system in a point $\vec{r}$ is described by the impulse $\vec{p} = \partial h/\partial \vec{v} = \rho \vec{v}$. The reactive part of the equation of motion then reads $\rho \dot{\vec{v}} = -\nabla p$, where $\dot{\vec{v}}$ is the material time derivative of the velocity, $\dot{\vec{v}} = \partial \vec{v}/\partial t + (\vec{v} \cdot \nabla)\vec{v}$. Taking into account the dissipative nature of the motion, $X_{\vec{p}} = -(1/T)\nabla \cdot (\partial a_{\min}/\partial \nabla \vec{p})$, where we have taken into account that $a_{\min}$ depends solely on gradient of the velocity. From this, the equation of motion reads

$$\rho \dot{\vec{v}} = -\nabla h + \nabla \cdot \frac{\partial \mathcal{D}}{\partial \nabla \vec{v}}, \tag{2.51}$$

where $(\partial \mathcal{D}/\partial \nabla \vec{v}) = \underline{\gamma}(\partial a_{\min}/\partial \nabla \vec{v})$ and $\mathcal{D}$ is the dissipation function which is in the case of isotropic fluid $\mathcal{D} = [\eta'(\nabla \vec{v}) : (\nabla \vec{v}) + \eta'' \operatorname{tr}(\nabla \vec{v})^2 + \eta'''(\operatorname{tr} \nabla \vec{v})^2]/2$. The viscous coefficients η', η'', and η''' are determined phenomenologically. In incompressible fluids $\eta''' \equiv 0$, whereas $\eta' = \eta''$ because $\mathcal{D}$ must be zero for pure rotations, $\vec{v} = \vec{\omega} \times \vec{r}$. Taking into account all these, the Eq. (2.51) reduces to the well-known Navier–Stokes equation,

$$\rho \frac{\partial \vec{v}}{\partial t} + \rho(\vec{v} \cdot \nabla)\vec{v} = -\nabla p + \eta' \nabla^2 \vec{v}. \tag{2.52}$$

In the anisotropic liquid, the dissipation is also due to variations of the order parameter(s). Therefore, first, terms bilinear in invariants of the order parameter and, secondly, terms coupling the order and the motion of the system, have to be added in the dissipation function. The latter terms, denoted as $\mathcal{D}^a$, depend on the character of the order parameter and will be written out at the end of this Section. The dissipative terms related solely to the variations of order can be written out in terms of linear laws,

$$\dot{\eta} = -\gamma' X_\eta - \frac{\partial \mathcal{D}^a}{\partial \eta}, \tag{2.53}$$

where by definition $X_\eta = \nabla \cdot [\partial s/\partial(\nabla \eta)] - (\partial s/\partial \eta)$. The change of the entropy density due to variations of the order parameter, $s = -f(\eta, \nabla \eta)/T$, thus,

$$\dot{\eta} = \gamma \left(\nabla \cdot \frac{\partial f}{\partial \nabla \eta} - \frac{\partial f}{\partial \eta} \right) - \frac{\partial \mathcal{D}^a}{\partial \eta}. \tag{2.54}$$

The left-hand side of Eq. (2.54) and the second term of its right-hand side are associated with the friction whereas the force X_η corresponds to the generalized elastic force which is due to the macroscopic order. In equilibrium, both forces are equal to 0. Due to the macroscopic order the equation of motion changes as well,

$$\rho\frac{\partial\vec{v}}{\partial t}+\rho(\vec{v}\cdot\nabla)\vec{v}=-\nabla p+\eta'\nabla^2\vec{v}+\nabla\cdot\frac{\partial\mathcal{D}^a}{\partial\nabla\vec{v}}. \tag{2.55}$$

The part of the dissipation function which couples the macroscopic flow and the order in the system is a bilinear form of gradients of velocity and the order parameter. In the case of a **scalar order parameter** bilinear invariants coincide with scalar invariants of gradients of velocity, thus,

$$\mathcal{D}^a=\frac{1}{2}\alpha_1\eta^2(\,\mathrm{tr}\,\nabla\vec{v})^2+\frac{1}{2}\alpha_2\eta^2\,\mathrm{tr}\,(\nabla\vec{v})^2+\frac{1}{2}\alpha_3\eta^2\nabla\vec{v}:\nabla\vec{v}. \tag{2.56}$$

For the **vectorial order parameter**, $\eta\rightarrow\vec{\eta}$,

$$\mathcal{D}^a=\frac{1}{2}\alpha_1(\vec{\eta}\cdot\nabla\vec{v})^2+\frac{1}{2}\alpha_2(\nabla\vec{v}\cdot\vec{\eta})^2+\frac{1}{2}\alpha_3(\vec{\eta}\cdot\nabla\vec{v})\cdot(\nabla\vec{v}\cdot\vec{\eta}), \tag{2.57}$$

whereas in the case of a **tensorial order parameter**, $\eta\rightarrow\underline{\eta}$,

$$\begin{aligned}\mathcal{D}^a &= \frac{1}{2}\alpha_1(\underline{\eta}:\nabla\vec{v})^2+\frac{1}{2}\alpha_2(\nabla\vec{v}\underline{\eta}):(\nabla\vec{v}\underline{\eta})+\frac{1}{2}\alpha_3(\nabla\vec{v}\underline{\eta}):(\underline{\eta}\nabla\vec{v})\\ &+\frac{1}{2}\alpha_4(\underline{\eta}\nabla\vec{v}):(\nabla\vec{v}\underline{\eta})+\frac{1}{2}\alpha_5(\underline{\eta}\nabla\vec{v}):(\underline{\eta}\nabla\vec{v})+\frac{1}{2}\alpha_6(\nabla\vec{v}:\underline{\eta})(\underline{\eta}:\nabla\vec{v})\\ &+\frac{1}{2}\alpha_7[\,\mathrm{tr}\,(\underline{\eta}\nabla\vec{v})]^2+\frac{1}{2}\alpha_8\,\mathrm{tr}\,(\underline{\eta}\nabla\vec{v}\nabla\vec{v}\underline{\eta})+\frac{1}{2}\alpha_9\,\mathrm{tr}\,(\underline{\eta}\nabla\vec{v})^2.\end{aligned} \tag{2.58}$$

In the case of a symmetric, traceless, second rank tensor the dissipation function $\mathcal{D}^a$ is less complicated since $(\underline{\eta}:\nabla\vec{v})^2=(\nabla\vec{v}\underline{\eta}):(\underline{\eta}\nabla\vec{v})=(\underline{\eta}\nabla\vec{v}):(\nabla\vec{v}\underline{\eta})=(\nabla\vec{v}:\underline{\eta})(\underline{\eta}:\nabla\vec{v})=[\,\mathrm{tr}\,(\underline{\eta}\nabla\vec{v})]^2=\,\mathrm{tr}\,(\underline{\eta}\nabla\vec{v})^2=[\hat{n}\cdot\nabla\vec{v}\cdot\hat{n}]^2$.

In the case of anisotropic liquids, due to the coupling between the macroscopic motion and the order of the system the description of dissipative processes is rather complex. One has to deal with (1 + 3 + the number of components of the order parameter) coupled partial differential equations: $\nabla\cdot\vec{v}=0$ for the incompressible fluid, and Eqs. (2.55) and (2.54), for the same number of observables: pressure, 3 components of the velocity field, and independent degrees of freedom of the order parameter. However, in nematic liquid crystals the typical time for equilibration of the velocity field, $\tau_{\vec{v}}\propto 1/\eta'$, is several orders of magnitude smaller than the typical time $\tau_{\hat{n}}$ for the relaxation of the nematic director, $\tau_{\vec{v}}/\tau_{\hat{n}}\sim 10^{-6}$ [4,56]. Thus, the adiabatic approximation which assumes the velocity field to immediately follow the orientational changes of the system is not far from reality. In the following, we will be interested in pretransitional dynamics of the liquid crystal without any macroscopic

motion. If there is no macroscopic velocity when the system is far from the phase transition and if the transition is approached with small and slow changes, within the adiabatic approximation, no motion will be induced. In that case the dissipative equations derived in this Section reduce to

$$\frac{\partial \eta}{\partial t} = -\gamma \frac{\delta f}{\delta \eta}, \tag{2.59}$$

where $\delta/\delta\eta = \partial/\partial\eta - \nabla\cdot(\partial/\partial\nabla\eta)$ denotes functional derivative with respect to η and γ^{-1} is a generalized viscosity associated with the relaxation of the order parameter.

The same result could be obtained also directly from the Landau–Khalatnikov equation [7]. In 1954 Landau and Khalatnikov proposed that in the case of a non-equilibrium configuration of the order parameter the latter relaxes to the equilibrium value as $\mathrm{d}\eta/\mathrm{d}t = -\Gamma^{-1}\partial\Phi/\partial\eta$, where Φ is the appropriate thermodynamic potential, and Γ is a generalized viscosity coefficient. Now, the equation is known also as a time-dependent Ginzburg–Landau model (TDGL) [38]. The Landau–Khalatnikov equation obtained in Eq. (2.59) can be understood as follows: The equilibrium configuration of the order parameter is determined by the minimum of the free energy, $\delta\mathcal{F} = \int \mathrm{d}\mathcal{V}\delta f(\eta, \nabla\eta) = \int \mathrm{d}\mathcal{V}(\delta f/\delta\eta)\delta\eta$, which is satisfied for $\delta f/\delta\eta = 0$. If the system is out of the equilibrium $\delta f/\delta\eta$ acts like a generalized elastic force which is balanced by viscous forces. When the macroscopic velocity can be neglected the viscosity is related solely to the rate of change of the order parameter $\dot{\eta}$.

2.3.1 Pretransitional collective dynamics in a nematic liquid crystal

In the equilibrium, the macroscopic order corresponds to the minimum of the free energy. Due to $T > 0$ there are motions on the microscopic level which can result in a collective motion — thermal excitations with characteristic energy $k_B T$. When the system is excited out of the equilibrium it relaxes back following the relaxation equation [Eq. (2.59)]. For the nematic liquid crystal with a tensorial order parameter the generalized viscosity is in general a tensor. In the ordered phase, one can expect that due to the anisotropy of the order the viscosities differ with respect to directions along different eigenvectors. In nonhomogeneously ordered nematic the generalized viscosity can be also spatially dependent. However, in order to simplify the description the generalized viscosity will be assumed to be isotropic with the effective value equal to the average viscosity, $\underline{\gamma}^{-1} = \gamma^{-1}\mathsf{I}$. In the case of a nematic liquid crystal with the free energy density written out in Eqs. (2.32) and (2.33) the relaxation equation reads

$$\frac{\partial \mathsf{Q}}{\partial t} = -\theta\mathsf{Q} + 3\sqrt{6}\,\overleftrightarrow{\mathsf{Q}^2} - 2\mathsf{Q}\,\mathrm{tr}\,\mathsf{Q}^2 + \zeta^2\nabla^2\mathsf{Q}, \tag{2.60}$$

where time is measured in units of time $\tau_a = 27C\gamma^{-1}/B^2$, which is related to the relaxation of the alignment, $t \leftarrow t/\tau_a$. The value of $\tau_a \sim 10^{-8}$ s is determined phenomenologically [32]; typical values of the effective generalized viscosity are $\gamma^{-1} \sim 0.01$ kg/ms [4]. The operator $\overleftrightarrow{\ldots}$ denotes the traceless part of the tensor in question. The surface part of the free energy is non-negligible only in the immediate proximity of the confining wall, thus, it reduces to boundary conditions for the order parameter,

$$(\hat{n}_S \cdot \nabla)\mathsf{Q} = \pm\frac{g}{\zeta^2}\left(\mathsf{Q} - \mathsf{Q}_S\right)\Big|_{\text{on surface}}, \tag{2.61}$$

where $\hat{n}_S$ is the surface normal and $\pm$ correspond to the wall placed at $\vec{r}_S$ where $\vec{r}_S + \vec{\epsilon}$ is either within the liquid crystal or outside, respectively. As already mentioned, the dissipation of energy on the confining substrates is neglected in this study. Usually, the motion of molecules close to the substrates is hindered due to the anchoring and the energy dissipated at the substrate can be assumed very small. If this would not be the case, the second term in Eq. (2.47) would contribute to the boundary conditions as well.

In the equilibrium, $\mathsf{Q} = \sum_{i=-2}^{2} a_i(\vec{r})\mathsf{T}_i$ is not time-dependent and the Eq. (2.60) reduces to five coupled, scalar, differential equations for five scalar amplitudes $a_i(\vec{r})$,

$$0 = -\left(\theta - \zeta^2\nabla^2\right)a_i + 3\sqrt{6}\sum_{j,k=-2}^{2} a_j a_k \,\mathrm{tr}\left(\mathsf{T}_i\mathsf{T}_j\mathsf{T}_k\right) - 2a_i\sum_{j=-2}^{2} a_j^2, \tag{2.62}$$

with boundary conditions

$$(\hat{n}_S \cdot \nabla)a_i = \pm\frac{g}{\zeta^2}(a_i - a_{i,S})\Big|_{\text{on surface}}. \tag{2.63}$$

Here, it was assumed that the system can be described by a constant set of base tensors T_i which is usually true in planar geometry and in some special cases in curved geometries. In a particular geometry and with given anchoring conditions the problem is generally simplified, since due to the symmetry reasons some of the amplitudes are equal to 0. In addition to that, only few of the products $\mathsf{T}_i\mathsf{T}_j\mathsf{T}_k$ have a nonzero trace; the combinations of base tensors which have a nonzero trace are listed in Table 2.1. In planar geometry, in the case of a uniaxial nematic order ($a_{i\neq 0} = 0$) one is left with only one scalar equation.

When considering pretransitional collective dynamics let us repeat that the derived equations hold for states not far from the equilibrium. Thus, the order can be assumed to be only slightly perturbed with respect to the equilibrium value, $\mathsf{Q}(\vec{r},t) = \mathsf{A}(\vec{r}) + \mathsf{B}(\vec{r},t)$, where A is the equilibrium order parameter determined by the mean-field theory [Eq. (2.62)] and B is a small fluctuating part,

Table 2.1 List of products of up to three base tensors T_α with nonzero trace: $\mathrm{tr}\,\mathsf{T}_i = 0$, $\mathrm{tr}\,(\mathsf{T}_i\mathsf{T}_j) = \delta_{i,j}$, and $\mathrm{tr}\,(\mathsf{T}_i\mathsf{T}_j\mathsf{T}_k)$ is as follows in the Table. Base tensors are defined in Eq. (2.6).

i	j	k	$\mathrm{tr}\,(\mathsf{T}_i\mathsf{T}_j\mathsf{T}_k)$
0	0	0	$1/\sqrt{6}$
0	±1	±1	$-1/\sqrt{6}$
0	±2	±2	$1/2\sqrt{6}$
1	±2	±2	$\pm1/2^{3/2}$
2	-1	-2	$1/2^{3/2}$

$\|\mathsf{B}\| \ll \|\mathsf{A}\|$. If B is small it can be assumed to be governed by a linearized form of equation of motion [Eq. (2.60)], which is equivalent to describing fluctuations within the harmonic approximation. The linearized form of the relaxation equation, $\dot{\mathsf{B}} = -(\partial^2 f/\partial\mathsf{A}^2)\mathsf{B} + \zeta^2\nabla^2\mathsf{B}$, reads

$$\frac{\partial\mathsf{B}}{\partial t} = -\theta\mathsf{B} + 3\sqrt{6}(\mathsf{AB}+\mathsf{BA}) - 2\mathsf{B}\,\mathrm{tr}\,\mathsf{A}^2 - 4\mathsf{A}\,\mathrm{tr}\,(\mathsf{AB}) + \zeta^2\nabla^2\mathsf{B}, \tag{2.64}$$

or in terms of amplitudes b_i, $\mathsf{B}(\vec{r},t) = \sum_{i=-2}^{2} b_i(\vec{r},t)\mathsf{T}_i$,

$$\frac{\partial b_i}{\partial t} = -\theta b_i + 6\sqrt{6}\sum_{j,k=-2}^{2} a_j b_k\,\mathrm{tr}\,(\mathsf{T}_i\mathsf{T}_j\mathsf{T}_k) - 2b_i\sum_{j=-2}^{2} a_j^2 - 4a_i\sum_{j=-2}^{2} a_j b_j + \zeta^2\nabla^2 b_i \tag{2.65}$$

with boundary conditions

$$(\hat{n}_S\cdot\nabla)b_i = \pm\frac{g}{\zeta^2}b_i\Big|_{\text{on surface}}. \tag{2.66}$$

In general, the fluctuations of five independent degrees of freedom of the nematic order are a solution of five coupled scalar, partial differential equations. In the case of a uniaxial equilibrium nematic order, when only the amplitude a_0 is nonzero, the Eqs. (2.65) uncouple. They correspond to fluctuations of the scalar order parameter, fluctuations of the biaxiality, and director fluctuations as denoted in Section 2.2.3 and schematically represented in Fig. 2.1 (c). Time dependence of the fluctuation modes which are described by relaxation is the exponential decay, $b_i \propto \mathrm{e}^{-\mu_i t}$, where μ_i is the relaxation rate of a given fluctuation mode. If we take into account this and compare Eq. (2.64) to Eqs. (2.20) and (2.24) we can see that $\mu_i = \zeta^2(\xi_i^{-2} + \nabla^2)$ is closely related to the free energy of the corresponding mode, which we have already used in the discussion of soft and Goldstone modes.

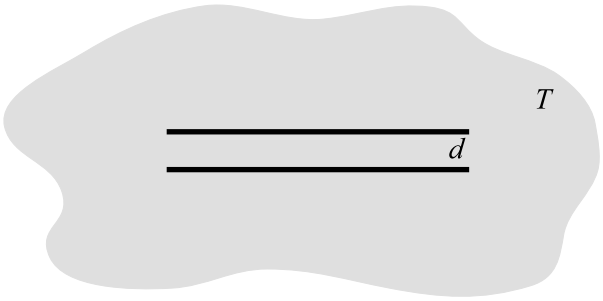

Figure 2.6 Schematic representation of the confined liquid-crystalline system in which by changing the distance between the confining walls the volume and the surface of the liquid crystal are preserved.

2.4 Forces acting on a thin liquid-crystalline film

The presence of walls causes the change of the energy of the system. In general, this change depends on the separation between the walls which, thus, results in an attractive or repulsive force between them. In this thesis, the state of the system will be described by a free energy rather than by its energy. Here, by system we refer to the liquid crystal in which the confining walls are immersed, so that the volume and the surface of the liquid crystal are preserved by changing the separation between walls (see Fig. 2.6). To relate the free energy of the system to the force, the force is expressed as a gradient of a potential, i.e., $\vec{F} = -\nabla\phi$, which can be done for all conservative forces. Here, $\mathrm{d}\phi = A$ is the amount of work required in order to move the walls to a new separation $\vec{r} + \mathrm{d}\vec{r}$. The free energy of the system and the work are related by the thermodynamic relation, $\mathrm{d}\mathcal{F} = \mathrm{d}A - \mathcal{S}\mathrm{d}T$, where $\mathcal{S}$ is the entropy of the system. In an isothermal process the force is related to the free energy of a system as

$$\vec{F} = -\frac{\partial \mathcal{F}}{\partial \vec{r}}. \tag{2.67}$$

In the planar parallel system consisting of two infinitely large surfaces, the force is perpendicular to the surfaces and, consequently, $F = -(\partial\mathcal{F}/\partial d)$, where d is the separation between the two objects. The positive value of F corresponds to repulsive force and the negative value corresponds to the attractive force.

In all studied systems it is assumed that there are no free electric charges. Further, the permanent electric dipoles of the liquid-crystalline molecules are assumed small, so that the electrostatic interaction can be safely neglected. The thermal fluctuations of the electromagnetic field in a confined dielectric medium give rise to a van der Waals interaction. Since this interaction is of my special interest and because I derive some new results for the van der Waals interaction it will be discussed in detail in the following Chapter. Here, we will proceed with forces which are due to the order in a liquid crystal.

First observations of forces in liquid crystal were performed in the 80's by Horn *et. al* [57]. They studied the force between two mica plates separated by a liquid crystal 5CB using the X-ray surface forces apparatus [57,58]. The observed forces were resulting from the elastic deformations in liquid crystal, from the enhanced order close to the substrate, and the oscillating part of the force originated in the substrate-induced smectic layering. Later on, the forces due to the structure were only briefly discussed by Poniewierski and Sluckin [59], however, a detailed study of forces due to mean-field nematic order was performed by Borštnik and Žumer at the end of 90's [60]. The interactions in the presmectic fluid were studied by de Gennes [61]. In the meantime, much attention was paid to the fluctuation-induced forces started by studies of Ajdari *et. al* [27,62], and Li and Kardar [63,64]. Ajdari *et. al* studied the fluctuation-induced force in liquid crystals with homogeneous mean-field order, either nematic or smectic. Later, the pseudo-Casimir forces were studied in various liquid-crystalline systems by Ziherl *et. al* [28,65,66]. The theoretical interest was accompanied by experimental studies of forces in presmectic lyotropic systems performed with surface forces apparatus by Moreau *et. al* [22] and by observations of interfacial forces in various thermotropic liquid crystals performed with the atomic force microscope by Kočevar and Muševič [67].

Structural force

The confinement has, especially in the vicinity of phase and structural transitions, great impact on the equilibrium order of the liquid crystal. The force arising from the change of the corresponding part of the free energy will be denoted as a *structural force*. In principle, the free energy of a system associated to its structure corresponds to both, the equilibrium average order and to order related to collective fluctuations. In this thesis, the free energy of a system is determined by means of the phenomenological mean-field theory and the structural force denotes the force associated with the equilibrium order obtained within this theory,

$$\vec{F}_{struct.} = -\frac{\partial \Delta \mathcal{F}_{MF}}{\partial \vec{r}} = -\frac{\partial \mathcal{F}_{MF}}{\partial \vec{r}} + f_{bulk}\mathcal{A}. \tag{2.68}$$

$\Delta\mathcal{F}_{MF}$ is the variation of the free energy of the system in the framework of mean-field theory with respect to the free energy of the same amount of the liquid crystal in bulk, $\mathcal{F}_{MF}^{bulk} = f_{bulk}\mathcal{V}$.

Pseudo-Casimir force

In practice, the equilibrium order determined within the mean-field theory is perturbed due to thermal fluctuations which give rise to collective excitations. Except in the close vicinity of the phase/structural transitions, the thermal fluctuations of

the order parameter can be assumed small, and the free energy of fluctuations can be considered a correction to the mean-field free energy. In such a case, the fluctuations of liquid-crystalline order are described consistently by harmonic a Hamiltonian of the form

$$\mathcal{H}[b] = \frac{L}{2}\left\{\int \left[\xi^{-2}b^2 + (\nabla b)^2\right] \mathrm{d}\mathcal{V} + \sum_{i=1,2} \lambda_i^{-1} \int b^2 \mathrm{d}\mathcal{A}_i \right\}, \tag{2.69}$$

where b stands for each of the fluctuating degrees of freedom of the order parameter and ξ is a generalized correlation length characteristic of a particular type of fluctuations. From the discussion of fluctuations in previous Sections,

$$\xi^{-2} = \frac{1}{L}\frac{\partial^2 f}{\partial \eta^2}\Big|_{\eta=\eta_0}, \tag{2.70}$$

where ξ corresponds to fluctuations of the order parameter η whose equilibrium mean-field value is η_0. In the case of a uniform nematic order parameter tensor the relevant temperature-dependent correlation lengths are the ones introduced in Eqs. (2.36) and (2.37) for the isotropic and nematic phase, respectively.

We have divided the free energy of the system associated to the equilibrium order into the mean-field part corresponding to the order calculated by means of a phenomenological mean-field theory and to the part associated with collective thermal fluctuations, $\mathcal{F}_{CAS}$. The latter is given by a partition function

$$\mathcal{F}_{CAS} = -k_B T \ln\left(\int \mathcal{D}b\, \mathrm{e}^{-\mathcal{H}[b]/k_B T}\right), \tag{2.71}$$

where k_B is the Boltzmann constant, T is the temperature, and the integral is over all configurations of a fluctuating field b which satisfy boundary conditions [54,38].

The name pseudo-Casimir force for the fluctuation-induced interaction is due to the analogy with a Casimir effect which was first recognized by Casimir in 1948 [68]. In his study he found out that at $T = 0$ quantum fluctuations of the electromagnetic field in a cavity yield a weak yet measurable attraction between the walls of the cavity. Because the force between the walls is determined by a derivative of the free energy of a system rather than by a derivative of its energy similar effect is expected above absolute zero where the interaction is not just due to quantum but also due to thermal fluctuations. In liquid crystals, the fluctuation-induced interaction is due to thermal fluctuations of order parameter field instead of the electromagnetic field.

The main problem when calculating the pseudo-Casmir force is in fact that the total free energy of collective excitations diverges within the continuum description. Within the theory of the Casimir effect there are many methods for determining the finite interacting part from the divergent total free energy, such as dimensional regularization, the introduction of the lower limit of the wavelength of excitations,

Zeta regularization, methods based on Green's function of fluctuations, etc. Describing techniques of calculation of the pseudo-Casmir force is beyond the scope of this thesis. When needed, we will just quote the results already obtained by others.

To get the feeling about the pseudo-Casimir force few basic characteristics should be known. Depending on the boundary conditions the fluctuation-induced interaction can be either repulsive or attractive [27,63,64]. Its magnitude depends strongly on the surface interaction. In general, the sign of the pseudo-Casimir interaction is determined by the type of the boundary conditions, provided that the system is not subject to electric or magnetic field; $b(z = 0, d) = (\lambda/d)\ b'(z = 0, d)$, where $b' = \mathrm{d}b/\mathrm{d}z$ and d is the separation between the walls [see Section 2.3.1 and Eq. (2.66)]. Fluctuation modes constrained by strong, $\lambda_{1,2} \ll d$, or weak, $\lambda_{1,2} \gg d$, anchoring at both substrates lead to an attractive force. In a mathematical language this corresponds to Dirichlet, $b(z = 0) = b(z = d) = 0$, or Neumann, $b'(z = 0) = b'(z = d) = 0$, boundary conditions at both substrates. In contrast the asymmetric situation with one surface enforcing a strong anchoring and the other a weak anchoring yields a repulsive force (mixed boundary conditions). This is the universal property of Casimir forces [69–71].

2.4.1 Stability of thin liquid films

Imagine a thin liquid film deposited on a solid substrate so that it has a free liquid–air interface. Due to thermal fluctuations the free interface of the film is not flat but rather wrinkled. The fluctuation waves of the interface are known as *capillary waves*. Because of the interfacial interactions and long-range interactions, such as the van der Waals interaction, and structural and pseudo-Casimir interaction in an ordered liquid, the total pressure in the film depends on its thickness, being either higher or lower than the external pressure. This difference in pressures, $\Pi = p_0 - p$ where p_0 is the external pressure, is denoted as a *disjoining pressure*. The term disjoining pressure was first introduced by Derjaguin as a pressure due to the van der Waals interaction [72]. Later, its use was extended also to structural interaction [59]. Here, it will denote the total pressure which is due to interactions in the film. The disjoining pressure can be either repulsive, $\Pi > 0$, or attractive, $\Pi < 0$, and it has to vanish in the limit of infinitely thick film. Thus, if the disjoining pressure is characterized by a monotonic behavior the magnitude of the disjoining pressure is larger for smaller film thicknesses. The two possible situations for the monotonic disjoining pressure are depicted in Fig. 2.7 (top). Imagine now a film whose interface is perturbed at a given moment. If the disjoining pressure is repulsive the repulsion is stronger in a thinner region of film. Thus, the tendency to thicken the thinner part of the film will be stronger than to thicken the thicker part and the differences

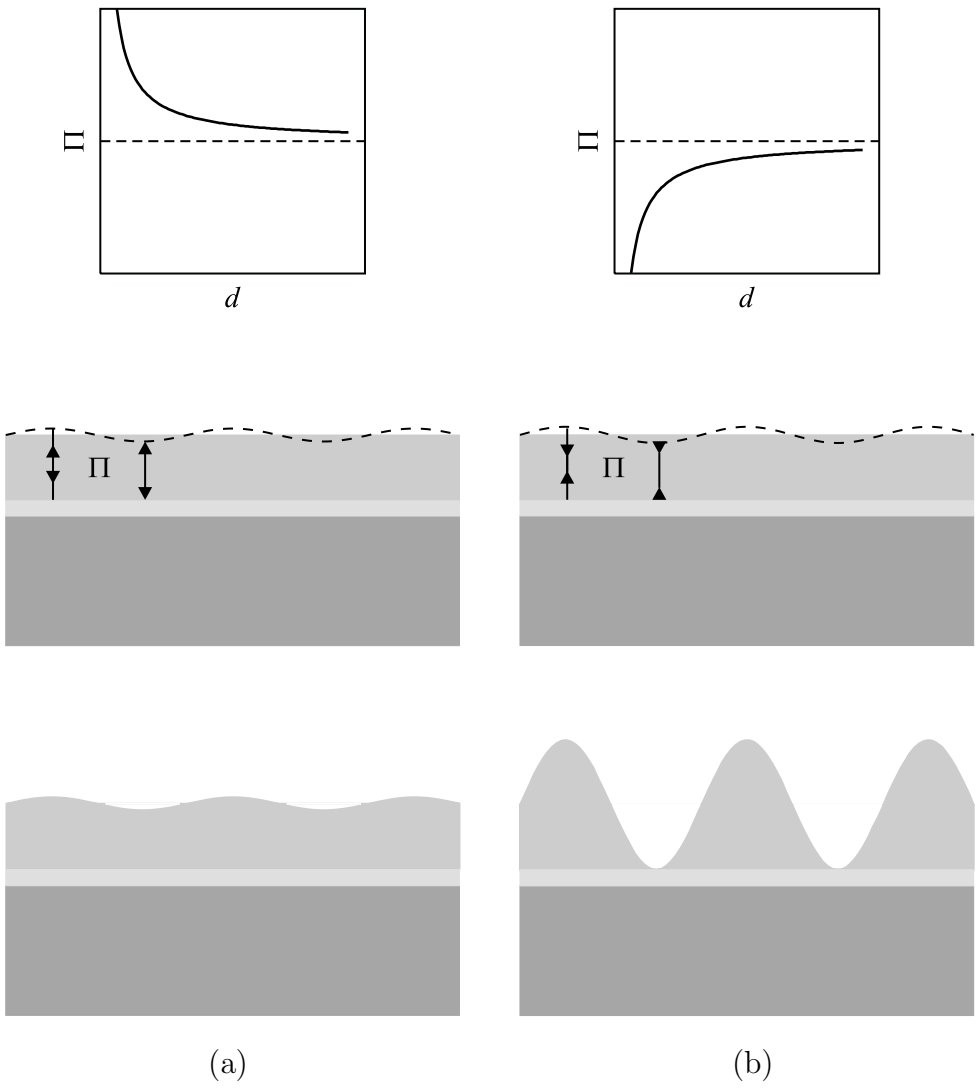

Figure 2.7 Schematic representation of conditions for the stability of thin liquid films. Thermal fluctuations of the free liquid–air interface are (a) diminished and (b) amplified, resulting in stable film or decomposition of the film in liquid drops and dry patches, respectively. Top: schematic representation of the disjoining pressure; middle: uniform film with a thickness equal to its average value and a sketch of a capillary wave with a disjoining pressure indicating the sign and the magnitude; bottom: resulting film profile.

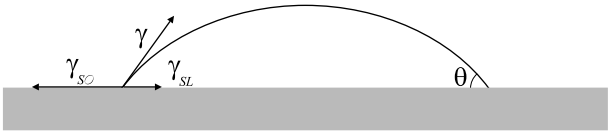

Figure 2.8 A liquid droplet on a solid substrate in the equilibrium; θ is the contact angle.

in the film thickness will be smeared. On the other hand, if the disjoining pressure is attractive the stronger attraction in thinner regions yields amplified differences in the film thickness when finally the thickness of thinner regions drops to zero and dry patches occur. These situations are schematically presented in Fig. 2.7 (a) and Fig. 2.7 (b), respectively. The described mechanism of a decomposition of a film is called the *spinodal dewetting*.

Once we are familiar with basic relations between the disjoining pressure and the stability of a thin film the stability conditions will be derived quantitatively. In the derivation we will follow the calculations made by de Gennes [73] and Brochard-Wyart and Daillant [74].

The spreading of the liquid on the solid substrate is determined by a spreading coefficient

$$S = \gamma_{SO} - (\gamma_{SL} + \gamma) \tag{2.72}$$

where $\gamma_{SO}\mathcal{A}$ is the interfacial energy of the bare solid, $\gamma_{SL}\mathcal{A}$ is the interfacial energy of the solid–liquid interface, and $\gamma\mathcal{A}$ is the interfacial energy of the liquid–air interface; $\mathcal{A}$ is the surface area. $S > 0$ leads to a *complete wetting* of the solid by liquid whereas for $S < 0$ the wetting is only *partial*. On the other hand, the wettability of the liquid is described by a contact angle θ_e as it is plotted in Fig. 2.8. The subscript e denotes that θ refers to contact angle in the equilibrium with the vapor. The contact angle and the interfacial energies are related through the Young's relation, $\gamma_{SV} - \gamma_{SL} - \gamma\cos\theta_e = 0$, where $\gamma_{SV}\mathcal{A}$ is the interfacial energy of the solid–vapor interface [75]. For organic liquids the difference $\gamma_{SO} - \gamma_{SV} > 0$ is usually very small. The energy of a liquid film is

$$\mathcal{F} = \mathcal{F}_0 - S\mathcal{A} + \mathcal{P}(d)\mathcal{A}, \tag{2.73}$$

where $\mathcal{P}(d)$ represents the energy of interactions which contribute to the disjoining pressure, $\Pi = -\partial\mathcal{P}/\partial d$. The equilibrium thickness of a film, d_e, is defined by the minimum of the energy while the volume $\mathcal{V} = \mathcal{A}d$ of the liquid is preserved, $S = \mathcal{P}(d_e) + \Pi(d_e)d_e$.

Imagine now a film with the average thickness d_0, however, with small deviations of the thickness with respect to the coordinate x parallel to the solid substrate, $\zeta(x)$.

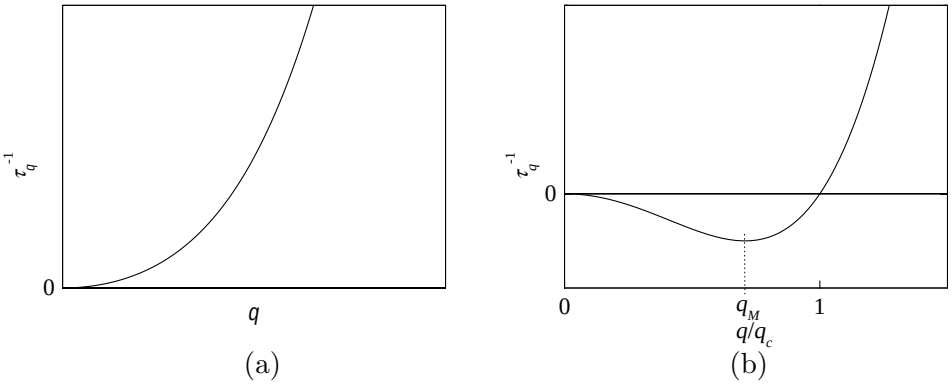

(a) (b)

Figure 2.9 The inverse relaxation rate of capillary waves as a function of a wavevector for (a) repulsive disjoining pressure and (b) attractive disjoining pressure. In the latter, for $q < q_c$ the fluctuations are amplified.

The pressure distribution in a film is then

$$p(x) = p_0 - \gamma \frac{\partial^2 \zeta}{\partial x^2} - \Pi(\zeta), \tag{2.74}$$

where the term with γ corresponds to the pressure due to the curved interface ($1/R = \partial^2\zeta/\partial^2 x$, where R is the radius of the curved path). In the lubrication approximation (flat liquid film and Poiseuille type of flow), the horizontal current in the liquid is given by

$$j = \zeta v = \frac{\zeta^3}{3\eta}\left(-\frac{\partial p}{\partial x}\right), \tag{2.75}$$

where v is the average horizontal velocity. In addition, the mass conservation law gives $\partial j/\partial x + \partial\zeta/\partial t = 0$. Consider now the expansion of the deviations of the film thickness from its average value

$$\zeta(x) = d_0 + \sum_q u_q \, \mathrm{e}^{iqx} \, \mathrm{e}^{-t/\tau_q}. \tag{2.76}$$

Here, τ_q is the relaxation time of the capillary wave with wavevector q and $u_q \ll d_0$ is the amplitude of a given capillary wave. Using the ansatz defined in Eq. (2.76) in Eq. (2.75), considering the mass conservation, and linearizing the obtained equations one is able to determine the relaxation times,

$$\frac{1}{\tau_q} = \frac{d_0^3}{3\eta}\left[\gamma q^4 - q^2 \Pi'(d_0)\right]. \tag{2.77}$$

For $\Pi'(d_0) < 0$, which corresponds to repulsive disjoining pressure, $\tau_q > 0$ for every q and fluctuations decrease exponentially after they are excited. On the other hand, if $\Pi'(d_0) > 0$ a wavevector q_c can be found so that $\tau_{q<q_c} < 0$. Negative relaxation time means that the given fluctuation mode is amplified in time and the film is

not stable. The obtained results confirm the arguments used at the beginning of the Section to describe relations between the disjoining pressure and stability of the film. The critical wavevector of capillary waves reads

$$q_c = \sqrt{\frac{\Pi'(d_0)}{\gamma}}. \tag{2.78}$$

The capillary wave which is the most amplified ($\partial\tau_q/\partial q = 0$) corresponds to $q_M = \sqrt{\Pi'(d_0)/2\gamma} = q_c/\sqrt{2}$, with the relaxation time

$$\tau_M = -\frac{d_0^3\Pi'(d_0)^2}{12\eta\gamma}. \tag{2.79}$$

Thus, typical wavelength of drops which result from the spinodal dewetting of a film corresponds to the capillary wave with

$$\lambda_M = \frac{2\pi}{q_M} = \sqrt{\frac{8\pi^2\gamma}{\Pi'(d_0)}}. \tag{2.80}$$

The inverse relaxation rate of capillary waves is plotted in Fig. 2.9.

3

Van der Waals force

In the last decades, the van der Waals interaction between macroscopic bodies was assumed to be a solved problem. However, new technological applications demand smaller and smaller systems whose stability is strongly influenced even by as weak interactions as is the van der Waals interaction which, thus, should be determined as accurately as possible [74,76]. Especially intriguing are electronic devices incorporating strongly confined liquid-crystalline materials, polymers, and other materials which are characterized by highly anisotropic macroscopic physical properties [77–81]. In addition, a lot of experimental and theoretical work is focused to studies of stability of nanostructures characterized by highly uniaxial macroscopic molecular arrangement, such as in self-assemblies of long organic molecules forming films, membranes, colloids, etc [82–85]. These materials are all characterized by anisotropic order (usually close to being uniaxial) and correspondingly by anisotropic permittivity tensor. Therefore, the dependence of the van der Waals interaction on the anisotropic permittivity tensor is required.

Although many decades ago Kihara and Honda [86] introduced the van der Waals interaction energy for the three-slab system of uniaxial media, generally, the van der Waals force for anisotropic media, such as liquid crystals, is still calculated by use of isotropic, yet average macroscopic physical quantities. The anisotropy of interacting media has been avoided in studies considering anisotropic media with only few exceptions. Okano and Murakami calculated the dispersion interaction contribution to the interfacial free energy of nematic liquid crystals taking into account the uniaxial symmetry of the nematic order and neglecting retardation [87]. The interaction was calculated between half spaces of air and nematic liquid crystal separated by a gap of vacuum in the limit where the thickness of the gap was 0. The optical axis of the nematic liquid crystal was either perpendicular or parallel to the air–liquid crystal interface. Podgornik and Parsegian studied the static part of the van der Waals interaction energy between rodlike polyelectrolytes: regions

consisting of uniaxially ordered rodlike polyelectrolytes separated by an isotropic gap [88]. The optical axes of uniaxial media were taken to lie in the plane of the interface and were rotated with respect to each other. In experimental studies, the results from theoretical studies of the anisotropic van der Waals force are not considered. Here, the reason for neglecting the anisotropy of permittivity tensor can not be the insignificance of the anisotropy of relevant quantities but rather the fact, that there are no known simplified expressions to calculate the van der Waals force, whereas for the isotropic media there is a well known approximate analytic expression (see e.g. [89]). On the other hand, the general calculation of the van der Waals force is in the case of anisotropic permittivity tensor even more complex than it is in the case of isotropic interacting media.

In this Chapter, the influence of anisotropy of permittivity tensor of a medium on the van der Waals force will be discussed through the simplest example of anisotropy — the uniaxial symmetry. In addition, the approximate expression for the van der Waals interaction will be derived for the same symmetry of the permittivity tensor. There are two reasons for choosing the uniaxial symmetry. First, as already noted in the introductory paragraph, there are many important physical and biological systems consisting of soft layers characterized by highly uniaxial molecular arrangement. In these, the correct dependence of the van der Waals force on the anisotropic refractive indices and static dielectric constants is needed for adequate explanations of experiments. Secondly, the uniaxial symmetry is the highest symmetry yielding the analytic solution for the surface electromagnetic fluctuation modes which determine the van der Waals force. Here the term *surface electromagnetic modes* is used to emphasize the influence of the walls on the electromagnetic modes rather than to denote the modes which would be strictly localized at the walls.

The calculation is performed for the simple planar parallel geometry: two macroscopic bodies separated by a layer of an uniaxial medium, as shown schematically in Fig. 3.1. Often, the results of the study of interactions in planar parallel systems can be applied also to curved bodies with small curvature, i.e., for locally planar parallel systems, by using standard Derjaguin procedure [90]. Here, due to the anisotropy of permittivity tensor the correspondence between different geometries can not be expected to be strictly explicit as it will be evident from the following calculation, therefore, the precision of a result obtained by Derjaguin procedure, even if only as a rough approximation, is rather questionable. Using the same arguments as when arguing the choice of the uniaxial symmetry of the permittivity tensor, the optical axis of the interposed uniaxial medium is assumed to be perpendicular to the gap between the macroscopic bodies. For optical axes lying either in the plane of the gap or even in an arbitrary direction the van der Waals interaction can be calcu-

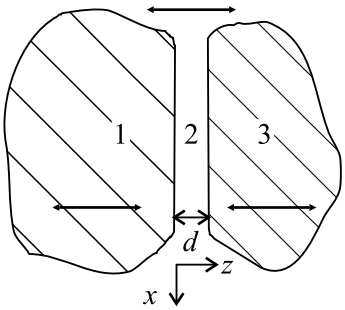

Figure 3.1 Schematic representation of the system for which the van der Waals force is calculated: two semi-infinite macroscopic bodies separated by the third medium. The arrows denote the orientation of optical axis in each medium, the closest distance between the two bodies d is in text referred as the separation between the bodies, and the numbers 1,2, and 3 denote different media.

lated only numerically and within the nonretarded approximation. Since the general cases are beyond the scope of this thesis, the calculations for them will be omitted here. However, at the appropriate steps the difficulties, which are encountered when dealing with systems which do not preserve the axis of full rotational symmetry, will be pointed out.

In the systems referred to, the uniaxial layer is surrounded by isotropic media, either some glassy materials, liquid, or air. Often, especially when talking about liquid crystals, the uniaxial order of the layer in question is obtained by inducing the order with some other uniaxially ordered material. In such case, the system consists of two or three uniaxial media with parallel optical axes. In the following the calculation will be performed for the general case of three/four uniaxial media with parallel optical axes. The transformation to the case of isotropic macroscopic bodies will be evident.

In the following Section the van der Waals interaction between macroscopic bodies is introduced. In Section 3.2 the electromagnetic field modes are calculated and the secular equation, which determines the frequencies of the surface modes is derived. In Section 3.3 the procedure of calculating free energy of electromagnetic field surface modes from the secular equation is reviewed. In Section 3.4 the van der Waals interaction mediated by uniaxial layer is calculated. The final expression can only be calculated numerically, however, in Section 3.5 the approximate analytic expression is calculated within the nonretarded limit. The Chapter is concluded by a general discussion of the obtained result and by arguing its validity. Further accounts concerning the van der Waals force follow in Sections 4.4 and 5.4 where the obtained results for the anisotropic van der Waals force are used in specific liquid-crystalline systems.

Figure 3.2 Schematic representation of van der Waals interaction between (a) two neutral molecules and (b) two macroscopic bodies.

3.1 Van der Waals interaction

Van der Waals interaction is a common name for the dispersion interaction, which originates in the pair-wise interaction of fluctuating dipoles arising from dynamic redistribution of electrons in molecules, and the orientational interaction which results from the interaction of permanent yet fluctuating electric dipoles. The value of the interaction is the quantum mechanic expectation value of the corresponding interaction term in the Hamiltonian. For small separations, the interaction energy is proportional to $1/d^6$, whereas for large separations the dispersion interaction falls off faster and approaches $1/d^7$ behavior. The decrease of the dispersion interaction is a consequence of finite velocity of light; when the time it takes for the electromagnetic field of one molecule to reach the second one and to return becomes comparable to the period of the fluctuating dipole (usually, $d > 100$ nm) the phase coherence between the two interacting molecules is getting lost. The effect is known as *retardation*. The $1/d^7$ behavior of the dispersion interaction in the limit of high retardation which was first calculated by quantum electrodynamic approach developed by Casimir and Polder [91,68]. The orientational interaction is proportional to $1/d^6$ for all separations. For materials with small permanent electric dipoles and for distances up to 100 nm the dispersion interaction dominates over the orientational one.

Several approaches have been employed to calculate the van der Waals interaction between macroscopic bodies. The simplest way, known as the Hamaker approach [92], is to sum all pair-wise interactions between constituent molecules. In condensed media these are not independent but rather strongly influenced by the surrounding medium, therefore, taking into account many-body interactions becomes essential. On the mesoscopic and macroscopic scale the many-body system can be regarded as a continuum and can be described by macroscopic quantities, such as permittivity, which take into account the screening of the surrounding molecules.

The continuum approach is known as the Lifshitz approach. Lifshitz was the first who calculated the van der Waals interaction energy between two semi-infinite dielectric bodies separated by a gap of vacuum [93]. Later, the interaction energy for the system with a gap filled with an isotropic dielectric medium was calculated by Dzyaloshinskii *et. al* [94,95]. The basic idea of the continuum theory is that the interaction between the bodies is considered to take place through a fluctuating electromagnetic field. The interaction arises from the change in the zero-point energy of the electromagnetic field modes when the latter are perturbed by the coupling of the field with the polarization currents induced on the molecules. The electromagnetic field modes are obtained by solving Maxwell's equations. These findings were obtained by a quantum field theory approach based on determination of the Green's function for the electromagnetic field in the presence of molecules in a dielectric media characterized by isotropic permittivities. The poles of the Green's function represent the electromagnetic field resonances of the system. There are two sources of poles: the poles of the permittivity, $\epsilon(\omega) = 0$, and the poles of the denominator of the Green's function, $\mathcal{D}(\omega) = 0$. The former modes refer to bulk modes and they do not depend on the separation between the macroscopic bodies. The poles arising from the secular equation $\mathcal{D}(\omega) = 0$ refer to the surface modes and are responsible for the change of the zero-point energy of the electromagnetic field modes. Once it is recognized that the van der Waals interaction arises from the change of the electromagnetic field surface modes, the latter can be determined directly by solving Maxwell's equations in a classical way. The equivalence of the van der Waals force between macroscopic bodies and the surface modes interaction was first shown by van Kampen *et. al* [96] for the non-retarded interaction, and later it was extended by Gerlach [97] and Schram [98] for the retarded interaction. The change of the free energy of a perturbed system for temperatures $T > 0$ instead of the change of the energy of a perturbed system at $T = 0$ was first introduced by Ninham *et. al* [99]. In the following Sections the continuum procedure will be used to derive the van der Waals interaction between uniaxial macroscopic bodies.

Before we start with the derivation of the van der Waals force for uniaxial media we shell first quote the known expression for a three-layer system of isotropic media (see e.g. [100]),

$$\begin{aligned} \Pi &= \frac{k_B T}{16\pi d^3}\int_0^\infty \mathrm{d}x\; x^2 \frac{\bar{\Delta}_{12}\bar{\Delta}_{23}\,\mathrm{e}^{-x}}{1-\bar{\Delta}_{12}\bar{\Delta}_{23}\,\mathrm{e}^{-x}} \\ &\quad + \frac{k_B T}{\pi d^3}\sum_{n=1}^{\infty}{}' \tilde{d}^3 \int_1^\infty \mathrm{d}p\; p^2 \left(\frac{\Delta_{12}^R \Delta_{23}^R\,\mathrm{e}^{-2p\tilde{d}}}{1-\Delta_{12}^R\Delta_{23}^R\,\mathrm{e}^{-2p\tilde{d}}} + \frac{\bar{\Delta}_{12}^R \bar{\Delta}_{23}^R\,\mathrm{e}^{-2p\tilde{d}}}{1-\bar{\Delta}_{12}^R\bar{\Delta}_{23}^R\,\mathrm{e}^{-2p\tilde{d}}} \right). \end{aligned} \tag{3.1}$$

Here, d is a thickness of a gap between two semi-infinite media 1 and 3, and the gap is filled with material 2; $\tilde{d} = d\sqrt{\epsilon_2}\xi_n/c$ and Δ_{ij}'s are functions of frequency dependent

permittivities of the media. They are defined in Section 3.2 [Eqs. (3.24) and (3.36)]. It should be noted, that in general there is no explicit separation dependence of the van der Waals force. Except for very large separations the second term in Eq. (3.1) is dominant. At small d's it reduces to an expression similar to the first term, and the force has a $1/d^3$ separation dependence. For intermediate separations the force falls off quicker, and would obtain a $1/d^4$ dependence. However, for very large separations the second term becomes negligible comparing to the first one, and the $1/d^3$ separation dependence is recovered. In practice, the van der Waals force is calculated by using the well-known approximate expression $\Pi = -A/6\pi d^3$ (see e.g. [89]), which is in a good agreement with Eq. (3.1) for separations of order of few nanometers and provides satisfactory qualitative insight in the van der Waals force for larger separations. Here A is a Hamaker constant,

$$A = \frac{3}{4}k_B T \frac{\epsilon_1 - \epsilon_2}{\epsilon_1 + \epsilon_2}\frac{\epsilon_3 - \epsilon_2}{\epsilon_3 + \epsilon_2} + \frac{3\hbar\omega_e}{8\sqrt{2}} \frac{(n_1^2 - n_2^2)(n_3^2 - n_2^2)}{\sqrt{n_1^2 + n_2^2}\sqrt{n_3^2 + n_2^2}(\sqrt{n_1^2 + n_2^2} + \sqrt{n_3^2 + n_2^2})}, \quad (3.2)$$

ϵ_i is the static dielectric constant of a medium i, n_i is its refractive index in visible, and ω_e is the plasma frequency of a medium, taken to be equal for all media.

3.2 Electromagnetic field surface modes

In this Section the spectrum of electromagnetic field modes in the gap between two dielectric macroscopic bodies will be calculated for the system with no external electromagnetic field and no macroscopic electric charges and dipoles. The fluctuations of the electromagnetic field are a consequence of a dynamic redistributions of electrons in molecules due to thermal fluctuations. However, the interest is not in fluctuations of a single molecule, but in collective behavior on the macroscopic scale. Therefore, the electromagnetic field in the gap is to be determined. The field obeys Maxwell's equations

$$\begin{aligned} \nabla \times \vec{E} = -\frac{\partial \vec{B}}{\partial t} \quad , \qquad \nabla \cdot \vec{D} = 0, \\ \nabla \times \vec{H} = \frac{\partial \vec{D}}{\partial t} \quad , \qquad \nabla \cdot \vec{B} = 0, \end{aligned} \quad (3.3)$$

and satisfies corresponding boundary conditions

$$\begin{aligned} \Delta\vec{D}_\perp\Big|_{boundary} = 0 \qquad \Delta\vec{E}_\parallel\Big|_{boundary} = 0 \\ \Delta\vec{B}_\perp\Big|_{boundary} = 0 \qquad \Delta\vec{H}_\parallel\Big|_{boundary} = 0. \end{aligned} \quad (3.4)$$

Here $\vec{D} = \epsilon_0 \underline{\epsilon} \vec{E}$ and $\vec{B} = \mu_0 \vec{H}$; $\underline{\epsilon}$ is permittivity tensor. It is not the subject of this thesis to calculate the electromagnetic field modes for general geometry of the

cavity and for general types of the wall. Therefore, as already stated in previous Section the electromagnetic field modes are calculated for the planar geometry. The coordinate system is set so that the z axis is perpendicular to the gap between the macroscopic bodies and axes x and y lie in the plane of one of the interfaces. In the lateral directions, there are no constraints for the electromagnetic field, therefore, the x and y dependencies of the electromagnetic field are the one of the plane wave. The dependence on the z coordinate is still to be determined. The ansatz function for the electromagnetic field is

$$\vec{A} = \vec{A}_0(z)\, \mathrm{e}^{i\vec{\kappa}\vec{r}}\, \mathrm{e}^{-i\omega t}, \tag{3.5}$$

where $\vec{A}$ stands for either electric field $\vec{E}$ or magnetic induction $\vec{B}$ and $\vec{\kappa} = (\kappa_x, \kappa_y, 0)$ is a wavevector in the plane of the boundary. In this study, the permittivity tensors of the macroscopic bodies as well as the permittivity of the interposed layer are uniaxial with eigenframes coinciding with the coordinate system,

$$\underline{\epsilon}_i = \begin{pmatrix} \epsilon_{i_\perp} & 0 & 0 \\ 0 & \epsilon_{i_\perp} & 0 \\ 0 & 0 & \epsilon_{i_\parallel} \end{pmatrix}. \tag{3.6}$$

Here, index $i = 1, 2,$ or 3, represents different media, and ϵ is frequency dependent. As already stated before, the uniaxial symmetry with perpendicular optical axis with respect to the gap is the only non-isotropic geometry, which allows one to calculate electromagnetic field modes quite easily. Even if the eigenframe of the permittivity tensor remains the same, but the optical axis lies in one of the lateral directions, the eigenmodes can not be calculated analytically, except in the nonretarded limit, which is equivalent to describing static fields. In the case of uniaxial symmetry and optical axis parallel to the gap normal, the full rotational symmetry around the z axis is preserved. This allows us to divide the eigenmodes in two groups: transverse magnetic modes (TM) and transverse electric (TE), as defined by Rayleigh already in 1897 [101].

Transverse magnetic modes

The TM waves are defined as waves with $B_z = 0$. By using this and the ansatz function for the electromagnetic field introduced in Eq. (3.5) to solve the Maxwell's equations the wave equation is obtained,

$$\Psi'' - \frac{\epsilon_\perp}{\epsilon_\parallel}\left(\kappa^2 - \frac{\omega^2}{c^2}\epsilon_\parallel\right)\Psi = 0, \tag{3.7}$$

with boundary conditions

$$\Delta\Psi\Big|_{boundary} = 0 \qquad \text{and} \qquad \Delta\frac{1}{\epsilon_\perp}\Psi'\Big|_{boundary} = 0. \tag{3.8}$$

Here, $\Psi' = \mathrm{d}\Psi/\mathrm{d}z$ and $\Psi(z)$ defines the z dependent amplitudes of corresponding components of the electromagnetic field,

$$\begin{aligned} B_x(\vec{r},t) &= B_0\Psi(z)\,\mathrm{e}^{i\vec{\kappa}\cdot\vec{r}-i\omega t}, \\ B_y(\vec{r},t) &= -B_0\frac{\kappa_x}{\kappa_y}\Psi(z)\,\mathrm{e}^{i\vec{\kappa}\cdot\vec{r}-i\omega t}, \\ E_x(\vec{r},t) &= -B_0\frac{c^2}{i\omega\epsilon_\perp}\frac{\kappa_x}{\kappa_y}\Psi'(z)\,\mathrm{e}^{i\vec{\kappa}\cdot\vec{r}-i\omega t}, \\ E_y(\vec{r},t) &= -B_0\frac{c^2}{i\omega\epsilon_\perp}\Psi'(z)\,\mathrm{e}^{i\vec{\kappa}\cdot\vec{r}-i\omega t}, \\ E_z(\vec{r},t) &= B_0\frac{c^2}{i\omega\epsilon_\parallel}\frac{i\kappa^2}{\kappa_y}\Psi(z)\,\mathrm{e}^{i\vec{\kappa}\cdot\vec{r}-i\omega t}. \end{aligned} \tag{3.9}$$

With respect to the coordinate normal to the gap, the electromagnetic field decays/grows exponentially with the inverse penetrations depth

$$\bar{\rho}(\omega) = \left[\frac{\epsilon_\perp}{\epsilon_\parallel}\left(\kappa^2 - \frac{\omega^2}{c^2}\epsilon_\parallel\right)\right]^{1/2}. \tag{3.10}$$

In a composed system of three dielectric media the amplitude Ψ has the following z dependence

$$\Psi(z) = \begin{cases} A\,\mathrm{e}^{\bar{\rho}_1 z} & ; \quad z < 0 \\ B\,\mathrm{e}^{\bar{\rho}_2 z} + C\,\mathrm{e}^{-\bar{\rho}_2 z} & ; \quad 0 < z < d \\ D\,\mathrm{e}^{-\bar{\rho}_3 z} & ; \quad z > d \end{cases}. \tag{3.11}$$

Taking into account the boundary conditions in Eq. (3.8) one ends up with a secular equation, which determines the dispersion relation for the TM surface modes

$$D^R_{TM}(\omega) = 1 + \bar{\Delta}^R_{12}(\omega)\bar{\Delta}^R_{23}(\omega)\mathrm{e}^{-2\bar{\rho}_2(\omega)d} = 0. \tag{3.12}$$

Here,

$$\bar{\Delta}^R_{ij}(\omega) = \frac{\epsilon_{i\perp}(\omega)\bar{\rho}_j(\omega) - \epsilon_{j\perp}(\omega)\bar{\rho}_i(\omega)}{\epsilon_{i\perp}(\omega)\bar{\rho}_j(\omega) + \epsilon_{j\perp}(\omega)\bar{\rho}_i(\omega)}. \tag{3.13}$$

Similarly, for the four-layer system one obtains the secular equation

$$\begin{aligned} D^R_{TM}(\omega) &= 1 + \bar{\Delta}^R_{12}(\omega)\bar{\Delta}^R_{23}(\omega)\mathrm{e}^{-2\bar{\rho}_2(\omega)d} + \bar{\Delta}^R_{23}(\omega)\bar{\Delta}^R_{34}(\omega)\mathrm{e}^{-2\bar{\rho}_3(\omega)t} \\ &\quad + \bar{\Delta}^R_{12}(\omega)\bar{\Delta}^R_{34}(\omega)\mathrm{e}^{-2\bar{\rho}_2(\omega)d}\mathrm{e}^{-2\bar{\rho}_3(\omega)t} = 0, \end{aligned} \tag{3.14}$$

where d and t are thicknesses of the layers of media 2 and 3, interposed between semi-infinite surrounding media.

Transverse electric modes

The TE waves are defined as waves with $E_z = 0$. Using the same procedure as when calculating TM modes the wave equation for the z dependent amplitude Ψ is

obtained,

$$\Psi'' - \left(\kappa^2 - \frac{\omega^2}{c^2}\epsilon_\perp\right)\Psi = 0, \tag{3.15}$$

with boundary conditions

$$\Delta\Psi\Big|_{boundary} = 0 \qquad \text{and} \qquad \Delta\Psi'\Big|_{boundary} = 0. \tag{3.16}$$

The components of the electromagnetic field depend on the function $\Psi(z)$ as

$$\begin{aligned}
E_x(\vec{r},t) &= E_0\Psi(z)\,\mathrm{e}^{i\vec{\kappa}\cdot\vec{r}-i\omega t},\\
E_y(\vec{r},t) &= -E_0\frac{\kappa_x}{\kappa_y}\Psi(z)\,\mathrm{e}^{i\vec{\kappa}\cdot\vec{r}-i\omega t},\\
B_x(\vec{r},t) &= E_0\frac{\kappa_x}{\kappa_y}\frac{1}{i\omega}\Psi'(z)\,\mathrm{e}^{i\vec{\kappa}\cdot\vec{r}-i\omega t},\\
B_y(\vec{r},t) &= E_0\frac{1}{i\omega}\Psi'(z)\,\mathrm{e}^{i\vec{\kappa}\cdot\vec{r}-i\omega t},\\
B_z(\vec{r},t) &= -E_0\frac{i\kappa^2}{\kappa_y}\frac{1}{i\omega}\Psi(z)\,\mathrm{e}^{i\vec{\kappa}\cdot\vec{r}-i\omega t}.
\end{aligned} \tag{3.17}$$

The characteristic length for the penetration of the TE waves into the dielectric walls is then

$$\rho(\omega) = \left(\kappa^2 - \frac{\omega^2}{c^2}\epsilon_\perp\right)^{1/2}. \tag{3.18}$$

In a composed system of three dielectric media the amplitude Ψ has the same z dependence as defined in Eq. (3.11), with ρ_i instead of $\bar{\rho}_i$. Taking into account the boundary conditions in Eq. (3.16) one ends up with a secular equation, which determines the dispersion relation for the TE surface modes

$$D^R_{TE}(\omega) = 1 + \Delta^R_{12}(\omega)\Delta^R_{23}(\omega)\mathrm{e}^{-2\rho_2(\omega)d} = 0. \tag{3.19}$$

Here,

$$\Delta^R_{ij}(\omega) = \frac{\rho_i(\omega) - \rho_j(\omega)}{\rho_i(\omega) + \rho_j(\omega)}. \tag{3.20}$$

Similarly, for the four-layer system one obtains the secular equation

$$\begin{aligned}
D^R_{TE}(\omega) &= 1 + \Delta^R_{12}(\omega)\Delta^R_{23}(\omega)\mathrm{e}^{-2\rho_2(\omega)d} + \Delta^R_{23}(\omega)\Delta^R_{34}(\omega)\mathrm{e}^{-2\rho_3(\omega)t}\\
&\quad + \Delta^R_{12}(\omega)\Delta^R_{34}(\omega)\mathrm{e}^{-2\rho_2(\omega)d}\mathrm{e}^{-2\rho_3(\omega)t} = 0,
\end{aligned} \tag{3.21}$$

where d and t are the thicknesses of the layers of media 2 and 3 interposed between semi-infinite surrounding media.

If all the media are isotropic, the electromagnetic field surface modes can still be divided into TM and TE but they are described by the same wave equation

$$\Psi'' - \left(\kappa^2 - \frac{\omega^2}{c^2}\epsilon\right)\Psi = 0 \tag{3.22}$$

with boundary conditions Eqs. (3.8) and (3.16) for TM and TE modes, respectively. Here, the transformation $\epsilon_\perp, \epsilon_\parallel \to \epsilon$ has to be made. The penetration depth of the modes is then

$$\rho(\omega) = \left(\kappa^2 - \frac{\omega^2}{c^2}\epsilon\right)^{1/2}, \tag{3.23}$$

and the secular equations for the three-layer system read

$$\begin{aligned} D^R_{TM}(\omega) &= 1 + \bar{\Delta}^R_{12}(\omega)\bar{\Delta}^R_{23}(\omega)\mathrm{e}^{-2\rho_2(\omega)d} = 0, \\ D^R_{TE}(\omega) &= 1 + \Delta^R_{12}(\omega)\Delta^R_{23}(\omega)\mathrm{e}^{-2\rho_2(\omega)d} = 0, \end{aligned} \tag{3.24}$$

where

$$\begin{aligned} \bar{\Delta}^R_{ij}(\omega) &= \frac{\epsilon_i(\omega)\bar{\rho}_j(\omega) - \epsilon_j(\omega)\bar{\rho}_i(\omega)}{\epsilon_i(\omega)\bar{\rho}_j(\omega) + \epsilon_j(\omega)\bar{\rho}_i(\omega)}, \\ \Delta^R_{ij}(\omega) &= \frac{\rho_i(\omega) - \rho_j(\omega)}{\rho_i(\omega) + \rho_j(\omega)}. \end{aligned} \tag{3.25}$$

3.3 The zero-point energy of surface modes

The roots of secular equations for TM and TE modes give frequencies of the corresponding modes, ω, as a function of a wave vector $\vec{\kappa}$, i.e., the dispersion relation for the surface modes. At the absolute zero, the interaction energy is then given by the difference of sums over the zero-point energies of each mode, $E = \hbar\omega/2$, for each value of the wave vector $\vec{\kappa}$, for the composed system of dielectric media with either finite thickness of the interposed medium or with $d \to \infty$,

$$\Delta E = \frac{\hbar}{2}\sum_{\vec{\kappa}}\left(\sum_i \omega_i - \sum_{i'}\omega_{i'}\right). \tag{3.26}$$

Here, ω_i's are the zero-point frequencies of the perturbed system and $\omega_{i'}$'s are the zero-point energies of unperturbed system (only the medium which is inbetween the walls). Solving the secular equations for the electromagnetic field surface modes is far from being easy, however, in the standard contour integral representation [102] the expression in Eq. (3.26) reduces to

$$\begin{aligned} \Delta E &= \frac{1}{2\pi i}\sum_{\vec{\kappa}}\oint \mathrm{d}\omega_{\vec{\kappa}}\frac{\hbar\omega_{\vec{\kappa}}}{2}\frac{\mathrm{d}}{\mathrm{d}\omega_{\vec{\kappa}}}\ln\frac{D(\omega_{\vec{\kappa}})}{D_0(\omega_{\vec{\kappa}})} \\ &= -\frac{\hbar}{4\pi i}\sum_{\vec{\kappa}}\oint \mathrm{d}\omega_{\vec{\kappa}}\ln\frac{D(\omega_{\vec{\kappa}})}{D_0(\omega_{\vec{\kappa}})}, \end{aligned} \tag{3.27}$$

where $D(\omega) = 0$ and $D_0(\omega) = 0$ are the secular equations for the perturbed and unperturbed systems, respectively. The secular equations derived in previous Sections are already the corresponding ratios, which can be easily tested by performing

the limit $d \to \infty$. The planar system is not bounded in the lateral directions, thus, the spectrum of wave vectors $\vec{\kappa}$ is continuous, and the sum over the wave vectors can be replaced by an integral, $\sum_{\vec{\kappa}} \to \frac{\mathcal{A}}{(2\pi)^2} \int \mathrm{d}^2\kappa$. Here, $\mathcal{A}$ is the surface area of the interfaces. In the case of optically isotropic media and uniaxial media with the optical axis parallel to the interface normal the frequencies ω depend only on the magnitude of the wave vector $\vec{\kappa}$, therefore, the zero-point energy reads

$$\Delta E = -\frac{\hbar\mathcal{A}}{8\pi^2 i} \oint \mathrm{d}\omega \int_0^\infty \kappa \mathrm{d}\kappa \ln \frac{D(\omega)}{D_0(\omega)}. \tag{3.28}$$

At the absolute zero, there are no excited states and the interaction is due to the change of the zero-point energy as derived above. At higher temperatures, not only the zero-point energy of the electromagnetic field is changed but also the occupancy of states. The whole information is gathered in the free energy of the system rather than in its energy. The free energy of the electromagnetic field with modes characterized by frequencies ω_i is then

$$\mathcal{F} = k_B T \sum_i \ln\left(2\sinh\frac{\beta\hbar\omega_i}{2}\right). \tag{3.29}$$

To calculate the interaction free energy of the perturbed system one has to substitute the energy of the system with the free energy, $\frac{\hbar\omega}{2} \to k_B T \ln(2\sinh\frac{\beta\hbar\omega}{2}) = \frac{\hbar\omega}{2} - k_B T \sum_{n=1}^\infty \frac{1}{n} \mathrm{e}^{-\beta\hbar\omega n}$. If a further substitution $\omega = i\xi$ is made we get the final expression for the change of the free energy of the electromagnetic field,

$$\begin{aligned}
\Delta\mathcal{F} &= \frac{\hbar\mathcal{A}}{8\pi^2} \int_0^\infty \mathrm{d}\kappa\kappa \int_{-\infty}^\infty \mathrm{d}\xi \Big(1 + 2\sum_{n=1}^\infty \mathrm{e}^{-i\beta\hbar\xi n}\Big) \ln\frac{D(i\xi)}{D_0(i\xi)} \\
&= \frac{\hbar\mathcal{A}}{4\pi^2} \int_0^\infty \mathrm{d}\kappa\kappa \int_0^\infty \mathrm{d}\xi \Big[1 + 2\sum_{n=1}^\infty \cos(\beta\hbar\xi n)\Big] \ln\frac{D(i\xi)}{D_0(i\xi)} \\
&= \frac{\hbar\mathcal{A}}{4\pi^2} \int_0^\infty \mathrm{d}\kappa\kappa \int_0^\infty \mathrm{d}\xi \left\{1 + 2\Big[\pi \sum_{n=-\infty}^\infty \delta(\beta\hbar\xi - 2\pi n) - \frac{1}{2}\Big]\right\} \ln\frac{D(i\xi)}{D_0(i\xi)} \\
&= \frac{k_B T\mathcal{A}}{2\pi} \int_0^\infty \mathrm{d}\kappa\kappa \sum_{n=-\infty}^\infty \ln\frac{D(i\xi_n)}{D_0(i\xi_n)}.
\end{aligned} \tag{3.30}$$

In Eq. (3.30) the second line is obtained by recognizing that $D(\omega)$ is an even function of ω, therefore, the odd, sine, part of the function under the integral gives 0 when integrating over the symmetric interval. The third line is obtained by using the equality $\sum_{n=1}^\infty \cos(nx) = \pi \sum_{n=-\infty}^\infty \delta(x - 2\pi n) - \frac{1}{2}$, which is derived from the Poisson sum formula [102]: $\sum_{n=-\infty}^\infty f(n) = 2\pi \sum_{m=-\infty}^\infty F(2\pi m)$, where F is Fourier transform of f. The last line is obtained by integrating over the frequencies ξ. In the final expression, $\xi_n = 2\pi k_B T n/\hbar$.

To relate the free energy of the van der Waals interaction to the van der Waals force we should use the thermodynamic definition of force written out in Eq. (2.67).

In the planar parallel system consisting of two infinitely large surfaces, the force is always perpendicular to the surfaces and, consequently,

$$F = -\left(\frac{\partial \mathcal{F}}{\partial d}\right)_{\mathcal{V},\mathcal{A}}, \tag{3.31}$$

where d is the separation between the two objects. The positive value of F corresponds to a repulsive force and the negative value corresponds to an attractive force.

3.4 Van der Waals force in a multi-layer system

As explained in previous Sections, the van der Waals force between macroscopic objects is due to the change of the free energy of electromagnetic field in a system perturbed by interfaces. By the definition of the force in Eq. (3.31) and the free energy of electromagnetic field surface modes obtained in Eq. (3.30) the van der Waals force per surface unit area, $\Pi = F/\mathcal{A}$, reads

$$\Pi = -\frac{k_B T}{2\pi} \int_0^\infty \mathrm{d}\kappa\kappa \sum_{n=-\infty}^{\infty} \sum_{\substack{\alpha= \\ TM,TR}} \frac{1}{D_\alpha(i\xi_n)} \frac{\partial D_\alpha(i\xi_n)}{\partial d}. \tag{3.32}$$

In order to evaluate the sum in Eq. (3.32) the frequency dependence of the permittivity tensor has to be known. The permittivity varies with frequency in much the same way as does the atomic polarizability of an atom, $\epsilon = 1+n\alpha/\epsilon_0$, where n is the density of molecules and α is their polarizability [101]. Basic polarization processes are reorientation of permanent dipoles and deformation of electronic configuration due to excited electrons. These yield $\epsilon(\omega) = 1+(\epsilon-n^2)/(1-i\omega/\omega_r)+(n^2-1)/(1-\omega^2/\omega_e^2)$ [100]. Here, ϵ and n stand for each of the components of the corresponding tensors, $\epsilon = \epsilon(0)$ is the static dielectric constant, n is the refractive index of the medium in the visible, ω_r is the molecular rotational frequency, and ω_e is the plasma frequency. Usually, $\omega_r < 10^{13}\ \mathrm{s}^{-1} \ll \omega_e \sim 2\pi \cdot 3 \cdot 10^{15}\ \mathrm{s}^{-1}$. Since $\xi_1 = 2.5 \cdot 10^{14}\ \mathrm{s}^{-1} \gg \omega_r$, the dispersion relation is determined solely by the electronic absorption,

$$\epsilon(i\xi_n) \approx 1 + \frac{n^2 - 1}{1 + \xi_n^2/\omega_e^2}, \tag{3.33}$$

In this case, $D(i\xi_n) = D(-i\xi_n)$ and

$$\Pi = -\frac{k_B T}{\pi} \int_0^\infty \mathrm{d}\kappa\kappa \sum_{n=0}^{\infty}{}' \frac{1}{D(i\xi_n)} \frac{\partial D(i\xi_n)}{\partial d}, \tag{3.34}$$

where prime over the sum denotes, that the term with $n = 0$ should be multiplied by $1/2$. From the secular equations determined in Section 3.2 the van der Waals

force per unit area between the two interfaces in the three-layer system reads

$$\begin{aligned}\Pi(d,T) &= \frac{k_BT}{16\pi d^3}\frac{\epsilon_{2_\parallel}(0)}{\epsilon_{2_\perp}(0)}\int_0^\infty \mathrm{d}x\; x^2 \frac{\bar\Delta_{12}\bar\Delta_{23}\,\mathrm{e}^{-x}}{1+\Delta_{12}\Delta_{23}\,\mathrm{e}^{-x}} \\ &+\frac{k_BT}{\pi d^3}\sum_{n=1}^{\infty}{}'\tilde d^3\int_1^\infty \mathrm{d}p\; p^2\left(\frac{\Delta^R_{12}\Delta^R_{23}\,\mathrm{e}^{-2p\tilde d}}{1+\Delta^R_{12}\Delta^R_{23}\,\mathrm{e}^{-2p\tilde d}}+\frac{\epsilon_{2_\parallel}}{\epsilon_{2_\perp}}\frac{\bar\Delta^R_{12}\bar\Delta^R_{23}\,\mathrm{e}^{-2p\tilde d}}{1+\bar\Delta^R_{12}\bar\Delta^R_{23}\,\mathrm{e}^{-2p\tilde d}}\right).\end{aligned} \tag{3.35}$$

The first term in the expression corresponds to the static response of the medium and the second term corresponds to the dynamic response. Functions $\bar\Delta_{ij}=\bar\Delta_{ij}(0)$, $\Delta^R_{ij}=\Delta^R_{ij}(i\xi_n)$ and $\bar\Delta^R_{ij}=\bar\Delta^R_{ij}(i\xi_n)$ are determined in Eqs. (3.13) and (3.20), and $\tilde d = d\sqrt{\epsilon_{2_\perp}}\xi_n/c$. In Eq. (3.35) the integration over the wavevector κ was substituted by the integration over a dimensionless parameter $p=\rho_2(\kappa)c/(\xi_n\sqrt{\epsilon_{2_\perp}})$, so that

$$\begin{aligned}\bar\Delta_{ij}&=\frac{\bar\epsilon_i-\bar\epsilon_j}{\bar\epsilon_i+\bar\epsilon_j} \quad , \quad \bar\epsilon_i=\sqrt{\epsilon_{i_\parallel}\epsilon_{i_\perp}},\\ \Delta^R_{ij}&=\frac{s_i-s_j}{s_i+s_j} \quad , \quad s_i=\sqrt{p^2-1+\epsilon_{i_\perp}/\epsilon_{2_\perp}},\\ \bar\Delta^R_{ij}&=\frac{\bar\epsilon_i\bar s_j-\bar\epsilon_j\bar s_i}{\bar\epsilon_i\bar s_j+\bar\epsilon_j\bar s_i} \quad , \quad \bar s_i=\sqrt{p^2-1+\epsilon_{i_\parallel}/\epsilon_{2_\parallel}},\end{aligned} \tag{3.36}$$

and $\epsilon_i=\epsilon_i(i\xi_n)$, unless stated otherwise.

By following the procedure of calculating the van der Waals force and by comparing the Eq. (3.35) to the Eq. (3.1) (or similarly, by comparing it to the limiting case of the Eq. (3.35) where $\epsilon_{i_\perp},\epsilon_{i_\parallel}\to\epsilon_i$), it can be seen that the influence of the anisotropy of the permittivity tensor affects the van der Waals interaction through the change of the penetration depths of the surface fluctuation modes and via changing the boundary conditions for the electromagnetic field at the interface between two different media. For the uniaxial permittivity the anisotropy of the interacting media 1 and 3 changes the interaction via renormalized effective permittivity, $\epsilon_i\to\sqrt{\epsilon_{i_\parallel}\epsilon_{i_\perp}}$. On the other hand, the uniaxiality of medium 2, which mediates the interaction between the other two media, does not only renormalize the effective permittivity but also explicitly affects the magnitude of the interaction. Beside these differences, the structure of van der Waals force for uniaxial media is similar to the one for the isotropic media. The properties of the force and the differences between the isotropic and uniaxial expressions will be discussed in more detail after the analytic expression for the force, i.e., the Hamaker constant, will be derived.

Often, in experimental set-up the solid substrate is covered by a natural oxide layer, a layer of condensed water, etc., and the system in question is at least four-layered (see Fig. 3.3). For such cases, combining relations for Hamaker constants are known [89] and are frequently used in practice. These relations are by itself approximate and beside that, they combine Hamaker constants, which are already

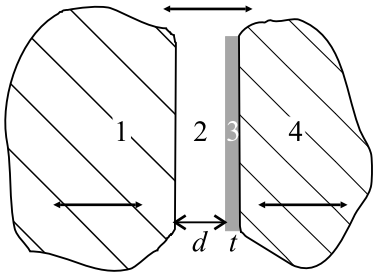

Figure 3.3 Schematic representation of the four-layer system: two semi-infinite macroscopic bodies separated by the third medium. One of the substrate is covered by an additional layer, e.g., a natural oxide layer or a layer of condensed water. The thickness of the additional layer is t and the separation between the macroscopic bodies, which is subject to change, is d.

obtained by some other approximations that will be discussed in the following Section. Therefore, the force calculated from a combined Hamaker constant can only serve as a qualitative measure of the force rather than a quantitative. From the secular equations obtained for the four-layer system [Eqs. (3.14) and (3.21)] and the definition of the van der Waals force [Eq. (3.34)], the expression for the force in a four-layer system can be easily determined. Both, the expression in Eq. (3.34) and the van der Waals force for the four-layer system can only be calculated numerically. Since the results of such numerical calculations will be used in the study of stability of thin nematic deposition, the expression for the van der Waals force acting on a layer of media 2 with thickness d, and surrounded by semi-infinite medium 1, a layer of medium 3 (thickness t), and semi-infinite medium 4, are written out as well,

$$\begin{aligned}\Pi \;=& \frac{k_B T}{16\pi d^3}\frac{\epsilon_{2_\parallel}(0)}{\epsilon_{2_\perp}(0)}\int_0^\infty \mathrm{d}x\; x^2 \frac{\bar\Delta_{12}\bar\Delta_{23}\,\mathrm{e}^{-x}+\bar\Delta_{12}\bar\Delta_{34}\,\mathrm{e}^{-x(1+a)}}{1+\bar\Delta_{12}\bar\Delta_{23}\,\mathrm{e}^{-x}+\bar\Delta_{23}\bar\Delta_{34}\,\mathrm{e}^{-xa}+\bar\Delta_{12}\bar\Delta_{34}\,\mathrm{e}^{-x(1+a)}} \\ &+\frac{k_B T}{\pi d^3}\sum_{n=1}^{\infty}{}'\tilde d^3\int_1^\infty \mathrm{d}p\; p^2\left(\frac{\Delta^R_{12}\Delta^R_{23}\,\mathrm{e}^{-2p\tilde d}+\Delta^R_{12}\Delta^R_{34}\,\mathrm{e}^{-2p\tilde d(1+a)}}{1+\Delta^R_{12}\Delta^R_{23}\,\mathrm{e}^{-2p\tilde d}+\Delta^R_{23}\Delta^R_{34}\,\mathrm{e}^{-2p\tilde da}+\Delta^R_{12}\Delta^R_{34}\,\mathrm{e}^{-2p\tilde d(1+a)}}\right. \\ &\left.+\frac{\epsilon_{2_\parallel}}{\epsilon_{2_\perp}}\frac{\bar\Delta^R_{12}\bar\Delta^R_{23}\,\mathrm{e}^{-2p\tilde d}+\bar\Delta^R_{12}\bar\Delta^R_{34}\,\mathrm{e}^{-2p\tilde d(1+a)}}{1+\bar\Delta^R_{12}\bar\Delta^R_{23}\,\mathrm{e}^{-2p\tilde d}+\bar\Delta^R_{23}\bar\Delta^R_{34}\,\mathrm{e}^{-2p\tilde da}+\bar\Delta^R_{12}\bar\Delta^R_{34}\,\mathrm{e}^{-2p\tilde d(1+a)}}\right). \end{aligned} \tag{3.37}$$

Here, $\tilde d = d\sqrt{\epsilon_{2_\perp}}\xi_n/c$, $a = t/d\sqrt{(\epsilon_{2_\parallel}/\epsilon_{2_\perp})(\epsilon_{3_\perp}/\epsilon_{3_\parallel})}$, and functions $\bar\Delta_{ij} = \bar\Delta_{ij}(0)$, $\Delta^R_{ij} = \Delta^R_{ij}(i\xi_n)$, $\bar\Delta^R_{ij} = \bar\Delta^R_{ij}(i\xi_n)$ are defined in Eq. (3.36). In a four-layer system, for small thicknesses d the van der Waals interaction is mostly due to the interaction between media 1 and 3 over a layer of medium 2, whereas for large separations d the effect of the additional layer 3 is negligible and the interaction is due to the interaction of media 1 and 4 over a medium 2. For intermediate separations the interaction is due to the non-trivial composition of layers and is not just a superposition of the two interactions described above. From the arguments just discussed the force can have

a non-monotonic behavior and the turn-over of the behavior of the force occurs at $d \sim t$.

3.5 Uniaxial Hamaker constant

Frequently, one is not interested in a precise separation dependence of the van der Waals force, but rather in its attractive/repulsive character and its order of magnitude. In such case, one is satisfied with the approximate analytic expression which is far easier to analyze and calculate with. For that reason the approximate analytic expression for the uniaxial van der Waals force is determined.

In the nonretarded limit the dependence on the separation between the two bodies can be extracted from the material properties and the van der Waals interaction can be written in a form of an explicit separation dependence and the "Hamaker" constant. In this limit the velocity of light is assumed to be infinitely large, so that the phase coherence between interacting fluctuating dipoles is not lost for any separation. This is always true for static electromagnetic fields, whereas for the dynamic electromagnetic fields it only holds approximately if the distance between the two interacting molecules is small comparing to the wavelength of the radiation of the fluctuating dipole. For most materials, $\lambda_e = c/\nu_e \sim 100$ nm. Neglecting the retardation, the expression in Eq. (3.32) reduces to $\Pi = -A/6\pi d^3$, where A is a Hamaker constant calculated from the Lifshitz theory,

$$A = -\frac{3k_BT}{4}\sum_{n=0}^{\infty}{}'\frac{\epsilon_{2_\parallel}(i\xi_n)}{\epsilon_{2_\perp}(i\xi_n)}\int_0^\infty \mathrm{d}x\; x^2 \frac{\bar{\Delta}_{12}(i\xi_n)\bar{\Delta}_{23}(i\xi_n)\mathrm{e}^{-x}}{1+\bar{\Delta}_{12}(i\xi_n)\bar{\Delta}_{23}(i\xi_n)\mathrm{e}^{-x}}. \tag{3.38}$$

Here, the prime over the sum denotes that the term with $n = 0$ should be multiplied by $1/2$ and the function $\bar{\Delta}_{ij} = \bar{\Delta}_{ij}(i\xi_n)$ is defined in Eq. (3.36). After performing the elementary integral in Eq. (3.38),

$$A = -\frac{3k_BT}{2}\sum_{n=0}^{\infty}{}'\frac{\epsilon_{2_\parallel}(i\xi_n)}{\epsilon_{2_\perp}(i\xi_n)}\bar{\Delta}_{12}\bar{\Delta}_{23}\left[1+\sum_{k=1}^{\infty}\frac{(-\bar{\Delta}_{12}\bar{\Delta}_{23})^k}{(k+1)^3}\right]. \tag{3.39}$$

Usually, $|\bar{\Delta}_{ij}| \ll 1$, except if $\bar{\epsilon}_i \ll \bar{\epsilon}_j$ or vice versa, which is usually not true. Therefore, the terms of higher orders of products $\bar{\Delta}_{12}\bar{\Delta}_{23}$ can be neglected — neglecting "many-body" interactions. Here, by analogy with the microscopic description, the contributions from different orders in $\Delta_{12}\Delta_{23}$ are termed as: "pair-wise" interaction, if only the first order is taken into account, and as "many-body" interaction, if the complete series of orders is considered. If the temperatures are not very high, the sum over n can be replaced by integral with respect to the frequency ξ. (For room temperatures, $\xi_1/\omega_e = (k_BT/\hbar c)\lambda_e \sim 1/80 \ll 1$, and the sum over discrete spectrum of frequencies ξ_n can be safely replaced by an integral.) In the case of

isotropic media, these approximations allow one to calculate the Hamaker constant analytically. Here, it should be taken into account that from Eqs. (3.36) and (3.33)

$$\bar{\Delta}_{ij}(i\xi) = \frac{n_i^2 - n_j^2}{n_i^2 + n_j^2 + 2\xi^2/\omega_e^2}. \tag{3.40}$$

For uniaxial media the latter expression, with the additional transformation $n_i \to \bar{n}_i$, is only approximately valid, since terms $[(\Delta n_i/n_{i_\parallel})^2 \pm (\Delta n_j/n_{j_\parallel})^2](\xi/\omega_e)^2$ and higher orders in both, $(\Delta n_i/n_{i_\parallel})$ and (ξ/ω_e), are neglected; $\Delta n_i = n_{i_\parallel} - n_{i_\perp}$, and is in liquid-crystalline systems up to 10% of $n_{i_\parallel}$, thus, neglecting the higher orders contributes the error not larger than few percents. With this additional approximation, the Hamaker constant for uniaxial media can be determined:

$$\begin{aligned} A \;=\; A^{\nu=0} + A^{\nu>0} &= \frac{3}{4}k_BT\frac{\epsilon_{2_\parallel}}{\epsilon_{2_\perp}}\frac{\bar{\epsilon}_1 - \bar{\epsilon}_2}{\bar{\epsilon}_1 + \bar{\epsilon}_2}\frac{\bar{\epsilon}_3 - \bar{\epsilon}_2}{\bar{\epsilon}_3 + \bar{\epsilon}_2} \\ &+ \frac{3\hbar\omega_e}{8\sqrt{2}}(\bar{n}_1^2 - \bar{n}_2^2)(\bar{n}_3^2 - \bar{n}_2^2)\left[\frac{\sqrt{2}(n_{2_\parallel}^2 - n_{2_\perp}^2)}{n_{2_\perp}(2n_{2_\perp}^2 - \bar{n}_1^2 - \bar{n}_2^2)(2n_{2_\perp}^2 - \bar{n}_3^2 - \bar{n}_2^2)}\right. \\ &\left. - \frac{2n_{2_\parallel}^2 - \bar{n}_1^2 - \bar{n}_2^2}{\sqrt{\bar{n}_1^2 + \bar{n}_2^2}(2n_{2_\perp}^2 - \bar{n}_1^2 - \bar{n}_2^2)(\bar{n}_1^2 - \bar{n}_3^2)} + \frac{2n_{2_\parallel}^2 - \bar{n}_3^2 - \bar{n}_2^2}{\sqrt{\bar{n}_3^2 + \bar{n}_2^2}(2n_{2_\perp}^2 - \bar{n}_3^2 - \bar{n}_2^2)(\bar{n}_1^2 - \bar{n}_3^2)}\right], \end{aligned} \tag{3.41}$$

where $\bar{a}_i = \sqrt{a_{i_\parallel} a_{i_\perp}}$ and a stands for either static dielectric constant ϵ, or the refractive index in visible n. The first term in Eq. (3.41), $A^{\nu=0}$, corresponds to the static response of the media, and the second term, $A^{\nu>0}$, corresponds to dynamic response.

If the interacting macroscopic bodies are isotropic, the effective parameters $\bar{\epsilon}$ and $\bar{n}$ are replaced by isotropic parameters ϵ and n, respectively. In the case all three media are isotropic, the expression reduces to the well known formula written out in Eq. (3.2). Frequently, the two semi-infinite media are the same, e.g., free-standing liquid-crystalline film surrounded by air, membrane in a solution, etc., and the Hamaker constant reduces to

$$\begin{aligned} A \;=\; &\frac{3}{4}k_BT\frac{\epsilon_{2_\parallel}}{\epsilon_{2_\perp}}\frac{(\bar{\epsilon}_1 - \bar{\epsilon}_2)^2}{(\bar{\epsilon}_1 + \bar{\epsilon}_2)^2} + \frac{3\hbar\omega_e}{8\sqrt{2}}(\bar{n}_1^2 - \bar{n}_2^2)^2 \\ &\times \left[\frac{\sqrt{2}(n_{2_\parallel}^2 - n_{2_\perp}^2)}{n_{2_\perp}(2n_{2_\perp}^2 - \bar{n}_1^2 - \bar{n}_2^2)^2} + \frac{(\bar{n}_1^2 + \bar{n}_2^2)^2 + 4\bar{n}_2^4 - 2(\bar{n}_1^2 + \bar{n}_2^2)(3n_{2_\parallel}^2 - n_{2_\perp}^2)}{2(\bar{n}_1^2 + \bar{n}_2^2)^{3/2}(2n_{2_\perp}^2 - \bar{n}_1^2 - \bar{n}_2^2)^2}\right]. \end{aligned} \tag{3.42}$$

In the following, the derived Hamaker constant for uniaxial media [Eq. (3.41)] will be first compared to the isotropic Hamaker constant [Eq. (3.2)] and, secondly, its validity with respect to the full Lifshitz theory [Eq. (3.35)] will be discussed.

Uniaxial vs. isotropic

In the derived expressions, the difference between isotropic and uniaxial media is explicitly manifested: The relevant parameters, which determine the character of the interaction, are in the case of isotropic interacting media $\epsilon = \epsilon^{iso}$ and $n = n^{iso}$. In the case of uniaxial media the relevant parameters are not the traces of the corresponding tensors, $\epsilon^{iso} = (\epsilon_\parallel + 2\epsilon_\perp)/3$ and $(n^{iso})^2 = (n_\parallel^2 + 2n_\perp^2)/3$, but rather products of their eigenvalues, $\bar{\epsilon} = \sqrt{\epsilon_\parallel \epsilon_\perp}$ and $\bar{n} = \sqrt{n_\parallel n_\perp}$. The sign of the static part of the Hamaker constant depends on the relative sequence of the introduced renormalized static dielectric constants: for $\bar{\epsilon}_2 < \bar{\epsilon}_1, \bar{\epsilon}_3$ or $\bar{\epsilon}_2 > \bar{\epsilon}_1, \bar{\epsilon}_3$ the static Hamaker constant is positive and static part of the van der Waals interaction is attractive, whereas for $\bar{\epsilon}_1 < \bar{\epsilon}_2 < \bar{\epsilon}_3$ or $\bar{\epsilon}_1 > \bar{\epsilon}_2 > \bar{\epsilon}_3$ the static Hamaker constant is negative and the corresponding interaction is repulsive. Similar conditions can be determined for the dynamic part of the Hamaker constant. It can be shown that the part in the square brackets in Eq. (3.41) is positive definite, thus, the sign of the dynamic part of the Hamaker constant depends solely on the sign of the product $(\bar{n}_1^2 - \bar{n}_2^2)(\bar{n}_3^2 - \bar{n}_2^2)$. For $\bar{n}_2 < \bar{n}_1, \bar{n}_3$ or $\bar{n}_2 > \bar{n}_1, \bar{n}_3$ the dynamic Hamaker constant is positive and the dynamic part of the van der Waals interaction is attractive, whereas for $\bar{n}_1 < \bar{n}_2 < \bar{n}_3$ or $\bar{n}_1 > \bar{n}_2 > \bar{n}_3$ the dynamic Hamaker constant is negative and the corresponding interaction is repulsive. The sign of the isotropic Hamaker constant has the same sequence dependence as the uniaxial Hamaker constant, however, with isotropic parameters ϵ^{iso} and n^{iso} instead of effective $\bar{\epsilon}$ and $\bar{n}$, respectively.

As already noted, until now in studies concerning uniaxial layers the van der Waals interaction has been calculated by use of the isotropic Hamaker constant and isotropic parameters. There are two sources of mistakes when doing this. First, even if the effective parameters are very close to the isotropic parameters, the magnitude of obtained Hamaker constant differs from the uniaxial one because the anisotropies $\Delta\epsilon_2 = \epsilon_{2_\parallel} - \epsilon_{2_\perp}$ and $\Delta n_2 = n_{2_\parallel} - n_{2_\perp}$ are neglected. (The static part is always smaller whereas the dynamic part can be either smaller or larger.) In the static part, the neglected dependence is easily recognized in the ratio $\epsilon_{2_\parallel}/\epsilon_{2_\perp}$, which is by definition always larger than 1, whereas in the difference of the dynamic parts the dependence on the anisotropy is not that clear. Secondly, the difference between the isotropic and uniaxial Hamaker constants can be even more profound if the sequences of isotropic and effective parameters are different. In that case, the isotropic expression yields wrong sign of the interaction. The change of the sequences is very easily obtained with static dielectric constants, whereas the optical anisotropies are usually small and the sequences of isotropic and effective refractive indices change only in a very narrow range of possible combinations. Since the static Hamaker constant is about an order of magnitude smaller than its dynamic part the effect is not very common

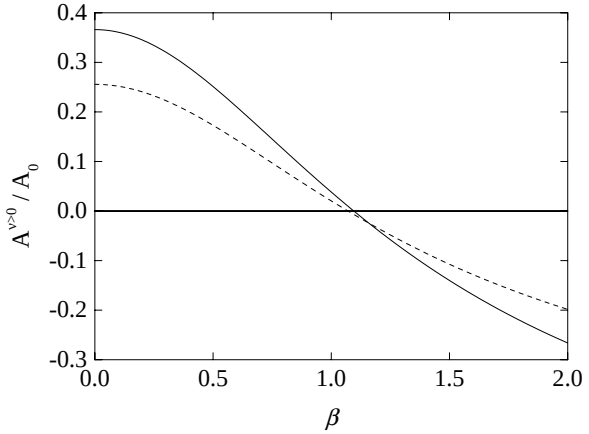

Figure 3.4 Dynamic part of Hamaker constant as a function of $\beta = n_1/n_{2_\perp}$. Solid line corresponds to reduced uniaxial and the dashed line to reduced isotropic Hamaker constant; $A_0 = 3\hbar\omega_e n_{2_\perp}/8\sqrt{2}$, $n_{2_\parallel}/n_{2_\perp} = 1.2$, and $n_3/n_{2_\perp} = 0.67$.

in experimental set-ups. The narrowness of possible combination of materials that satisfy the described conditions (see Fig. 3.4) could be one of the reasons why the problem of wrong sign of the Hamaker constant in systems consisting of uniaxial media has not been recognized before. However, it can be expected that the effect has already been observed but not recognized and/or understood. The explained change of the attractive/repulsive character of the van der Waals interaction to the repulsive/attractive character due to the increased optical anisotropy can be also one of the reasons for change in the stability of thin soft layers when crossing the (dis)ordering transition. As an example, the Hamaker constant is calculated for a system, which is often a part of the experimental set-up: a thin liquid-crystalline film deposited on a solid substrate and in contact with air on the other side. For liquid crystal 5CB ($\epsilon_\parallel = 18.5$, $\epsilon_\perp = 7$, $n_\parallel = 1.702$, and $n_\perp = 1.539$) on silica ($\epsilon = 14$ and $n = 1.5$) the van der Waals interaction is attractive in both, uniaxial and isotropic phase; for the same liquid crystal on a material with $\epsilon = 11$ and $n = 1.6$, which can be found among glassy materials, the interaction is repulsive in the isotropic and attractive in the uniaxial phase (see Fig. 3.5).

Hamaker vs. Lifshitz

After the comparison between the isotropic and uniaxial Hamaker constants the validity of the approximations that lead from the full Lifshitz theory to the derived Hamaker constant should be discussed. By comparing the Hamaker constants in which either "many-body" interactions [Eq. (3.35)] or just "pair-wise" interactions [Eq. (3.41)] are taken into account, it can be seen that in the nonretarded limit neglecting the higher orders does not considerably alter the magnitude of the inter-

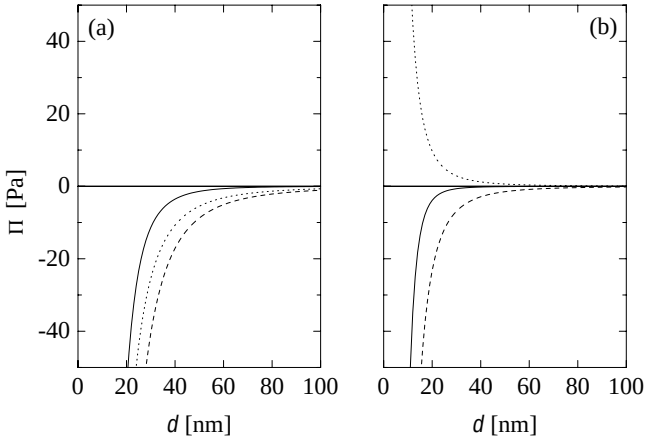

Figure 3.5 Van der Waals force per unit area in the layer of nematic liquid crystal ($\epsilon_\parallel = 18.5$, $\epsilon_\perp = 7$, $n_\parallel = 1.702$, and $n_\perp = 1.539$) in a contact with a solid substrate — (a) silica ($\epsilon = 14$, $n = 1.5$), (b) some glassy material ($\epsilon = 11$, $n = 1.6$) — and air. Solid curves correspond to full Lifshitz theory for uniaxial media, dashed curves are the van der Waals force per unit area calculated with uniaxial Hamaker constant, and dotted lines are calculated with Hamaker constant for isotropic media.

action. Nevertheless, one should bear in mind that the screening of the surrounding molecules decreases the interaction, however, for realistic parameters $\sim 5\%$ at the most. As already known, the main defect of the introduced "Hamaker" procedure is not in neglecting "many-body" interactions but in neglecting the retardation. The latter becomes important when the time it takes for the electromagnetic field of one molecule to reach the second one and to return becomes comparable to the period of the fluctuating dipole. Usually, this happens when the interacting molecules are about ten nanometers apart. In Figs. 3.5 and 3.6 the van der Waals force as calculated from the full Lifshitz theory for uniaxial media is compared to the forces in the nonretarded limit, either taking into account or neglecting the anisotropy.

Although, strictly speaking, approximation of no retardation is valid only when the interacting bodies are in close proximity to each other one should keep in mind that the retardation does not change the character of the interaction but only decreases its magnitude when the separation between the bodies is increased. If there is another, stronger interaction, which acts in the system, and the van der Waals interaction contributes only a correction to the primary interaction or if the van der Waals interaction is itself the primary interaction one can be satisfied with the approximate analytic expression which is far easier to calculate with and gives better insight in the effect of dielectric and optical properties of constituent media on the van der Waals interaction. Here is the opportunity for the analytic expression derived here. Especially lately, in studies, which aim to explain the experiments of

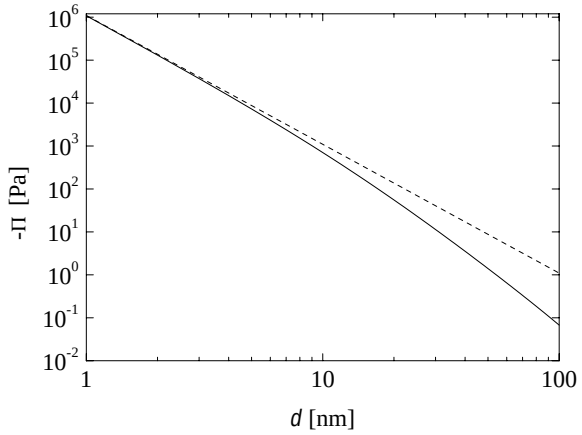

Figure 3.6 Van der Waals force per unit area in the layer of nematic liquid crystal in a contact with silica and air. Solid curve corresponds to the full Lifshitz theory for uniaxial media and dashed curve to the van der Waals force per unit area calculated with uniaxial Hamaker constant. Parameters used are the same as in Fig. 3.5.

spinodal dewetting of thin soft organic materials usually characterized by uniaxial dielectric permittivity and refractive index, the correct determination of at least the character of van der Waals interaction is very important [103,104].

4

Heterophase nematogenic system

In this study of influence of the confining substrates onto the equilibrium order and pretransitional dynamics of the nematic liquid crystal we will first stop at substrate-induced effects which are localized in the vicinity of confining walls. They are characteristic for systems in which there is no competition between antagonistic fields inducing preferred direction of the nematic order in different directions, such as the surface, magnetic, etc., fields. Here, we are interested in systems that are subject to surface-induced nematic order. Especially interesting is the case, in which the surface potential is such as to induce a sufficiently large orientational ordering as compared with the bulk phase — a *paranematic system*. Then, a mesoscopic layer of nematic phase intervenes at the substrate–isotropic phase interface as the isotropic–nematic transition is approached from above [see Fig. 4.1 (a)]. The described situation is known as (orientational) *wetting*; the wetting can be either partial or complete. In the case of complete wetting, a *surface transition* occurs prior to the isotropic–nematic phase transition; the former being associated with the occurrence of the well defined layer of a nematic phase. The thickness of the surface-induced ordered layer diverges at the isotropic–nematic phase transition which, thus, becomes continuous. Above the surface critical point (G_{SC}, T_{SC}) the surface-induced layer grows continuously. In the case of partial wetting, the thickness of the surface-induced layer is saturated before the isotropic–nematic phase transition and the transition remains discontinuous. By changing the aligning power of the substrate, i.e., changing the anchoring strength and/or changing the value of the induced nematic order, the complete wetting can change to partial wetting (or vice versa) between which the *wetting transition* occurs. Temperature dependence of surface-induced wetting layers in the case of complete and partial wetting is plotted in Fig. 4.2.

The surface interaction may also have a disordering effect if, for example, the inner surface of the host material is rough [105–107]. In this case a reduction of the degree of order in the boundary layer is expected below the phase transition tem-

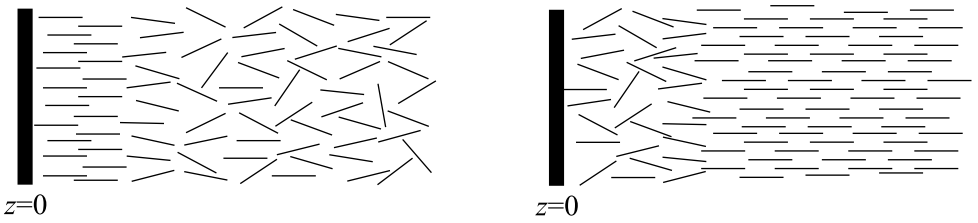

Figure 4.1 Schematic representation of the order of molecules close to the substrate in the system with surface-induced (a) nematic order and (b) disorder.

perature, and the substrate induces wetting by the isotropic phase [see Fig. 4.1 (b)]. Again, the complete wetting refers to the case where the thickness of the surface-induced isotropic layer diverges on approaching the isotropic–nematic phase transition from below whereas the wetting is partial if the thickness of the wetting layer remains finite at the transition. The divergent nature of the thickness of the wetting layer, either isotropic in a nematic phase or nematic in isotropic phase, is associated with the surface aligned semi-infinite nematic systems. In the case the liquid crystal is bounded from more than one side, the thickness of the wetting layer can not diverge because the wetting layers get in contact before that. Still, the discontinuity of the isotropic–nematic phase transition can be significantly reduced. In highly constrained surface-aligned nematic systems the transition between the isotropic and nematic phase can be lost whereas the nematic order grows gradually on lowering the temperature.

The interest in wetting transitions was initiated by study of Sheng in 1976 in which it was found that above some critical film thickness the isotropic–nematic phase transition in a surface aligned nematic can become continuous [18]. The original study of a nematic in contact with two substrates with infinitely strong anchoring was extended to cases of oblique anchoring strength [50]. Allender *et. al* studied extensively a semi-infinite nematic wetting system for which they determined in an analytical manner the scalar order parameter profiles in stable and metastable phases above and below the isotropic–nematic phase transition [108]. The isotropic–nematic phase transition in restricted geometries was further studied by Sluckin and Poniewierski [109,59], both, for the case of homeotropic and planar anchoring. In the latter, the nematic order in the wetting layer is biaxial due to the broken symmetry in the plane of the confining substrate. Telo da Gama *et. al* studied the wetting and interfacial phenomena by use of the density functional method [110,111]. In highly restricted geometry, the pretransitional nematic order and the structural force among the confining substrates was studied by Borštnik and Žumer [60]. Studies of equilibrium order were followed by studies

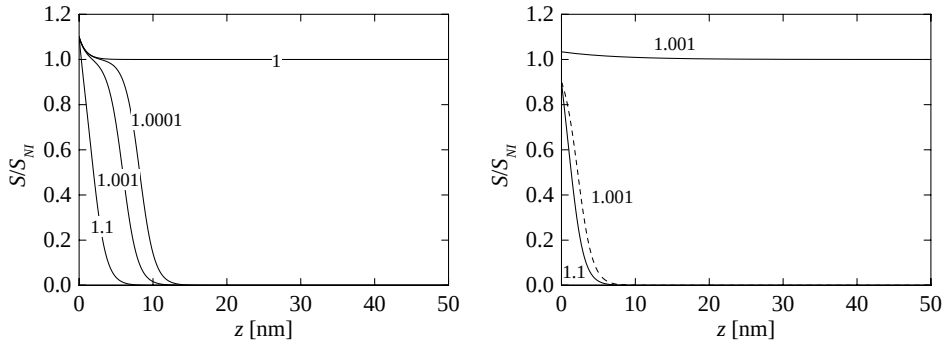

Figure 4.2 Portrait of profiles of the scalar order parameter for various temperatures for the case of (a) complete wetting and (b) partial wetting (dashed line corresponds to the metastable paranematic solution). The scalar order parameter S is measured in units of bulk value of the order parameter at the phase transition, S_{NI}.

of pretransitional collective dynamics in wetting systems. First, pretransitional excitations were determined for the paranematic slab above the phase transition by Ziherl *et. al* [14] which was followed by an extended study in the inverse case of a nematic sandwiched between order melting substrates [15]. The analytical solutions in a semi-infinite system were derived by Ivanov [112]. Beside theoretical studies, the wetting and wetting transitions were subject of series of experimental studies since they reveal anchoring and interfacial properties of the liquid crystal in contact with substrates. The studies performed by means of optical ellipsometry methods are due to Miyano [113], Yokoyama [114], Moses [106], and many others, and lately, the experiments involving the force microscopy were performed by Moreau *et. al* [22] and Kočevar *et. al* [115,67]. Similar effect as in the case of surface-aligned nematic order is observed also for the case of smectic order — wetting by a smectic phase — which is associated with both, the vicinity of the transition to the smectic A phase and with the fact that the presence of the wall breaks the continuous translational symmetry resulting in a smectic-like order close to the confining substrate. The former effect was studied mostly by Moses *et. al* [116], and the latter effect was studied by Rosenblatt [117], Ocko *et. al* [118], etc.

As it can be noted from the above review of work done in the field of wetting by isotropic or nematic phase there was not much known about the pretransitional collective dynamics in wetting systems before our study was performed. Though, it can be expected that the pretransitional dynamics of wetting systems should differ significantly from pretransitional dynamics in bulk systems, especially, when the conditions for the complete wetting are fulfilled. If the average equilibrium order in the wetting systems reveals the anchoring properties of the confining substrates and

the nature of the liquid crystal interface the study of pretransitional dynamics offers insight into the evolution of the order characteristic for the low-temperature phase in the case of paranematic system and the evolution of the disorder in the case of a nematic confined by "order-melting" substrates. Regardless of the geometry of the host medium, these systems are characterized by high surface-to-volume ratio and, thus, they are very susceptible to any interaction between the constituent molecules and the surrounding walls. The surface coupling encountered in actual confined systems is usually not strong enough to be describable by a fixed value of the degree of order at the wall which was assumed in the study of pretransitional collective dynamics in the paranematic system [14], however, it reveals the basic physics behind the phenomena studied. Secondly, as it has been already discussed, the surface interaction may also have a disordering effect which is realized in the case of silica and some other materials for various kinds of the surface treatment [107]. It is evident, that there are a number of parameters of wetting in liquid-crystalline systems that seem to be pertinent to the behavior of collective excitations of the ordering in the vicinity of the isotropic–nematic phase transition. In order to provide a complete account of the phenomenon first discussed in a preliminary study of Ziherl and Žumer [14], I elaborate some of them theoretically by (i) comparing the spectra of fluctuations in geometries with surface-induced order and disorder, and (ii) by extending the analysis to substrates with finite strength of the surface interaction. For the case of "order-melting" substrates I present a detailed study of both, equilibrium order determined within the phenomenological mean-field theory and collective pretransitional dynamics.

One of the difficulties encountered in any theoretical description of confined liquid crystals is the curved or even irregular and random internal geometry of the host material, which is often not easy to model. However, in the case of wetting, the anchoring effect of the confining surface is either partly or completely screened, and thus the actual topology of walls is not really important: it can be expected that the basic physics of these systems can be captured by a model planar geometry consisting of a nematic liquid crystal sandwiched between two parallel substrates, which is adopted in the present analysis. Schematic representation of the modeled system is visualized in Fig. 4.3. Two types of walls are considered: The *disordering substrate* gives rise to an isotropic boundary layer below the isotropic–nematic phase transition temperature, where the largest part of the sample is nematic, and to perfectly isotropic phase above the transition. The system will be termed as the *surface-molten nematic system*. Second type of walls pertains to the *ordering substrate* and the corresponding liquid-crystalline system is *paranematic*. In the paranematic system, the equilibrium configuration is nematic below T_{NI}, and above T_{NI} it remains

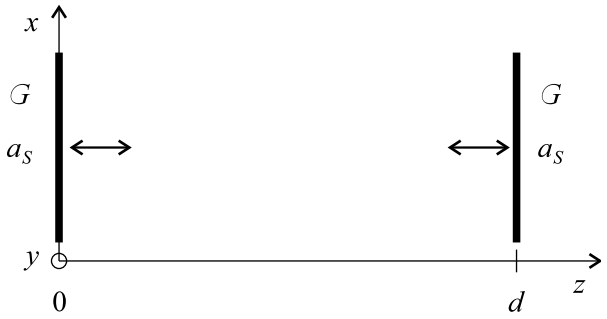

Figure 4.3 Schematic representation of the studied system. Nematic liquid crystal is sandwiched between two parallel planar substrates with equal anchoring properties. They either induce uniaxial nematic order in the homeotropic direction (paranematic system) or they decrease the nematic order (surface-molten nematic system).

nematic within the boundary layer whereas the core melts into isotropic phase.

The forthcoming analysis is based on the Landau–de Gennes model of the phase transition and the nematic is described by a tensorial order parameter. In the study, the surface-induced smectic layering is not considered since in the case of liquid crystals which can be found in nematic phase but do not form smectic layers in the bulk (which is the case for 5CB I refer to all through the thesis) the smectic layering is not very pronounced. Further, it is assumed that the average nematic director is homogeneous in the system and only the scalar order parameter varies as a function of a coordinate z perpendicular to the confining substrates. Skačej *et. al* showed that when the elastic constants associated to splay and bend deformations of the nematic director are different form the twist elastic constant (which is usual in liquid-crystalline materials) a spatial variation of the scalar order parameter induces variation of the director [119]. However, the coupling and the resulting variation of the director is very small and it is safe to adopt the one-elastic-constant approximation in which this effect can not arise. In 1996 Braun *et. al* studied wetting in the system where there was a competition between the surface-induced direction for the director and the preferred orientation of the director at the nematic–isotropic interface [120]. There are many experimental [121,122] and theoretical [123–125] studies considering the orientation of the director at the nematic–isotropic interface and also at the free nematic or isotropic surface. In most of them, the reported measured directions are in the range of 40° to 60°, however, from the Landau–de Gennes theory with assuming uniaxial nematic order only homeotropic and planar molecular arrangements can be obtained [123]. Marcus removed the assumption of uniaxial nematic order and showed that the order at the nematic–isotropic interface is highly biaxial and that the angle between the interface normal and the nematic director can be oblique [124]. However, in all cases the anchoring strength at the

nematic–isotropic interface is rather weak, $\sim 10^{-5}$ J/m^2, [107] so that it can be assumed that the orientation of the director is determined by the stronger anchoring of the substrate in the case of a paranematic system whereas in the case of a nematic in contact with disordering substrates the homeotropic direction is maintained by the aligning action of the magnetic field. In order to compete with the anchoring at the nematic–isotropic interface, $B \gtrsim 0.01$ T, which is very weak and, thus, its contribution to the free energy of the system need not to be considered explicitly. The case where the competing antagonistic preferred orientations of the director are comparable will be studied in the following Chapter which deals with the hybrid nematic cell.

In the following, the equilibrium profiles of the nematic order are calculated within the phenomenological mean-field theory (Section 4.1). The pretransitional dynamics of all five degrees of freedom of the order is determined in Section 4.2. Structural forces which arise among the confining substrates because of their (dis)-ordering action are discussed in Section 4.3. Last Section in the Chapter deals with the van der Waals force acting on a wetting layer due to the inhomogeneity of the order.

4.1 Equilibrium profiles

For a uniform director field with $\hat{n} = \hat{e}_z$, the base tensors T_i [Eq. (2.6)] are uniform themselves provided that the orientation of the two arbitrary vectors $\hat{e}_1$ and $\hat{e}_2$ is also position-independent, e.g., identified by $\hat{e}_x$ and $\hat{e}_y$. Being uniaxial, wetting structures are characterized by an inhomogeneous profile of the degree of order, $S/S_{NI} = a_0$. The lateral dimensions of the system are much larger than its thickness, $L_x, L_y \gg d$, thus, a_0 depends only on the distance from (one of) the substrates. Since the confining substrates are equal the profile of the degree of order is symmetric with respect to the plane in the middle of the liquid-crystalline cell. Thus, it will only be calculated in one half of the cell. The other four coefficients in the expansion $\mathsf{A} = \sum_{i=-2}^{2} a_i(\vec{r})\mathsf{T}_i$ are all equal to 0. The Euler–Lagrange equation [Eq. (2.62)], which determines the profile of a_0, reduces to

$$\zeta^2 a_0'' - \theta a_0 + 3a_0^2 - 2a_0^3 = 0, \tag{4.1}$$

where prime denotes $\mathrm{d}/\mathrm{d}z$. Since Q_S is assumed uniaxial and homeotropic, $\mathsf{Q}_S = a_S\mathsf{T}_0$, the boundary conditions at $z = 0$ and $z = 1/2$ read

$$a_0' = \frac{g}{\zeta^2}\left(a_0 - a_S\right), \tag{4.2}$$

where a_S is the preferred degree of order at the substrate, and

$$a_0' = 0, \tag{4.3}$$

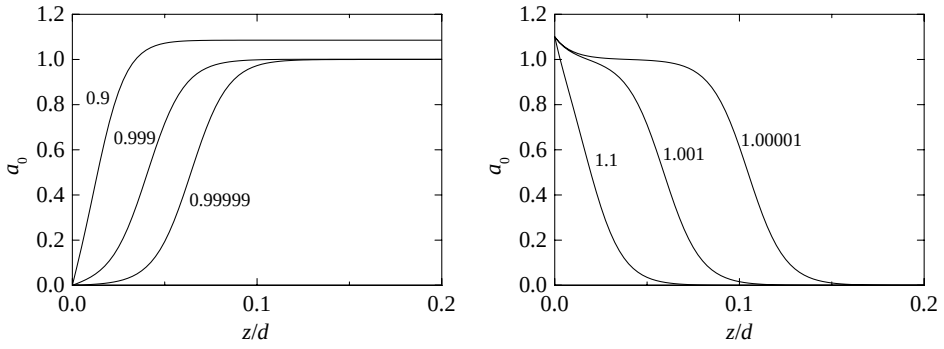

(a) (b)

Figure 4.4 Equilibrium profiles of the degree of order in the vicinity of (a) a disordering substrate at $\theta = 1 - 10^{-1}, 1 - 10^{-3}$, and $1 - 10^{-5}$, and (b) an ordering substrate at $\theta = 1 + 10^{-1}, 1 + 10^{-3}$, and $1 + 10^{-5}$. In both cases, the surface interaction is modeled by a prescribed degree of order equal to 0 and 1.1, respectively.

respectively. This and all further differential equations are solved numerically using the relaxation method [126].

In both wetting geometries the equilibrium profile of the degree of order exhibits a substrate-induced variation in the boundary layer and levels off at the bulk value in the center of the sample (Fig. 4.4). In the case the wetting is partial, the thickness of the wetting layer d_W has a very moderate temperature dependence whereas in the case of a complete wetting it exhibits a pronounced pretransitional increase. Since the thickness of the liquid crystal is finite the increase can not diverge like it diverges in the semi-infinite sample [108], however, as presented in Fig. 4.5 the actual temperature dependence is not far from the logarithmic behavior typical for semi-infinite samples. In the case of partial wetting, the thickness of the wetting layer levels off on approaching the bulk phase transition temperature. Temperature dependence of the thickness of the isotropic and nematic wetting layer in the case of complete and partial wetting is presented in Fig. 4.5.

Although the wetting behavior of liquid crystals can be quite complex as it was discussed in the beginning of this Chapter, complete wetting is generally related to substrates with large (dis)ordering power, whereas otherwise partial wetting is to be expected. For the quadratic surface interaction used in present study, complete wetting of the disordering wall occurs only if $a_S = 0$ and $G \gtrsim 0.0023$ J/m^2. In case of an order-inducing substrate the critical value of G depends on the preferred degree of order, which must exceed 1: for example, $G_c(a_S = 1.1) = 0.0006$ J/m^2. The obtained results are consistent with the results of the earlier study performed by Sheng [50], based on a somewhat different type of surface interaction. To illustrate the role of the strength of the surface interaction in the wetting behavior, some

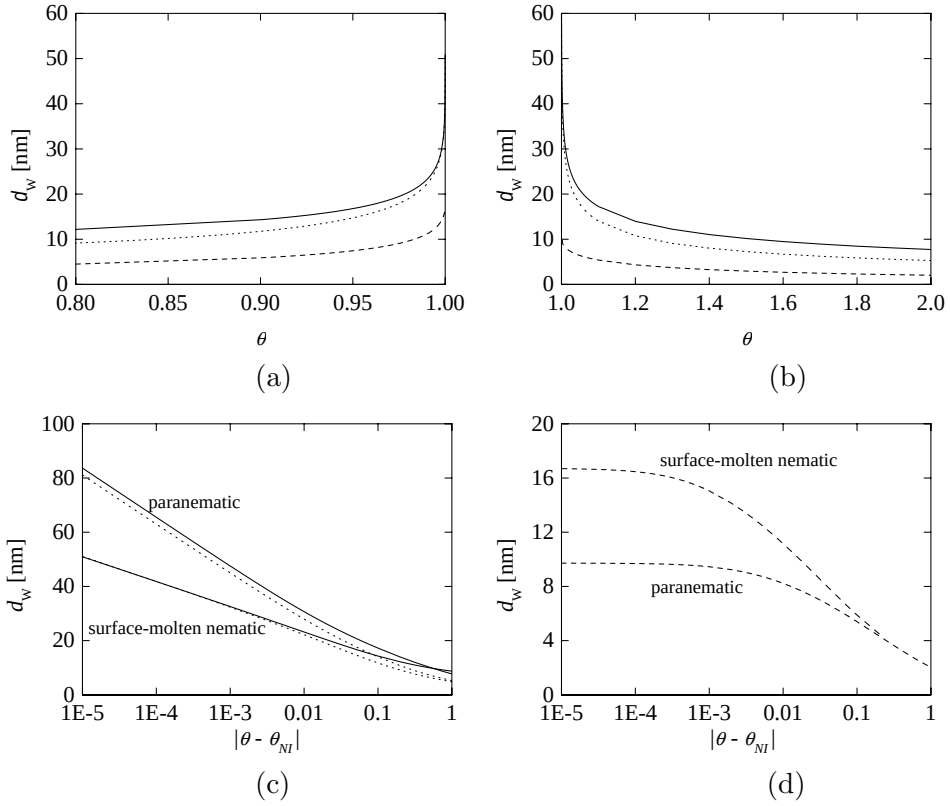

Figure 4.5 Temperature dependence of the thickness of the wetting layer d_W in (a) surface-molten nematic system and in (b) paranematic system in the case of complete (solid lines) and partial (dashed line) wetting. Dotted lines correspond to the thickness in the semi-infinite sample. Parameters used in the calculation of finite samples are for the surface-molten nematic system: $a_S = 0$, $d = 792$ nm, and $G \to \infty$ in the case of complete wetting and $G = 0.001$ J/m^2 in the case of partial wetting, and in the case of a paranematic system: $a_S = 1.1$, $d = 792$ nm, and $G \to \infty$ in the case of complete wetting and $G = 0.0006$ J/m^2 in the case of partial wetting. In the semi-infinite sample: $G \to \infty$ and $a_S = 0$ and $a_S = 1.1$, respectively. In (c) and (d), the curves are plotted in logarithmic scale.

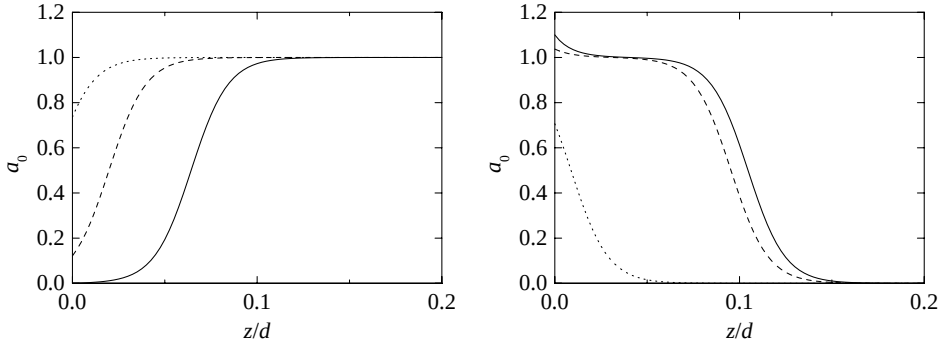

Figure 4.6 Some profiles of the degree of order in the finite anchoring model: (a) a disordering substrate at $\theta = 1-10^{-5}$ with $G \to \infty$ (solid line), 0.001 J/m^2 (dashed line), and 0.0003 J/m^2 (dotted line), (b) an ordering substrate at $\theta = 1 + 10^{-5}$ with $G \to \infty$ (solid line), 0.0007 J/m^2 (dashed line), and 0.0006 J/m^2 (dotted line).

equilibrium profiles of the degree of order in the two wetting systems are shown in Fig. 4.6.

As the thickness of the liquid-crystalline sample is varied the thickness of the wetting layer changes even though it looks like the two wetting layers do not interact with each other. In an earlier study within the Landau–Ginzburg theory, Gompper *et. al* studied a heterophase system of water confined with hydrophobic substrates. They derived the asymptotic behavior for the thickness dependence of the wetting layer thickness, $\partial d_W/\partial d \sim -\text{const.} \times \exp(-d/\xi)$ [127], where ξ is the correlation length of the degree of order in the bulk phase. In Fig. 4.7 the temperature dependence is presented for the case of complete and partial wetting in surface-molten nematic and paranematic systems. In both, d_W is a decreasing function of d and approaches the thickness corresponding to the semi-infinite sample. The behavior differs from the predicted asymptotic behavior, however, the latter is valid in the limit of large d's and small d_W's. On decreasing the sample thickness, the bulk-like core of the sample is more and more affected by the presence of the wall and finally the two wetting layers merge.

In a confined geometry, the transition between a surface-induced heterophase ordering and a homophase structure occurs at a temperature somewhat different from the clearing point. In case of disordering walls, the transition from the low-temperature phase characterized by molten boundary layer to the high-temperature isotropic phase is shifted below the nematic-isotropic phase transition temperature. Conversely, in the order-inducing geometry the transition from nematic to paranematic phase takes place above θ_{NI}. The actual magnitude of the shift depends on the size of the sample and on the parameters of the surface interaction, and is prac-

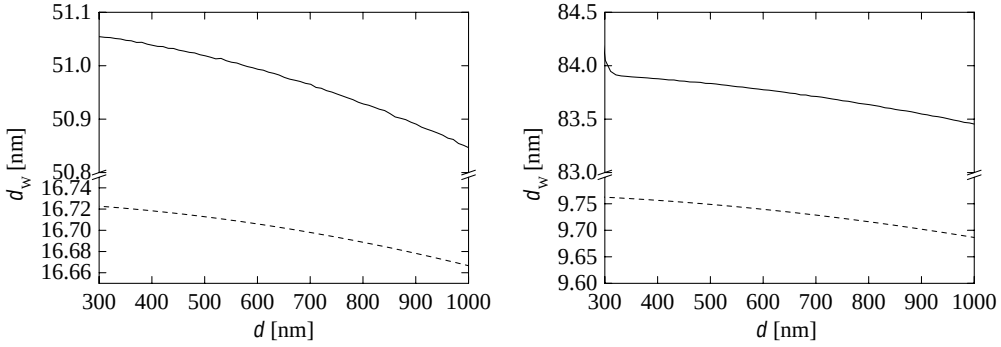

(a) (b)

Figure 4.7 Thickness of the wetting layer as a function of the thickness of the (a) nematic and (b) paranematic sample. Solid lines correspond to the regime of the complete wetting and dashed lines correspond to partial wetting. In semi-infinite sample, the corresponding thicknesses are in the nematic case 50.6 nm and 16.3 nm, and in the paranematic case 81.1 nm and 9.4 nm, respectively. Parameters used in calculation are in the surface-molten nematic case: $a_S = 0$, $\theta = 1 - 10^{-5}$, and $G \to \infty$ (complete wetting) and $G = 0.001$ J/m^2 (partial wetting), and in the paranematic case: $a_S = 1.1$, $\theta = 1 + 10^{-5}$, and $G \to \infty$ (complete wetting) and $G = 0.0006$ J/m^2 (partial wetting).

tically negligible in micron-size cavities: For example, for $\zeta = 0.01$ ($d = 792$ nm) and perfectly disordering wall with $G \to \infty$ and $a_S = 0$, the transition occurs at $\theta = 0.99274$. In the paranematic system with the same thickness and anchoring strength but with $a_S = 1.1$, the transition occurs at $\theta = 1.0073$. Both examples indicate that the shifts do not exceed 0.01 K. However, in smaller cavities the effect can be far more prominent. Below some cell thickness, which depends on the anchoring properties of the confinement, the phase transition is lost and the order grows continuously which is in agreement with experimental studies [128,129].

4.2 Pretransitional dynamics

Once the relevant equilibrium structures in the two wetting geometries have been described, the scene is set for the analysis of fluctuations. The dynamics of the five scalar components of collective excitations — introduced by the expansion $\mathsf{B}(\vec{r},t) = \sum_{i=-2}^{2} b_i(\vec{r},t)\mathsf{T}_i$ — is derived by projecting the equation of motion [Eq. (2.64)] onto the base tensors. Because the equilibrium order is characterized by only one nonzero amplitude, a_0, the five fluctuation modes are uncoupled. In addition, due to the uniaxial symmetry of the system the two biaxial modes are degenerate and so are the two director modes. Since the mean-field equilibrium profiles depend on the

z-coordinate only, the normal modes can be factorized as follows:

$$b_i(\vec{r},t) = \mathrm{e}^{i(k_x x + k_y y)}\beta_i(z)\,\mathrm{e}^{-\mu_i t}, \tag{4.4}$$

where μ_i's are the dimensionless relaxation rates of the eigenmodes measured in units of $\tau_a^{-1} \sim 10^8\ \mathrm{s}^{-1}$ [Eq. (2.60)]. Their normal components β_i are uncoupled and determined by

$$\begin{aligned} \zeta^2\beta_0'' - \left(\theta - 6a_0 + 6a_0^2 - \lambda_0\right)\beta_0 &= 0, \\ \zeta^2\beta_{\pm1}'' - \left(\theta + 6a_0 + 2a_0^2 - \lambda_{\pm1}\right)\beta_{\pm1} &= 0, \\ \zeta^2\beta_{\pm2} - \left(\theta - 3a_0 + 2a_0^2 - \lambda_{\pm2}\right)\beta_{\pm2} &= 0, \end{aligned} \tag{4.5}$$

where $\beta_i' = \mathrm{d}\beta_i/\mathrm{d}z$ and $\lambda_i = \mu_i - \zeta^2(k_x^2 + k_y^2)$ are the reduced relaxation rates of the modes. The in-plane components of the wave vector, k_x and k_y, are assumed to be subject to periodic boundary conditions. In terms of correlation lengths $\lambda_i = \xi_i^{-2}/\xi_{NI}^{-2} + \zeta^2 q_z^2$, where ξ_i's are the corresponding correlation lengths introduced in Eq. (2.35) and q_z is the wavevector of the deformation parallel to the substrate normal. In case of finite anchoring strength, the corresponding boundary condition at the substrate is given by

$$\beta_i'(0) = \frac{g}{\zeta^2}\beta_i(0), \tag{4.6}$$

and otherwise $\beta_i(0) = 0$. Due to symmetry arguments, the normal modes must be either even or odd with respect to the center of the sample, thus, $\beta_i'(1/2) = 0$ in the former case and $\beta_i(1/2) = 0$ in the latter case. (Since the equilibrium mean-field profile a_0 is even with respect to the plane in the middle of the cell and parallel to the confining substrates the corresponding potentials for the fluctuation modes are even as well. In the case of even potential the modes are know to be of the two types — either even or odd with respect to the same symmetry plane [130].)

Homophase ordering

If a nematic layer is bounded by the walls characterized by strong surface interaction and a bulk-like value of the preferred degree of order, β_i's reduce to sine waves, and their relaxation rates may be cast into

$$\widetilde{\lambda}_i = \xi_{N,i}^{-2}/\xi_{NI}^{-2} + \zeta^2\left[(n+1)\,\pi\right]^2, \tag{4.7}$$

which is the same as in bulk except that due to the finite dimension in the z direction the wavevector q_z can only have discrete values, $q_{z,n} = \zeta(n+1)\pi$, where n is the number of nodes of the sine function between the two substrates. In confined sample, the minimum wavevector is $\zeta\pi \neq 0$, thus, even the relaxation rate of the Goldstone

director mode is finite, though, it is very small. $\xi_{N,i}$'s are defined in Eq. (2.37) and their temperature dependence is presented in Fig. 2.5.

Above the clearing point, a disordering wall produces a perfectly isotropic phase. In this case, all five types of fluctuations are degenerate, and their relaxation rate is determined by

$$\widetilde{\lambda}_i = \xi_I^{-2}/\xi_{NI}^{-2} + \zeta^2 \left[(n+1)\,\pi\right]^2 . \tag{4.8}$$

ξ_I is introduced in Eq. (2.36) and its temperature dependence is plotted in Fig. 2.5. It should be stressed again that the hardness of a given type of fluctuations can be characterized by its correlation length: the shorter the correlation length, the higher the energy of fluctuations. To understand the pretransitional behavior of the system, it is important to know how the energy levels of excitations in nematic phase compare with those in isotropic phase. In the vicinity of the phase transition, fluctuations of the degree of order are equally hard in both phases. In nematic phase, the biaxial modes are energetically far more costly than in isotropic phase — as opposed to the director modes, which are characterized by an infinite correlation length in nematic phase, whereas ξ_I is finite at the phase transition temperature. At the phase transition, the correlation lengths of the scalar order parameter are equally hard in both, nematic and isotropic phase, because at the transition both phases are in equilibrium.

In general, the surface-induced degree of order differs form the bulk value and the profile of the degree of order is inhomogeneous. Thus, the generalized correlation lengths of the fluctuation modes are spatially dependent and the eigenmodes of fluctuations in the two wetting geometries can only be determined numerically. In the following, the spectra of collective excitations in nematic phase with molten boundary layers and in paranematic phase are interpreted simultaneously.

Fluctuations of Degree of Order

In both systems, the primary effect of wetting is related to the existence of a slow mode characterized by soft dispersion of its relaxation rate, whereas the upper part of the spectrum remains more or less the same as in homophase system (Figs. 4.8 and 4.9). The elementary mode of fluctuations of the degree of order is localized at the phase boundary between the wetting layer and the bulk phase, and since it is even with respect to the center of the sample, it corresponds to fluctuations of thickness of the central part of the slab. Similarly, the lowest odd mode — also localized at the nematic-isotropic interface — represents fluctuations of position of the core. However, the relaxation rates of these two modes are the same within numerical accuracy, indicating that the two wetting layers are effectively uncoupled.

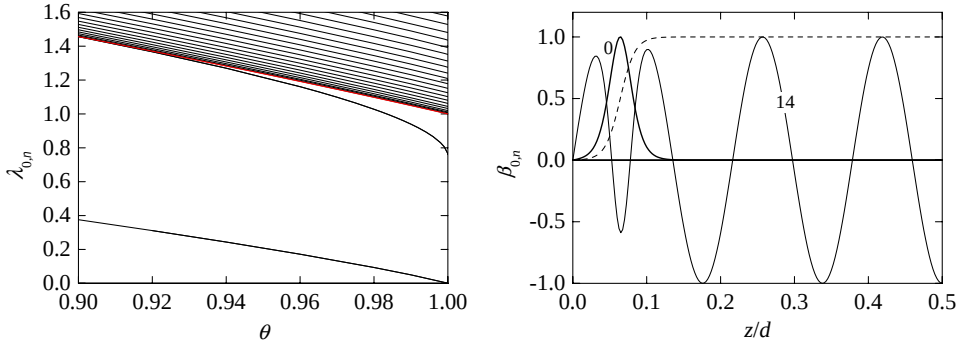

(a) (b)

Figure 4.8 Disordering substrate: (a) spectrum of fluctuations of the degree of order, illustrated by the portraits of a few typical modes labeled by the number of nodes (b); $\theta = 1 - 10^{-5}$. The lowest mode characterized by soft dispersion of the relaxation rate corresponds to fluctuations of the thickness of the wetting layer, whereas the upper part of the spectrum is basically the same as in purely nematic sample and the corresponding fluctuations disturb the whole sample. Red line in (a) represents the lower limit of the spectrum of a homophase system and the dashed line in (b) corresponds to the equilibrium profile of the degree of order; $G \to \infty$ and $a_S = 0$.

This is directly related to the thickness of the sample, which is much larger than $\xi_{N,0}$, the typical length scale of the variation of the degree of order. Were the system thinner, the correlation between the (dis)ordered regions induced by the two substrates would be stronger and the degeneracy of the lowest two normal modes would be removed.

In the complete wetting regime, the relaxation rate of the elementary excitations of the degree of order exhibits a linear critical temperature dependence typical for soft modes:

$$\lambda_{0,0} = \pm C_{\pm}(\theta - 1), \tag{4.9}$$

where '−' and '+' correspond to nematic phase with molten boundary layer and paranematic phase, respectively. The difference between the coefficients C_- and C_+, which are approximately equal to 5.6 and 3.0, can be attributed to the fact that the thickness of the isotropic wetting layer at the disordering wall at $\theta = 1 - \delta$ is half of the thickness of the nematic wetting layer at the ordering substrate at $\theta = 1 + \delta$; cf. Fig. 4.4 (a) and Fig. 4.4 (b). The slowdown of the relaxation rates of the surface-induced soft modes, i.e., the divergence of their relaxation times, at the phase transition temperature is a well-known and clear signature of the continuity of the transition, which is actually just another face of the advancing phase boundary in any complete wetting geometry [18,113]. In a finite system, however, a wetting-driven phase transition can never be truly continuous, because the heterophase

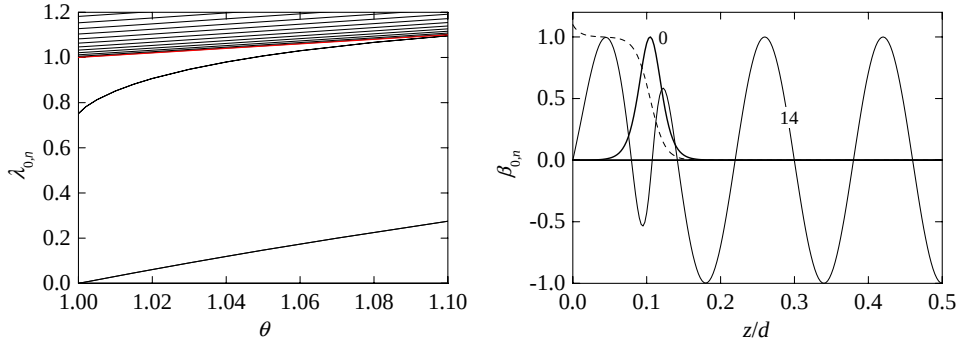

(a) (b)

Figure 4.9 Ordering substrate: (a) relaxation rates of fluctuations of the degree of order in paranematic phase, and (b) some typical modes for $\theta = 1 + 10^{-5}$. As in Fig. 4.8, the soft mode represents fluctuations of the thickness of the wetting layer, and the upper part of the spectrum is more or less the same as in perfectly isotropic sample, which is also reflected in the sinusoidal behavior of $\beta_{0,n>1}(z)$. Again, the red line is (a) is associated to the lower limit of the spectrum in a homophase system and in (b) the equilibrium profile of the degree of order is plotted with the dashed line; $G \to \infty$ and $a_S = 1.1$.

configuration eventually becomes unstable in the immediate vicinity of the clearing point — but in samples of thickness $\gtrsim 100$ nm this effect is detectable only if the temperature resolution of the experimental method is better than ~ 0.01 K.

In both wetting geometries, the upper part of the spectrum is more or less the same as its homophase (i.e., nematic and isotropic) counterpart, which is reflected in its regularity as well as in the sinusoidal profiles of the normal modes (Figs. 4.8 and 4.9). This also means that the upper, quasi-homophase modes are more or less independent on the strength of the surface interaction, which has been verified numerically. On the other hand, the behavior of the wetting-induced elementary mode does depend strongly on the magnitude of the anchoring strength, G: if the wetting is partial instead of complete, the pretransitional decrease of the localized modes' relaxation rates is less pronounced. They do not drop to 0 but remain finite at $\theta_{NI} = 1$, so that the transition from surface-molten nematic to isotropic phase or from nematic to paranematic phase is discontinuous even in semi-infinite systems. Though, the corresponding latent heat may be reduced considerably compared to the bulk isotropic–nematic transition. The temperature variation of the relaxation rates of the lowest modes remains linear, implying that the underlying mechanism is basically the same as in the complete wetting geometry. These findings are quantitatively summarized in Fig. 4.10, where the lowest mode's relaxation rate at the isotropic–nematic phase transition temperature is plotted as a function of the anchoring strength. In the partial wetting regime, which corresponds to small

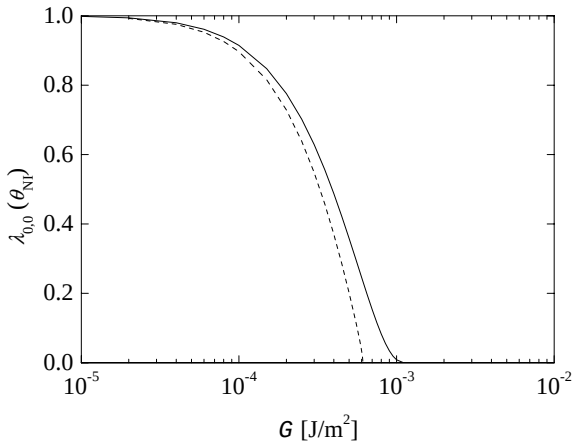

Figure 4.10 Relaxation rate of fluctuations of the thickness of the boundary layer in disordering (solid line) and ordering wetting geometry (dashed line) as a function of the strength of the surface interaction. In both cases, $\lambda_{0,0}$ is finite for $G < G_c$ (partial wetting) and 0 otherwise (complete wetting), the critical values of G being equal to 0.0023 J/m^2 for disordering substrates and 0.0006 J/m^2 for order-inducing walls. Note that the two geometries differ in the type of the behavior of $\lambda_{0,0}$ in the vicinity of G_c.

G's, $\lambda_{0,0}$ is finite; in the complete wetting regime, on the other hand, it is (within numerical accuracy) equal to 0. The two geometries give rise to slightly different behavior of $\lambda_{0,0}$ in the vicinity of the critical strength of the surface interaction: in case of disordering wall, $\lambda_{0,0}$ approaches 0 somewhat more slowly than in case of an order-inducing wall which is due to the fact that in the former case the regime of the complete wetting is bounded to the very edge of the phase diagram (G, a_S), i.e., to $a_S = 0$.

In addition to the two elementary modes corresponding to fluctuations of thickness of the boundary layers there are actually two more localized modes with relaxation rates that do depart from the quasi-homophase spectrum although not as distinctly as the soft dispersion of $\lambda_{0,0}$. These modes represent fluctuations of the shape of the phase boundaries: the even one is related to simultaneous sharpening/flattening of the phase boundaries, whereas the odd one describes out-of-phase fluctuations of their slope. The relaxation rates of these two modes are degenerate, which is, as it has already been established, related to the fact that the system considered is rather thick, so that the correlation between the two wetting layers is very weak. These modes are depicted in Fig. 4.11.

There are, therefore, two localized modes associated to each interface between nematic and isotropic phase: one of them corresponds to fluctuations of the position of the phase boundary, and the other one changes its profile. Since the theoretical approach used in this analysis is quite universal in its very nature, it seems that the

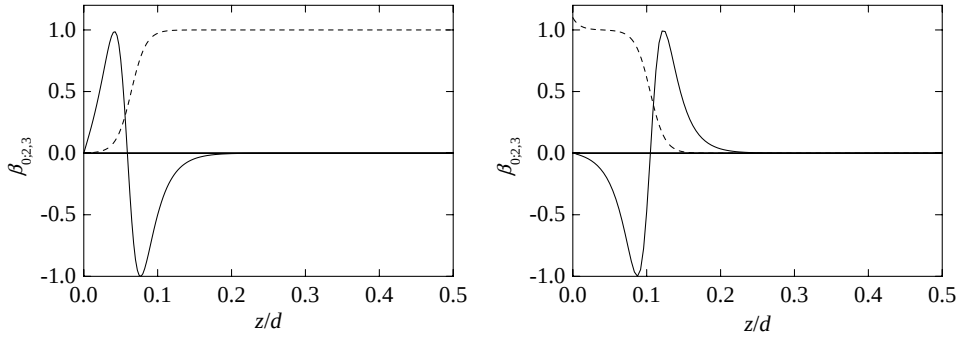

Figure 4.11 Portrait of the second-lowest order parameter modes in the case of (a) disordering and (b) ordering substrates. The even mode is responsible for simultaneous sharpening/flattening of the phase boundaries and the odd one describes out-of-phase fluctuations of their shape. The modes are degenerate within the numerical accuracy.

same should hold true for any interface that can be described by a scalar variable. However, in case of a phase boundary with a more complex structure, additional and more sophisticated localized modes are expected.

As the mean-field structures discussed here are characterized by inhomogeneous profiles of the degree of order and homogeneous profiles of the degree of biaxiality and director fields, the wetting-specific dynamics is primarily related to fluctuations of the degree of order. On the other hand, any critical behavior of the biaxial and director modes is merely an indirect effect of the surface-induced heterophase ordering.

Biaxial fluctuations

Biaxial modes are the hardest type of fluctuations in uniaxial nematic phase, which is related to the fact that thermal excitations of transverse molecular order have to compete with the existing uniaxial alignment. In systems with intrinsic biaxiality, biaxial fluctuations are much softer which will be evident in the hybrid nematic system studied in the following Chapter. At the phase transition temperature, the lower limit of the relaxation rates of biaxial fluctuations in nematic phase is 9 times larger than in isotropic phase [cf. Eqs. (4.7), (4.8) and Eqs. (2.37), (2.36)]. This considerable difference in the energy levels of biaxial modes in the two phases is reflected in their spectra in the two wetting geometries.

In case of nematic phase confined by a disordering wall, the lowest modes are bounded to the isotropic wetting layer. A strong elastic deformation of the modes in the thin isotropic region of the sample is energetically more favorable than a moder-

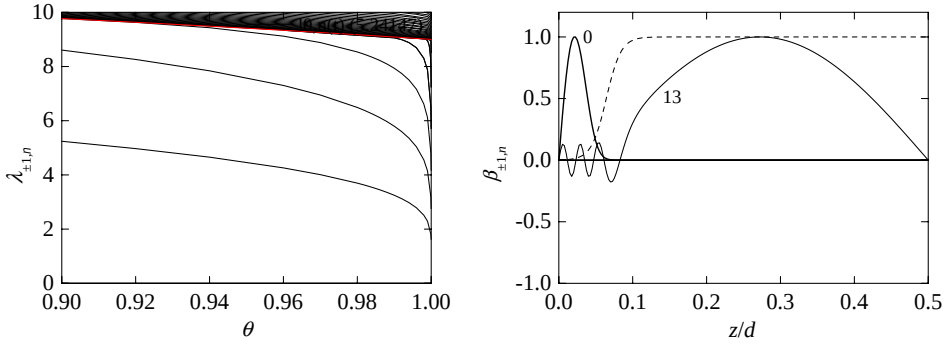

(a) (b)

Figure 4.12 Biaxial modes in a nematic sample bounded by disordering substrates: (a) the lowest modes exhibit pretransitional slowdown on approaching the clearing point and are confined to the isotropic wetting layer (b); $\theta = 1 - 10^{-5}$, $a_S = 0$, $G \to \infty$. The upper part of the spectrum is more or less nematic-like, the modes being spread over the whole slab. Red line represents the lower limit of the spectrum in a homophase system and the dashed line corresponds to the equilibrium profile.

ate deformation in the thick nematic core (see Fig. 4.12). The number of bounded modes depends on the thickness of the wetting layer and, thus, on temperature: as the sample is heated towards the clearing point, more and more levels depart from the upper, nematic-like part of the spectrum, which corresponds to modes that disturb the whole sample.

In paranematic phase induced by the ordering substrate, biaxial fluctuations are, conversely, expelled from the ordered boundary layer (see Fig. 4.13), so that the allowed wavelengths of the normal modes are determined by the thickness of the central isotropic part, not by the actual thickness of the sample. The difference between these two is not significant except in the vicinity of the phase transition temperature, where the nematic wetting layers squeeze the isotropic core and speed up the relaxation rates of the biaxial modes.

Director fluctuations

Director modes are, as opposed to biaxial fluctuations, excited very easily in nematic phase, where their Hamiltonian is purely elastic, whereas in isotropic phase they are characterized by finite correlation length [Eqs. (2.37) and (2.36)]. This implies that their wetting-induced behavior should be quite the inverse of what is predicted for the biaxial modes.

In the disordering geometry, the director modes are forced out of the substrate-induced isotropic boundary layer into the nematic core (see Fig. 4.14) just like the biaxial modes are expelled from the nematic boundary layer into the isotropic core

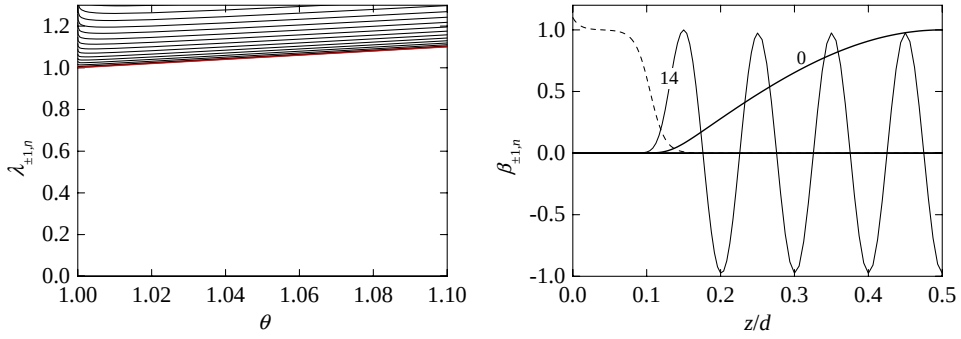

(a) (b)

Figure 4.13 Biaxial modes in paranematic phase are all expelled from the quasi-nematic boundary layer (b); $\theta = 1 + 10^{-5}$, $a_S = 1.1$, and $G \to 0$; and on approaching θ_{NI} their relaxation rates must therefore increase along with the thickness of the boundary layer (a). Red line represents the lower limit of the spectrum of a homophase system and the dashed line depicts the equilibrium profile.

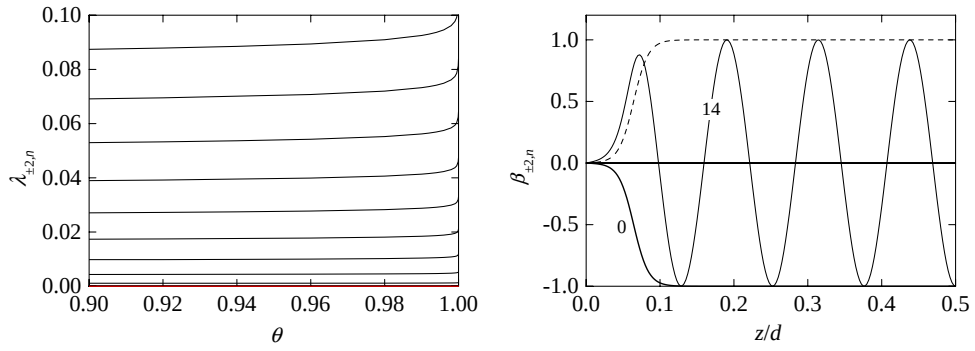

(a) (b)

Figure 4.14 Director modes in a nematic sample bounded by disordering substrates: (b) director fluctuations are forced out of the boundary layer; $\theta = 1 - 10^{-5}$, $a_S = 0$, and $G \to \infty$; and must speed up on approaching the clearing point (a), just like the biaxial modes in paranematic phase (Fig. 4.13). Red line represents the lower limit of the corresponding spectrum in a homophase system and the dashed line depicts the equilibrium profile.

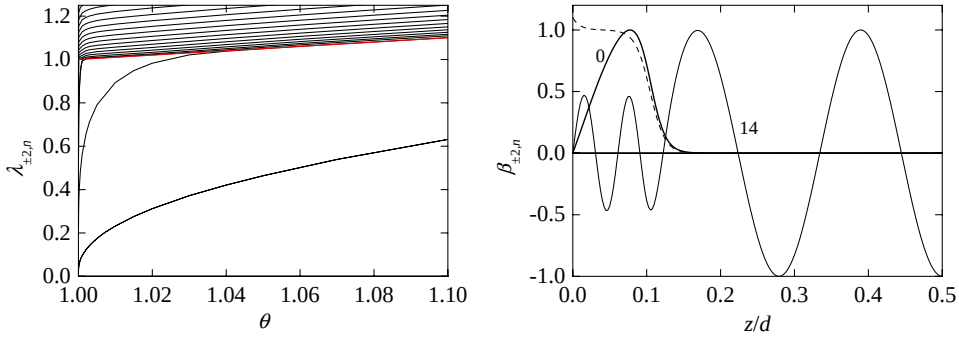

(a) (b)

Figure 4.15 Director modes in paranematic phase: (a) the relaxation rates of the lowest modes, which are restricted to the nematic wetting layer (b); $\theta = 1 + 10^{-5}$, $a_S = 1.1$, and $G \to \infty$; decrease to 0 as $\theta \to 1$ due to the growth of the wetting layer (cf. Fig. 4.13). Red line represents the lower limit of the corresponding spectrum in a homophase system and the dashed line depicts the equilibrium profile.

of the paranematic phase induced by the ordering substrate. Far from the phase transition temperature, their relaxation rates are temperature-independent, whereas in the vicinity of the clearing point they all increase because of rapid growth of the wetting layer.

In paranematic phase a few lowest director modes are confined to the nematic boundary layer, whereas the upper ones extend over the whole sample and are more or less the same as in perfectly isotropic phase (see Fig. 4.15). The relaxation rates of the lowest modes exhibit a cusplike slowdown similar to that observed in biaxial modes in a disordering geometry (Fig. 4.12). Moreover, their pretransitional slowdown resulting from the increase of the thickness of the wetting layer is actually critical, since in this case the fluctuations confined to the wetting layer are Goldstone modes.

The discussed results correspond to infinitely strong surface interaction. For G's which are large enough to induce complete wetting, the spectra of fluctuations remain qualitatively the same, whereas otherwise the slow modes are no longer critical. Eventually, if the strength of the surface interaction is very weak, all fluctuations become cosine-like and their spectrum is described by Eqs. (4.7) and (4.8).

The analysis has revealed a close relationship between the wetting regime induced by (dis)ordering substrates and the pretransitional behavior of thermal fluctuations of the ordering in confined liquid crystals. Both geometries are characterized by a wetting-induced interface between nematic and isotropic phase, which gives rise to two localized normal modes: the first one represents fluctuations of the position

of the phase boundary and is characterized by a soft dispersion of its relaxation rate (provided that the wetting is complete), and the second one corresponds to fluctuations of the shape of the interface. Moreover, there are a few additional slow modes, which are restricted to the wetting layer and whose pretransitional behavior is related to its growth. If the wetting is partial, the slowdown of the localized modes is not as pronounced as in complete wetting regime, but the underlying physics remains the same.

The wetting-induced pretransitional behavior of the fluctuations of the liquid-crystalline ordering is certainly not limited to geometries discussed in this study. A similar phenomenon is expected in nematic and isotropic samples with substrate-stabilized smectic boundary layer, which should exhibit critical slowdown in the vicinity of the nematic–smectic and isotropic–smectic phase transition, respectively. But the analogy with the substrate-stabilized nematic layer above the isotropic–nematic phase transition is not complete due to layered structure of the smectic ordering, which presumably gives rise to nontrivial features of the wetting-induced fluctuations in this system.

It seems possible that the effect described here has already been detected experimentally in some microconfined liquid-crystalline systems, where a huge increase of the decay time of fluctuations has been observed in the vicinity of isotropic–nematic [9] and nematic–smectic A phase transition [131]. However, conclusive evidence could only be provided by a detailed and comprehensive analysis of the existing data or by an experiment designed to probe the dynamics within the boundary layer. The latter could be based on, for example, the evanescent light scattering technique [132,24].

The results of the study can be extrapolated beyond the geometries discussed once it has been realized that the slow dynamics of the localized modes is actually directly related to the existence of the phase boundary and that the wetting itself is merely a mechanism which introduces a heterophase structure — and, therefore, a phase boundary — into the system. In confined liquid crystals, heterophase ordering is very often induced by topological constraints imposed by curved walls, which result in singularities of the director field, where very strong elastic deformation of the nematic phase is avoided by reducing the degree of order. Since the disordered regions called defects are more complex than the planar nematic-isotropic interface [133–135], they should be accompanied by several localized modes related to fluctuations of their structure as well as those corresponding to fluctuations of their size, position, and shape. This indicates that the defects should be considered as possible generators of slow nondirector fluctuations in confined liquid crystals. Another aspect of structure and pretransitional dynamics applicable to defects in

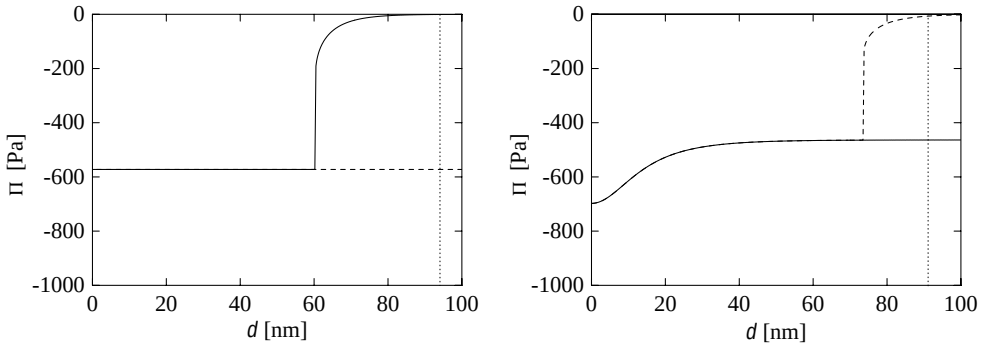

Figure 4.16 Structural force in a nematic system confined with (a) disordering substrates ($\theta = 0.9$, $a_S = 0$, and $G \to \infty$) and (b) ordering substrates ($\theta = 1.1$, $a_S = 1.1$, and $G \to \infty$). Solid lines correspond to the force in the nematic phase and dashed lines correspond to the force in the isotropic phase. Dotted verticals denote the thickness at which the isotropic phase becomes metastable in the surface-molten nematic system (94.6 nm) and the nematic phase becomes metastable in the paranematic system (91.3 nm), respectively.

nematic liquid crystals is given in Chapter 5.

4.3 Structural and pseudo-Casimir forces

Structural force

The structural force in nematogenic heterophase systems studied in this thesis arises from the deformation of the scalar order parameter. Thus, the force is short-range and attractive. A detailed study of structural forces in a paranematic system was performed by Borštnik and Žumer [60]. Similarly, the structural force can be calculated also for the nematic system with molten wetting layers. Typical thickness dependence of the structural forces in both nematogenic systems is presented in Fig. 4.16.

The order in thin cells is determined by the surface interaction. If the cell thickness is increased the corresponding amount of the liquid-crystalline material enters the cell and its order is changed from the bulk order to the one induced by the substrates. Thus, the free energy of the system changes for $(f - f_{bulk})\mathcal{V}$ which produces a constant force between the confining walls. The force is attractive, because in the given systems the surface-induced order corresponds to higher free energy. In thick enough cells, the order parameter profile is characterized by a bulk-like core and surface-induced wetting layers. Now the change of the free energy of the system when changing the cell thickness is due to the minor changes in the order parameter profile while most of the material enters the core of the cell, thus, its free

energy is not changed. In this regime, the structural force decays exponentially with respect to the cell thickness,

$$\Pi \propto \exp(-d/\xi), \tag{4.10}$$

where $\xi = \xi_{N,0}$ in the case of a nematic with molten wetting layers and $\xi = \xi_I$ in the case of a paranematic cell. In Fig. 4.16 hysteresis loops can be clearly seen — they are the evidence of the metastable phases. Details of the profile of structural force depend on details of the surface-induced interaction, whereas the existence of the hysteresis depends on the temperature.

Pseudo-Casimir force

For the sake of completeness, in this Section, I will quote the main results of fluctuation-induced force in the paranematic phase which were obtained by Ziherl *et. al* [28]. As we have seen, there is a strong correspondence between the paranematic system and the surface-molten nematic system. Thus, the main features of the pseudo-Casimir force in the surface-molten nematic system, as they can be predicted from the anchoring properties and fluctuation modes, will be discussed at the end of this Section.

The pseudo-Casimir force in a heterophase system can be interpreted in terms of two contributions: (i) the interaction between the substrates and the phase boundaries and (ii) the interaction between the two phase boundaries.

Interaction between solid substrate and phase boundary consists of three contributions corresponding to three non-degenerated fluctuation modes. The fluctuations of the degree of order and biaxial fluctuations give rise to a short-range repulsion between the substrate and the phase boundary proportional to $\exp(-2d_W/\xi)$, where d_W is the thickness of the wetting layer and $\xi = \xi_{N,0}$ or $\xi_{N,\pm1}$ for order parameter and biaxial fluctuations, respectively. The short-range of the interaction is a consequence of finite correlations in both nematic and isotropic phase. The repulsion between the substrate and the phase boundary can be understood in terms of boundary conditions. The anchoring at the substrates is strong, whereas the maxima of the order fluctuation modes at the phase boundaries (see Fig. 4.9) indicate that these modes experience effectively weak "anchoring" conditions. Because of the dissimilarity of the boundary conditions the interaction due to fluctuation of the degree of order is repulsive. A similar argument applies to biaxial fluctuations. Here weak "anchoring" condition at the phase boundary can be understood as a consequence of the fact that biaxial fluctuations are much more favorable in the isotropic phase than in the nematic phase. The main contribution to the interaction between the solid substrate and the phase boundary is induced by the director fluctuations,

which are characterized by an infinite correlation length in the nematic phase. The leading term of this interaction reads

$$-\frac{k_B T S \zeta(3)}{4\pi d_W^2}, \tag{4.11}$$

where ζ is the Riemann zeta function. This long-range interaction is attractive which can again be interpreted in terms of (dis)similarity of boundary conditions. In the isotropic phase, the director fluctuations are very "hard" compared to the ones in the nematic phase, therefore, as we have seen (Fig. 4.15), the lowest normal modes are actually confined to the nematic surface layer. The effective boundary condition at the phase boundary is very similar to strong anchoring at the solid substrate, and the force induced by director fluctuations is attractive.

Interaction between phase boundaries gives rise to an attractive fluctuation-induced force which is proportional to $\exp\left(-2(d-2d_W)/\xi_I\right)$. The attraction is due to the identical boundary conditions. Except in the vicinity of the metastability limit of the paranematic phase, the distance between the substrate and the phase boundary is much smaller than the distance between the two boundaries, and the interaction between the phase boundaries is very weak. The range of the pseudo-Casimir interaction between the phase boundaries is half of the range of the structural interaction [Eq. (4.10)]. Thus, for $d_W \ll d$ the attractive structural contribution is dominant. In very thin cells the distance between the two phase boundaries becomes comparable to the thickness of the wetting layers and in this range the attractive fluctuation-induced interaction between the phase boundaries becomes dominant.

Effective interaction between solid substrates is a superposition of the two contributions discussed above. In the range of stable paranematic phase ($\theta > 1$, $d_W \ll d$) the fluctuation-induced force between the two substrates is governed by the interaction between the solid substrate and the phase boundary. It is mediated by the structural interaction which determines functional dependence of the wetting layer thickness on the sample thickness which has already been discussed to be $\partial d_W/\partial d \approx -\text{const.} \times \exp(-d/\xi_I)$ [127]. Therefore, the leading term in the substrate-to-substrate fluctuation-induced force

$$F_{CAS} \approx -\frac{k_B T S \zeta(3)}{2\pi d_W^3} \frac{\partial d_w}{\partial d} \propto \mathrm{e}^{-d/\xi_I} \tag{4.12}$$

is repulsive and short-range. Its range, ξ_I, is identical to the range of the structural force, whereas its magnitude is smaller but comparable to the magnitude of the structural attraction. Since the two forces have the same range, the structural force is proportionally diminished by fluctuation-induced contribution.

The pseudo-Casimir force in a surface-molten nematic system: From the knowledge of general properties of the pseudo-Casimir force and by being familiar with fluctuations in the system the force can be predicted also for the case opposite to the paranematic, for the nematic in contact with disordering walls. Here, the wetting layers are in the isotropic phase where all fluctuations modes are characterized by the same, finite correlation length, thus, all the corresponding contributions to the fluctuation-induced force are short-range and proportional to $\exp(-2d_W/\xi_I)$. Fluctuations of the degree of order and director fluctuations yield a repulsive interaction because they both experience effectively weak "anchoring" at the phase boundary. In the case of former fluctuations, this is indicated by the position of their maxima whereas in the case of the latter, the "weak" anchoring is due to the fact that the director fluctuations are much more favorable in the nematic core. Biaxial fluctuations give rise to a short-range attraction because they experience effectively strong "anchoring" at the phase boundary which results from the fact that biaxial fluctuations are extremely "hard" in the nematic phase and, thus, they are localized to the wetting layers. On the other hand, the fluctuation-induced interaction between the two phase boundaries is dominated by Goldstone director fluctuations which give rise to a long-range attractive interaction proportional to $(d - 2d_W)^{-2}$. Fluctuations of the degree of order and biaxial fluctuations yield short-range attraction. From this, it can be expected that the pseudo-Casimir force in the nematic system with molten wetting layers should be long-range and attractive and it should dominate the structural force since the range of the latter is finite, i.e., $\xi_{N,0}$.

4.4 Van der Waals force in heterophase liquid-crystalline systems

As it has been derived in previous Chapter dealing with the van der Waals force, two media with the same "isotropic" dielectric and optical properties (here, isotropic quantities are $a^{iso} \propto \operatorname{tr} \mathsf{a}$ and a is the corresponding tensor), however, with different symmetry of relevant tensors, have different effect on the electromagnetic field modes. In a heterophase system, the two phases — the nematic and isotropic phase — have the described properties. Therefore, the isotropic–nematic phase boundary acts as an additional wall in the system and it forms, together with the solid–liquid-crystalline interface, a cavity which perturbs the electromagnetic field modes. The van der Waals interaction originating in different symmetries of the phases together with the pseudo-Casimir interaction, thus, yields a correction to the equilibrium thickness of the (dis)ordered wetting layer.

In Chapter 3, the van der Waals force was determined for a system characterized

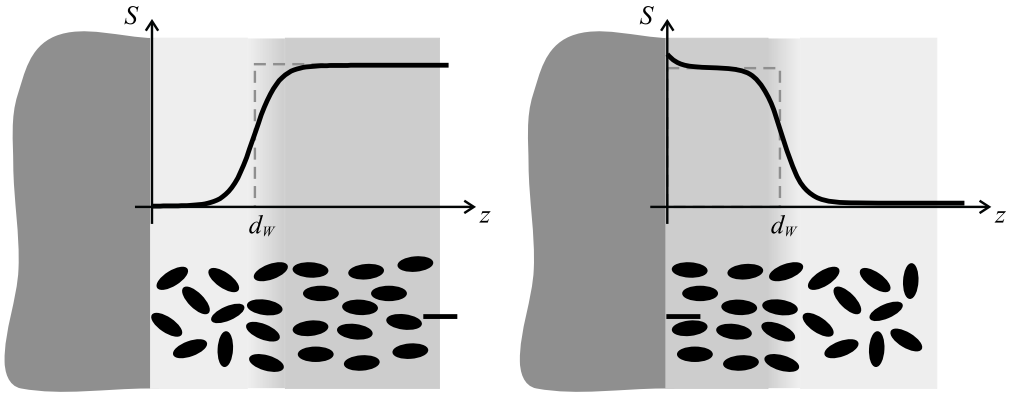

(a) (b)

Figure 4.17 Cartoon of the nematic–isotropic heterophase system: semi-infinite nematic liquid crystal in a contact with a solid substrate which (a) induces high uniaxial homeotropic nematic order or (b) melts the nematic order. In a graph, the solid line corresponds to the spatial dependence of the scalar order parameter S and the dotted line corresponds to the modeled function. d_W is the thickness of the (a) disordered isotropic wetting layer in the bulk uniaxial nematic liquid crystal or (b) ordered uniaxial wetting layer in the bulk isotropic liquid.

by sharp, discontinuous changes in the dielectric (and optical) properties at the walls whereas these properties were constant between two walls. The obtained results are applicable to the systems where the thickness of the interface between two distinct media is finite, however, much smaller than typical dimensions in the system, i.e., the gap between the walls, and the wavelength λ_e. In wetting system close to the isotropic–nematic phase transition, the interface between the two phases is well defined and the order parameter profile can be approximated by a step-like function, as is schematically represented in Fig. 4.17. The approximation is the better the closer is the temperature to the phase transition. (In the immediate proximity of the phase transition, the thickness of the region where the nematic order falls off to the isotropic phase or, similarly, where the isotropic order grows to the nematic phase, is well below the thickness of the wetting layer as it is shown in Figs. 4.2 and 4.4.)

In the case of a two-phase system the separation d_W between the two "semi-infinite" media — solid substrate and the bulk liquid-crystalline phase — is not a directly controllable parameter, instead, it corresponds to the minimum of the free energy of the system; it can be changed by changing the temperature of the system. In Section 4.1 only the mean-field part of the free energy was taken into account to determine the equilibrium state of the heterophase system. However, there are at least two sources of correction to that description. The fluctuations of

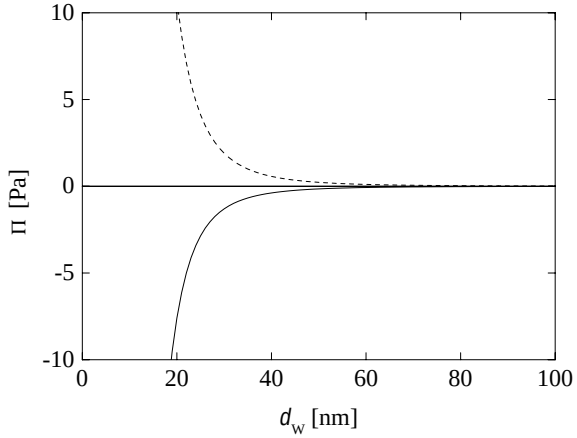

Figure 4.18 Van der Waals force per unit area acting on a wetting layer in a surface-molten nematic system (solid line) or in a paranematic system (dashed line).

the order parameter tensor contribute to the pseudo-Casimir interaction between the interfaces; the leading term of the interaction energy in the paranematic system is written out in Eq. (4.11) [28]. Another contribution to the free energy of a heterophase system is due to the spatial dependence of the permittivity tensor which yields nonzero van der Waals interaction. The interaction is very weak, because the difference in the permittivities of two of the media — the isotropic and nematic part of the system — is only due to different eigenvalues of the permittivity tensors, whereas the traces of the tensors are the same.

In Fig. 4.18 the van der Waals force acting on a wetting layer is plotted for a typical liquid-crystalline heterophase system. Although the thickness of the wetting layer is not subject to direct change, the force has been calculated as it has been defined in Eq. (3.31), i.e., as a derivative of the corresponding free energy with respect to the gap between the walls. One can imagine that due to thermal order parameter fluctuations the thickness of the wetting layer can change. The van der Waals force acting on such wetting layer is then the change of the interaction free energy of the system because of the changed separation between the walls. In a system with silica as a solid substrate the van der Waals force between solid–liquid-crystalline and nematic–isotropic interface is attractive in the surface-molten nematic system and it is repulsive in the paranematic system. In the surface-molten nematic system the thickness of the equilibrium isotropic wetting layer is decreased due to the nonzero van der Waals interaction; in the paranematic system, the thickness of the ordered wetting layer is increased.

To determine quantitatively the change of the equilibrium wetting layer thickness the van der Waals free energy should be included in the total free energy which is subject to minimization. However, the van der Waals interaction is very weak.

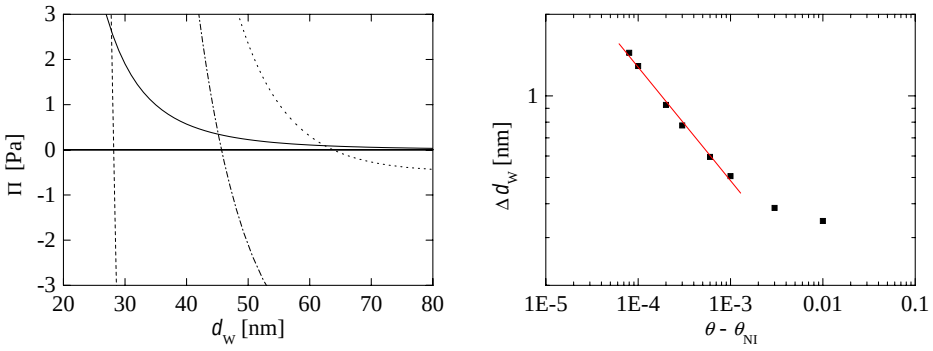

(a) (b)

Figure 4.19 (a) Van der Waals force (solid line) and structural force per unit area in the wetting layer of a nematic liquid crystal at the order-inducing solid substrate for various temperatures close to the isotropic–nematic phase transition: $T - T_{NI} = 10^{-2}$ K (dashed line), $T - T_{NI} = 10^{-3}$ K (dash-dotted line), and $T - T_{NI} = 10^{-4}$ K (dotted line). The nonzero van der Waals force yields the increase of the equilibrium wetting layer thickness. (b) Close to the phase transition, the temperature dependence of the correction of the equilibrium wetting layer thickness exhibits power-law behavior, $\Delta d_W \propto (T - T_{NI})^{-\nu}$, where $\nu = 0.42$ is obtained from fitting the corresponding data (red line). In the limit $T - T_{NI} \to 0$, $\nu = 0.5$.

Therefore, the forces acting on the wetting layer will be compared rather than the corresponding free energies. Here again, one should imagine that due to thermal fluctuations a heterophase structure with different wetting layer thickness is established. Since that structure is not the equilibrium one its mean-field counterpart of the free energy is raised with respect to the equilibrium value and an effective structural force starts acting in the system in order to reestablish the equilibrium state. In Fig. 4.19 (a) the structural force acting on the ordered wetting layer in the paranematic system is plotted together with the van der Waals force. The effective structural force is repulsive if the layer thickness is smaller than the equilibrium thickness, and it is attractive if the thickness is larger than the equilibrium thickness. In the equilibrium, there is no force acting on the layer. If the van der Waals force is taken into account the point of zero force is moved towards larger layer thicknesses. The increase of the equilibrium layer thickness is in the range of few nanometers. In 5CB in contact with order-inducing silica, at $T - T_{NI} = 10^{-2}$ K the equilibrium layer thickness determined from the phenomenological mean-field approach, $d_{MF} = 28.13$ nm, is increased by 0.34 nm, at $T - T_{NI} = 10^{-3}$ K the equilibrium layer thickness $d_{MF} = 45.28$ nm is increased by 0.51 nm, and at $T - T_{NI} = 10^{-4}$ K the equilibrium layer thickness $d_{MF} = 63.39$ nm is increased by 1.29 nm. Temperature dependence of the van der Waals induced correction is presented in Fig. 4.19 (b). On approaching the bulk phase transition temperature Δd_W exhibits critical power-law

behavior, $\Delta d_W \propto (T - T_{NI})^{-\nu}$, where $\nu = 0.5$. Due to the van der Waals interaction between the solid–liquid-crystalline and two phase interface the critical behavior of the growth of the wetting layer changes — critical behavior determined from the mean-field phenomenological approach is characterized by a critical exponent 0 (logarithmic divergence).

Except in immediate proximity of the phase transition where Δd_W diverges the correction due to the van der Waals force is rather small and, thus, experimentally undetectable. However, it should be noted that for the sake of simplicity the structural force has been determined in the limit of infinitely strong surface anchoring which yields larger deformations and therefore larger forces and stronger thickness dependence as compared to more realistic values of the surface coupling. On the other hand, in calculation of the van der Waals force the usual experimentally determined values of dielectric permittivity and refractive indices have been used [136]. Therefore, in real wetting systems the effect of the van der Waals force is stronger and can be estimated to contribute up to 10% to the structural force and, therefore, also to the equilibrium wetting layer thickness. In the immediate vicinity of the phase transition, the order parameter fluctuations become critical and the fluctuation-induced interaction exceeds the structural interaction. Thus, to probe the critical exponent due to the effect of the van der Waals interaction the mean-field theory should be renormalized also by the fluctuationg-induced contribution.

Further from the phase transition, the effect of the van der Waals interaction should be more prominent in systems with substrate-induced smectic layering. In such systems, the layer of the surface-induced order and the corresponding phase interface are better defined even further from the phase transition. In the case of presmectic layering in the isotropic phase the two phases — smectic A and isotropic phase — differ more than do the smectic A and nematic phase in the case of presmectic layering in the nematic phase. Thus, in the former case the van der Waals interaction between the solid substrate and the phase boundary is stronger than it is in the latter case.

5

Hybrid nematic cell

In hybrid nematic cells the liquid crystal is confined by substrates inducing nematic order in different directions, often close to being perpendicular. In such systems the nematic order can not be unperturbed. Due to the frustrating boundary conditions the equilibrium order usually results in a nonlocally perturbed, both, director field and degree of nematic order. Hybrid nematic cells are mainly used for studying anchoring properties of the confining substrates but also as optical switches.

In practice the hybrid frustration can be achieved by several ways: (i) If the nematic liquid crystal is confined with substrates that have been prepared in a way to induce nematic order one in homeotropic direction and the other in one of the lateral directions. (ii) If the nematic liquid crystal is deposited on the solid substrate whereas on the other sides it has free liquid-crystalline–air interface. In many liquid crystals the free liquid-crystalline–air interface induces rather strong homeotropic anchoring of the nematic liquid crystal. Thus, in combination with a solid substrate which induces nematic order in a direction in the plane of the substrate such liquid crystal is subject to frustrating hybrid conditions. (iii) The hybrid situation can also be a result of geometrical constraints such as in cylindrical cavity with homeotropic anchoring at the wall whereas the geometry of the cavity prefers orientation along the symmetry axis. Different possibilities of achieving hybrid nematic cells are schematically represented in Fig. 5.1.

Possible technological applications have stimulated the increase of interest in hybrid nematic geometries [137]. Using a quasi-elastic light scattering method Wittebrood *et. al* experimentally studied thickness dependence of the nematic-isotropic phase transition temperature and stability of ordered structures in a hybrid nematic film obtained after a spread of a liquid crystal droplet on a solid substrate [138]. In their experimental setup with unequal anchoring strengths of the confining substrates (solid substrate and a free liquid crystal interface) they were able to determine the critical cell thickness for the hybridly aligned order which was in good agreement

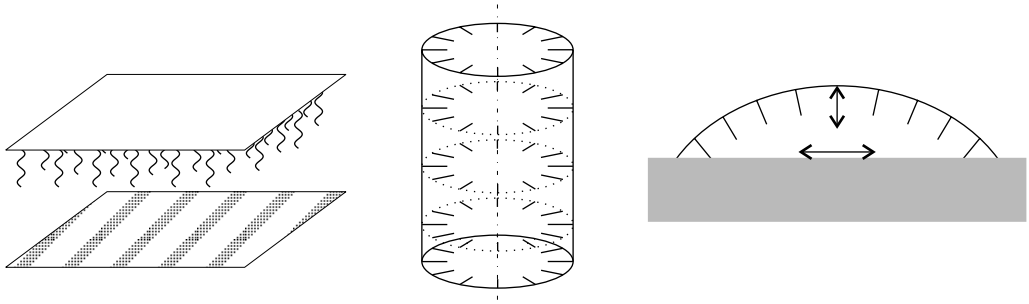

Figure 5.1 Schematic representation of different systems characterized by hybrid frustration: (a) Confining substrates prepared in a different way, so that one induces homeotropic anchoring and the other homogeneous planar anchoring. (b) Hybrid frustration due to opposing geometry induced direction of order and the direction induced by anchoring. (c) Liquid crystal in a contact with a solid substrate and with a free liquid-crystalline–air interface.

with the theoretical expression obtained long ago by Barbero and Barberi [19]. In their study an approximate director picture omitting positional dependence of the scalar order parameter and biaxiality was used. In the framework of Frank elastic theory an extensive study of pretransitional director dynamics in a hybrid cell was done by Stallinga *et. al* [12]. Using the director description of the nematic liquid-crystalline ordering they calculated relaxation times for tilt and twist fluctuations in hybridly aligned structure and director fluctuations in uniform director field structure. However, in their study they neglected spatial dependence of the uniaxial and biaxial degrees of nematic order, which are quite important in the case of strong anchoring and thin cells. A couple of years ago, Palffy-Muhoray *et. al* [20] showed that in highly constrained hybrid cells the nematic order can be either biaxial with the steplike profile of the director's tilt angle or the director field can be bent continuously. They predicted a structural transition between the two possible ordered configurations but did not probe the stability of both configurations. A more detailed description of the nematic order in planar hybrid geometry has been provided by Galabova *et. al* [139]. They calculated the phase diagrams for a hybrid cell in relation to film thickness and anchoring strength of one of the surfaces. Another aspect of a nematic liquid crystal in a planar hybrid geometry are stripe domains studied by Pergamenshchik [140]. In his study, using Frank elastic theory with surface terms, it was shown that equilibrium modulated structures can appear. However, in that study only spatial dependence of the nematic director was taken into account whereas other degrees of freedom of the nematic order have been neglected. In a cylindrical geometry Ziherl and Žumer [13] studied director fluctuations in the vicinity of a disclination line of strength 1 whose structure is similar

to structures in hybrid cells. They extended the approach based on Frank elastic theory by introducing spatially dependent rotational viscosity and elastic constants. More extensive study of structure of point and line defects in a capillary was carried out by Kralj *et. al* [25]. They described the nematic order in an infinite cylindrical cavity with three parameters, scalar order parameter, parameter of biaxiality, and the angle between the local director and capillary long axis. However, they assumed $\mathrm{tr}\,\mathsf{Q}^2$ to be a constant, which leaves only one, either the scalar order parameter or the parameter of biaxiality, independent. Furthermore, they neglected the third order term in the expansion of the free energy density. The obtained results have the expected resemblance to results of our study [21]. Lately, an increased interest was focused in the field of fluctuation-induced forces. Ziherl *et. al* determined the pseudo-Casimir force in the hybrid cell with degenerate planar anchoring in the most simple case, where the equilibrium nematic director is not perturbed. The force was calculated within the bare director picture and the Frank elastic theory.

This brief review shows that there was a lack of information on the dynamics related to the structural transition between different nematic configurations in highly constrained systems when nondirector degrees of freedom are crucial. This motivated us to start our analysis. In order to provide a simple but detailed description of a highly frustrated system a thin planar film with hybrid surface conditions was examined. In contrast to previous studies [19,12,13] we have focused our attention on highly constrained films where biaxiality and nonhomogeneous degree of nematic order play an important role. Although the origins of the high frustration in a system can be different, i.e., specific confining substrates in planar geometry or geometry induced hybrid properties (see Fig. 5.1), its effects on the liquid-crystalline order and pretransitional dynamics are similar [25,21,134,135,141]. Therefore one can study the basic effects of high frustration within the analysis of a planar system.

Our model system is a very thin hybrid film consisting of a nematic liquid crystal confined by two parallel substrates inducing uniaxial nematic order in mutually perpendicular directions. The hybrid frustration can be also achieved if both substrates induce order with the nematic director perpendicular to the substrates, however, with positive scalar order parameter at one of the substrates and with a negative scalar parameter at the other. The latter case — the degenerate planar anchoring — corresponds to molecules lying in the plane of the substrate, but being randomly distributed around the substrate normal. A system with such boundary conditions possesses full rotational symmetry around the substrate normal, whereas the equilibrium bent director structure breaks this symmetry. Breaking of the symmetry results in an infinite number of equilibrium states with the same energy and

Figure 5.2 Schematic representation of the model system. The substrate at $z = 0$ induces uniaxial nematic order in a particular direction in the plane of the confining substrate, say parallel to the x axis. The other substrate, in the plane $z = d$, is then characterized by a homeotropic anchoring. $\hat{k}_i$ is the easy axes of the i-th substrate, $a_{S\,i}$ is the induced degree of uniaxial nematic order, and G_i is the free energy associated with the anchoring of the i-th substrate. The lateral dimensions of the cell are much larger than its thickness, $L_x, L_y \gg d$.

characterized by a mirror plane, which contains the previous axis of full rotational symmetry. Such system is easily described within a director picture and Frank elastic theory. In that way Lavrentovich *et. al* have studied point defects which are due to infinite degeneracy of equilibrium states [142,143]. On the other hand, the same system is hard to handle within the phenomenological description and the tensorial order parameter which favors the nonfrustrated solution because it preserves the original symmetry on expense of varying the scalar order parameter. In practice the full rotational symmetry at the planar substrate is never ideally realized and there exists a locally preferred direction. Therefore, if one is interested in defect free structures even the hybrid situation with degenerate planar anchoring can be described by a hybrid cell with two well defined preferred directions.

In order to simplify the description it is assumed that there is no surface induced smectic order although at least partial formation of smectic layers is often observed [117,144]. Suppose that the first substrate ($z = 0$) induces uniaxial nematic order in a particular direction in the plane of the confining substrate (say parallel to the x axis); the other substrate (in the plane $z = d$) is then characterized by a homeotropic anchoring. Here, d is the thickness of the nematic film which is much smaller than the lateral dimensions of the system, $d \ll L_x, L_y$. Since the liquid crystal is not confined in the lateral dimensions and we are not interested in modulated stripe domain structures which are sometimes observed [43] the nematic order is not perturbed with respect to the coordinates x and y. Thus, describing the planar hybrid film reduces to solving a one-dimensional problem. The geometry of the model hybrid film is shown schematically in Fig. 5.2.

Usually, the elastic distortions in such films are studied within the Frank elastic theory [42], where the nematic order is assumed to be uniaxial with the director field continuously bent from one substrate to the other; the scalar order parameter and the elastic constants are assumed to be temperature dependent only. However, long ago Barbero and Barberi [19] showed that in a hybrid film with different surface anchoring strengths the bent-director configuration can only exist if the film is thicker than the critical thickness, $d_c \equiv K(1/W_2 - 1/W_1)$, where K is the elastic constant in the one-elastic-constant approximation ($K_{ii} = K$), and $W_2 < W_1$ are the out-of-plane strengths of the surface interaction at the two confining substrates, respectively. In thinner films the director field is uniform with the nematic director in the direction of the easy axis of the substrate with stronger anchoring. For a typical liquid-crystalline material (such as 8CB; $K \approx 4.4 \times 10^{-12}$ N) in a contact with an in-plane aligning substrate yet homeotropically ordered at free surfaces ($W_1 \gg W_2 \approx 1.1 \times 10^{-5}$ J/m^2) the critical film thickness is found to be approximately 0.4 μm [138]. However, in the case of two confining substrates (without free surface) with very different surface anchorings (such as substrates modified with different aliphatic acids with, e.g., $W_1 \approx 10^{-3}$ J/m^2 and $W_2 \approx 10^{-4}$ J/m^2 [51]) the critical value would be as small as $d_c \approx 40$ nm. As implied by the above expression for the critical film thickness this value would be even smaller if the anchoring strengths of the confining substrates would be comparable, therefore, in such hybrid films the order would always be distorted. However, in the case of hybrid yet equally strong anchoring conditions the director field is uniform below a finite critical film thickness, whereas the boundary conditions are fulfilled with the eigenvalue or director exchange [20,21]. Here the term "uniform director field" refers to the corresponding uniform orthonormal triad, whereas the director's tilt angle exhibits a steplike change [see Fig. 5.3(b)]. The other interesting consequence of equivalent confining substrates is a geometry induced biaxial ordering of a uniaxial nematic liquid crystal. The effect is interesting because in thermotropic nematic liquid crystals biaxiality cannot be observed very often.

In the following Sections first different possible equilibrium structures in a hybrid film are described in detail, and the structural transition toward the bent director structure is discussed. In Section 5.1.1 the comparison between the phenomenological description and the results from the Monte Carlo simulations is provided [145,146]. Next, in Section 5.2 the pretransitional orientational dynamics is determined for the biaxial structure, which is characteristic for highly constrained hybrid systems. The perturbed equilibrium nematic order and the changed spectrum of thermal fluctuations give rise to structural forces discussed in Section 5.3. Once acquainted with the forces acting on a slab of a nematic liquid crystal the

stability of thin liquid-crystalline depositions are discussed in Section 5.4.

5.1 Equilibrium structures

The free energy of liquid-crystalline system consists of terms of three different types. The bulk-like terms control the melting/growing of the nematic order. If the order is smaller or larger than its bulk value these terms contribute to the increase of the free energy. If the nematic order is spatially dependent the free energy of the system increases due to the elasticity related to deformations of the tensorial order parameter. The elastic part of the free energy corresponds either to variations of the uniaxial and biaxial parameters of the order around the director or to elastic deformations of the director field. The larger the nematic order the bigger the resistance of the system toward the elastic deformations of the director field; the elastic energy related to deformations of the director scales as S^2, if S is the degree of the nematic order. The third contribution to the free energy of a confined nematic liquid-crystalline system is the free energy associated with (dis)obeying the substrate-induced order.

The system reaches its thermal equilibrium when its free energy is minimal. In a hybrid cell the confinement induces deformation of the director field. If other degrees of freedom of the tensorial order parameter are neglected, the minimum of the free energy is reached by the interplay of energetic penalty for violating the surface-induced order and the energy due to elastic distortions. In a one-elastic-constant approximation, for $d > d_c$ elastic deformations are more favorable than severe violation of the surface anchoring, whereas for $d < d_c$ it is energetically more favorable to disobey surface anchoring than to be submitted to elastic deformation. However, the nematic order has also other degrees of freedom. If these are taken into account the increase of the free energy due to elastic deformations can be compensated by localization of elastic deformation together with melting the nematic order in the region of high deformations. The violation of the surface-induced order can be also balanced by decreased nematic order at the surface with the mismatched director and the surface easy axis. In addition to melting of the nematic order the uniaxial distribution of molecules around the director can become biaxial.

The equilibrium ordering of a hybrid nematic film can exhibit either distorted (hybridly bent) or undistorted director structure (see Fig. 5.3). The undistorted structure is characterized by either biaxial director exchange configuration in the case of equally strong but hybrid surface anchorings or uniform director field in the case of hybrid confining substrates characterized one by a strong anchoring and other by a weak anchoring. Which of the two possible configurations — distorted or undistorted — will actually occur depends on the temperature and film thickness.

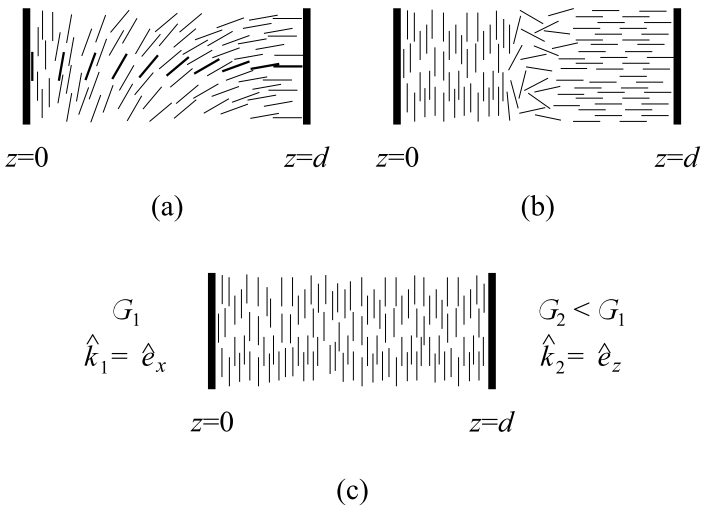

Figure 5.3 Schematic representation of three possible ordered configurations in a hybrid film: (a) the bent-director structure, (b) biaxial structure with director exchange, and (c) uniform director structure.

However, the existence of either of the two undistorted structures depends on the strength of the surface coupling.

Both distorted and undistorted structures are studied using the same free energy density expansion [Eqs. (2.32) and (2.33)]. By comparing the total free energy dependencies on temperature and film thickness the structural transition is determined. The nematic order is described by a tensorial order parameter, however, only the nontrivial degrees of freedom are actually taken into account. Each particular parametrization of the order parameter tensor is described when describing the corresponding structure. The obtained differential equations are solved numerically using the relaxation method [126].

Uniform director field

If the antagonistic anchorings are very different in magnitude it is energetically more favorable to disobey one of the surface anchorings than to be subject to elastic deformation. In order to minimize the surface contribution to the free energy the nematic director will lie in the direction of the easy axis of the substrate with stronger anchoring, say the substrate at $z = d$, i.e., $G_2 > G_1$. Thus the nematic order can be described with a scalar order parameter S and, in general, with the additional parameter P measuring biaxiality of the order; $\mathsf{Q} = S\mathsf{T}_0 + P\mathsf{T}_1$, with the orthonormal triad $\hat{n} = \hat{e}_z$, $\hat{e}_1 = \hat{e}_x$, and $\hat{e}_2 = \hat{e}_y$. Usually, the biaxiality of the nematic order is neglected in calculations but in highly frustrated systems such an approximation is not justified. The positional dependence of the two chosen

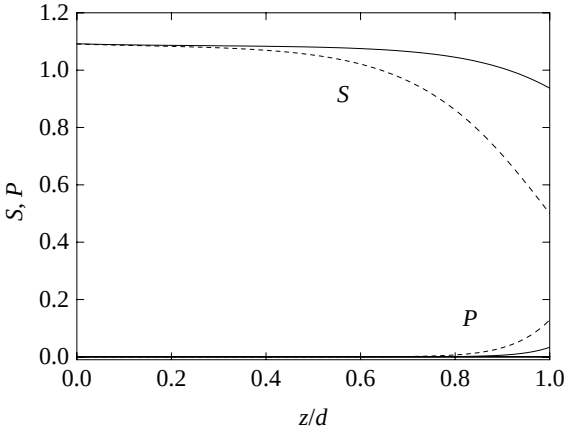

Figure 5.4 Uniform director structure in a hybrid film with unequal anchoring strengths. Equilibrium profile is characterized by a spatially dependent degree of nematic order and increasing biaxiality profile when approaching the substrate with weaker anchoring. Parameters used in calculation were $\theta = 0.9$, $\zeta^2 = 0.03$, $a_S = 1.1$, $G_1 = 1.2 \times 10^{-3}$ J/m^2, and $G_2 = 1.2 \times 10^{-4}$ J/m^2 (solid line), $G_2 = 4 \times 10^{-4}$ J/m^2 (dashed line).

parameters can be obtained by solving Euler-Lagrange equations

$$\begin{aligned} \zeta^2 S'' - \theta S + 3S^2 - 2S^3 - 3P^2 - 2SP^2 &= 0, \\ \zeta^2 P'' - \theta P - 2P^3 - 6SP - 2S^2 P &= 0, \end{aligned} \tag{5.1}$$

where the prime denotes d/dz, $S = S(z)$, and $P = P(z)$. The corresponding boundary conditions are determined by

$$\begin{aligned} S' &= -\frac{g_1}{\zeta^2}\left(S + \frac{a_S}{2}\right)\Big|_{z=0}, \\ P' &= -\frac{g_1}{\zeta^2}\left(P + \frac{a_S\sqrt{3}}{2}\right)\Big|_{z=0}, \\ S' &= \frac{g_2}{\zeta^2}(S - a_S)\Big|_{z=1}, \\ P' &= \frac{g_2}{\zeta^2}P\Big|_{z=1}, \end{aligned} \tag{5.2}$$

where a_S is the preferred value of the scalar order parameter which is taken to be equal at both substrates and $g_i = (\xi_{NI}^2/Ld)G_i$ is the dimensionless strength of the surface interaction. The dimensionless parameters used in this calculation are the same as introduced in Eqs. (2.32) and (2.33) and discussed on page 33.

Since the confining substrates induce uniaxial order the biaxiality is small, especially near the substrate whose easy axis is parallel to the nematic director (Fig. 5.4). By increasing the weaker anchoring the biaxiality increases as well. Progressively increasing biaxiality and simultaneously decreasing degree of nematic order along

the director lead to transformation of the uniform structure to the biaxial structure. The transformation does not correspond to a structural transition. If one of the confining substrates is characterized by very weak anchoring ($g \to 0$) the parameter of biaxial order can be omitted and the equations reduce to $\zeta^2 S'' - \theta S + 3S^2 - 2S^3 = 0$, i.e., describing Sheng's surface aligned nematic ordered structures [18].

Bent-director structure

The discussion of the bent-director configuration is only slightly simplified by the assumption that the order is uniaxial but it allows both positionally dependent scalar order parameter and director field, whereas in most previous studies only the variation of the director field has been taken into account. The effect of biaxiality can be neglected since it is very small comparing to the scalar order parameter, especially, deep in the nematic phase. If one minimizes the free energy of the hybrid system with constant parameters S, P, and $\phi' \approx \pi/2$, deep in the nematic phase, the value of biaxiality can be estimated to be no larger than $P = (\pi^2/4\sqrt{3})\zeta^2 \ll S \sim 1$. The biaxiality is negligible for hybrid cells with $d \gtrsim 100$ nm ($P < 0.01$).

Using the dimensionless form of the free energy density expansion [Eq. (2.32)] and the ansatz $\mathsf{Q}(z) = S(z)(3\hat{n} \otimes \hat{n} - \mathsf{I})/\sqrt{6}$, where the nematic director has the form $\hat{n} = (\sin\phi, 0, \cos\phi)$ and $\phi = \phi(z)$, the two independent parameters S — the scalar order parameter — and ϕ — the angle between the nematic director and the substrate normal — are determined by the equations

$$\begin{aligned} \zeta^2 S'' - \theta S + 3S^2 - 2S^3 - 3\zeta^2 S(\phi')^2 = 0, \\ (S^2\phi')' = 0. \end{aligned} \tag{5.3}$$

In the case of a very strong surface anchoring the boundary values of S and ϕ are set to the values preferred by the confining substrates [$S = a_S$ and $\phi(z = 0, d) = \phi_{S_{1,2}}$, where $\phi_{S_1} = \pi/2$ and $\phi_{S_2} = 0$] otherwise they are determined with boundary conditions

$$\begin{aligned} S' &= \pm\frac{g_i}{2\zeta^2}\left[2S + a_S - 3a_S\cos^2(\phi - \phi_{S_i})\right]\Big|_{z=0,1}, \\ S\phi' &= -\frac{g_i}{2\zeta^2}\, a_S \sin 2\phi\,\Big|_{z=0,1}, \end{aligned} \tag{5.4}$$

where the signs + and −, and the subscripts $i = 1, 2$ correspond to $z = 0$ and $z = 1$, respectively. If spatial variations of the scalar order parameter are neglected the Eq. (5.3) reduces to the well known equation for the director's tilt angle which can be derived from the Frank elastic description within the director picture, $\phi'' = 0$. Resulting director field is characterized by a linearly varying director's tilt angle with boundary conditions $\phi'(z = 0, 1) = -(g_{1,2}/2\zeta^2)\sin 2\phi(z = 0, 1)$. Meanwhile,

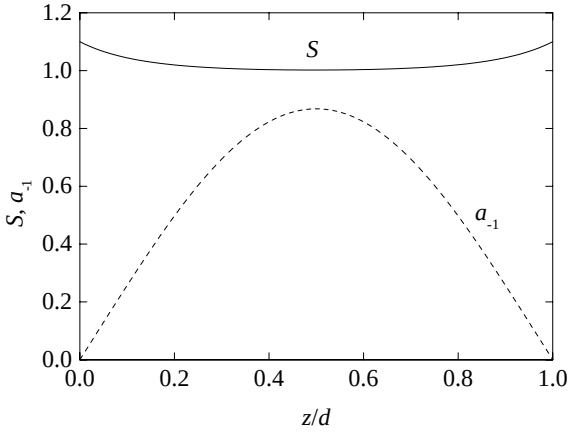

Figure 5.5 Equilibrium bent-director structure in a hybrid film. The solid line corresponds to the scalar order parameter and the dashed line represents the $a_{-1} = (\sqrt{3}/2)S\sin 2\phi$ amplitude of the tensor order parameter, which describes the bending of the director field in the plane (x, z). Parameters used in calculation are $\theta = 0.9$, $\zeta^2 = 0.01258$, $g_1 = g_2 \to \infty$, and $a_S = 1.1$.

the scalar order parameter is constant through the liquid-crystalline film and its temperature dependence is described by the equation $\theta_{\text{eff}}S - 3S^2 + 2S^3 = 0$, where

$$\theta_{\text{eff}} = \theta + (3\pi^2/4)\zeta^2. \tag{5.5}$$

Thus, the scalar order parameter corresponds to its bulk value at the increased temperature [cf. Eqs. (2.15) and (5.5)]. Due to elastic deformation of the director field the temperature of the hybrid system effectively increases. The increase of the effective temperature results in a smaller degree of order along the director with respect to the degree of order in bulk where there are no elastic deformations. The latter fact is often forgotten in studies within the bare director description. However, these difference is in micron-size cells, which are usually studied within the bare director description, negligible; for a typical liquid crystal $T_{\text{eff}} - T \approx 0.5$ mK.

As suggested, above the critical film thickness or below the critical temperature (with constant temperature or film thickness, respectively) the order in a hybrid nematic film can be described by a bent-director field. Since we allow the scalar order parameter to vary with the distance from one of the substrates the director tilt angle is not changing linearly as it would in the case of the uniform scalar order parameter (see Figs. 5.5 and 5.6). However, the difference is very small and, as expected, decreases further with the increasing film thickness and when the boundary value of the scalar order parameter is getting closer to the value $S_b(\theta_{\text{eff}})$. Here, $S_b(\theta) = 0.75(1 + \sqrt{1 - 8\theta/9})$ is the bulk degree of the nematic order and θ_{eff} is the renormalized dimensionless temperature defined in Eq. (5.5). In the case of strong surface anchoring the discrepancies from the case of uniform scalar order parameter

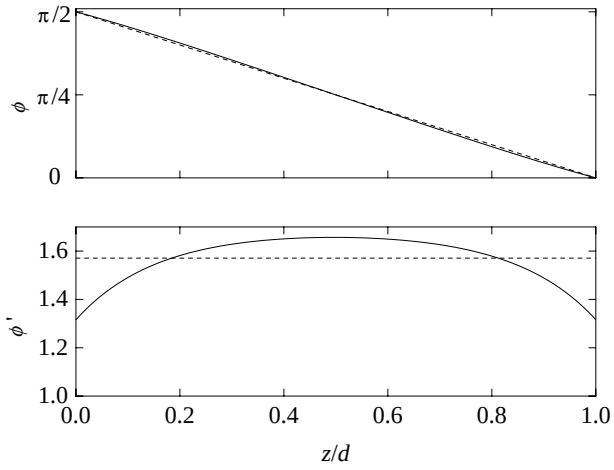

Figure 5.6 Spatial dependence of the tilt angle (top) and its derivative (bottom) for the bent-director structure. Dashed lines correspond to the appropriate parameters in the case of the uniform scalar order parameter. Parameters used in calculation are $\theta = 0.9$, $\zeta^2 = 0.0126$, $a_S = 1.1$, and $g_1 = g_2 \to \infty$.

are $\Delta S = S(0) - S(1/2) \approx a_S - S_b$ and $\Delta\phi' = \phi'(0) - \phi'(1/2) \approx \pi(a_S^2 - S_b^2)/(a_S^2 + S_b^2)$, where $S_b = S_b(\theta_{\text{eff}})$. On approaching the transition to either of the uniform director structures, i.e., by increasing the temperature or decreasing the film thickness, the discrepancies become larger. Simultaneously, the biaxiality becomes larger and the assumption of its negligibility is not justified anymore.

Biaxial configuration

As already mentioned in the introduction of the Chapter, the biaxial configuration was introduced by Palffy-Muhoray *et. al* [20] and later discussed by Galabova *et. al* [139]. However, their studies were made for a special case where the temperature corresponded to the bulk supercooling limit ($T = T^*$), whereas some other choices of temperature give rise to different physical phenomena. In order to better understand the pretransitional dynamics in such biaxially ordered structure, a detailed description of the biaxial configuration is presented.

In general, in the case of a hybrid film the director field is not uniform. However, the easy axes of the confining substrates are one in the direction of the x axis and the other parallel to the z axis; therefore it can be assumed that the director will lie in the plane (x, z), i.e., perpendicular to the y axis. Thus $\hat{n} = \hat{e}_y$, $\hat{e}_1 = \hat{e}_z$, and $\hat{e}_2 = \hat{e}_x$ can form a suitable uniform orthonormal triad.

The biaxial configuration is determined by using the expansion of the tensor order parameter in terms of the base tensors, $\mathsf{A}(\vec{r}) = \sum_{i=-2}^{2} a_i(z)\mathsf{T}_i$. Due to the symmetry reasons and boundary conditions, the configuration can be described by two amplitudes, a_0 and a_1. The former refers to the scalar order parameter with

respect to the y axis, whereas the latter denotes biaxiality of the order in perpendicular directions. In our case, the negative/positive sign of the amplitude a_1 tells whether the actual director is in the direction of the x or z axis, respectively. Both nonzero amplitudes are the solutions of two coupled equations arising from minimization of the free energy [Eqs. (2.28) and (2.62)] and the expansion of the tensor order parameter in terms of the base tensors,

$$\begin{aligned} \zeta^2 a_0'' - \theta a_0 + 3(a_0^2 - a_1^2) - 2a_0(a_0^2 + a_1^2) &= 0, \\ \zeta^2 a_1'' - \theta a_1 - 6a_0 a_1 - 2a_1(a_0^2 + a_1^2) &= 0, \end{aligned} \tag{5.6}$$

where the prime denotes d/dz. The boundary conditions are determined by the surface interaction. In our case, the induced order is assumed to be uniaxial at both substrates but in mutually perpendicular directions, therefore $\mathsf{Q}_S(0) = a_S(3\hat{e}_x \otimes \hat{e}_x - \mathsf{I})/\sqrt{6}$ and $\mathsf{Q}_S(1) = a_S(3\hat{e}_z \otimes \hat{e}_z - \mathsf{I})/\sqrt{6}$, where $a_S \geq S_b(\theta)$ is the preferred degree of order at the substrates (and is assumed to be equal at both substrates). Thus, the boundary conditions read

$$\begin{aligned} a_0' &= \pm\frac{g_{1,2}}{\zeta^2}\Big[a_0 + a_S/2\Big]\,\Big|_{z=0,1}, \\ a_1' &= \pm\frac{g_{1,2}}{\zeta^2}\Big[a_1 \pm a_S\sqrt{3}/2\Big]\,\Big|_{z=0,1}, \end{aligned} \tag{5.7}$$

where the signs + and −, and the subscripts 1 and 2 correspond to $z = 0$ and $z = 1$, respectively. If the anchoring is very strong ($g \to \infty$), the order at the surface is the same as the one preferred by the confining substrate, otherwise, the parameters can differ from the preferred ones.

The actual significance of the two nonzero amplitudes is obvious when they are rewritten into $a_0^x = -(a_0 + \sqrt{3}a_1)/2$ and $a_0^z = (-a_0 + \sqrt{3}a_1)/2$, where the former sum refers to the scalar order parameter with respect to the director $\hat{n} = \hat{e}_x$ and the latter sum denotes the scalar order parameter with respect to the director $\hat{n} = \hat{e}_z$. As shown in Fig. 5.7, on the average, near the first surface ($z = 0$) the liquid-crystal molecules are oriented parallel to the x axis while they are parallel to the z axis close to the other substrate ($z = 1$). In the vicinity of the surfaces the order is uniaxial, however, with increasing distance from the substrates it becomes slightly biaxial. In the case of equal anchoring strengths, both, biaxiality and order parameter profiles are symmetric with respect to the middle of the film (plane $z = 1/2$). The biaxiality profile has two maxima near the symmetry plane. In between them the molecular ordering can be described with a director perpendicular to the plane of the molecules ($\hat{n} = \hat{e}_y$), yet the scalar order parameter is negative. In the region of negative scalar order parameter the director or eigenvalue exchange occurs.

The maximum biaxiality and the thickness of the exchange region depend on the film thickness, the temperature, and the anchoring strength. The biaxiality is more

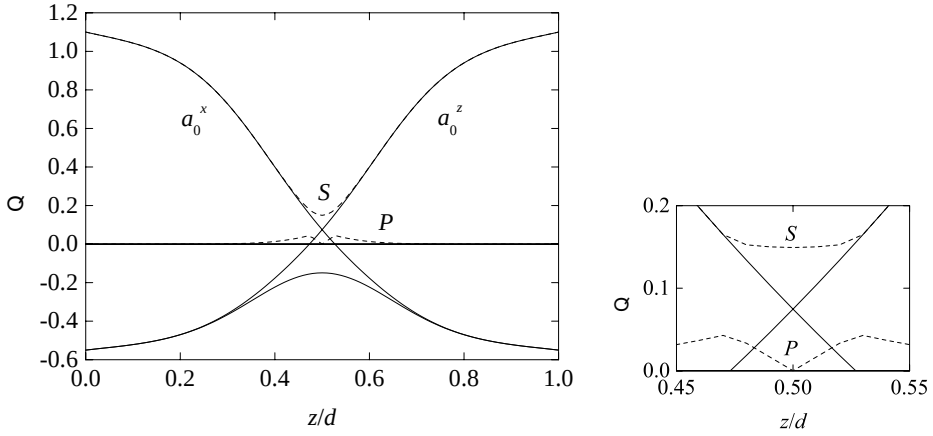

Figure 5.7 (a) Equilibrium profiles of the nonzero degrees of freedom. Thin solid line refers to the scalar order parameter with respect to the uniform director $\hat{e}_y$, whereas thicker lines represent scalar order parameters with respect to the easy axes x and z, $a_0^x = -(a_0 + \sqrt{3}a_1)/2$ and $a_0^z = (-a_0 + \sqrt{3}a_1)/2$, respectively. Dashed lines correspond to scalar order parameter [$S = (\sqrt{6}/2)|\mathsf{Q}_{ii}|$, where Q_{ii} has a sign opposite to that of the two other eigenvalues of Q] and biaxiality of the order ($P = |\mathsf{Q}_{jj} - \mathsf{Q}_{kk}|/\sqrt{2}$, where $j, k \neq i$), respectively. (b) Magnified detail of the profiles in the exchange region. Parameters used in calculation are $\theta = 0.9$, $\zeta^2 = 0.01258$, $a_S = 1.1$, and $g_1 = g_2 \to \infty$.

pronounced in thinner films and when the temperature is closer to the phase transition temperature. From the point where the surface wetting layers are in contact the exchange region thickness is — within the numerical accuracy — independent of temperature. On the other hand, the relative exchange region increases with decreasing film thickness, however, the absolute exchange region thickness decreases.

The biaxially ordered configuration is typical for highly constrained nematic liquid crystals, i.e., systems with high surface-to-volume ratio and strong surface anchoring ($G \gtrsim 10^{-3}$ J/m^2). In such systems the surface wetting layers may be in contact with each other, thus, the structure they form becomes progressively ordered on approaching the phase transition temperature. Because of the continuous growth of the ordered biaxial structure there is no nematic-isotropic phase transition. However, there is the transition to the low-temperature bent-director field configuration. Because the initial structure is ordered too, the transition between the two phases is structural rather than the phase one.

In the case of unequal but strong surface anchorings the high-temperature phase is biaxial as well, but the exchange region is located closer to the surface with weaker anchoring (Fig. 5.8). As already discussed before, biaxial structure reduces to the uniform director field state with spatially dependent degree of nematic order and negligible biaxiality (except at the substrate where the nematic director is perpen-

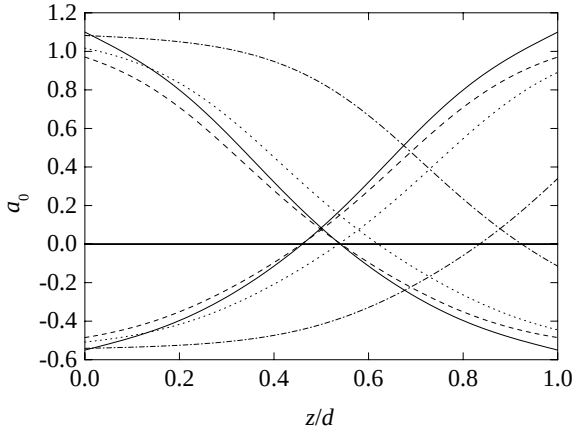

Figure 5.8 The degree of nematic order with respect to mutually perpendicular directors $\hat{n} = \hat{e}_x$ and $\hat{n} = \hat{e}_z$. Different lines correspond to different anchoring strengths: $G_1, G_2 \to \infty$ (solid line), $G_1 = G_2 = 1.2 \times 10^{-3}$ J/m^2 (dashed line), $G_1 = 1.2 \times 10^{-3}$ J/m^2 and $G_2 = 1.1 \times 10^{-3}$ J/m^2 (dotted line), and $G_1 = 1.2 \times 10^{-3}$ J/m^2 and $G_2 = 0.6 \times 10^{-3}$ J/m^2 (dash-dotted line). Parameters used in calculation are $\theta = 0.9$, $\zeta^2 = 0.03$, and $a_S = 1.1$.

dicular to the easy axis) if one of the confining substrates is characterized by weaker anchoring ($G \lesssim 10^{-4}$ J/m^2).

Structural transition between bent-director structure and biaxial structure

By comparing the total free energies of the two ordered configurations we determine the structural transition film thickness. However, the bent-director structure was determined approximately, therefore, the total free energy of the actual configuration is lower than the one obtained in our calculations. Since the neglected biaxiality is of order of $P \sim c\zeta^2$, where $0 < c < 1$, the difference between the actual and approximated free energy should be very small, i.e., $\mathcal{F} - \mathcal{F}_{\text{approx}} \sim -\zeta^4[c(\pi^2\sqrt{3}/4)S - c^2(\theta/2 + 3S + S^2)]$, where $S = S_b(\theta)$ is the bulk degree of nematic order parallel to the director. As expected, the correction is getting smaller as the film thickness is increased.

Near the isotropic–nematic phase transition temperature ($T_{NI} - T = 0.1$ K) and in a hybrid film of a typical liquid-crystalline material (such as 5CB) the nematic order is distorted if the film is thicker than $d_t \approx 47$ nm, whereas the metastable biaxial structure ceases to exist if the film thickness is larger than $d_s \approx 71$ nm. The latter critical thickness is determined by pretransitional dynamics, which will be discussed in detail in Section 5.2. As the temperature is decreased both values are decreased too and so is the difference between them. The same structural transition can be realized if the film thickness is held constant and the temperature is varied.

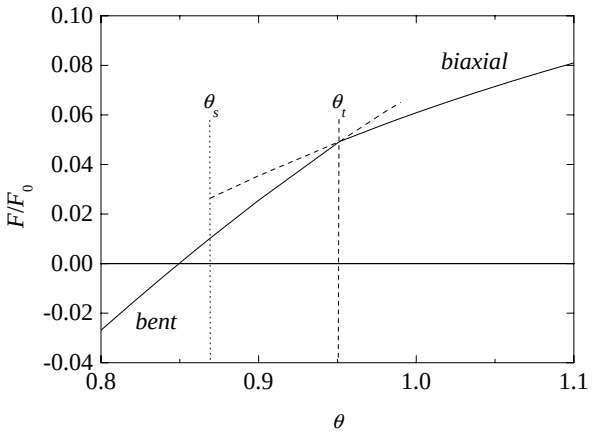

Figure 5.9 Temperature dependence of the total free energy of biaxial and bent-director structure. The structural transition occurs at the point where the free energies of the two configurations are equal ($\theta_t = 0.951$), whereas $\theta_s = 0.869$ represents the "supercooling" limit of the biaxial structure. In a typical liquid-crystalline material, the difference between the two temperatures is very small, $\Delta T = T_s - T_t \sim 0.09$ K, and the corresponding latent heat is by an order of magnitude smaller than the latent heat of the nematic-isotropic phase transition. The dashed continuation of the total free energy represents the region where the given structure is metastable. Parameters used in calculation are $\zeta^2 = 0.02$, $a_S = 1.1$, and $g_1 = g_2 \to \infty$.

A typical temperature dependence of the free energies of both ordered phases at constant film thickness ($\zeta^2 = 0.02$) is shown in Fig. 5.9. It is obvious that the slopes of the functions are not equal at the transition point, so that the structural transition is discontinuous. However, the corresponding latent heat, $q_l = \Delta(\partial\mathcal{F}/\partial T)T_t = \Delta(\partial\mathcal{F}/\partial\theta)[\theta_t + T^*/(T_{NI} - T^*)] \approx 8 \times 10^4$ J/m^3, is even smaller than the isotropic–nematic phase transition latent heat ($\approx 1.5{\times}10^6$ J/m^3) [147], therefore the structural transition is only weakly discontinuous.

The (dis)continuity of the structural transition can be changed if the temperature and film thickness are low enough. Within our approximation, in such case the free energies of bent and biaxial structures do not intersect and the free energy of the bent structure exceeds the biaxial one at the "supercooling" limit. This can be understood if one considers the approximate determination of the bent-director structure in which the biaxiality was omitted. However, even a rough calculation such as the one introduced at the beginning of this section shows that taking into account the estimated biaxiality lowers the free energy of the bent structure so that the transition becomes continuous. Such nature of the structural transition was found also in studies of Palffy-Muhoray *et. al* [20] and Galabova *et. al* [139]. The two different regimes are separated with a tricritical point (tricritical temperature and film thickness) below which the transition is continuous. Because of the approximate

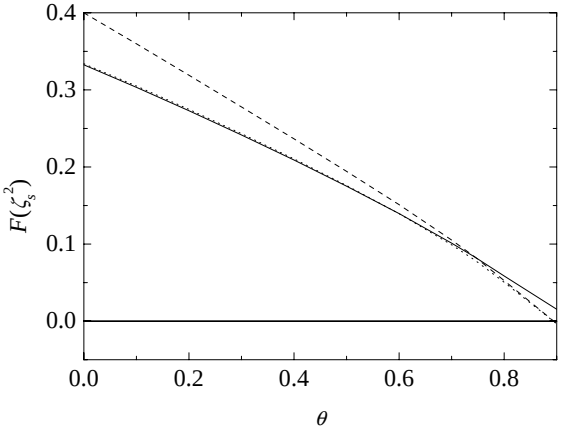

Figure 5.10 Temperature dependence of the total free energy of biaxial and bent-director structure at the "supercooling" film thickness [$\zeta_s = \zeta_s(\theta)$]. Because of the approximate determination of bent director structure the corresponding free energy is too high but even rough calculation shows that the correction (dotted line) would cause the transition to become continuous below some critical temperature and film thickness (tricritical point). Above the tricritical point (the upper limit $\theta_{\mathrm{TP}} = 0.746$ and $\zeta^2_{\mathrm{TP}} = 0.054$) the transition becomes progressively discontinuous.

description of the bent-director structure only its upper limit has been determined: $\theta_{\mathrm{TP}} = 0.746$ and $\zeta^2_{\mathrm{TP}} = 0.054$, which corresponds to $T_{NI} - T_{\mathrm{TP}} = 0.28$ K and $d_{\mathrm{TP}} = 34$ nm for a typical nematic liquid crystal, such as 5CB. In Fig. 5.10 the temperature dependence of total free energies of both ordered structures at the "supercooling" film thickness is shown. One should notice that the dimensionless total free energies are decreasing functions of temperature. That indicates that in the range of film thicknesses where biaxial structure can be realized the elastic part of the free energy is dominant over the ordering terms. The elastic term whose magnitude is determined by $\zeta^2 \propto 1/d^2$ is decreasing with temperature because the "supercooling" film thickness is an increasing function of temperature.

5.1.1 Monte Carlo simulations of a hybrid cell

Theoretical description of physical phenomena has its purpose when the results can be related to the observed phenomena. In the case of hybrid nematic cell, the distorted bent-director structure and undistorted uniform structure have been probed by many experimental methods taking advantage of the effect of certain ordered structure on physical observables, such as dielectric and optical properties, etc. On the other hand, the experimental evidence of biaxial structure is rather limited since the existence of this structure is very delicately tuned by the anchoring properties of the confining substrates and since it is only realized in a very narrow temperature in-

terval. However, the results can also be compared to the ones obtained by computer simulations which act not only as a bridge between microscopic and macroscopic length and time scales but also as a bridge between a theory and experiment.

In computer simulations we provide a guess for the interactions between molecules and probe it by comparing predicted macroscopic physical properties of a system with its actual properties. Once the model interactions between molecules are set the computer simulations can be used as an "experimental" method which may also reveal hidden details behind macroscopic observables. There are two basic types of computer simulations, molecular dynamics and Monte Carlo simulations. The former method consists of a brute-force solution of Newton's equations of motion, therefore, it corresponds to what happens in "real life" — it generates configurations time step after time step in their natural time sequence. On the other hand, the latter method can be thought of as a prescription for sampling configurations from a statistical ensemble; on achieving the equilibrium the system goes from one state to the next, not necessarily in a proper order [148,149].

Here, I present results obtained from the Monte Carlo simulation of the hybrid nematic film which was performed by the group of Pasini and prof. Zannoni in Bologna in collaboration with me and prof. Žumer. Further, I suggest some preliminary correspondence between outcome of the phenomenological theory and computer simulation.

The hybrid nematic film is simulated using a well known cubic-lattice spin system put forward by Lebwohl and Lasher [150]. It is based on modeling the interactions between the molecules through a second rank Lebwohl-Lasher potential

$$U_{ij} = \epsilon_{ij} P_2(\cos \beta_{ij}), \tag{5.8}$$

where ϵ_{ij} equals $\epsilon > 0$ for nearest-neighbor particles i and j, and it is zero elsewhere. P_2 is the second rank Legendre polynomial and β_{ij} is the angle between the long axes of the corresponding spins; spin denotes either a single molecule or a cluster of molecules whose short-range order is maintained in the examined temperature interval [151]. The only free parameter of the model is the temperature of the system, $T^{MC} = k_B T/\epsilon$. The model reproduces well the behavior of bulk nematic liquid crystals, particularly, it reproduces a weakly discontinuous phase transition and the correct temperature dependence of the order parameter [150,152]. The bulk isotropic–nematic phase transition occurs at $T_{NI}^{MC} = 1.1232$ [152], which yields for 5CB with $T_{NI} = 308.3$ K the inter-spin interaction strength $\epsilon = 0.0237$ eV (comparing this to the phenomenological estimate $A(T_{NI} - T^*)\mathcal{V}_0$ one would get for the volume of correlated molecules $\mathcal{V}_0 \sim 26$ nm^3 with the corresponding correlation length $\sqrt[3]{\mathcal{V}} \sim 3$ nm which is comparable to the phenomenological value $\xi_{NI} \sim 8$ nm).

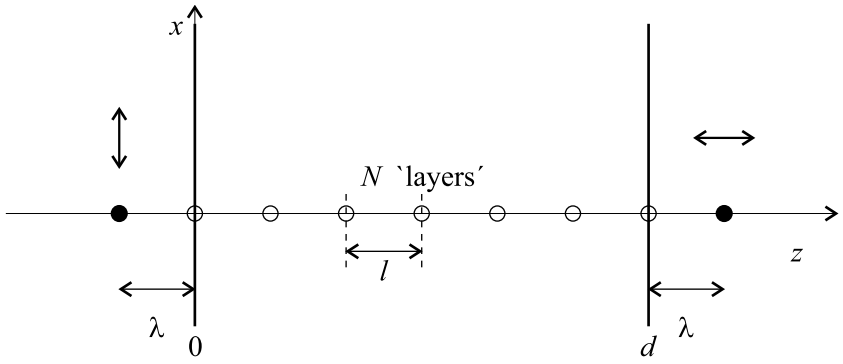

Figure 5.11 Schematic representation of the model system: the system consists of N layers of nematic spins and two additional layers of fixed spins which mimic the confining substrates. The layer distance l represents the extrapolation length λ — the distance on which the order is extrapolated to the one preferred by the substrates.

In the last decade, the Lebwohl-Lasher model has been successfully employed in simulations of confined nematic systems [149]. In the case of hybrid nematic system it has already been used in the study of point defects in hybrid nematic film [143]. The confinement is introduced as an additional layer of fixed spins whose orientation corresponds to the direction preferred by the confinement. The interaction between the fixed "substrate's" spins and the nematic spins is taken to be equal to the nematic–nematic interaction, therefore, the separation between the fixed layer and the first nematic layer has a clear physical significance — it is the extrapolation length. Its value is closely related to the number of molecules representing one spin — it is assumed that if a volume belonging to each molecule is $\mathcal{V}_1$ (for a typical liquid-crystalline molecule with a length $\sim$ 2 nm, $\mathcal{V}_1 \sim 8$ nm^3) then the corresponding volume of one spin is $\mathcal{V}_0 = N\mathcal{V}_1 = l^3$ where l is the layer separation. Variation of anchoring strength can be obtained either by changing the strength of the substrate-nematic spin interaction or as in our case by changing the number of layers. As it is known, what determines the strength of the surface-induced interaction is not just the absolute value of the corresponding energy but rather the ratio between surface-induced interaction and energy of elastic deformations; this is equivalent to the ratio λ/d. With equal λ the anchoring is effectively stronger in thicker films. Schematic representation of the model system is represented in Fig. 5.11. Large dimensions in the lateral directions are obtained by periodic boundary conditions. In the present study, the simulation boxes have dimensions $30 \times 30 \times N'$ particle, where $N' = N + 2$ corresponds to N layers of "nematic" spins and to 2 parallel layers of fixed spins on each side.

In order to determine the type of the ordered configuration obtained after the equilibration with the Monte Carlo method the components of the order parameter

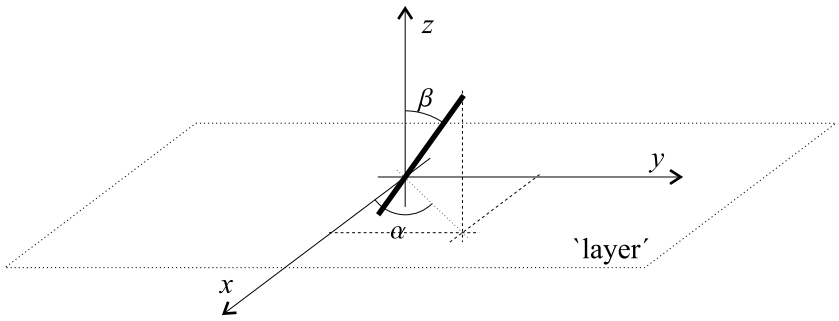

Figure 5.12 Schematic representation of a spin in the coordinate system: coordinate axes x and y lie in the plane of a substrate with the preferred orientation of the director parallel to x, and the other substrate is located at $z = Nl = d$. "Layers" are planes parallel to the substrates. The order in a film is measured with respect to the fixed orthonormal triad $\hat{n} = \hat{e}_z$, $\hat{e}_1 = \hat{e}_x$, and $\hat{e}_2 = \hat{e}_y$.

tensor are calculated as an average over distinct layers. The relevant parameters are the order with respect to the film normal which is measured by the degree of order

$$a_0^z = \frac{1}{2}\langle 3\cos^2\beta - 1\rangle = -\frac{1}{2}a_0 + \frac{\sqrt{3}}{2}a_1 \tag{5.9}$$

and parameter of biaxiality

$$a_1^z = \frac{\sqrt{3}}{2}\langle \sin^2\beta\cos 2\alpha\rangle = -\frac{\sqrt{3}}{2}a_0 - \frac{1}{2}a_1, \tag{5.10}$$

whereas the parameter

$$a_{-1} = \frac{3}{2}\langle \sin 2\beta\cos\alpha\rangle \tag{5.11}$$

measures the possible bending of the director field in the plane of the two easy axes. Here $\langle\cdots\rangle$ represent the average over the spins in a layer over several MC steps after the equilibrium has been reached. The amplitudes a_i correspond to the same parametrization of the order parameter tensor as used in the phenomenological description. In Fig. 5.12, a spin is shown with respect to the layer and coordinate system together with representative parameters.

The results of the simulation of the hybrid nematic film with mutually perpendicular preferred orientations at the substrates, however, with equal anchoring strength, reveal three different states: disordered phase with progressively growing order in layers close to the substrates and two ordered structures, biaxial and bent-director structure. In ordered structures, the liquid crystal is ordered in the whole film, whereas in the high temperature disordered phase there is no order in the core of the film. Order in the middle of the film develops below T_1^{MC}; in a 14-layer hybrid film $T_1^{MC} \approx 1.17$. Temperature dependence of the degree of order with respect to the distance from (one of) the substrates is presented in Fig. 5.13 (a). Due to the high

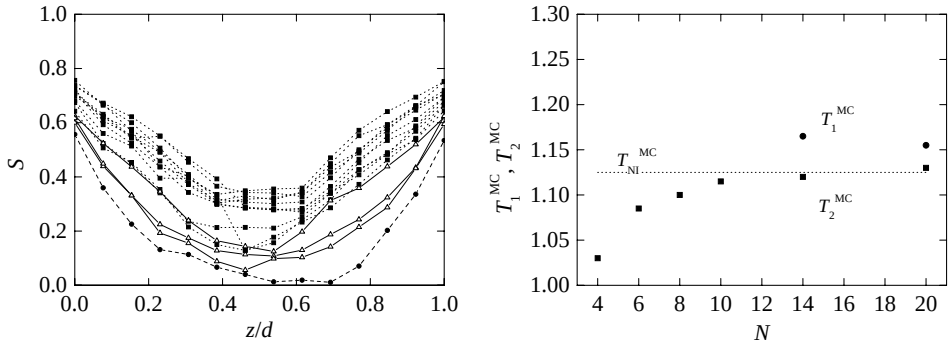

(a) (b)

Figure 5.13 (a) Scalar order parameter in a 14-layer hybrid film as a function of distance from (one of) the substrates for various temperatures below (full squares and triangles) and above (full circles) the ordering transition to the biaxial phase; $T^{MC} \in [0.90, 1.18]$ and the temperature step is 0.02. Curves with triangles correspond to the ordered phase with undistorted director field — biaxial structure — which is stable between T_2^{MC} and T_1^{MC}. Lines are guides to the eye. (b) Transition temperatures T_1^{MC} and T_2^{MC} as a function of number of layers; dotted line corresponds to the bulk ordering transition temperature.

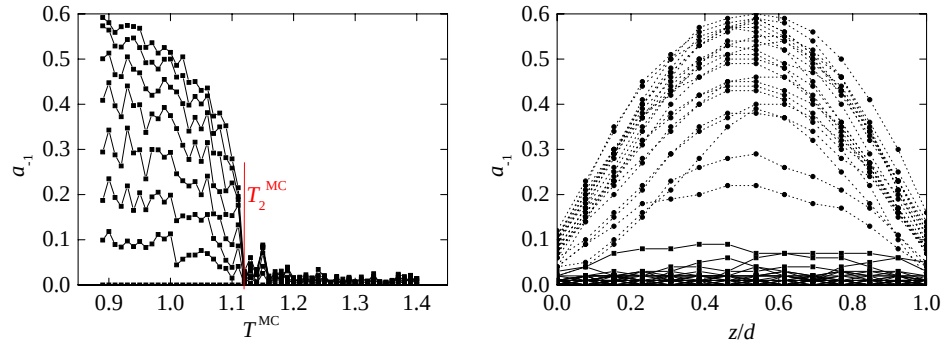

(a) (b)

Figure 5.14 Bending parameter a_{-1} in a 14-layer hybrid film: (a) a_{-1} as a function of temperature for distinct layers of the film (the upper the curve the closer the layer to the middle of the film). (b) a_{-1} as a function of distance from (one of) the substrates for various temperatures below (circles) and above (squares) the transition to the bent-director structure; $T^{MC} \in [0.89, 1.40]$ and the temperature step is 0.01. The corresponding transition temperature is denoted as T_2^{MC}. Lines are guides to the eye.

surface-induced order the ordering-transition temperature T_1^{MC} is higher than the ordering-transition temperature in bulk which has already been discussed in the case of heterophase nematogenic systems. This surface-induced effect is weaker in larger films, thus, T_1^{MC} is a decreasing function of the film thickness [see Fig. 5.13 (b)]. On the other hand, in very thin films ($d \gtrsim \xi_{NI}$) the order in the middle of the film is subject to a continuous evolution and the ordering transition is lost.

On lowering the temperature, first the order in the middle of the film grows and then, below some temperature the director field starts to bend. The corresponding temperature of the structural transition between undistorted biaxial and distorted bent-director structure is denoted as T_2^{MC}; in a 14-layer hybrid film $T_2^{MC} \approx 1.12$. Temperature dependence of the bending parameter a_1 as a function of temperature and distance from (one of) the substrates is presented in Fig. 5.14. Structural transition temperature is lower than the bulk transition temperature. This difference with respect to the T_{NI}^{MC} is a consequence of the elastic deformations which are due to the frustrating boundary conditions. The effect has already been discussed within the phenomenological theory. Elastic deformations are stronger in thinner films, thus, the temperature T_2^{MC} is an increasing function of the film thickness which is presented in Fig. 5.13 (b). Increasing the film thickness the temperature interval of the stable biaxial structure decreases and in very thick films the two transitions would merge; the remaining transition would correspond to a direct change from the disordered to ordered bent-director structure.

The existing transitions can also be recognized as peaks in the heat capacity of the film. In Fig. 5.15, the temperature dependence of the internal energy of the 14-layer film and the corresponding heat capacity are shown. The well developed peak corresponds to the transition to the bent-director structure. Smaller peak, which is to some extent hidden by the higher one, is associated with the change of the ordering in the core of the film.

The results obtained from the Monte Carlo simulation confirm the existence of the biaxial structure and the corresponding transitions between (dis)ordered configurations. In some other simulation study of a hybrid film [153], the biaxial structure was not found which was due to the choice of the surface potential which yielded extremely unsymmetric properties for the homeotropic and planar anchoring. Still, some further work is needed to establish the closer quantitative correspondence between the results obtained from Monte Carlo simulations and from the phenomenological description.

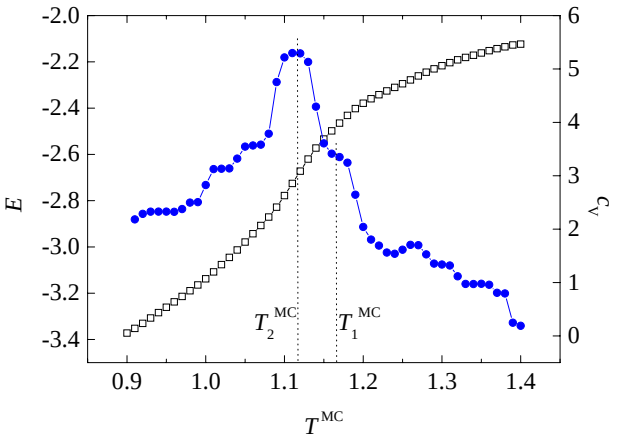

Figure 5.15 Energy of the 14-layer hybrid nematic film (squares) and the corresponding specific heat (full circles). The highest peak located at $T_2^{MC} \approx 1.12$ corresponds to the structural transition between bent-director and biaxial structures and the lower peak which is masked by the higher one corresponds to the ordering transition and is associated to the middle of the film, $T_1^{MC} \approx 1.17$. Lines are guides to the eye.

5.2 Pretransitional dynamics

Once we have calculated and tested the equilibrium profiles we can begin with the analysis of fluctuations. Here, the analysis is restricted to fluctuations in the biaxial (director exchange) structure with equal anchoring strengths. We study their temperature/film thickness dependence when approaching the structural transition to the bent-director configuration and the "supercooling" limit. The same approach can be used also with the uniform director structure. This analysis is not performed here because due to very small biaxiality the fluctuations do not differ much from fluctuations in homogeneous systems which are discussed in Section 2.2.2 and Section 4.2 on page 83. The detailed analysis of the pretransitional dynamics of all five degrees of freedom around the bent-director configuration is somewhat more complicated because of the nonuniformity of the base tensors. The simplified description within the director picture was studied in detail by Stallinga *et. al* [12], however, the results are not quoted here.

The Gaussian dynamics of five scalar components of collective excitations — introduced by the expansion $\mathsf{B}(\vec{r},t) = \sum_{i=-2}^{2} b_i(\vec{r},t)\mathsf{T}_i$ — is derived by projecting the linearized form of the relaxation equation [Eq. (2.64)] onto the base tensors. Since the equilibrium profiles depend on the z coordinate only, the normal modes can be factorized as follows,

$$b_i(\vec{r},t) = \mathrm{e}^{i(k_x x + k_y y)} \beta_i(z)\, \mathrm{e}^{-\mu_i t}, \tag{5.12}$$

where k_x and k_y are the in-plane components of dimensionless wave vector of fluc-

tuations which are assumed to be subject to periodic boundary conditions, μ_i's are the dimensionless relaxation rates of the eigenmodes, and time is measured in units of $\tau_a = (27C/B^2)\Gamma \sim 10^{-8}$ s [32]. Considering the introduced ansatz [Eq. (5.12)] and the equilibrium profiles of the system the amplitudes $\beta_i(z)$ are determined by the equations

$$\begin{aligned}
\zeta^2\beta_0'' - (\theta - \lambda_{0,1} - 6a_0 + 6a_0^2 + 2a_1^2)\beta_0 - 2a_1(3+2a_0)\beta_1 &= 0,\\
\zeta^2\beta_1'' - (\theta - \lambda_{0,1} + 6a_0 + 2a_0^2 + 6a_1^2)\beta_1 - 2a_1(3+2a_0)\beta_0 &= 0,\\
\zeta^2\beta_{-1}'' - (\theta - \lambda_{-1} + 6a_0 + 2a_0^2 + 2a_1^2)\beta_{-1} &= 0,\\
\zeta^2\beta_{\pm 2}'' - (\theta - \lambda_{\pm 2} - 3a_0 \mp 3\sqrt{3}a_1 + 2a_0^2 + 2a_1^2)\beta_{\pm 2} &= 0,
\end{aligned} \tag{5.13}$$

where $\beta_i' = d\beta_i/dz$ and $\lambda_i = \mu_i - \zeta^2(k_x^2 + k_y^2)$ are the reduced relaxation rates of the modes. When deriving these equations, one must consider that the modes which are coupled relax with the same relaxation rate, therefore $\lambda_0 = \lambda_1 = \lambda_{0,1}$. In the case of a very strong surface anchoring ($g \to \infty$) no fluctuations are allowed at the substrate, thus $\beta_i(z = 0, 1) = 0$, otherwise the boundary conditions read

$$\beta_i' = \pm\frac{g_{1,2}}{\zeta^2}\beta_i \Big|_{z=0,1}, \tag{5.14}$$

where the signs + and −, and the subscripts 1 and 2 refer to $z = 0$ and $z = 1$, respectively.

In the case of a purely uniaxial nematic ordering and uniform director field ($a_i = 0$, $i \neq 0$) the five fluctuating modes are independent, therefore the two equations for the amplitudes $\beta_0(z)$ and $\beta_1(z)$ are uncoupled. Furthermore, due to the symmetry reasons the two biaxial modes (b_i with indices $i = \pm 1$) are degenerate and so are the two director modes (indices $i = \pm 2$). The system reduces to the one studied in Chapter 4.

As implied by equations in Eq. (5.13) this is not the case when dealing with fluctuations in a biaxially ordered hybrid film. Since the equilibrium profiles are described by two nonzero amplitudes, a_0 and a_1, the corresponding fluctuation modes, β_0 and β_1, are coupled. The significance of these modes is transparent when considering their linear combinations $\beta_{0,1}^x = -(\beta_0 + \sqrt{3}\beta_1)/2$ and $\beta_{0,1}^z = -(\beta_0 - \sqrt{3}\beta_1)/2$, which denote the order parameter fluctuations with respect to the nematic director parallel to the x and z axis, respectively. The other three fluctuation modes are uncoupled and represent either director fluctuations (β_{-1} modes and low $\beta_{\pm 2}$ modes) or biaxial fluctuations, high $\beta_{\pm 2}$ modes.

Due to the inhomogeneous equilibrium profiles the eigenmodes of fluctuations can only be determined numerically. In the following, the spectra of collective excitations and the eigenamplitudes for different fluctuating modes will be interpreted.

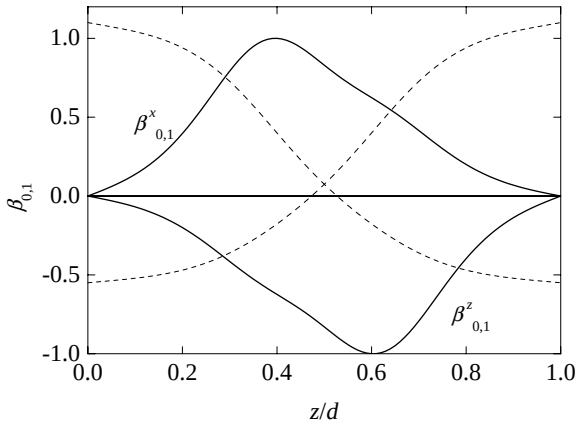

Figure 5.16 Spatial dependence of the lowest order parameter mode. Solid lines correspond to coupled fluctuations of the degree of order with respect to the two mutually perpendicular easy axes. Dashed lines correspond to the equilibrium profiles (Fig. 5.7). Parameters used in calculation are $\theta = 0.9$, $\zeta^2 = 0.01258$, $a_S = 1.1$, and $g_1 = g_2 \to \infty$.

Order parameter fluctuations

The term order parameter fluctuations denotes coupled fluctuations of the two nonzero equilibrium amplitudes. As it is well known the eigenfunctions of an operator invariant to the space reflection are either symmetric or antisymmetric with respect to the same transformation [130]. Since the operator which governs the order parameter fluctuations [see Eq. (5.13) and the results for the equilibrium profiles a_0 and a_1] is symmetric with respect to the plane $z = 1/2$ the eigenfunctions of the system can be divided into two classes, i.e., the symmetric and antisymmetric functions with respect to the symmetry plane. The lowest symmetric mode is associated with fluctuations of the thickness of the central director exchange region and therefore also with the fluctuations of the magnitude of biaxiality of the nematic order. However, the lowest antisymmetric mode corresponds to fluctuations of the position of the boundary between the two parts of the film which are determined by mutually perpendicular nematic directors. The portrait of the lowest antisymmetric order parameter mode is plotted in Fig. 5.16. It can be noticed that the two corresponding profiles, $\beta^x_{0,1}$ and $\beta^z_{0,1}$, are "localized" at the part of the film with director $\hat{e}_x$ and $\hat{e}_z$, respectively. The positions of their maxima coincide with the position of maximum slope of the scalar order parameter. Thus, the lowest antisymmetric order parameter mode is responsible for the growth of the surface wetting layers. The same fluctuation mode was found also in heterophase systems (see Section 4.2). Higher symmetric and antisymmetric modes change the shape of the exchange region in a symmetric or an antisymmetric manner, respectively.

The lowest relaxation rate corresponds to the lowest antisymmetric mode. When

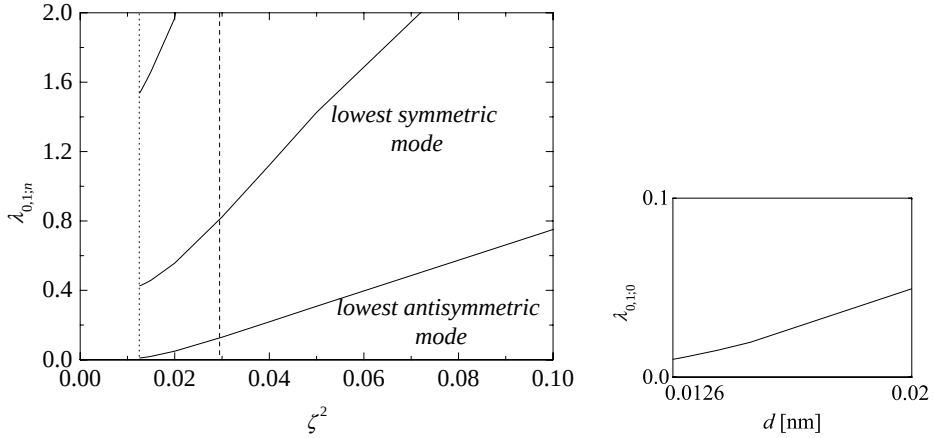

Figure 5.17 (a) Lower part of the spectrum of collective order parameter excitations with respect to the film thickness. Dotted and dashed verticals denote the "supercooling" and the structural transition film thickness, respectively. (b) Magnified detail of the lowest order parameter relaxation rate. Notice that the relaxation rate remains finite even at the "supercooling" limit and approaches the limit with the zero slope. Parameters used in calculation are $\theta = 0.9$, $a_S = 1.1$, and $g_1 = g_2 \to \infty$.

increasing the film thickness toward the structural transition thickness (decreasing the parameter ζ^2) all the relaxation rates are decreased, especially the lowest one (see Fig. 5.17). However, it stays finite ($\lambda_{0,1;n=0} > 0$) even at the "supercooling" limit/transition point above/below the tricritical point, respectively. Similarly, the relaxation rates decrease with decreasing temperature. At this point it should be emphasized again that the film thickness turns out to be a parameter that rescales the temperature [Eq. (5.5)].

Director fluctuations

Director fluctuations β_{-1} represent changes of the orientation of the nematic director in the plane of the two easy axes. They bend the nematic director in the $\hat{n} = \hat{e}_x$ half of the film toward the direction $\hat{e}_z$ and the $\hat{n} = \hat{e}_z$ director in the other half toward the perpendicular x direction. The corresponding eigenmodes are spread over the whole sample and are similar to the sine functions as it is shown in Fig. 5.18. The lowest director mode represents the change of the tensor order parameter that is similar to the one characteristic for the bent-director configuration plotted in Fig. 5.5. Its relaxation rate exhibits a critical slowdown when the film thickness approaches the "supercooling" limit/transition point above/below the tricritical point, respectively. In the case of discontinuous structural transition the lowest director mode is almost critical even at the structural transition, which is in agreement with our previous

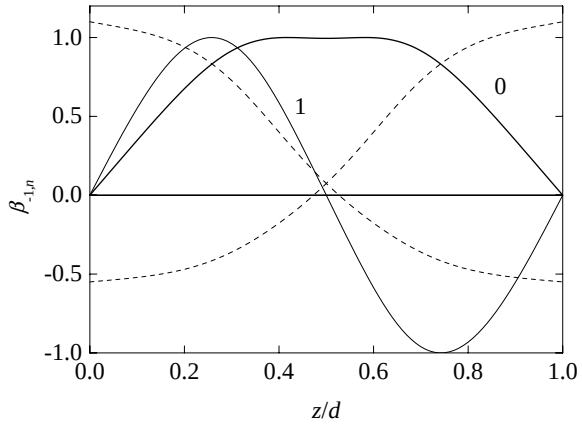

Figure 5.18 Spatial dependence of the lowest two director modes labeled by the number of nodes. Dashed lines correspond to the equilibrium profiles plotted in Fig. 5.7. Parameters used in calculation are $\theta = 0.9$, $\zeta^2 = 0.01258$, $a_S = 1.1$, and $g_1 = g_2 \to \infty$.

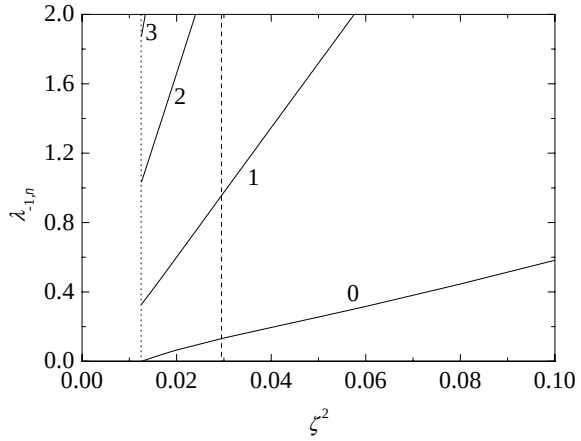

Figure 5.19 A few lowest relaxation rates of director modes versus film thickness. The rates are decreasing with increasing film thickness, especially the lowest mode's rate which drops to zero as the film thickness approaches the "supercooling" limit. Dotted and dashed verticals denote the "supercooling" and the structural transition film thickness, respectively. Parameters used in calculation are $\theta = 0.9$, $a_S = 1.1$, and $g_1 = g_2 \to \infty$.

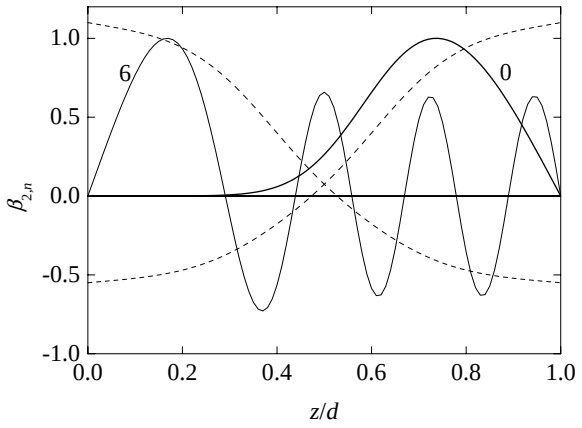

Figure 5.20 Portrait of two typical biaxial fluctuation modes β_2 (the β_{-2} modes are just their mirror images with respect to the symmetry plane $z = 1/2$). The lowest modes are expelled from the part of the film where these fluctuations represent biaxial fluctuations. Higher modes are spread over the whole sample. Labels denote the number of nodes of the mode and the dashed lines correspond to the equilibrium profiles of biaxial structure. Parameters used in calculation are $\theta = 0.9$, $\zeta^2 = 0.01258$, $a_S = 1.1$, and $g_1 = g_2 \to \infty$.

conclusion that the transition is only weakly discontinuous. Therefore, in both regimes the soft director mode can be assumed to govern the structural transition between the two ordered configurations. As shown in Fig. 5.19, higher modes relax faster and do not contribute essentially to the pretransitional change in the director field.

Biaxial fluctuations

Biaxial fluctuations $\beta_{\pm 2}$ are described by the last two equations in Eq. (5.13). If these equations are rewritten in more appropriate form

$$\zeta^2 \beta''_{\pm 2} - [\theta - \lambda_{\pm 2} + 6a_0^{x,z} + 2(a_0^2 + a_1^2)]\beta_{\pm 2} = 0, \tag{5.15}$$

and the symmetry relations between the equilibrium amplitudes a_0^x and a_0^z are considered (see Fig. 5.7) it can be easily seen that the spectra for the two biaxial modes are degenerated, whereas the eigenfunctions are just mirror images with respect to the plane $z = 1/2$.

As shown in Fig. 5.20 the few lowest modes of fluctuations $\beta_2(z)$ and $\beta_{-2}(z)$ are expelled from the part of the film which is characterized by directors $\hat{e}_x$ and $\hat{e}_z$, respectively. This can be easily understood if we consider that $\beta_{\pm 2}$ represent amplitudes of the projection of the tensor order parameter along the base tensors $\mathsf{T}_{\pm 2}$ which couple directions y and z or y and x, respectively. That means that β_2 refers to director fluctuations in the $\hat{n} = \hat{e}_z$ part of the film but to biaxial

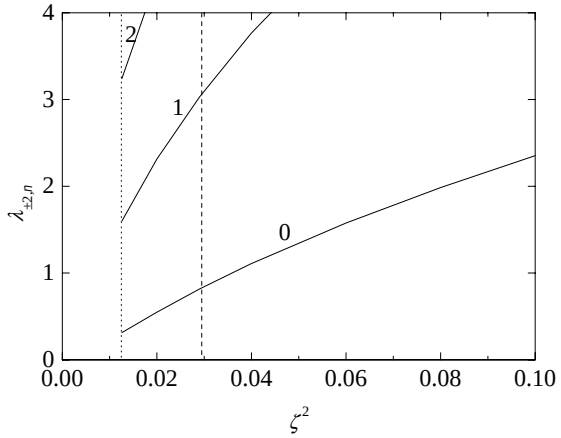

Figure 5.21 The lowest part of the spectrum of relaxation rates of biaxial fluctuations. Note that the relaxation rates are higher than the relaxation rates of other modes (cf. Figs. 5.17 and 5.19). Since the biaxial fluctuations represent deformations of the order parameter in the y direction they do not play any important role at the structural transition. Dotted and dashed verticals denote the "supercooling" and the structural transition film thickness, respectively. Parameters used in calculation are $\theta = 0.9$, $a_S = 1.1$, and $g_1 = g_2 \to \infty$.

fluctuations in the other part, and vice versa for the β_{-2} fluctuation modes. Since in the uniaxial nematic phase director fluctuations are much more favorable than biaxial fluctuations [15], $\beta_{\pm 2}$ fluctuations tend to be localized at the appropriate half of the film only. Higher modes are spread over the whole film whereas the unfavorable manner of biaxial fluctuations is compensated by the shorter wave vector of a deformation. In addition, it is well known that the higher the modes, the smaller the effect of the shape of the potential on them.

The biaxial relaxation rates are higher than the rates of other fluctuation modes, therefore the biaxial fluctuations do not play any important role in the structural transition discussed. The spectrum of biaxial relaxation rates is plotted in Fig. 5.21.

5.3 Structural and pseudo-Casimir forces

Structural force

The common feature of all ordered structures in hybrid nematic cell is the repulsive character of the structural force for separations above a few nanometers. The repulsion is due to the antagonistic boundary conditions, which always lead to at least small deformation, and to the fact that within certain ordered structure the frustration is stronger if the confining substrates are brought closer to each other. The magnitude of the force is tuned by the anchoring strength at both substrates

whereas its functional form depends on the structure in question.

The *uniform director structure* is characterized by a weak localized deformation of the nematic scalar order parameter whereas the director field is undeformed. The corresponding structural force is short-range and very weak comparing to the structural forces characteristic for other configurations in a hybrid film. Depending on the details of the induced order the force can be either monotonically repulsive or can exhibit a nonmonotonic behavior characterized by attraction at very small film thicknesses and a weak repulsion for larger separations (see Fig. 5.22). The latter case corresponds to the substrates that induce strong order, higher than characteristic for given temperature. (E.g., the excess order at the free surface of some nematic liquid crystals observed by Kasten *et. al* [122] and studied theoretically by means of density functional approach by Martin del Rio *et. al* [125].) Here, the turn-over between the regime of the increasing/decreasing force with the increasing film thickness is related to the fact that above certain film thickness the order at the side with stronger anchoring is above its bulk value whereas it is below it on the other side. If the spatial variation of the scalar order parameter is neglected the free energy of the uniform director structure corresponds only to the penalty for violating the induced order at the substrate with weaker anchoring,

$$\mathcal{F} = \frac{3}{2} G S^2 \mathcal{A}, \tag{5.16}$$

where G is related to the substrate with weaker anchoring, S is the uniform degree of the nematic order, and $\mathcal{A}$ is the surface area of the confining substrate. This free energy does not depend on the separation between the two confining substrates and, thus, does not give rise to the structural force.

Within the bare director picture there is no structural force in the uniform director structure, however, the elastic deformation of the director field in the *bent-director structure* gives rise to strong structural repulsion even within the simplified description. In this structure, in the limit of infinitely strong surface anchorings the elastic contribution to the free energy reads

$$\mathcal{F} = \frac{3}{2} L S^2 \mathcal{A} d \int_0^1 \mathrm{d}z (\phi')^2 = \frac{3\pi^2 L S^2 \mathcal{A}}{8d}, \tag{5.17}$$

which is only slightly perturbed by the coupling with the deformed field of the scalar order parameter. From Eq. (5.17) in the bent director structure the structural force per unit area is roughly given by

$$\Pi = \frac{3\pi^2 L S^2}{8d^2}. \tag{5.18}$$

For finite anchorings the structural pressure becomes $\Pi \approx (3/2) L S^2 (\phi_1 - \phi_2)^2 d^{-2}$, where ϕ_1 and ϕ_2 are the director's tilt angles at the substrates located at $z = 0$ and

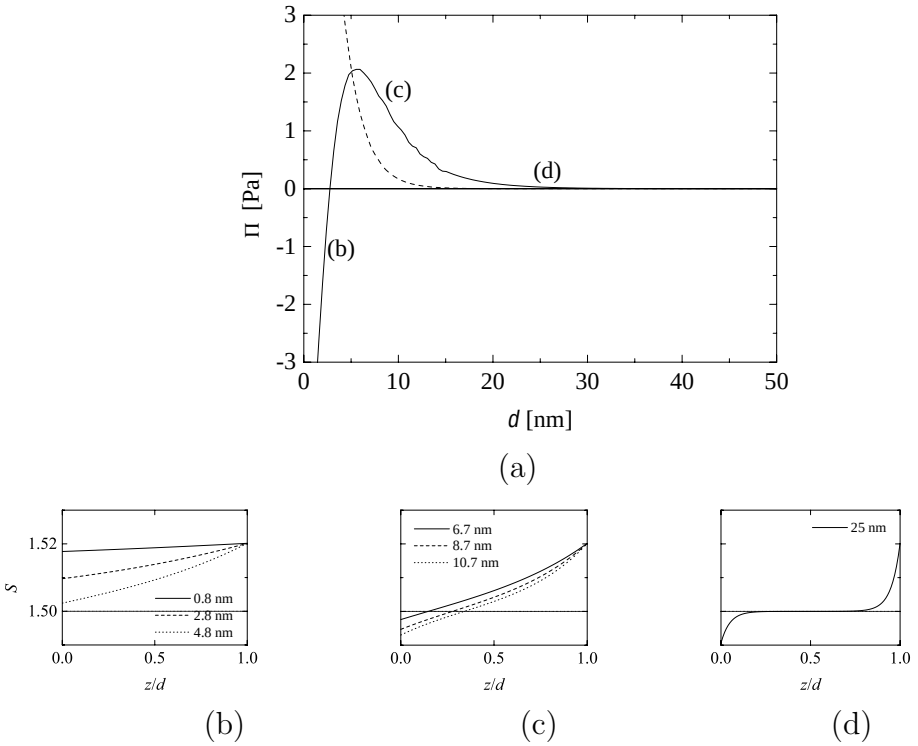

Figure 5.22 (a) Structural force per unit area in a hybrid cell characterized by the uniform director structure. Solid line corresponds to confining substrates which induce high nematic order [$a_S = 1.01 S_b(\theta)$] and the dashed line corresponds to the hybrid cell with substrates with no excess order [$a_S = S_b(\theta)$]. Labels (b) – (d) refer to the corresponding equilibrium profiles of the scalar order parameter in a hybrid cell confined by substrates characterized by the induced excess order. Parameters used in calculation are $\theta = 0$, $G_1 = 2 \cdot 10^{-5}$ J/m^2, and $G_2 \to \infty$.

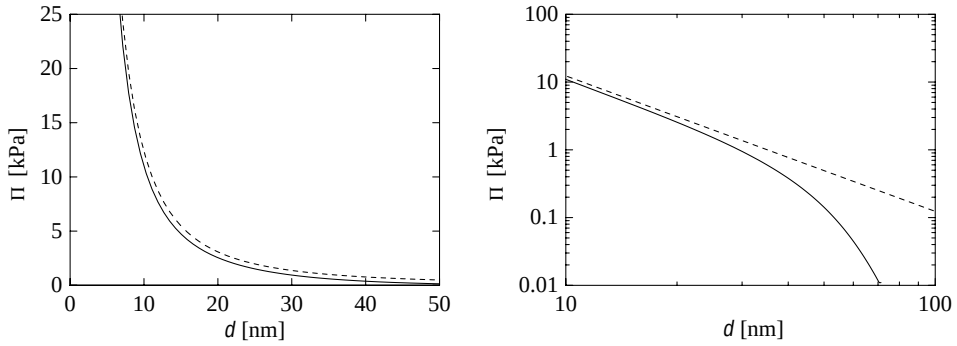

(a) (b)

Figure 5.23 (a) Structural force per unit area in the bent-director structure (dashed line) and in the biaxial structure (solid line). In (b) the same plot in the logarithmic scale where it can be clearly seen that for large cell thicknesses the localization of the deformation in the biaxial structure results in shortened range of the structural force.

$z = d$, respectively. They are determined by Eq. (5.4) and depend on the separation between the two confining substrates. The structural force in the bent-director structure is plotted in Figs. 5.23 (a) and 5.23 (b).

In *biaxial structure*, the force is repulsive and exhibits $1/d^2$ behavior at small cell thicknesses whereas at large d's the exponent of the power law is smaller than -2 which is clearly evident from Fig. 5.23 (b). For small cell thicknesses, the elastic deformation, although of the scalar fields rather than the director field, is spread over the whole cell and the force exhibits typical elastic dependence. The decrease of the range of the force for larger cell thicknesses is a consequence of the localization of the deformation when approaching the stability limit of this structure.

Pseudo-Casimir force

As we have seen, depending on the temperature, surface anchorings, and the thickness of the cell the nematic liquid crystal in a hybrid cell can be found in one of the three ordered structures described in previous Sections. Unlike in the case of the heterophase nematic system, where a systematic study of the pseudo-Casimir force was performed by Ziherl *et. al* [154,28], in the hybrid cell the pseudo-Casimir force has only been calculated for the simplest ordered configuration, i.e., the uniform director structure (Ziherl *et. al* [65]). The studied hybrid cell was characterized by stronger homeotropic and weaker degenerate planar boundary conditions yielding homeotropic director field below the critical thickness d_c which preserves the full rotational symmetry with respect to the normal to the planar parallel cell. The study was performed within the bare director description. In the cell with the uniform nematic order the effective correlation length in the Hamiltonian of the correspond-

ing fluctuating mode [Eq. (2.69)] is a constant and the partition function of the fluctuation modes can be derived analytically.

In this thesis, we do not intend to present any new results for the pseudo-Casimir force in the hybrid cell although to complete the description of the nematic liquid crystal in a hybrid geometry pseudo-Casimir force should be determined also in other possible structures, i.e., the bent-director structure and biaxial structure. Determination of the force in the latter structure is more complex due to deformed equilibrium order.

In the following Section the stability of thin nematic depositions subject to hybrid boundary conditions will be studied. In the system, the pseudo-Casimir force plays crucial role for the mechanical stability of the film and, thus, has to be taken into account. In the study, we will use the results obtained by Ziherl *et. al* [65], however, in this Section, we present in short the calculation of the pseudo-Casimir force in the given system and we discuss the obtained results.

In the uniform director structure with homeotropic and planar boundary conditions the Hamiltonian of the liquid-crystalline system consists of elastic and surface terms. As already done in previous studies of order parameter fluctuations, the calculation is restricted to harmonic approximation, therefore, the director is expanded around the equilibrium configuration and only the lowest-order terms are kept. The corresponding Hamiltonian of fluctuations is diagonal

$$\mathcal{H}[n_x, n_y] = \mathcal{H}[n_x] + \mathcal{H}[n_x], \tag{5.19}$$

where in the one-elastic-constant approximation

$$\mathcal{H}[n] = \frac{K}{2}\left[\int (\nabla n)^2 \mathrm{d}V - \lambda_P^{-1}\int n^2 \mathrm{d}S_P + \lambda_H^{-1}\int n^2 \mathrm{d}S_H\right]. \tag{5.20}$$

Here, n is either of the two fluctuating scalar director fields, $K = 3LS^2$, and $\lambda_{P,H}$ are the extrapolation lengths of the degenerate planar and homeotropic substrate, respectively. The negative sign of the planar surface term indicates the frustrating role of the two competing substrates, which eventually destabilizes the uniform structure.

The interaction free energy of the two degenerate director modes is determined by the partition function written out in Eq. (2.71). Due to the in-plane translational invariance of the system the modes can be Fourier decomposed, $n(\vec{r}) = \sum_{\vec{q}} \exp(i\vec{q}\cdot\vec{r}_\perp)\tilde{n}_{\vec{q}}(z)$ — $\vec{q}$ is the in-plane wavevector and $\vec{r}_\perp$ is the projection of the vector $\vec{r}$ onto the plane of the confining substrate —, in to the ensemble of independent one-dimensional harmonic oscillators. The corresponding partition function is

factorized, $\Xi = \Pi_{\vec{q}} \Xi_{\vec{q}}$, where

$$\Xi_{\vec{q}} = \int \mathcal{D}\tilde{n}_{\vec{q}}\, \mathrm{e}^{-\beta \mathcal{H}[\tilde{n}_{\vec{q}}]} \tag{5.21}$$

and

$$\mathcal{H}[\tilde{n}_{\vec{q}}] = \frac{K\mathcal{A}}{2} \left[\int_0^d \left(\tilde{n}_{\vec{q}}'^2 + q^2 \tilde{n}_{\vec{q}}^2 \right) \mathrm{d}z - \lambda_P^{-1} \tilde{n}_{\vec{q},-}^2 + \lambda_H^{-1} \tilde{n}_{\vec{q},+}^2 \right]. \tag{5.22}$$

Here, $\mathcal{A}$ is the substrate surface area, the prime denotes $\mathrm{d}/\mathrm{d}z$, and $\tilde{n}_{\pm} = \tilde{n}(z = 0, d)$. Further calculation of the partition function is based on the analogy with the calculation of the probability for a particle with the Hamiltonian $\mathcal{H}$ to remain at a given point within a certain time interval [155]. According to this,

$$\Xi_{\vec{q}} \propto \int_{-\infty}^{\infty} \mathrm{d}\tilde{n}_{\vec{q},-} \int_{-\infty}^{\infty} \mathrm{d}\tilde{n}_{\vec{q},+} \exp\left(\frac{K\mathcal{A}}{2k_B T} \left(\lambda_P^{-1} \tilde{n}_{\vec{q},-}^2 - \lambda_H^{-1} \tilde{n}_{\vec{q},+}^2 \right) \right) \Xi_{\vec{q};\tilde{n}_{\vec{q},-},\tilde{n}_{\vec{q},+}} \tag{5.23}$$

and

$$\Xi_{\vec{q};\tilde{n}_{\vec{q},-},\tilde{n}_{\vec{q},+}} \propto \sqrt{\frac{1}{\sinh(qd)}} \exp\left(-\frac{K\mathcal{A}}{2k_B T} \left[\left(\tilde{n}_{\vec{q},-}^2 + \tilde{n}_{\vec{q},+}^2 \right) \coth(qd) - \frac{2\tilde{n}_{\vec{q},-}\tilde{n}_{\vec{q},+}}{\sinh(qd)} \right] \right), \tag{5.24}$$

where we have disposed of irrelevant multipliers. Here, $\Xi_{\vec{q};\tilde{n}_{\vec{q},-},\tilde{n}_{\vec{q},+}}$ is the partition function associated with the fluctuation modes with boundary conditions $\tilde{n}_{\vec{q},-}$ and $\tilde{n}_{\vec{q},+}$, and $\Xi_{\vec{q}}$ in Eq. (5.23) is obtained by an extension of a point-to-point Green function to a region-to-region Green function, where the width of each region is defined by a characteristic length scale analogous to the extrapolation length [155]. In practice this means, that a finite surface interaction with a given easy axis is represented by a superposition of strong surface interactions each characterized by some easy axis and multiplied by a statistical weight corresponding to the energetic penalty for the deviation from the given easy orientation. The integrals in Eq. (5.23) can be calculated analytically and by omitting further irrelevant multipliers we obtain the final expression for the interaction free energy,

$$\begin{aligned} \mathcal{F} &= -k_B T \sum_{\vec{q}} \Xi_{\vec{q}} \\ &\propto -k_B T \sum_{\vec{q}} \left[\frac{q^2 - \lambda_P^{-1}\lambda_H^{-1}}{q\left(-\lambda_P^{-1} + \lambda_H^{-1}\right)} \sinh(qd) + \cosh(qd) \right]^{-1/2}. \end{aligned} \tag{5.25}$$

Here, we stress that by replacing $-\lambda_P$ with $\lambda_{H'}$ the obtained result corresponds also to the free energy of fluctuations between two substrates with homeotropic anchoring and with different anchoring strengths characterized by extrapolation lengths $\lambda_{H'}$ and λ_H.

Rather than in the free energy of the interaction we are interested in the force acting between the two confining substrates. The force is, like in the case of the

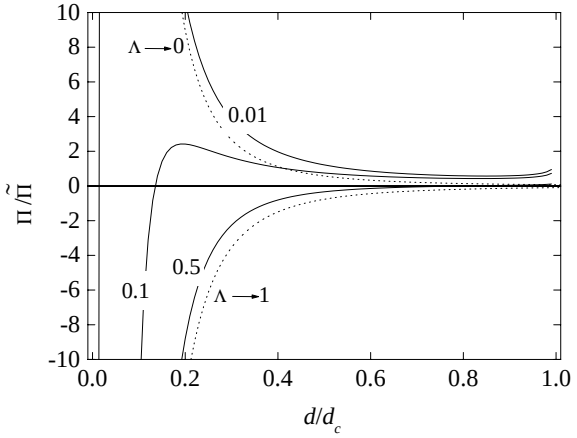

Figure 5.24 Pseudo-Casimir force for different values of $\Lambda = \lambda_H/\lambda_P$ in unit of $\tilde{\Pi} = (k_B T/d_c^3)$. Dotted lines correspond to the pseudo-Casimir force in the two analytical limits, $\Lambda \to 0$ (only the zeroth-order) and $\Lambda \to 1$.

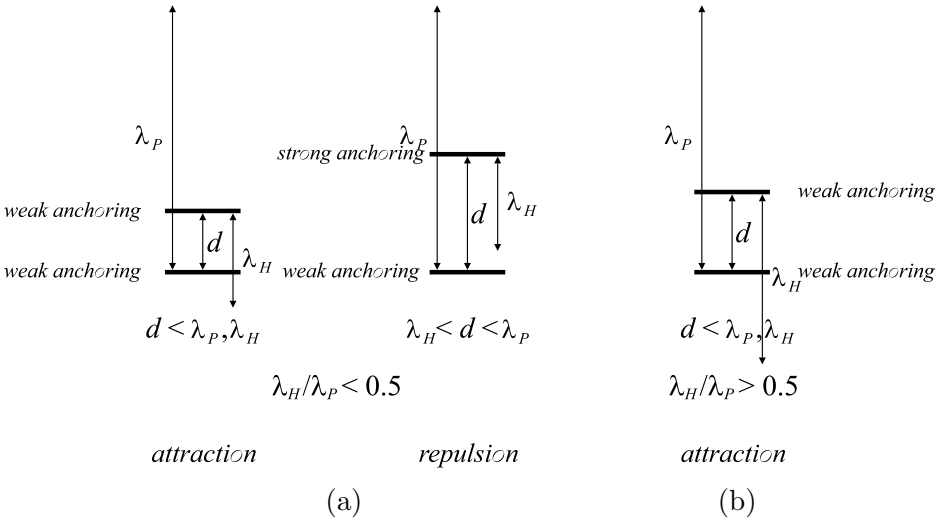

Figure 5.25 Relation between the cell thickness and the effective anchoring strength in hybrid cell below the critical thickness d_c. (a) For $d < \lambda_H, \lambda_P$ both anchorings are effectively weak whereas for $\lambda_H < d < \lambda_P$ the homeotropic anchoring becomes effectively strong. (b) For $\lambda_H/\lambda_P \geq 0.5$ both anchorings are effectively weak for all thicknesses $d < d_c$.

structural force, obtained by the derivative of the corresponding part of the free energy of the system with respect to the distance between the substrates. According to this and by replacing the sum over $\vec{q}$ by an integral, $\sum_{\vec{q}} \to (2\pi)^{-2} \int \mathrm{d}^2 q$, the pseudo-Casimir force per unit area reads

$$\Pi = -\frac{k_B T}{\pi d_c^3} \int_0^\infty \frac{p^2 \mathrm{d}p}{\frac{p-1+\Lambda}{p+1-\Lambda} \frac{p+\Lambda^{-1}-1}{p-\Lambda^{-1}+1} \mathrm{e}^{2px} - 1}, \tag{5.26}$$

where $\Lambda = \lambda_H/\lambda_P$ and $x = d/d_c$. The shape of the pseudo-Casimir force depends on the ratio between the two extrapolation lengths whereas its magnitude is tuned by the difference between them, i.e., the critical thickness d_c for the existence of the uniform director configuration.

The above expression can not be calculated analytically except in few limiting cases. For the finite but similar extrapolation lengths ($\Lambda \to 1$) the force is attractive and decreases as d^{-3} which is a typical behavior for equal boundary conditions [27,63],

$$\Pi\,(\Lambda \to 1) \approx -\frac{k_B T}{2\pi} \frac{\zeta(3)}{2d^3}, \tag{5.27}$$

where $\zeta(r) = \sum_{m=1}^{r} m^{-r}$ is the Riemann zeta function. In the case of infinitely strong homeotropic anchoring ($\Lambda \to 0$) the system reduces to mixed boundary conditions for the fluctuation modes and the zeroth-order of the pseudo-Casimir force has a typical monotonic repulsive behavior with the characteristic separation dependence $1/d^3$,

$$\Pi\,(\Lambda \to 0) \approx \frac{k_B T}{2\pi} \left[\frac{3\zeta(3)}{8d^3} + \frac{\ln 2}{\lambda_P d^2} \right]. \tag{5.28}$$

The second term in Eq. (5.28) is related to the fact that the substrate with weak planar anchoring promotes fluctuations and therefore enhances the discrepancy between the two effective boundary conditions which gives rise to an additional repulsion. In real hybrid systems with both λ_P and $\lambda_H > 0$, the fluctuation-induced force is attractive at small d/d_c's, then it becomes repulsive and may reach a local maximum before the pretransitional logarithmic singularity, which is common for all combinations of extrapolation lengths in the hybrid geometry [65]. However, it should be stressed that in the vicinity of the structural transition to the bent-director structure the anharmonic fluctuations may also play an important role. Nevertheless, the higher-order corrections are expected not to modify the divergent pretransitional behavior qualitatively [65]. The portrait of the pseudo-Casimir force for few values of the ratio λ_H/λ_P is plotted in Fig. 5.24. The nonmonotonic behavior of the pseudo-Casimir force can be simply understood by means of the influence of the type of the boundary conditions for the fluctuating modes on to

the fluctuation-induced force which we have already met in the introductory Section 2.4. At very small thicknesses ($d/d_c \ll 1$) both extrapolation lengths are larger than the thickness of the cell, therefore both surface interactions are effectively weak resulting in an attractive pseudo-Casimir interaction. On increasing the distance, the fluctuation-induced force becomes repulsive when the homeotropic extrapolation length becomes smaller than the cell thickness: for $\lambda_H < d < \lambda_P$, the homeotropic anchoring is strong whereas the planar anchoring is weak. For $\lambda_H/\lambda_P > 0.5$ both extrapolation lengths are larger than the cell thickness for all thicknesses yielding the uniform director configuration and the nonmonotonic behavior of the pseudo-Casimir force is lost. The numerical calculation gives for this critical ratio of the two extrapolation lengths the value 0.7; above this, the pseudo-Casimir force is attractive almost right up to the structural transition to the bent-director configuration. The described relations between extrapolation lengths and the effective strength of the anchorings are schematically represented in Fig. 5.25.

5.4 Stability of thin hybrid nematic films

In this Section the stability of a thin liquid-crystalline film is discussed in terms of enhanced/diminished capillary waves which cause the film to decompose through a process known as *spinodal dewetting*. As discussed in Section 2.4.1 the possible enhancement of thermal fluctuations of a free liquid–air interface is driven by disjoining force of the interactions acting between the two confining surfaces. The sum of all forces per unit area acting on a thin film is therefore denoted as a *disjoining pressure*. As already noted, the relevant physical quantity is the slope of the disjoining pressure rather than its sign. In the liquid-crystalline film the disjoining pressure consists of van der Waals interaction discussed in Chapter 3, and structural force and pseudo-Casimir force discussed in this Chapter. The electrostatic interactions are neglected here, since we assume that there are no free charges.

Lately, there has been an increased interest in the study of stability of thin films, not only liquid-crystalline films but also depositions of liquid metal [156], polymers [103,76], and protein solutions [157]. The reason for that is both, technological interest in stability of thin depositions and the interest in basic physical phenomena involved in the process of spinodal decomposition. Our study was stimulated by the results of the experiment performed by Vandenbrouck *et. al* [104,158]. In their experimental set-up the system consisted of a nematic liquid crystal 5CB spun cast on a silicon wafer bearing a natural oxide layer. Depending on the initial thickness of the liquid-crystalline film the film either remained stable for days or it dewetted into islands of liquid-crystalline drops and dry patches. The dewetting was moni-

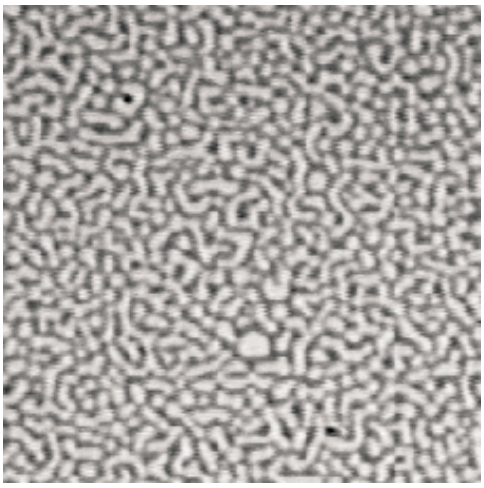

Figure 5.26 Photograph of a film after it has decomposed via spinodal dewetting. The picture was taken by F. Vandenbrouck *et. al* and is published in Phys. Rev. Lett. **82**, 2693 (1999).

tored using a polarized optical microscopy. A typical picture of a film after it has decomposed via spinodal dewetting is shown in Fig. 5.26. The original experiment was performed at the room temperature and the main conclusion was that the disjoining pressure exhibits nonmonotonic behavior with the marginal thickness for the dewetting of the film larger than 17 nm and smaller than 20 nm [104]. Later, the experiment was repeated for various temperatures within the nematic phase [158].

As we have seen in Sections 3.4 and 5.3 all forces contributing to the disjoining pressure can exhibit a nonmonotonic behavior. The portrait of the van der Waals force for the system in question is plotted in Fig. 5.27. Since the silicon wafer bears a natural oxide layer of silica the system is at least four-layered. As discussed in Section 3.4 in that case the van der Waals force can exhibit a nonmonotonic behavior if the van der Waals forces in different three-layer systems composed of the given materials have different signs. Here, the interaction between silicon and air across the nematic liquid crystal is repulsive whereas the interaction between silica and air across the same liquid crystal is attractive. Roughly speaking, one would expect that for film thicknesses below the thickness of the oxide layer the interaction would be mostly due to the interaction of silica and air whereas for large film thicknesses the existence of the additional layer would be negligible. Indeed, in Fig. 5.27 we can recognize the explained behavior. The marginal thickness (turnover thickness) is comparable to the thickness of the oxide layer, which is considered to be approximately 2 nm thick. Actually, the value of the marginal thickness can differ from the thickness of the additional layer if the two competing interactions are very different in magnitude. The dielectric and optical parameters characteristic for the given materials are written out in Table 5.1.

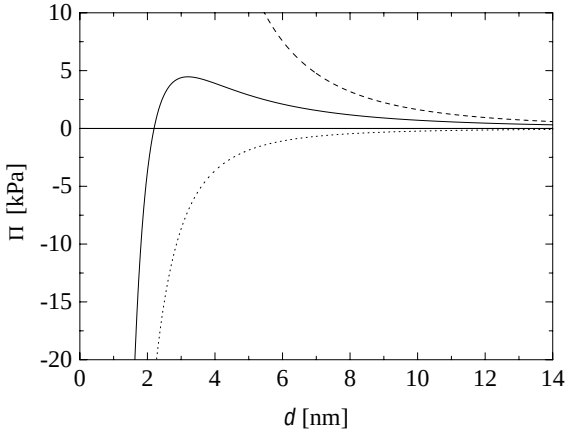

Figure 5.27 Van der Waals force per unit area acting on the liquid-crystalline film in contact with a solid substrate bearing an additional layer and a free liquid–air interface. Dashed and dotted lines correspond to the van der Waals force for the partial three-layer systems silicon–5CB–air and silica–5CB–air, respectively.

Although the van der Waals force possesses the needed nonmonotonic behavior the marginal thickness is an order of magnitude smaller than the observed value and can not be increased to the appropriate value just by small corrections due to better precision of the input parameters. Similar arguments can be stated also for the structural force which is in addition far too weak to have any significant influence on the disjoining pressure. On the contrary, the pseudo-Casimir force together with the van der Waals force yields suitable set of interactions to describe the process of spinodal decomposition. This was first recognized by Ziherl *et. al* [28]. In their study they determined the van der Waals and pseudo-Casimir forces acting in the described system and obtained the appropriate marginal thickness within the reasonable set of parameters describing optical and anchoring properties of the materials in question. Here, we present the results of a similar study, however,

Table 5.1 Material properties of the media constituting the system for studying spinodal dewetting. ϵ is the static dielectric constant and n is the refractive index of the medium in visible. All parameters are given at the room temperature.

material	ϵ		n	
silicon	12		3.5	
silica	14		1.5	
5CB	$\epsilon_\parallel$	$\epsilon_\perp$	$n_\parallel$	$n_\perp$
	18.5	7	1.71	1.53

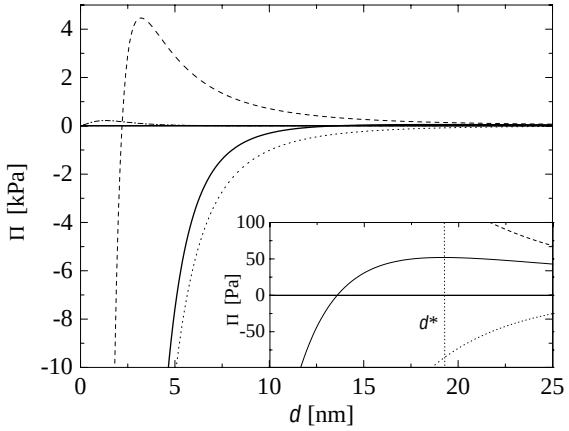

Figure 5.28 Disjoining pressure within the liquid crystal in contact with a solid substrate and air (solid line) deep in the nematic phase. The dashed line corresponds to van der Waals force, whereas the dotted and dash-dotted lines depict the pseudo-Casimir and structural contributions, respectively. Inset: behavior of the disjoining pressure in the vicinity of the marginal thickness.

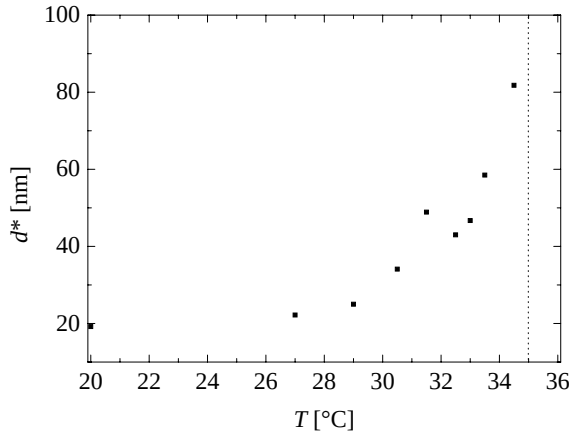

Figure 5.29 Temperature dependence of the marginal thickness for the spinodal dewetting of 5CB obtained by Valignat *et. al* [158].

with the improved determination of the van der Waals force which in the original study suffered from some defects. Since the van der Waals force is relatively strong in the interval of relevant film thicknesses its best determination is most important. The disjoining pressure on a slab of a liquid-crystalline material subject to spinodal dewetting together with the individual forces taking part in the total force is plotted in Fig. 5.28. In the calculation of the pseudo-Casimir force the extrapolation lengths were taken to be $\lambda_H = 33$ nm and $\lambda_P = 133$ nm which yields $\Lambda = 0.25$. The parameters used are comparable to the ones reported in previous studies [159,43,28].

As the temperature is varied the observed marginal thickness changes [158]: Deep in the nematic phase the marginal thickness only slightly increases with the increased temperature. On approaching the isotropic–nematic phase transition temperature

the marginal thickness exhibits a pretransitional singular-like behavior. The experimental values obtained by Valignat *et. al* are plotted in Fig. 5.29. The pretransitional "singularity" of the marginal thickness for the stability of a film is not just a consequence of the changed occupancy of the fluctuation states, either of thermal fluctuations of order parameter or fluctuations of the instantaneous electromagnetic fields. This explicit temperature dependence induces only weak temperature dependence of the corresponding forces, far from being singular. Within the mean-field theory used in this thesis only the order parameters change with the temperature. They indeed affect the tensorial physical quantities like the permittivity tensor, however, this again only weakly perturbs the van der Waals force through the temperature dependent refractive indices. The extrapolation lengths, being the ratio of the free energy related to elastic deformations and the energetic penalty for violating boundary conditions, are constant within the mean-field description and, thus, do not yield any temperature dependence of the pseudo-Casimir force. However, in experimental studies the extrapolation lengths were found to have a strong temperature dependence characterized by a "critical" increase on approaching the isotropic–nematic phase transition [17,46–48,16]. In their study, Mertelj *et. al* report this temperature dependence to be approximately $\lambda \propto (T_{NI} - T)^{-1}$ where T_{NI} corresponds to the bulk isotropic–nematic phase transition [16]. The power law indicates that the extrapolation lengths are inversely proportional to the square of the degree of nematic order. As already noted, within the mean-field theory and with lowest nontrivial terms, both, the elastic free energy and free energy corresponding to the interaction of the nematic liquid-crystalline material with solid substrate, are proportional to $S^2(T)$, thus, the corresponding extrapolation length is temperature independent. The observed temperature dependence of the extrapolation length indicates that close to the phase transition higher orders in the interaction between nematic liquid crystal and solid substrate should be taken into account. Considering the quadrupolar symmetry of the constituting molecules up to the fourth order term the surface part of the free energy reads

$$\mathcal{F}_{sur} = \frac{L\mathcal{A}}{2}\lambda^{-1}\left\{ \mathrm{tr}\,(\mathsf{Q}-\mathsf{Q}_S)^2 + \alpha\left[\mathrm{tr}\,(\mathsf{Q}-\mathsf{Q}_S)^2\right]^2\right\}, \tag{5.29}$$

where α is the ratio of the free energies associated with the second and fourth order terms. For the uniaxial nematic order $\mathsf{Q} = (S/\sqrt{6})(3\hat{n}\otimes\hat{n} - \mathsf{I})$ and, correspondingly, $\mathsf{Q}_S = (a_S/\sqrt{6})(3\hat{k}\otimes\hat{k} - \mathsf{I})$ if the confining substrate induces uniaxial nematic order with the easy axis $\hat{k}$ and the preferred degree of nematic order a_S. In the case with the uniform degree of nematic order through the film, $S = a_S = S_b(T)$, the effective extrapolation length reads approximately

$$\lambda_{eff}(T) = \frac{\lambda}{1 + \alpha' S_b^2(T)}, \tag{5.30}$$

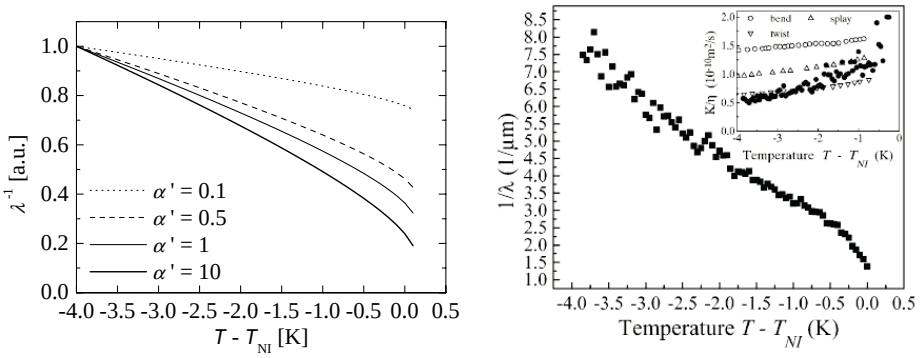

(a) (b)

Figure 5.30 (a) Temperature dependence of the extrapolation length for various values of the parameter α'. Large values of α' correspond to dominant fourth-order term which fits well the experimentally obtained behavior. Parameter λ is chosen in a way to fit the value of the extrapolation length deep in the nematic phase. (b) Experimental data for extrapolation length in 5CB in polycarbonate Nucleopore membrane reported by Mertelj and Čopič [Phys. Rev. Lett. **81**, 5844 (1998)].

where α' is related to α. On approaching the nematic–isotropic phase transition the nematic order decreases and, effectively, the anchoring strength decreases as well. Therefore, the effective extrapolation length increases on approaching the transition to the disordered phase. In Fig. 5.30 the temperature dependence of the extrapolation length is plotted for various values of the parameter α'. There are, however, some other approaches which lead to the increase of the extrapolation length in the vicinity of phase transition. They are based on the renormalization of the anchoring energy due to variations of the degree of nematic order [17] or due to thermal fluctuations [160].

To model the temperature dependence of the marginal thickness for the stability of a thin nematic liquid-crystalline film we have assumed the simplest temperature dependence of the extrapolation lengths: both extrapolation lengths are assumed to change with temperature in the same way, $\lambda \propto S^{-2}(T)$. In that case, the relevant ratio which changes the pseudo-Casimir interaction, $\Lambda = \lambda_H/\lambda_P$, is constant whereas the critical thickness for the structural transition between uniform and bent director configuration changes with temperature. As shown in Fig. 5.31, depending on the value of this ratio, however, with the same extrapolation lengths deep in the nematic phase, temperature dependence can vary from a very weak temperature dependence up to the dependence characterized by a pronounced pretransitional increase. Comparing the results from our model with the experimental results presented in Fig. 5.29 the best fit was obtained for $\Lambda = 0.25$, and $\lambda_H = 33$ nm and $\lambda_P = 133$ nm at $T = 293$ K. The used parameters fit well with the reported values

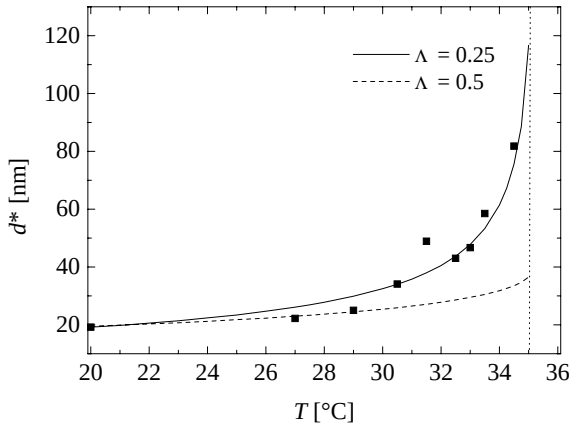

Figure 5.31 Temperature dependence of the marginal thickness for different Λ's. Squares correspond to experimental results obtained by Valignat *et. al* [158].

of extrapolation lengths at free nematic surface of 5CB and with the extrapolation length of 5CB in contact with silica, respectively. Within this, depending on the temperature the marginal thickness of the disjoining pressure is in the interval from 10 nm deep in the nematic phase up to 100 nm close to the transition to the isotropic phase. It should be stressed that the extrapolation lengths and the marginal thickness exhibit a pronounced increase in the vicinity of the phase transition, however, they do not diverge at the phase transition. In the literature this increase is often denoted as a pretransitional singularity although there is no reason for that at the discontinuous transition form the nematic to the isotropic phase.

6

Conclusion

The primary aim of my thesis was to study the effects of the confinement onto the nematic order parameter fluctuations. These are affected directly by the changed boundary conditions for the fluctuation modes and indirectly through the changed potential arising from the average equilibrium order. The surface-induced effects can be either localized at the confining substrates or the surface-induced deformation can extend over the whole liquid-crystalline sample. On the other hand, the spectrum of fluctuations indicates whether the corresponding transition is continuous or discontinuous, which is the mechanism responsible for the change of the order at the transition, etc. The variation of order on the macroscopic scale can be monitored through changed optical properties of the system, by its influence on the NMR response, etc. One of the principal physical observables are, however, the forces. Forces acting among the walls that confine the liquid crystal can be monitored either directly by force spectroscopy methods, such as with surface force apparatus, atomic force microscopy, etc., or indirectly via the effect of the interactions in the system onto the mechanical stability of liquid films — via their ability to wet solid substrates. It was found out by other authors that experiments taking advantage of spinodal dewetting of liquid-crystalline depositions are most promising for the observation of fluctuation-induced forces [161]. However, the fluctuation-induced force is just one of the forces among all that are acting on a film and it is far from being the only one relevant. Thus, other forces have to be considered as accurately as possible in order to provide an adequate mechanism for observing the fluctuation-induced forces. There was a lack of knowledge of the influence of the anisotropy of order onto the electromagnetic field fluctuations which give rise to the van der Waals interaction. Although they are not strictly related to the order parameter fluctuations they were studied here because of their relevance for the observation of fluctuation-induced forces and because they are too affected by the ordering power of the confining walls.

First, the collective fluctuations were studied in a heterophase system in which the surface-induced change of the order is localized at the confining wall. The analysis has revealed a close relationship between the wetting regime induced by disordering substrates and the pretransitional behavior of thermal fluctuations of the ordering in confined liquid crystals. The disordering action of the confining surface results below the isotropic–nematic phase transition in a heterophase structure consisting of an isotropic wetting layer and a nematic core. The system is characterized by a wetting-induced interface between nematic and isotropic phase, which gives rise to two localized normal modes: the first one represents fluctuations of the position of the phase boundary and is characterized by a soft dispersion of its relaxation rate (provided that the conditions for the complete wetting are fulfilled), and the second one corresponds to fluctuations of the shape of the interface. Moreover, there are a few additional softened biaxial modes, which are restricted to the wetting layer and whose pretransitional behavior is related to its growth. The spectrum of director fluctuations is Goldstone like and the corresponding fluctuation modes are accommodated by the nematic core. If the wetting is partial, the slowdown of the localized modes is not as pronounced as in complete wetting regime, but the underlying physics remains the same. In systems with complete wetting the isotropic–nematic phase transition becomes continuous provided that the thickness of the nematic cell is large compared to the nematic correlation length.

The surface-induced influence which perturbs the whole system was studied on the example of the hybrid nematic film. The analysis of nematic liquid crystals confined to highly constrained hybrid films with a biaxial structure has revealed a soft-mode or soft-mode-like dynamics in the vicinity of the structural transition toward hybridly aligned bent-director structure. The soft fluctuation manner is related to the bending director fluctuations which deform the undistorted director profile in biaxial configuration toward the continuously bent-director field in a usual hybridly distorted structure. In addition to this fluctuation mode the lowest order parameter mode exhibits similar slowdown of the relaxation rate, however, it remains finite even at the "supercooling" limit of the biaxial configuration. This mode is related to fluctuations of the position of the interface between the two uniaxial parts of the film. Other fluctuation modes do not contribute to the structural transition. However, low biaxial modes are interesting because they are localized in one half of the film only. The structural transition between the biaxial and bent-director phase can be either continuous or discontinuous — the two regimes are separated by a tricritical point $(T_{\mathrm{TP}}, d_{\mathrm{TP}})$. Above the tricritical point, the continuous structural transition becomes progressively discontinuous. The results of the phenomenological description were compared to the ones obtained by the computer simulation of the

hybrid nematic cell and a good qualitative agreement was found between the two approaches. Another test for the phenomenological description was the study of stability of thin hybrid films. It has revealed that the van der Waals and pseudo-Casimir forces are both important for the stability of the film. We managed to model the temperature dependence for the marginal thickness which is in good agreement with the observed dependence.

In order to study the stability of thin hybrid nematic depositions we have derived an improved analytic expression for the van der Waals interaction between macroscopic bodies, characterized by uniaxial permittivity tensor. We have shown that neglecting the anisotropy of static dielectric constants and refractive indices can yield wrong character of the interaction leading to incorrect interpretation or prediction of stability of thin uniaxial depositions. The anisotropic van der Waals interaction yields also a correction to the equilibrium order in heterophase nematic and smectic systems. In paranematic systems this changes the critical exponent of the wetting layer thickness.

Open problems

There are, however, some aspects of the surface-induced influence on the nematic order fluctuations which are not discussed here.

Due to the broken translational symmetry of the phases caused by the presence of walls surface-induced layering is expected in the vicinity of walls. The effect is more pronounced in systems with spontaneous smectic layering, however, to some extent it is observed also in nematogenic liquid crystals. The effect of smectic layering onto the fluctuations of the nematic order parameter is still to be investigated.

Another influence on the nematic order fluctuations, especially in heterophase systems, is due to the van der Waals interaction which yields a correction to the equilibrium order. This is quite substantial in the vicinity of the phase transition and even changes the critical exponent for the wetting layer thickness. In the complete wetting regime, this behavior is critical even within the phenomenological description used in our study, therefore, the basic properties of the fluctuation spectra are not expected to be changed. It might, however, change the behavior in the regime of partial wetting or at least renormalize the conditions for the complete wetting.

In the description of fluctuations it was assumed that the energy is dissipated only in the interior of the system whereas the dissipation at the surfaces was neglected. In order to provide the complete account of the influence of the surfaces the surface viscosity should be discussed in the future.

The studied behavior of the nematic ordering and pretransitional dynamics of a liquid crystal is certainly not limited to the simple planar geometry discussed in this

thesis. Similar phenomena are expected in systems where the heterophase or hybrid order of the nematic liquid crystal is induced by topological constraints imposed by curved walls, such as in cylindrical cavities, in the vicinity of line and point defect, etc. In these, the equilibrium order is already recognized to be characterized by partially molten nematic order characteristic for either of the two systems discussed in the thesis instead of exhibiting deformations of the director field. Thus, it can be expected that the collective modes associated with these geometries are basically the same as described here. However, in curved geometry in both of the discussed systems the director field can not be uniform due to the shape of the confinement. In order to make a quantitative analysis of collective modes in the vicinity of defects and, thus, of their growth, the analysis should be performed from the beginning.

⋆ ⋆ ⋆

The nature of the research work is such as to always open new questions and so the work seems to be never finished and the aim never fulfilled. On my way to prepare this thesis, many new interesting aspects of confined liquid crystals were raised; some of them gave the results presented in this work, some of them led to the dead end, and some of them still have to be investigated. However, this is what makes the research work interesting and what gives the assurance that there will be always something new to work on. Working on this thesis helped in deriving or becoming familiar with certain theories, methods, and models to describe physical phenomena of confined systems and provided some basic concepts characteristic for them.

Bibliography

[1] G. Friedel, Ann. Physique **18**, 273 (1922).
[2] R. Reinitzer, Monatsch Chem. **9**, 421 (1888).
[3] O. Lehman, Z. Physikal Chem. **4**, 462 (1889).
[4] P. G. de Gennes and J. Prost, *The Physics of Liquid Crystals* (Clarendon Press, Oxford, 1993).
[5] S. Chandresekhar, *Liquid crystals*, 2 ed. (Cambridge University Press, Cambridge, 1992).
[6] P. Chatelain, Acta Cristallogr. **1**, 315 (1948).
[7] L. D. Landau and I. M. Khalatnikov, Dokl. Akad. Nauk SSSR **96**, 469 (1954).
[8] *Liquid Crystals in Complex Geometries*, edited by G. P. Crawford and S. Žumer (Taylor & Francis, London, 1996).
[9] X. I. Wu, W. I. Goldburg, M. X. Liu, and J. Z. Xue, Phys. Rev. Lett. **69**, 470 (1992).
[10] G. Schwalb and F. W. Deeg, Phys. Rev. Lett. **74**, 1383 (1995).
[11] F. M. Aliev, in *Liquid crystals in complex geometries*, edited by G. P. Crawford and S. Žumer (Taylor & Francis, London, 1996).
[12] S. Stallinga, M. M. Wittebrood, D. H. Luijendijk, and T. Rasing, Phys. Rev. E **53**, 6085 (1996).
[13] P. Ziherl and S. Žumer, Liq. Cryst. **21**, 871 (1996).
[14] P. Ziherl and S. Žumer, Phys. Rev. Lett. **78**, 682 (1997).
[15] P. Ziherl, A. Šarlah, and S. Žumer, Phys. Rev. E **58**, 602 (1998).
[16] A. Mertelj and M. Čopič, Phys. Rev. Lett. **81**, 5844 (1998).
[17] M. Nobili and G. Durand, Phys. Rev. A **46**, R6174 (1992).
[18] P. Sheng, Phys. Rev. Lett. **37**, 1059 (1976).
[19] G. Barbero and R. Barberi, J. Phys. (Paris) **44**, 609 (1983).
[20] P. Palffy-Muhoray, E. C. Gartland, and J. R. Kelly, Liq. Cryst. **16**, 713 (1994).
[21] A. Šarlah and S. Žumer, Phys. Rev. E **60**, 1821 (1999).
[22] L. Moreau, P. Richetti, and P. Barois, Phys. Rev. Lett. **73**, 3556 (1994).
[23] A. Šarlah, P. Ziherl, and S. Žumer, Mol. Cryst. Liq. Cryst. **329**, 413 (1999).
[24] A. Šarlah, P. Ziherl, and S. Žumer, Mol. Cryst. Liq. Cryst. **320**, 231 (1998).
[25] S. Kralj, E. G. Virga, and S. Žumer, Phys. Rev. E **60**, 1858 (1999).
[26] A. Šarlah, P. Pasini, C. Chiccoli, C. Zannoni, and S. Žumer (unpublished).
[27] A. Ajdari, L. Peliti, and J. Prost, Phys. Rev. Lett. **66**, 1481 (1991).

[28] P. Ziherl, R. Podgornik, and S. Žumer, Phys. Rev. Lett. **82**, 1189 (1999).
[29] S. Žumer, A. Šarlah, P. Ziherl, and R. Podgornik, Mol. Cryst. Liq. Cryst. **358**, 83 (2001).
[30] A. Šarlah, P. Ziherl, and S. Žumer, accepted for publication in Mol. Cryst. Liq. Cryst. (unpublished).
[31] A. Šarlah and S. Žumer, accepted for publication in Phys. Rev. E (unpublished).
[32] S. Hess, Z. Naturforsch. Teil A **30**, 728 (1975).
[33] V. L. Pokrovskii and E. I. Kats, Zh. Eksp. Teor. Fiz. **73**, 774 (1977), [Sov. Phys. JETP **46**, 405 (1977)].
[34] L. D. Landau, Fiz. Z. Sowejetunion **11**, 26 (1937).
[35] Y. Nambu, Phys. Rev. Lett. **4**, 380 (1960).
[36] J. Goldstone, Nuovo Cimento **19**, 155 (1961).
[37] K. Huang, *Statistical Mechanics* (Wiley, New York, 1987).
[38] P. M. Chaikin and T. C. Lubensky, *Principles of condensed matter physics* (Cambridge University Press, Cambridge, 1995).
[39] V. L. Ginzburg, Fiz. Tverd. Tela. **2**, 2031 (1960), [Sov. Phys. Solid State **2**, 1824 (1961).].
[40] D. Monselesan and H.-R. Trebin, Phys. Stat. Sol. (b) **155**, 349 (1989).
[41] A. L. Alexe-Ionescu, G. Barbero, and G. Durand, J. Phys. II (Paris) **3**, 1247 (1993).
[42] F. C. Frank, Discuss. Faraday Soc. **25**, 19 (1958).
[43] O. D. Lavrentovich and V. M. Pergamenshchik, Phys. Rev. Lett. **73**, 979 (1994).
[44] V. M. Pergamenshchik, Phys. Rev. E **61**, 3936 (2000).
[45] J. L. Ericksen, Phys. Fluids **9**, 1205 (1966).
[46] K. H. Yang and C. Rosenblatt, Appl. Phys. Lett. **43**, 62 (1983).
[47] H. Yokoyama, S. Kobayashi, and H. Kamei, J. Appl. Phys. **61**, 4501 (1987).
[48] L. M. Blinov, A. Y. Kabayenkov, and A. A. Sonin, Liq. Cryst. **5**, 645 (1989).
[49] A. Rapini and M. Papoular, J. Phys. Colloq. **40**, C3 (1969).
[50] P. Sheng, Phys. Rev. A **26**, 1610 (1982).
[51] G. P. Crawford, R. J. Ondris-Crawford, J. W. Doane, and S. Žumer, Phys. Rev. E **53**, 3647 (1996).
[52] E. M. Lifshitz and L. P. Pitaevskii, *Statistical Physics, Part 1* (Pergamon Press, Oxford, 1980).
[53] L. D. Landau and E. M. Lifshitz, *Theory of Elasticity*, 3 ed. (Pergamon Press, Oxford, 1986), first published in English by Pergamon Press plc 1959.
[54] R. Kubo, *Statistical mechanics* (North-Holland Publishing Company, Amsterdam, 1965).
[55] L. O. Onsager, Phys. Rev. **37**, 405 (1931).
[56] D. Svenšek and S. Žumer, Liq. Cryst. **28**, 1389 (2001).
[57] R. G. Horn, J. N. Israelachvili, and E. Perez, J. Phys. (Paris) **42**, 39 (1981).
[58] S. H. J. Idziak *et al.*, Science **264**, 1915 (1994).

[59] A. Poniewierski and T. J. Sluckin, Liq. Cryst. **2**, 281 (1987).
[60] A. Borštnik and S. Žumer, Phys. Rev. E **56**, 3021 (1997).
[61] P. G. de Gennes, Langmuir **6**, 1448 (1990).
[62] A. Ajdari, B. Duplantier, D. Hone, L. Peliti, and J. Prost, J. Phys. II (Paris) **2**, 487 (1992).
[63] H. Li and M. Kardar, Phys. Rev. Lett. **67**, 3275 (1991).
[64] H. Li and M. Kardar, Phys. Rev. A **46**, 6490 (1992).
[65] P. Ziherl, F. K. P. Haddadan, R. Podgornik, and S. Žumer, Phys. Rev. E **61**, 5361 (2000).
[66] P. Ziherl, Phys. Rev. E **61**, 4636 (2000).
[67] K. Kočevar and I. Muševič, Liq. Cryst. **28**, 599 (2001).
[68] H. B. G. Casimir, Proc. Kon. Ned. Akad. Wet. **51**, 793 (1948).
[69] M. E. Fisher and P. G. de Gennes, C. R. Acad. Ser. B **287**, 207 (1978).
[70] V. Privman and M. E. Fisher, Phys. Rev. B **30**, 322 (1984).
[71] H. W. J. Bloete, J. L. Cardy, and M. P. Nightingale, Phys. Rev. Lett. **56**, 742 (1986).
[72] B. V. Derjaguin, A. S. Titijevskaja, I. I. Abricossova, and A. D. Malkina, Discuss. Faraday Soc. **18**, 24 (1954).
[73] P. G. de Gennes, Rev. Mod. Phys. **57**, 827 (1985).
[74] F. Brochard-Wyart and J. Daillant, Can. J. Phys. **68**, 1084 (1990).
[75] T. Young, Philos. Trans. R. Soc. London **95**, 65 (1805).
[76] M. Sferrazza *et al.*, Phys. Rev. Lett. **81**, 5173 (1998).
[77] M. Ibn-Elhaj and M. Schadt, Nature **410**, 796 (2001).
[78] H. Sirringhaus *et al.*, Nature **401**, 685 (1999).
[79] S. H. Chen *et al.*, Nature **397**, 506 (1999).
[80] K. M. Lenahan, Y. Liu, and R. O. Claus, Proceedings of the SPIE—The Interational Society for Optical Engineering **3675**, 74 (1999).
[81] P. Krecmer *et al.*, Science **277**, 1799 (1997).
[82] B. A. Grzybowski, H. A. Stone, and G. M. Whitesides, Nature **405**, 1033 (2000).
[83] H. G. F. Coster, A. J. Phys. **52**, 117 (1999).
[84] P. Poulin, H. Stark, T. C. Lubensky, and D. A. Weitz, Science **275**, 1770 (1997).
[85] A. Borštnik, H. Stark, and S. Žumer, Phys. Rev. E **61**, 2831 (2000).
[86] T. Kihara and N. Honda, J. Phys. Soc. Jap. **20**, 15 (1965).
[87] K. Okano and J. Murakami, J. Phys. Coll. **40**, 525 (1979).
[88] R. Podgornik and V. A. Parsegian, Phys. Rev. Lett. **80**, 1560 (1998).
[89] J. Israelachvili, *Intermolecular & Surface Forces* (Academic Press, London, 1985).
[90] B. V. Derjaguin, Kolloid Z. **69**, 155 (1943).
[91] H. B. G. Casimir and D. Polder, Nature **158**, 787 (1946).
[92] H. Hamaker, Physica **4**, 1058 (1937).

[93] E. M. Lifshitz, Zh. Eksp. Teor. Fiz. **29**, 94 (1955), [Sov. Phys. JETP **2**, 73, (1956)].
[94] I. E. Dzyaloshinskii and L. P. Pitayevskii, Zh. Eksp. Teor. Fiz. **36**, 1797 (1959), [Sov. Phys. JETP **9**, 1282 (1959)].
[95] I. E. Dzyaloshinskii, E. M. Lifshitz, and L. P. Pitayevskii, Advan. Phys. **10**, 165 (1961).
[96] N. G. van Kampen, B. R. A. Nijboer, and K. Schram, Phys. Lett. **26A**, 307 (1968).
[97] E. Gerlach, Phys. Rev. B **4**, 393 (1971).
[98] K. Schram, Phys. Lett. **43**, 282 (1973).
[99] B. W. Ninham and V. A. Parsegian, Biophys. J. **10**, 646 (1970).
[100] J. Mahanty and B. W. Ninham, *Dispersion Forces* (Academic Press, London, 1976).
[101] L. D. Landau and E. M. Lifshitz, *Electrodynamics of Continuous Media*, 2 ed. (Butterworth-Heinemann, Oxford, 1984), first published in English by Pergamon Press plc 1960.
[102] P. M. Morse and H. Feshbach, *Methods of theoretical physics* (Mc Graw Hill, Boston, 1953).
[103] G. Reiter, Phys. Rev. Lett. **68**, 75 (1992).
[104] F. Vandenbrouck, M. P. Valignat, and A. M. Cazabat, Phys. Rev. Lett. **82**, 2693 (1999).
[105] R. Barberi and G. Durand, Phys. Rev. A **41**, 2207 (1990).
[106] T. Moses and Y. R. Shen, Phys. Rev. Lett. **67**, 2033 (1991).
[107] H. Yokoyama, in *Handbook of Liquid Crystal Research*, edited by P. J. Collings and J. S. Patel (Qxford University Press, New York, 1997).
[108] D. Allender, G. L. Henderson, and D. L. Johnson, Phys. Rev. A **24**, 1086 (1981).
[109] T. J. Sluckin and A. Poniewierski, Phys. Rev. Lett. **26**, 2907 (1985).
[110] M. M. Telo da Gama, Mol. Phys. **52**, 611 (1984).
[111] M. M. Telo da Gama, Phys. Rev. Lett. **59**, 154 (1987).
[112] N. B. Ivanov, Phys. Rev. E **60**, 7596 (1999).
[113] K. Miyano, Phys. Rev. Lett. **43**, 51 (1979).
[114] H. Yokoyama, S. Kobayashi, and H. Kamei, Mol. Cryst. Liq. Cryst. **99**, 39 (1983).
[115] K. Kočevar, R. Blinc, and I. Muševič, Phys. Rev. E **62**, R3055 (2000).
[116] T. Moses, Y. Ouchi, W. Chen, and Y. R. Shen, Mol. Cryst. Liq. Cryst. **225**, 55 (1993).
[117] C. Rosenblatt, Phys. Rev. Lett. **53**, 791 (1984).
[118] B. M. Ocko, A. Braslau, P. S. Pershan, J. Als-Nielsen, and M. Deutsch, Phys. Rev. Lett. **57**, 94 (1986).
[119] G. Skačej, A. L. Alexe-Ionescu, G. Barbero, and S. Žumer, Phys. Rev. E **57**, 1780 (1998).
[120] F. N. Braun, T. J. Sluckin, and E. Velasco, J. Phys. Con. Matt. **8**, 2741 (1996).

[121] S. Faetti and V. Palleschi, Phys. Rev. A **30**, 3241 (1984).
[122] H. Kasten and J. Strobl, J. Chem. Phys. **103**, 6768 (1995).
[123] P. G. de Gennes, Mol. Cryst. Liq. Cryst. **12**, 193 (1971).
[124] M. A. Marcus, Mol. Cryst. Liq. Cryst. **100**, 253 (1983).
[125] E. Martin del Rio, M. M. Telo da Gama, E. de Miguel, and L. F. Rull, Europhys. Lett. **35**, 189 (1996).
[126] W. H. Press, S. A. Teukolsky, W. T. Vetterling, and B. P. Flannery, *Numerical recipes in C: The art of scientific computing*, 2 ed. (Cambridge University Press, Cambridge, 1992).
[127] G. Gompper, M. Hauser, and A. A. Kornyshev, J. Chem. Phys. **101**, 3378 (1994).
[128] T. Bellini *et al.*, Phys. Rev. Lett. **69**, 788 (1992).
[129] G. S. Iannacchione, G. P. Crawford, S. Žumer, J. W. Doane, and D. Finotello, Phys. Rev. Lett. **71**, 2595 (1993).
[130] W. Greiner and B. Muller, *Quantum Mechanics – Symmetries* (Springer–Verlag, Berlin, 1989).
[131] T. Bellini, N. A. Clark, and D. W. Schaefer, Phys. Rev. Lett. **74**, 2740 (1995).
[132] C. S. Park, M. Čopič, R. Mahmood, and N. A. Clark, Liq. Cryst. **16**, 135 (1994).
[133] I. F. Lyuksyutov, Zh. Eksp. Teor. Fiz. **75**, 358 (1978), [Sov. Phys. JETP **48**, 178 (1978)].
[134] N. Schopohl and T. J. Sluckin, Phys. Rev. Lett. **59**, 2582 (1987).
[135] A. Sonnet, A. Kilian, and S. Hess, Phys. Rev. E **52**, 718 (1995).
[136] *Handbook of liquid crystals*, edited by D. Demus, J. W. Goodby, G. W. Gray, and H.-W. Speiss (Wiley-VCH, Weinheim, 1998).
[137] D. Andrienko, Y. Kurioz, Y. Reznikov, and V. Reshetnyak, Sov. Phys. JETP **85**, 1119 (1997).
[138] M. M. Wittebrood, T. Rasing, S. Stallinga, and I. Muševič, Phys. Rev. Lett. **80**, 1232 (1998).
[139] H. G. Galabova, N. Kothekar, and D. W. Allender, Liq. Cryst. **23**, 803 (1997).
[140] V. M. Pergamenshchik, Phys. Rev. E **47**, 1881 (1993).
[141] E. C. Gartland, P. Palffy-Muhoray, and R. S. Varga, Mol. Cryst. Liq. Cryst. **199**, 429 (1991).
[142] O. D. Lavrentovich, Phys. Scr. **T39**, 394 (1991).
[143] C. Chiccoli, O. D. Lavrentovich, P. Pasini, , and C. Zannoni, Phys. Rev. Lett. **79**, 4401 (1997).
[144] J. Stelzer, P. Galatola, G. Barbero, and L. Longa, Phys. Rev. E **55**, 477 (1997).
[145] P. Pasini, private communication.
[146] C. Chiccoli, P. Pasini, A. Šarlah, C. Zannoni, and S. Žumer (unpublished).
[147] P. P. Karat and N. V. Madhusudana, Mol. Cryst. Liq. Cryst. **40**, 953 (1977).
[148] M. P. Allen and D. J. Tildesley, *Computer simulation of liquids* (Clarendon Press, Oxford, 1989).

[149] *Advances in the Computer Simulations of Liquid Crystals*, edited by P. Pasini and C. Zannoni (Kluwer, Dordrecht, 2000).
[150] P. A. Lebwohl and G. Lasher, Phys. Rev. A **6**, 426 (1972).
[151] E. Berggren, C. Zannoni, C. Chiccoli, P. Pasini, and F. Semeria, Phys. Rev. E **50**, 2929 (1994).
[152] U. Fabbri and C. Zannoni, Mol. Phy. **58**, 763 (1986).
[153] D. J. Cleaver and P. I. C. Teixeira, Chem. Phys. Lett **338**, 1 (2001).
[154] P. Ziherl, Ph.D. thesis, University of Ljubljana, Ljubljana, 1998.
[155] H. Kleinert and F. Langhammer, Phys. Rev. A **44**, 6686 (1991).
[156] J. Bischof, D. Scherer, S. Herminghaus, and P. Leiderer, Phys. Rev. Lett. **77**, 1536 (1996).
[157] U. Thiele, M. Mertig, and W. Pompe, Phys. Rev. Lett. **80**, 2869 (1998).
[158] M.-P. Valignat and F. Vandenbrouck, private communication.
[159] J. E. Proust, Colloid Polym. Sci. **254**, 672 (1976).
[160] G. Barbero and A. K. Zvezdin, Phys. Rev. E **62**, 6711 (2000).
[161] P. Ziherl and I. Muševič, accepted for publication in Liq. Cryst. (unpublished).

Izjava

Izjavljam, da sem v disertaciji predstavila rezultate lastnega znanstvenoraziskovalnega dela.

Ljubljana, 27. 9. 2001 Andreja Šarlah